Collective effects in many-body systems: The case of quantum batteries and photon condensation

PhD program

Nanoscience

Academic year

2019/2020

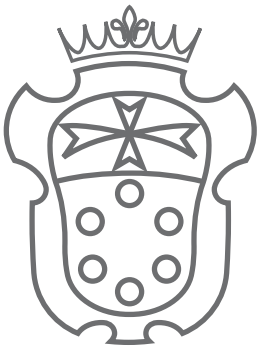

SCUOLA NORMALE SUPERIORE

Candidate

Gian Marcello Andolina

Supervisors

Prof. Marco Polini

Prof. Vittorio Giovannetti

Acknowledgements

Quattro anni di dottorato sono volati. Questo lo devo senz'altro alle tante persone che hanno arricchito questi anni. Per prima cosa devo ringraziare i miei supervisors: il Prof. Marco Polini e il Prof. Vittorio Giovannetti. Lavorare con Marco non è mai banale, facile o rilassante. Al contrario si è constantemente spronati a capire profondamente le cose. Il progetto cruciale, quello cui essere entusiasti, è quello su cui si sta lavorando adesso. Non avrei potuto chiedere di meglio. Vittorio è un esempio di passione genuina nel risolvere problemi di fisica e di matematica. Molti risultati di questa tesi non ci sarebbero se non avessi passato diverse ore a discutere ininterrotamente alla lavagna con lui.

Questa tesi tratta di due argomenti diversi: batterie quantistiche e transizioni di fase superradianti. Ho affrontato ciascuno di questi due argomenti fianco a fianco con due amici: il Dr. Maximilian Keck e il Dr. Francesco Pellegrino, rispettivamente. Devo ringraziare Max per essere stato un constante sprone (talora brutale) ad affrontare la ricerca seriamente e con spirito critico. Ho lavorato con Ciccio (Francesco) fin dal primo giorno del mio dottorato e tuttora lavoriamo assieme giornalmente. Immagino che non finirà qui. Nel frattempo lo ringrazio per essere per me un esempio scientifico e umano. Vorrei ringraziare anche il Prof. Davide Rossini per la proficua collaborazione, contraddistinta da una grande pazienza e disponiblità da parte sua, e per le sue straordinarie abilità di programmazione numerica. Ringrazio tutti coloro con cui ho collaborato e che hanno contribuito al materiale di questa tesi: la Dr.ssa Antonella De Pasquale, il Dr. Andrea Mari, il Prof. Allan MacDonald, il Prof. Frank Koppens, il Dr. Dario Ferraro, il Dr. Dario Rosa, Donato Farina, il Dr. Matteo Carrega, il Prof. Omar di Stefano, il Prof. Salvatore Savasta e il Dr. Vittorio Pellegrini. In questi anni ho avuto la fortuna di seguire alcuni tesisti: Francesco, Johannes e Lorenzo. Ciascuno di loro mi ha insegnato qualcosa. Grazie.

Devo ringraziare inoltre tutto il gruppo di ricerca di informazione quantistica e materia condensata della Scuola Normale, per i tanti momenti passati assieme e per le innumerevoli discussioni, scientifiche e non. Ringrazio Paolo per i tanti consigli scientifici davvero illuminanti e per la sua amiciza sincera che lo costringe a sopportarmi; Pietro per avere sempre un'opinione interessante (che esprime solo sotto richiesta esplicita) e per la riservatezza; Stefano Cusumano per la lotta politica e per i tanti momenti goliardici; il "generale" Vasco per l'inesauribile umorismo; Salvatore per il suo febbricitante entusiasmo; Gianmichele per il forbito dark humor e per le sue capacità eclettiche; Iacopo per la pazienza e il suo formidabile aiuto con certi conti; Bibek per la cucina esotica e per i momenti di condivisione tra coinquilini; Marco Fanizza per essere il "luminoso contrario"; Stefano Chessa per l'ironia tagliente; Donato per il laborioso impegno; Federico per il suo sguardo sul mondo così originale; Farzad per il suo altruismo e la sua rilassatezza. Ringrazio tutti coloro che hanno speso del tempo per rileggere questa tesi e darmi utili consigli: Antonella, Max, Alessandro, Lorenzo, Gianmichele, Francesco, Salvatore, Paolo e Pietro, grazie!

Ringrazio anche gli amici dei tempi dell'università, in particolare "la Spezia gang (ovvero

Giulia, Paolo e Francesco) che ha formato la mia capacità di polemizzare. Tra gli amici univeritari, un ringraziamento speciale va a Federico Tonielli, che è venuto a mancare quest'anno. Per me è sempre stato un esempio di tenacia e di volontà di comprendere. Non lo dimenticherò. Ringrazio anche gli amici di Spezia con cui ho condiviso questi anni, ovvero lo "zio" Mattia, la "cugina" Davide e le mie due "sorelle": Nicolò ed Alessandro. Un ringraziamento speciale va ad Alessandro con cui condivido l'amore per le storie.

Ringrazio i miei nonni: Piero e Maria Pia, Sebastiano ed Erminia e i miei genitori: Marcello per l'amore incondizionato e Germana per avermi insegnato a lottare. L'ultimo ringraziamento è per Giulia. Nulla di tutto questo sarebbe stato possibile senza di te. Ti prometto che torneremo ancora a viaggare e vedere il mondo assieme. Per ora, grazie di esserci sempre stata!

List of Publications

- **G.M. Andolina**, F.M.D. Pellegrino, F.H.L. Koppens, and M. Polini,
Quantum nonlocal theory of topological Fermi arc plasmons in Weyl semimetals,
Phys. Rev. B **97**, 125431 (2018).

- D. Ferraro, **G.M. Andolina**, M. Campisi, V. Pellegrini and M. Polini,
High-Power Collective Charging of a Solid-State Quantum Battery, Editor's Suggestion,
Phys. Rev. Lett. **120**, 117702 (2018).

- **G.M. Andolina**, D. Farina, A. Mari, V. Pellegrini, V. Giovannetti, and M. Polini,
Charger-mediated energy transfer in exactly solvable models for quantum batteries,
Phys. Rev. B **98**, 205423 (2018).

- **G.M. Andolina**, M. Keck, A. Mari, M. Campisi, V. Giovannetti und M. Polini,
Extractable work, the role of correlations, and asymptotic freedom in quantum batteries,
Phys. Rev. Lett. **122**, 047702 (2019).

- D. Farina, **G.M. Andolina**, A. Mari, M. Polini, and V. Giovannetti,
Charger-mediated energy transfer in exactly solvable models for quantum batteries,
Phys. Rev. B **99**, 035421 (2019).

- **G.M. Andolina**, M. Keck, A. Mari, V. Giovannetti, and M. Polini,
Quantum versus classical many-body batteries,
Phys. Rev. B **99**, 205437 (2019).

- D. Ferraro, M. Campisi, **G.M. Andolina**, V. Pellegrini and M. Polini,
Quantum supercapacitors, Editor's Suggestion,
Phys. Rev. B **100**, 075433 (2019).

- **G.M. Andolina**, F.M D. Pellegrino, V. Giovannetti, A.H. MacDonald, and M. Polini,
Cavity quantum electrodynamics of strongly correlated electron systems: A no-go theorem for photon condensation, Rapid Communication,
Phys. Rev. B **100**, 121109(R) (2019) .

- D. Rossini, **G.M. Andolina**, and M. Polini,
Many-body localized quantum batteries,
Phys. Rev. B **100**, 115142 (2019) .

- D. Rossini, **G.M. Andolina**, D. Rosa, M .Carrega, and M. Polini,
Quantum charging supremacy via Sachdev-Ye-Kitaev batteries, Editor's Suggestion,
Phys. Rev. Lett. **125**, 236402 (2020).

- D. Rosa, D. Rossini, **G.M. Andolina**, M. Polini, and M. Carrega,
Ultra stable charging of fastest scrambling quantum batteries,
J. High Energ. Phys. **2020**, 67 (2020).

- **G.M. Andolina**, F.M.D. Pellegrino, V. Giovannetti, A.H. MacDonald, and M. Polini, *Theory of Photon Condensation in a Spatially-Varying Electromagnetic Field*, Editor's Suggestion,
  Phys. Rev. B **102**, 125137 (2020).

Abstract

This thesis studies problems concerning light-matter interaction in the context of many-body systems and the exploitation of these systems in the context of the emerging field of quantum batteries (QBs). We start by introducing the necessary theoretical concepts and tools forming the basis of this manuscript. Among these, the Dicke Hamiltonian, a paradigmatic model which describes an ensemble of N atoms interacting with the same electromagnetic mode, is introduced. This model represents a key concept on which the thesis is developed.

The remaining chapters contain original results and can be conceptually split into two parts. The first one deals with the study of many-body QBs, quantum mechanical systems with many degrees of freedom which can be used to store energy and that display fast charging. The second part studies equilibrium superradiant quantum phase transition, (which we dub, to avoid confusion with many superradiant phenomena, systems "photon condensation"), in the context of many-body strongly-correlated system.

Quantum information theorems state that it is possible to exploit collective quantum resources to greatly enhance the charging power of QBs made of many identical elementary units. We here present and solve a model of a QB that can be engineered in solid-state architectures. It consists of N two-level systems coupled to a single photonic mode in a cavity. We contrast this collective model ("Dicke QB"), whereby entanglement is genuinely created by the common photonic mode, to the one in which each two-level system is coupled to its own separate cavity mode ("Rabi QB"). By employing exact diagonalization, we demonstrate the emergence of a collective advantage in the charging power of Dicke QBs, which scales like $\sqrt{N}$ for $N \gg 1$.

We study a simplified version of a Dicke QB, where non energy-conserving interactions are neglected. In such so-called Tavis-Cummings QB, we quantify the fraction $\mathcal{E}_{\mathrm{B}}^{(N)}$ of energy stored in the battery that can be extracted in order to perform thermodynamic work. We first demonstrate that $\mathcal{E}_{\mathrm{B}}^{(N)}$ is highly reduced by the presence of correlations between the charger and the battery or between the two-level systems composing the battery. We then show that the correlation-induced suppression of extractable energy, however, can be mitigated by preparing the charger in a coherent optical state. We conclude by proving that the charger-battery system is asymptotically free of such locking correlations in the $N \to \infty$ limit.

At this point, the physics behind fast charging in a Dicke QB is still unclear. Is this just due to the collective behavior of the underlying interacting many-body system or does it have its roots in the quantum mechanical nature of the system itself? We address these questions by studying three examples of quantum-mechanical many-body batteries with rigorous classical analogs. We find that quantum and classical models perform with the same scaling with the number of battery units N. Within these models it is possible to find only parametric advantages (i.e. advantages independent of N), which are model dependent and, even within the same model, depend on the value of the coupling constant that controls the interaction between the charger and the battery itself.

We introduce a different model of charging, which relies on a quantum quench base on the Sachdev-Ye-Kitaev (SYK) model. The exactly-solvable SYK model has recently received considerable attention in both condensed matter and high energy physics because it describes quantum matter without quasiparticles, while being at the same time the holographic dual of a quantum black hole. Here, we examine SYK-based charging protocols of quantum batteries with N quantum cells. The complexity of the SYK problem prevents us from employing analytic techniques and thus we rely on a fully numerical approach. Extensive calculations based on exact diagonalization for N up to 16 strongly suggest that the optimal charging power of our SYK quantum batteries displays a super-extensive scaling with N that stems from genuine quantum mechanical effects. To the best of our knowledge, this is the first quantum many-body battery model where fast charging occurs due to the maximally-entangling underlying quantum dynamics.

Lastly, we study photon condensation in strongly-interacting many-body systems. Despite decades of work it has remained unclear whether or not photon condensation can occur an equilibrium. We first show that when a non-relativistic quantum many-body system is coupled to a spatially-uniform quantum cavity field, gauge invariance forbids photon condensation. We then present a microscopic theory of the cavity quantum electrodynamics of an extended Falicov-Kimball model, showing that, in agreement with the general theorem, its insulating ferroelectric and exciton condensate phases are not altered by the cavity and do not support photon condensation.

Finally, we show that the no-go theorem does not apply to *spatially-varying* quantum cavity fields. We find a criterion for occurrence of photon condensation that depends solely on the static, non-local orbital magnetic susceptibility $\chi_{\rm orb}(q)$, of the electronic system (ES) evaluated at a cavity photon momentum $\hbar q$. Only 3D ESs satisfying the Condon inequality $\chi_{\rm orb}(q) > 1/(4\pi)$ can harbor photon condensation. For the experimentally relevant case of two-dimensional (2D) ESs embedded in quasi-2D cavities the criterion again involves $\chi_{\rm orb}(q)$ but also the vertical size of the cavity. We use these considerations to identify electronic properties that are ideal for photon condensation. Our theory is non-perturbative in the strength of electron-electron interaction and therefore applicable to strongly correlated ESs. We conclude the Thesis with a number of Appendices reporting useful technical details.

Contents

Part I

Introduction to relevant theoretical facts

"TE OCCIDERE POSSUNT SED TE EDERE NON POSSUNT NEFAS EST [a]"

D.F. Wallace - Infinite Jest

[a] Roughly, "They can kill you, but the legalities of eating you are quite a bit dicier"

1 Introduction

It is believed that we are at the midst of the *second quantum revolution* [1]. While the *first quantum revolution* consisted in recognizing that microscopic phenomena are correctly described by the laws of quantum mechanics, the second one actively exploits these laws to engineer novel more efficient technologies.

In the first thirty years of the 20th century the theory of quantum mechanics was developed. Plank [2] managed to explain the frequency distribution of black body radiation with the ad hoc hypothesis that electromagnetic energy can assume only discrete multiples of its frequency. Soon after, it was realized that this assumption can be justified if we admit that light, customary described as waves by classical electromagnetism, behaves as a particle in certain circumstances. Similarly, experimental data of atom emission spectra were found to be in good agreement with the hypothesis that electrons, which were thought as corpuscular particles, possess wave properties. Once we accept such counter-intuitive properties of microscopic constituents of matter a number of experimental facts can be explained with great accuracy. The successful quantum theory led to ground breaking inventions such as the transistor (1948) and the laser (1960), which are at the basis of our present technology. Computers and cellphones would not have been possible without the transistor, which is the fundamental unit of electronics. The laser has wide applications, ranging from communications to medicine.

This was the first quantum revolution. The second one is expected to have equally disruptive implications on human daily life. The typical example of what we could expect is quantum computation [3], where computing operations are performed on quantum bits (qubits) instead of classical bits. In this case, it is believed that quantum resources such as coherence and entanglement can be used to greatly speed-up the computing process. In 1994, Peter Shor [4] proposed a quantum algorithm that factorizes an integer in a polynomial number of computational steps. Factorizing an integer number, finding its prime factors, it is known to be a hard problem. All known classical algorithms for integer factorization require an exponential number of computational steps. As such, for classical algorithms cannot be applied to for large enough numbers due to the rapid increasing of computational time. In practice, this means that a quantum computer can perform a task which is believed to be unattainable for

a classical computer. This exponential speed-up fueled by quantum resources goes under the name of "quantum supremacy". A first experimental proof of principle of such computational speed-up appeared in 2019 [5].

Remarkably, one of the most used encryption methods, the so-called public-key cryptography, relies on the impossibility for a third malevolent part to find the prime factors of a large number in a feasible amount of time. While this assumption is true for a classical computer, a quantum computer is supposed to easily break the security of such encryption, meaning that quantum computation can be a threat for secure communication. Quantum mechanics itself offers a solution to this problem. It has been shown that the quantum version of the public key encryption, the quantum key distribution [3], is unconditionally secure. The only presence of a third malevolent part eavesdropping the communication would spoil the message, since in quantum mechanics the presence of an observer causes the collapse of the quantum state. The receiver would immediately recognize that conversation has been spied and ask the sender to stop the communication. Quantum phenomena can have many other technological applications such as: quantum simulators [6, 7] and quantum metrology [8, 9]. The key idea behind all these applications is to exploit quantum resources to achieve unprecedented results.

As the quantum revolutions are based on quantum theory, also other previous technological revolutions were driven by a new scientific theory. Indeed, the success of the first industrial revolution was deeply intertwined the development of thermodynamics. Thermodynamics is an empirical theory that studies the transformation of energy into heat and work [10]. Such theory was developed with the clear goal of optimizing the steam engines efficiency. Unlike statistical mechanics, which starting from a microscopic description of the constituents tries to find a link among macroscopic quantities, thermodynamics starts from some fundamental laws that are assumed as postulates based on experience and conclusions are drawn from them, without entering into the specific microscopic detail of the phenomena. This approach has the advantage of being independent of the specific microscopic model. The laws of thermodynamics therefore have a universal character, which ignores the specific details of the system and connects macroscopic quantities of practical interest, such as work, heat and temperature [10].

Given this context, it is natural to ask ourselves if quantum resources can be exploited in order to improve thermodynamic performances. The research field which studies thermodynamic quantities in a quantum regime has been named quantum thermodynamics [11–19]. At first glance, there seems to be no place for quantum supremacy in quantum thermodynamics. As stated before, the laws of thermodynamics possess a universal character which transcend the specific microscopic model. For example, it is not possible to perform a transformation which has the only effect to transfer heat from a cold to an hot bath, even employing quantum resources. Equivalently, the efficiency of a quantum heat engine can not surpass the Carnot limit (which sets the maximum efficiency compatible with the laws of thermodynamics).

Nevertheless, thermodynamics does not set bounds on the timescale of such transformations. If there is a place where a quantum advantage can be found that should be finite-time (or out of equilibrium) quantum thermodynamics. Indeed, seminal papers [20–23] showed that entangling operations can speed-up the charging process of a quantum battery (QB), a system able to store energy and perform useful work. In these systems, at set of entangled states represents a shortcut in the Hilbert space which allows a fast charging process. Basic theoretical tools of QBs and a brief review of the related Literature are provided in Chap. 2.

The quantum advantage in QBs relies on the usage of highly non-local operations acting simultaneously on all the battery units that form the QB. Such non-local interactions may be

difficult to be realized in practice. In Ref. [24] we proposed an experimentally feasible set up to implement the fast charging of a QB, employing the Dicke model [25]. This model, which has a central role in describing collective effects in cavity and circuit quantum electrodynamics (QED), is presented in Chap. 3. The Dicke model describes an ensemble of atoms in an optical cavity as two-level systems (TLS) coupled with a single bosonic mode. Dicke [25] proposed a forerunner of such model and he employed it to predict superradiant emission, a collective phenomena where excited atoms interfere and simultaneously release photons in a bright flash. Hepp and Lieb [31], inspired by the pioneering work of Dicke, introduced the Dicke model in 1973 and they used it to predict the so-called superradiant phase transition.

The outline of the first part of the Thesis, devoted to quantum batteries, is the following: In Chap. 4 (based on Ref. [24]) we present the Dicke QB, showing that a collective charging protocol outperform an independent charging by a factor $\sqrt{N}$, where N is the number of battery units. The physics of this boost is rooted in the superradiant mechanism proposed by Dicke [25].

In Chap. 5 (based on Ref. [26]) we investigated the amount of energy that can be drawn from a QB, after the charging has occurred. Correlations, such as entanglement, between the battery and the charger can seriously limit the extractable work. Furthermore, we prove that, in integrable system, the charger-battery system is asymptotically free of such locking correlations in the $N \to \infty$ limit.

In Chap. 6 (based on Ref. [27]) we finally study a series of many-body QBs which posses a well-defined classical analogue. This enables us to prove that the power advantage of Ref. [24] has a collective many-body origin and does not effectively realize the entanglement shortcut foreseen by Refs. [22, 23].

In Chap. 7 (based on Ref. [28]), employing the Sachdev-Ye-Kitaev model [29, 30], we provide the first quantum many-body battery model where fast charging occurs due to the maximally-entangling underlying quantum dynamics envisioned in by Refs. [22, 23]. The answer of the main research question driving the topic of QB, "can quantum resources used to improve the performances of a battery?", as shown in this Chapter, is affirmative. This concludes the first part of this Thesis, devoted to QBs.

The second quantum revolution does not only deal with the production of new quantum devices but also aim to engineer new quantum phase of matter, such as photon condensation. This exotic phase, peculiar of strongly interacting light-matter systems, is characterized by a macroscopic number of photons in the equilibrium ground state.

The prototypical theoretical model showing such phase is the Dicke model [25], introduced in Chap. 3, which describes systems that can be engineered with cavity and circuit quantum electrodynamics (QED). Cavity QED deals with atoms in optical cavities while circuit QED referrers to experimental setups where artificial atoms, made by superconducting qubits, are coupled to microwave resonators. Several of the first implementations [3] of quantum computers rely on these platforms and they are one the most promising tools in the context of the second quantum revolution.

Let us briefly summarize experimental development in the context of light-matter interaction. In the 80s, experimental platforms achieved the strong coupling regime, where noise and losses can be neglected. This enables the manipulation of atoms and photons as isolated quantum objects [33–35]. Cavity QED was one of the first setups where it was possible to measure quantum features of a single photon, such as coherent superposition, quantum jumps, and of atom-photon entangled state such as Schrödinger cat states and time-resolved decoherence [34]. More recently these platforms reached the ultra-strong coupling regime

[36], where the light-matter coupling exceeds the bare energies of the non-interacting system. In this situation the intuitive picture of atoms absorbing and emitting photons ceases to be valid. Conversely, due to strong interactions, atoms and photons are strongly bounded in an emerging quasi-particle, the polariton.

In this exotic regime, the Dicke model shows the aforementioned photon condensation [31, 32, 37, 38]. As we show in Chap. 3 when the coupling exceeds a critical value the model enters in a "superradiant" phase, characterized by a macroscopic number of photons. In order to avoid any confusion with superradiant emission [25], we refer to this phase as photon condensation. A careful microscopic derivation of the Dicke model led to addition of an extra Hamiltonian term, known as diamagnetic term. This factor, which is crucial to enforce the gauge invariance of the model, forbids the phase transition to occur [39, 40]. However the Dicke model remains a simplified toy model, inadequate to describe all experimental situations, and whether or not photon condensation can occur in real systems remains an open and debated question.

The outline of the second part of the Thesis, devoted to photon condensation, is the following: In Chap. 8 (based on Ref. [41]), we generalize such "no-go" theorem to a generic non-relativistic electronic system. Our proof accounts for strong electronic interaction. As we demonstrate, this result is based on the correct gauge invariance of the system.

In Chap. 9 (based on Ref. [42]) we provide a path to circumvent the previous theorem and realize photon condensation, by considering a spatially varying electromagnetic field. This result paves the way for the realization of equilibrium photon condensation in solid-state systems.

Finally in Chap. 10 we draw the conclusions of this thesis.

2
Quantum batteries

Quantum batteries (QBs) are quantum systems which ideally can be fast charged, which can store energy for a long times and finally deliver such energy as useful thermodynamic work. Such quantum devices have to accomplish quite different tasks and their performance have to be judge based on different figure of merit, such as the *charging time*, the *storage time* and the *extractable work*. In this Chapter we focus on the fast charging of a QB, which is strongly intertwined with entanglement production, and subsequently we study the *extractable work* that can be drawn from QB.

QBs have first been proposed by Alicki and Fannes [20] in 2013. In their description, such a quantum battery system is composed by N quantum cells. After this seminal work, a number of theoretical studies [21–23] put on a solid ground the fact that entanglement can be exploited to boost the performances of a battery subject to the laws of quantum mechanics. Indeed, Alicki and Fannes [20] suggested that "entangling unitary controls", i.e. unitary operations acting globally on the state of the N quantum cells, lead to better work extraction capabilities from a QB, when compared to unitary operations acting in parallel on each quantum cell separately. This conjecture has been proven incorrect in Ref. [21]. In this work, the authors show that the same work extraction can be achieved without relying on entangling operations, at the cost of additional operation. This suggested that the enhancing effect of entanglement should be rather related to the reduction of the charging time, rather than the amount of extractable work. As a matter of fact, a dynamical evolution of the battery state which travels through highly entangled states corresponds to a shortcut in the Hilbert space [22, 23].

While all these studies were based on quantum-information concepts, a first realistic model which realizes a collective power speedup has been studied in Ref. [24]. The proposed setup is composed by N two-levels systems charged by a single cavity mode, namely this proposal exploits the Dicke model [25] to realize a QB. Details on the Dicke model are introduced in Chap. 3, while the Dicke QB [24] is described in Chap. 4. In this Chapter we review all the fundamental theoretical concepts of QBs necessary to understand our contribution to the field [24, 26–28] presented in Chaps. 4,5,6,7.

This Chapter is organized as follows. In Sect. 2.1 we introduce the charging protocol and we present the figures of merit we use to quantify the performance of a QB. In Sect. 2.2 we review the connection between fast-charging, entanglement and shortcuts in the Hilbert

space, put forward by Refs.[22, 23]. In Sect. 2.3 we present a further figure of merit of interest for QBs: *ergotropy*, which quantifies the amount of useful work that can be extracted from a quantum system. We conclude in Sect. 2.4, with a discussion of possible solid-states implementations of QBs.

2.1 Charging protocol and figures of merit

In this Section we introduce a unitary charging protocol, sketched in Fig. 2.1, and a number of figures of merit which quantifies the quality of the charging. We consider as a battery an isolated quantum system, composed of N identical battery cells. The energy of the system is measured with respect to a free and local *battery* Hamiltonian,

$$\hat{\mathcal{H}}_0 = \sum_{i=1}^{N} \hat{h}_i \ . \tag{2.1}$$

At the initial time $t = 0$, the system is considered to be in its ground state, $|\mathrm{G}\rangle = |\mathrm{g}, \mathrm{g}, \ldots, \mathrm{g}\rangle$, where $|\mathrm{g}\rangle_i$ is the local ground state of $\hat{h}_i$ representing the completely discharged battery cell. We then inject energy into the system, by suddenly switching on a *charging* Hamiltonian $\hat{\mathcal{H}}_1$ (and switching off $\hat{\mathcal{H}}_0$) for a finite amount of time τ. Our aim is to inject as much energy as possible into the battery in the shortest possible *charging time* τ.

The full Hamiltonian of the model can thus be written as

$$\hat{\mathcal{H}}(t) = \hat{\mathcal{H}}_0 + \lambda(t)\big(\hat{\mathcal{H}}_1 - \hat{\mathcal{H}}_0\big) \ , \tag{2.2}$$

where $\lambda(t)$ is a dimensionless classical parameter that represents the external control we exert on the system, equal to 1 for $t \in [0, \tau]$ and zero elsewhere. For a cartoon, see Fig. 2.1. The *charging* Hamiltonian $\hat{\mathcal{H}}_1$ dictates the evolution of the system from $t = 0$ to $t = \tau$, when the charging process ends. During this time interval, the evolved state reads $|\psi(t)\rangle = \exp(-i\hat{\mathcal{H}}_1 t/\hbar)\,|\mathrm{G}\rangle$.

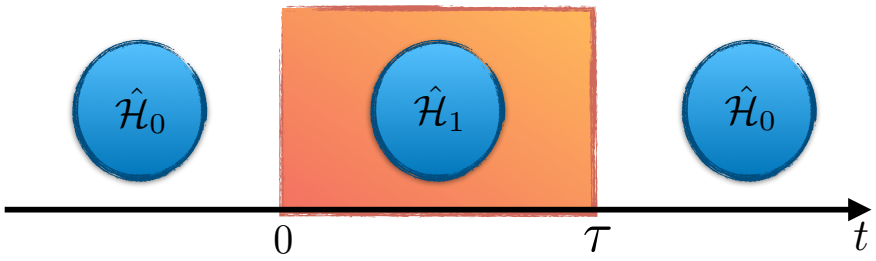

FIGURE 2.1: The time-dependent charging protocol that enables to charge the battery system, by the action of the charging Hamiltonian $\hat{\mathcal{H}}_1$ which is switched on during the time interval $0 < t < \tau$. Outside this interval the evolution of the system is ruled by the free local Hamiltonian $\hat{\mathcal{H}}_0$.

The energy injected into the battery can be expressed in terms of the difference between the final and the initial mean battery energy:

$$E^{(N)}(\tau) \equiv \langle\psi(\tau)|\hat{\mathcal{H}}_0|\psi(\tau)\rangle - \langle \mathrm{G}|\hat{\mathcal{H}}_0|\mathrm{G}\rangle \ . \tag{2.3}$$

We define the corresponding average charging power as

$$P^{(N)}(\tau) \equiv \frac{E^{(N)}(\tau)}{\tau} \ . \tag{2.4}$$

Upon optimization with respect to the charging time τ , we can extract from these functions a collection of *figures of merit* which quantify the quality of a given charging protocol from different perspectives. We define the maximum energy that can be injected into the battery,

$$\tilde{E}^{(N)} \equiv \max_{\tau}\Big[E^{(N)}(\tau)\Big] \equiv E^{(N)}(\tilde{\tau}) \ , \tag{2.5}$$

and the corresponding charging power $\tilde{P}^{(N)} \equiv P^{(N)}(\tilde{\tau})$. Similarly, we define the maximum average charging power

$$\bar{P}^{(N)} \equiv \max_{\tau}\Big[P^{(N)}(\tau)\Big] \equiv P^{(N)}(\bar{\tau}) \ . \tag{2.6}$$

We denote their corresponding optimal charging times as

$$\tilde{\tau} \equiv \min_{E^{(N)}(\tilde{\tau})=\tilde{E}^{(N)}}(\tau) \ , \qquad \bar{\tau} \equiv \min_{P^{(N)}(\bar{\tau})=\bar{P}^{(N)}}(\tau) \ . \tag{2.7}$$

Given these figures of merit we are ready to tackle a first explicit example of a charging protocol.

2.2 Entanglement induced speed-up in charging power

In this Section we present a charging protocol put forward in Refs. [22, 23]. This protocol relies on the use of a non-local charging Hamiltonian which drives the battery system trough a set of highly entangled states. As we will show, this protocol is superior to its local counterpart, where no entanglement between the quantum cells can be build. We start considering a collection of N two-level systems (TLs), described by the following battery Hamiltonian

$$\hat{\mathcal{H}}_0 = \sum_{i=1}^{N} \frac{\hbar\omega_0}{2}\hat{\sigma}_i^z \ , \tag{2.8}$$

where $\hbar\omega_0$ is the qubit energy, $\hat{\sigma}_i^z \equiv |\mathrm{e}\rangle_i \langle\mathrm{e}|_i - |\mathrm{g}\rangle_i \langle\mathrm{g}|_i$ and $|\mathrm{e}\rangle_i$ is the local excited state, corresponding to the fully charged battery cell. We consider two different charging protocols. On the one hand, each battery unit can be charged independently in a *parallel* fashion (denoted by the symbol $\|$) by the Hamiltonian

$$\hat{\mathcal{H}}_1^{\|} = \sum_{i=1}^{N} g_{\|}\hat{\sigma}_i^x \ , \tag{2.9}$$

where $g_{\|}$ sets the energy scale of this *parallel* charging Hamiltonian. On the other hand, all the battery units can be collectively manipulated in a *collective* fashion (denoted by the symbol $\sharp$). This collective charging is induced by

$$\hat{\mathcal{H}}_1^{\sharp} = g_{\sharp}\big(\,|\mathrm{G}\rangle\langle\mathrm{E}| + \mathrm{h.c.}\big) \ , \tag{2.10}$$

where $|\mathrm{E}\rangle = |\mathrm{e},\mathrm{e},\ldots,\mathrm{e}\rangle$ represents the fully charged battery state and the energy scale is set by the coupling $g_\sharp$. This is an highly non-local interaction which acts on all qubits simultaneously.

Considering the parallel protocol, the injected energy reads

$$E_\parallel^{(N)}(\tau) = N\hbar\omega_0 \sin^2\left(\frac{g_\parallel \tau}{\hbar}\right) . \tag{2.11}$$

We consider this quantity at the optimal time $\tilde{\tau}_\parallel$ such that the battery is fully charged, $\tilde{E}_\parallel^{(N)} = N\hbar\omega_0$. The optimal time reads $\tilde{\tau}_\parallel = \pi\hbar/(2g_\parallel)$. If the collective charging is considered, the injected energy has a similar dynamics

$$E_\sharp^{(N)}(\tau) = N\hbar\omega_0 \sin^2\left(\frac{g_\sharp \tau}{\hbar}\right) , \tag{2.12}$$

with the difference that the charging time scale is set by $g_\sharp$ instead of $g_\parallel$. The full charge $\tilde{E}_\sharp^{(N)} = N\hbar\omega_0$ is reached at the optimal time $\tilde{\tau}_\sharp = \pi\hbar/(2g_\sharp)$. In order to compare the two different protocols we introduce the *quantum advantage* as

$$\boxed{\Gamma \equiv \frac{\tilde{P}_\sharp^{(N)}}{\tilde{P}_\parallel^{(N)}} = \frac{\tilde{\tau}_\parallel}{\tilde{\tau}_\sharp} ,} \tag{2.13}$$

here "quantum" refers to an enhancement due to the entangling operations of the collective protocol.

From Eq.(2.11) and Eq.(2.12), the quantum advantage can be evaluated to be $\Gamma = g_\sharp/g_\parallel$. Hence, in order to compare the performance of the two different protocols we have to compare the two energy scales $g_\sharp$ and $g_\parallel$. Following Refs. [22, 23], in order to do a fair comparison we set to be equal, the norm of the parallel charging Hamiltonian $\|\hat{\mathcal{H}}_1^\parallel\|$ and the collective charging Hamiltonian $\|\hat{\mathcal{H}}_1^\sharp\|$, where $\|\hat{\mathcal{O}}\| = \mu_{\hat{\mathcal{O}}}^{\max} - \mu_{\hat{\mathcal{O}}}^{\min}$ defines the norm of the Hermitian operator $\hat{\mathcal{O}}$, $\mu_{\hat{\mathcal{O}}}^{\max}$ ($\mu_{\hat{\mathcal{O}}}^{\min}$) being its largest (smallest) eigenvalue.

We now diagonalize $\hat{\mathcal{H}}_1^\parallel$ and $\hat{\mathcal{H}}_1^\sharp$. Introducing the collective pseudo-spin $\hat{J}^x = \sum_{i=1}^N \hat{\sigma}_i^x/2$, the parallel Hamiltonian in Eq.(2.9) can be written as $\hat{\mathcal{H}}_1^\parallel = 2g_\parallel \hat{J}^x$. Eigenstates of such Hamiltonian are called Dicke state, which we denote as $|J,M\rangle_x$. We will discuss these states in details in Chap. 3. Here, it is sufficient to remind that $\hat{J}^x |J,M\rangle_x = M |J,M\rangle_x$, where $J = N/2, N/2-1,\ldots,0$ and $M = J, J-1,\ldots,-J$. [1] Hence, the spectrum of $\hat{\mathcal{H}}_1^\parallel$ is given by $g_\parallel M$ and its norm reads $\|\hat{\mathcal{H}}_1^\parallel\| = 2Ng_\parallel$. The norm of the collective charging Hamiltonian in Eq.(2.10) can be easily showed to be $\|\hat{\mathcal{H}}_1^\parallel\| = 2g_\sharp$, since $\hat{\mathcal{H}}_1^\parallel$ is a simple two-level Hamiltonian with eigenvalues $\pm g_\sharp$. The spectrum of $\hat{\mathcal{H}}_1^\parallel$ and $\hat{\mathcal{H}}_1^\sharp$ is sketched in Fig. 2.2.

Setting

$$\|\hat{\mathcal{H}}_1^\parallel\| = \|\hat{\mathcal{H}}_1^\sharp\| , \tag{2.14}$$

we obtain the following relation, $g_\sharp = Ng_\parallel$, which can be used to evaluate the quantum advantage,

$$\Gamma = N . \tag{2.15}$$

This equation shows that relying on a highly non-local charging Hamiltonian such as $\hat{\mathcal{H}}_1^\sharp$ greatly enhances the charging power in comparison with a local charging induced by $\hat{\mathcal{H}}_1^\parallel$.

[1] We suppose the number of quantum cells N to be even. A similar result applies even if an odd number is considered.

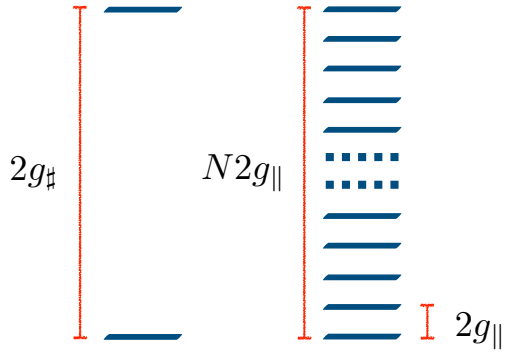

Figure 2.2: A pictorial representation of the spectra of $\hat{\mathcal{H}}_1^\sharp$ (left) and of $\hat{\mathcal{H}}_1^\parallel$ (right). Energy levels are rappresented by blu lines. The spectrum of $\hat{\mathcal{H}}_1^\sharp$ is given by $\pm g_\sharp$, while the spectrum of $\hat{\mathcal{H}}_1^\parallel$ reads $2Mg_\parallel$, where $M = N/2, N/2-1, \ldots, -N/2$. The mininum energy gap is $2g_\parallel$, while that bandwith is $2Ng_\parallel$.

Considering charging Hamiltonians with equal operator norms is not the unique procedure to evaluate the quantum advantage. Another possibility is to rely on the concept of quantum speed limits (QSLs). The QSL is the minimum time interval needed to evolve a quantum system between two orthogonal states (such as $|\mathrm{G}\rangle$ and $|\mathrm{E}\rangle$) under the action of a given Hamiltonian $\hat{\mathcal{H}}_1$ which generates the evolution. It can be expressed as

$$\tau^{\mathrm{QSL}} = \frac{\hbar\pi}{2}\frac{1}{\min\{\langle\hat{\mathcal{H}}_1\rangle, \langle\delta\hat{\mathcal{H}}_1\rangle\}}, \tag{2.16}$$

where $\langle\hat{\mathcal{H}}_1\rangle$ denotes the gap between the mean value and the ground-state energy of $\hat{\mathcal{H}}_1$, and $\langle\delta\hat{\mathcal{H}}_1\rangle$ is the square root of the variance of $\hat{\mathcal{H}}_1$. These quantum averages are evaluated on the initial state evaluated on the initial state $|\mathrm{G}\rangle$.

Considering the parallel charging, we can see by inspection that $\langle\hat{\mathcal{H}}_1^\parallel\rangle = Ng_\parallel$ and $\langle\delta\hat{\mathcal{H}}_1^\parallel\rangle = \sqrt{N}g_\parallel$. Hence, the QSL reads

$$\tau_\parallel^{\mathrm{QSL}} = \frac{\hbar\pi}{2g_\parallel\sqrt{N}}. \tag{2.17}$$

Comparing $\tau_\parallel^{\mathrm{QSL}}$ in Eq.(2.17) with the optimal charging time $\tilde{\tau}_\parallel = \hbar\pi/(2g_\parallel)$ we can see that the parallel protocol it is not optimal, in the sense that it does not evolve the ground state $|\mathrm{G}\rangle$ into the orthogonal excited state $|\mathrm{E}\rangle$ in the minimal time given by quantum mechanics, $\tau_\parallel^{\mathrm{QSL}}$. This is due to the fact that, before reaching the completely excited state, the system has to travel between a finite number of orthogonal states. While the QSL bound can be applied for each of these transitions, we should take into account that the system has to travel through many orthogonal states. Conversely, if the collective charging protocol is considered, $\langle\hat{\mathcal{H}}_1^\sharp\rangle = g_\sharp$ and $\langle\delta\hat{\mathcal{H}}_1^\sharp\rangle = g_\sharp$, and the QSL is given by

$$\tau_\sharp^{\mathrm{QSL}} = \frac{\hbar\pi}{2g_\sharp}. \tag{2.18}$$

Remarkably, in this case, the optimal charging time saturates the QSL, $\tau_\sharp^{\mathrm{QSL}} = \tilde{\tau}_\sharp = \hbar\pi/(2g_\sharp)$, meaning that the evolution follows the fastest path between $|\mathrm{G}\rangle$ and $|\mathrm{E}\rangle$. The

highly non-local Hamiltonian $\hat{\mathcal{H}}_1^{\sharp}$ drives the system trough a shortcut in the Hilbert space. The local charging Hamiltonian $\hat{\mathcal{H}}_1^{\parallel}$ cannot drive the system trough this shortcut, constituted by a set of highly entangled states.

Moreover, we can directly compare the collective and the charging protocol by setting the two QSLs to be equal,

$$\tau_{\parallel}^{\mathrm{QSL}} = \tau_{\sharp}^{\mathrm{QSL}} \ , \tag{2.19}$$

meaning that the two Hamiltonian induce two different evolutions with the same speed in the Hilbert space. With this procedure, the quantum advantage scales as the square-root of the number of battery units,

$$\Gamma = \sqrt{N} \ . \tag{2.20}$$

With both constrains in Eqs. (2.14,2.19), the power of the collective protocol outperforms the parallel one due to the effect of entangling operations.

Motivated by such result, we propose in Chap. 4 a many-body Dicke QB where collective effects can greatly enhance the charging process. However, as we show in Chap. 6 such collective effect does not rely on entanglement production and can be found in classical many-body models. A direct implementation of non-local charging of the collective protocol is shown in Chap. 7, where we employ the so-called SYK model [29, 30] to achieve a genuinely quantum advantage in the charging process.

2.3 Quantum work: Ergotropy

In this Section we introduce the maximum work that can be drawn from a quantum system according to quantum mechanics, i.e. *ergotropy*. Of course, the study of work extraction is closely related to the study of a QB: A good QB, should not only display fast charging/discharging, but also have the capability to fully deliver stored energy in order to perform useful work. The extractable work can be seen as another fundamental figure of merit, useful to quantify the performance of a QB.

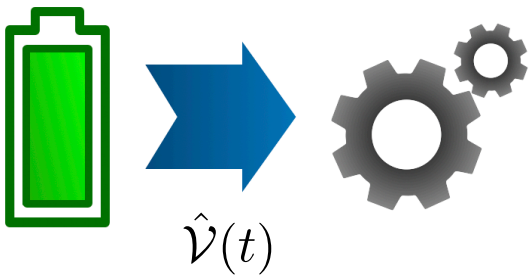

FIGURE 2.3: A sketch of quantum work. By driving the system with a time-dependent Hamiltonian $\hat{\mathcal{V}}(t)$ it is possible to extract an amount of energy W, that can be used to perform thermodynamical work.

Ergotropy [43] is the maximum work that can be extracted from a given state ρ via unitary transformation with respect to a reference Hamiltonian $\hat{\mathcal{H}}$. This definition is justified by the following scheme: we consider a time-dependent Hamiltonian $\hat{\mathcal{H}}(t)$ given by the sum of a fixed term $\hat{\mathcal{H}}$, and of a time-dependent cyclical potential$\hat{\mathcal{V}}(t)$ such that $\hat{\mathcal{V}}(t) = 0$ for $t \leq 0$ and

$t \geq T$. The idea is to extract work from the system through the time dependent potential. The dynamics up to time T is generated by the unitary operator

$$U = \hat{\mathcal{T}} \exp\Big\{ -i \int_0^T \frac{dt}{\hbar} \big[\hat{\mathcal{H}} + \hat{\mathcal{V}}(t)\big] \Big\} , \tag{2.21}$$

where $\hat{\mathcal{T}}$ is the time-ordering operator. The density matrix evolves accordingly, $\rho_U = U\rho U^\dagger$. The work extracted from the system is

$$W\big[\hat{\mathcal{H}}, \hat{\mathcal{V}}(t), \rho\big] = E(\rho) - E(\rho_U) , \tag{2.22}$$

where $E(\rho) = \mathrm{tr}[\rho\hat{\mathcal{H}}]$. Notice that W is a functional depending on the explicit form of the driving $\hat{\mathcal{V}}(t)$ at each intermediate time t. We can get rid of this explicit dependence considering the maximum amount of work that can be extracted among all possible cyclical potentials $\hat{\mathcal{V}}(t)$,

$$\boxed{\mathcal{E}\big(\rho, \hat{\mathcal{H}}\big) \equiv E(\rho) - \mathrm{min}_U \mathrm{tr}\big[\hat{\mathcal{H}} U\rho U^\dagger\big] \ .} \tag{2.23}$$

This is the so-called *ergotropy* (from the Greek words $\varepsilon\rho\gamma o\nu$: work; $\tau\rho o\pi\eta$: transformation), introduced by Ref. [43]. A closed expression for this quantity can be obtained in terms of the difference between the mean energy $E(\rho) = \mathrm{tr}[\hat{\mathcal{H}}\rho]$ of the state ρ and that of the passive counterpart $\tilde{\rho}$ of ρ [43–45], i.e. $E(\tilde{\rho}) = \mathrm{tr}[\hat{\mathcal{H}}\tilde{\rho}]$, i.e.

$$\mathcal{E}\big(\rho, \hat{\mathcal{H}}\big) = E(\rho) - E(\tilde{\rho}) \ . \tag{2.24}$$

A passive state $\tilde{\rho}$ is obtained from the corresponding density matrix ρ as follows. Consider $|\epsilon_n\rangle$ and $|r_n\rangle$ to be the eigenvectors of $\hat{\mathcal{H}}$ and ρ, respectively. We express $\hat{\mathcal{H}}$ and ρ in its own diagonal form, as follows

$$\rho = \ \sum_n r_n \, |r_n\rangle \langle r_n| \, , \qquad r_0 \geq r_1 \geq r_2 \geq \cdots \ , \tag{2.25}$$

$$\hat{\mathcal{H}} = \ \sum_n \epsilon_n \, |\epsilon_n\rangle \langle \epsilon_n| \ , \qquad \epsilon_0 \leq \epsilon_1 \leq \epsilon_2 \leq \cdots \ . \tag{2.26}$$

where a proper ordering of eigenvalues is considered. The passive state $\tilde{\rho}$ is build associating the descending eigenvalues of ρ with the eigenvectors of $\hat{\mathcal{H}}$, as follows

$$\tilde{\rho} = \sum_n r_n \, |\epsilon_n\rangle \langle \epsilon_n| \ . \tag{2.27}$$

Therefore $E(\tilde{\rho}) = \sum_n r_n \epsilon_n$. Notice that, if $\epsilon_0 = 0$ and the state ρ is pure, then $E(\tilde{\rho}) = 0$ and the ergotropy coincides with the mean energy of ρ, i.e. $\mathcal{E}(\rho, \hat{\mathcal{H}}) = E(\rho)$. On the contrary, if the state ρ is mixed, the extractable work is in general smaller than the mean energy, i.e. $\mathcal{E}(\rho, \hat{\mathcal{H}}) < E(\rho)$. If the whole-system wavefunction is considered to be pure, mixedness is due to quantum correlations established between the battery unit and the rest of the system. While entangling operations enable fast charging, entanglement can spoil the quality of energy stored in a quantum system, since it can create a gap between average energy and useful work that can be actually extracted, i.e. $E(\rho) - \mathcal{E}(\rho, \hat{\mathcal{H}})$. In Chap. 5 (and Ref.[26]) we investigate how correlations established between a QB and a quantum charger can limit work extraction.

Finally, it is worth noticing that all thermal states, $\rho_\beta = \exp(-\beta\hat{\mathcal{H}})/\mathrm{tr}\big[\exp(-\beta\hat{\mathcal{H}})\big]$, are passive states. This can be seen as a manifestation of the second law of thermodynamics: no work can be extracted by a single thermal bath with a given temperature.

In the following we analyze the ergotropy in to two simple examples [46]: a qubit (2.3.1) and a quantum harmonic oscillator (2.3.2).

2.3.1 Ergotropy of a qubit

Consider the case of a qubit with an Hamiltonian of the form $\hat{\mathcal{H}}_0 = \hbar\omega_0\big(\hat{\sigma}^z + \mathbb{I}\big)/2$ and a generic density matrix

$$\rho = \frac{1}{2}(\mathbb{I} + \sum_{i=1}^{3} r_i \hat{\sigma}^i) \ , \tag{2.28}$$

where $\mathbb{I}$ is the 2×2 identity and $\hat{\sigma}^i$ and r_i are the Pauli matrices and the i-th components of the Bloch vector, respectively. Simple algebraic manipulations yield [46]

$$\mathcal{E}\big(\rho, \hat{\mathcal{H}}_0\big) = \frac{\hbar\omega_0}{2}\left(r + r_z\right) \ , \tag{2.29}$$

with $r^2 = \sum_{i=1}^{3} r_i^2$. The gap between the energy and the extractable work, given by $E(\rho) - \mathcal{E}\big(\rho, \hat{\mathcal{H}}_0\big) = \hbar\omega_0\left(1 - r\right)/2$, is a monotonic function of the modulus of the Bloch vector r and it is zero for pure states ($r = 1$) and maximal for the completely mixed state ($r = 0$).

2.3.2 Ergotropy of a gaussian state

Consider a quantum harmonic oscillator with an Hamitonian given by $\hat{\mathcal{H}}_0 = \hbar\omega_0 \hat{a}^\dagger \hat{a}$. In this case, it is possible to express the ergotropy in a closed form for a restricted set of states, named Gaussian states. A Gaussian state ρ_{G} can be obtained from a thermal state $\rho_\beta = \exp(-\beta\hat{\mathcal{H}}_0)/\mathrm{tr}\big[\exp(-\beta\hat{\mathcal{H}}_0)\big]$, with a given inverse temperature β by using the following identity [47]:

$$\rho_{\mathrm{G}} = \hat{D}^\dagger(\alpha)\hat{S}^\dagger(\xi)\rho_\beta\hat{S}(\xi)\hat{D}(\alpha) \ , \tag{2.30}$$

where $\hat{D}(\alpha) = \exp(\alpha\hat{a}^\dagger - \alpha^*\hat{a})$ and $\hat{S}(\xi) = \exp[(\xi^*\hat{a}^2 - \xi\hat{a}^{\dagger\,2})/2]$ are displacement and squeezing operators, respectively. Here, α and ξ are the displacement and squeezing complex parameters [47] that identify the Gaussian state, together with the real parameter β. Since ρ_{G} is connected to the passive state ρ_β through the unitary $U = \hat{S}(\xi)\hat{D}(\alpha)$ the ergotropy reads [46],

$$\mathcal{E}\big(\rho_{\mathrm{G}}, \hat{\mathcal{H}}_0\big) = E(\rho_{\mathrm{G}}) - E(\rho_\beta) \ . \tag{2.31}$$

The energy of a bosonic thermal state can be expressed as a function of the Bose occupation factor $n_\beta = 1/(1 + e^{\beta\omega_0})$, $E(\rho_{\bar{\beta}}) \equiv \mathrm{tr}\big[\hat{\mathcal{H}}_0\rho_\beta\big] = \hbar\omega_0 n_\beta$. By noticing that n_β can be linked to the purity $\mathrm{tr}\big[\rho_\beta^2\big]$ by the identity $n_\beta = \big(1/\mathrm{tr}\big[\rho_\beta^2\big] - 1\big)/2$, and that $\mathrm{tr}\big[\rho_{\mathrm{G}}^2\big] = \mathrm{tr}\big[\rho_\beta^2\big]$ since purity is invariant under unitary transformation, we arrive to the expression:

$$\mathcal{E}\big(\rho_{\mathrm{G}}, \hat{\mathcal{H}}_0, \big) = E(\rho_{\mathrm{G}}) + \frac{\hbar\omega_0}{2}\Big(1 - \mathrm{tr}\big[\rho_{\mathrm{G}}^2\big]^{-1}\Big) \ . \tag{2.32}$$

The gap between the ergotropy and the energy is given by $E(\rho_{\mathrm{G}}) - \mathcal{E}\big(\rho_{\mathrm{G}}, \hat{\mathcal{H}}_0\big) = \big(\hbar\omega_0/2\big)$ $\big\{\mathrm{tr}\big[\rho_{\mathrm{G}}^2\big]^{-1} - 1\big\}$. The purity $\mathrm{tr}\big[\rho_{\mathrm{G}}^2\big]$ is bounded by one since $\mathrm{tr}\big[\rho_{\mathrm{G}}^2\big] \leq \mathrm{tr}\big[\rho_{\mathrm{G}}\big] = 1$ and this inequality is saturated only in the case of a pure state. The more a state is mixed, the smaller is the purity and the more energy cannot be extracted through unitary operations.

2.4 Solid-state implementation

We have seen that it is possible to exploit entangling operations to greatly enhance the charging power of a QB made of many cells. As summarized in Sect. 2.2 there exists a highly

non-local Hamiltonian which, by means of a global entangling operation, enables a superior performance in the average charging power as compared to parallel classical charging.

As noted in Ref. [24], however, such global entangling operations involve highly non-local interactions, which may be difficult to realize in practice. A major issue of this thesis is to bring the notion of QBs from the realm of quantum information theorems to that of microscopic theoretical models that can be simulated in laboratories using cold-atom, photonics, trapped-ion, and solid-state tecnologies. The key idea is to utilize ideas of cavity and circuit quantum electrodynamics to engineer non-local entangling interactions among the N quantum cells. In essence, by coupling all the qubits to the very same quantum energy source one realizes effective long-range interactions between all the elementary quantum units. This can be achieved relying on an ensemble of (artificial) atoms coupled to the same cavity, which mediates long-range interactions. Such system is described by the Dicke model. We will introduce such a model in the next Chapter, Chap. 3, deriving it from a microscopic model, and then propose a Dicke QB in Chap.4.

Moreover, the quantum advantage found in Sect. 2.2 relies on strong theoretical assumptions, namely the comparison between a parallel and collective charging is based on the concepts of speed limits and operator norms. Studying more concrete solid-state models is crucial to test whether or no such criteria are predictive when experimentally feasible couplings are considered.

We conclude by noticing that first seminal quantum-information works [20–23], and our solid-state proposal [24] were followed by a remarkable number of studies [26, 27, 46, 48–63], which further investigate both quantum-information theorems related to QBs and physical implementations.

3

Light-matter interactions: Superradiances

The Dicke model [25] consists of a collection of two-level systems (TLSs) cooperatively interacting with the same bosonic mode. This model plays a pivotal role in describing collective effects in cavity and circuit quantum electrodynamics (QED) [33, 36, 64, 65]. Dicke[25] used this model in 1954 to predict the collective emission of N excited atoms coherently coupled with the same dissipative mode. Remarkably, due to an interference effect, such emission is N times faster than independent atomic decay, a phenomena that has been dubbed "superradiance". This effect can be put in strong connection with the power QBs speed-up discussed in Chap. 2, where a similar collective effect is exploited to reduce the charging time. Starting from this analogy, in Chap. 4 we propose a high-power QB based on the Dicke model. Several further questions about such Dicke QB are answered in Chaps. 5,6.

Nowadays the Dicke model is still the subject of a great deal of interest, since only relatively recently experiments opened the possibility to access to new regimes of light-matter interaction. Dicke had in mind a situation where atoms and cavity are extremely lossy when he proposed his model. In 1983, the Haroche group [32], sending beams of Rydberg atoms trough a high-Q microwave cavity, realized a light-matter system in the strong coupling regime, where the light-matter coupling exceeds the losses. This experiment enabled the possibility to study atoms and photons as isolated quantum objects, getting rid of noise and losses that usually cover quantum features. This outstanding breakthrough was worth the award of the Nobel prize to Serge Haroche in 2012 [34]. Recently, experiments [66–68] managed to achieve the so-called ultra-strong coupling, a regime where the light-matter interaction is the dominant parameter, exceeding even the bare frequencies of the system. This opens a path to investigate radically new phenomena where atoms and photons strongly interact and customary perturbation theory is not predictive. As a notable example of these new aspects of strong light-matter interaction, the Dicke model displays a quantum phase transition driven by the coupling. When the interaction exceeds a critical value, such model enters in a new "superradiant" phase characterized by an equilibrium macroscopic number of photons. To avoid confusion with the superradiant emission originally proposed by Dicke [25], we dubbed this phase "photon condensation". As a caveat, a careful microscopic derivation leads to the addition of the so-called diamagnetic term to the standard Dicke model. The presence of this term forbids the occurrence of the phase transition. Many attempts [40, 69–72] were recently

done to overcome such "no-go" theorem. Whether or not photon condensation can be realized in practice is an open and debated question [73–75]. Along this line of research, we generalize the no-go theorem to arbitrary electronic systems in Chap. 8, while in Chap. 9 we provide a possible path to realize photon condensation, circumventing the theorem.

This Chapter is organized as follows. In Sect. 3.1 we derive the Dicke model from a microscopic model. The superradiant emission is discussed in Sect. 3.2 and we conclude with Sect. 3.3 discussing photon condensation and the related no-go theorem.

3.1 A microscopic derivation of the Dicke model

In this Section, we derive the Dicke model from a microscopic description of light and matter. In Subsect.3.1.1, we quantize the electromagnetic field showing how the vector potential can be written as a sum of independent quantum harmonic oscillators. In Subsect.3.1.2, we derive an effective Hamiltonian that describes an ensemble of atoms as a collection of two-level systems (TLS). Finally, light and matter are coupled through the *minimal coupling* and the Dicke model is obtained projecting the light-matter interaction onto the TLS basis in Subsect.3.1.3.

3.1.1 Light as oscillators

In this Subsection we will show that electromagnetic waves can be expanded as a sum of independent harmonic oscillators. Here we follow Ref.[76]. Electromagnetic waves are solutions of classical Maxwell equation in absence of any source [76]:

$$\boldsymbol{\nabla}\cdot\boldsymbol{E}(\boldsymbol{r},t) = 0\,, \tag{3.1}$$

$$\boldsymbol{\nabla}\cdot\boldsymbol{B}(\boldsymbol{r},t) = 0\,, \tag{3.2}$$

$$\boldsymbol{\nabla}\times\boldsymbol{E}(\boldsymbol{r},t) = -\frac{1}{c}\frac{\partial\boldsymbol{B}(\boldsymbol{r},t)}{\partial t}\,, \tag{3.3}$$

$$\boldsymbol{\nabla}\times\boldsymbol{B}(\boldsymbol{r},t) = \frac{1}{c}\frac{\partial\boldsymbol{E}(\boldsymbol{r},t)}{\partial t}\,, \tag{3.4}$$

where $\boldsymbol{E}(\boldsymbol{r},t)$ ($\boldsymbol{B}(\boldsymbol{r},t)$) is the electric (magnetic) field and c is the speed of light. A convenient choice of gauge in quantum optics is the Coulomb gauge. In this gauge, both $\boldsymbol{E}(\boldsymbol{r},t)$ and $\boldsymbol{B}(\boldsymbol{r},t)$ can be expressed as a functions of the vector potential $\boldsymbol{A}(\boldsymbol{r},t)$:

$$\boldsymbol{E}(\boldsymbol{r},t) = -\frac{1}{c}\frac{\partial\boldsymbol{A}(\boldsymbol{r},t)}{\partial t}\,, \tag{3.5}$$

$$\boldsymbol{B}(\boldsymbol{r},t) = \boldsymbol{\nabla}\times\boldsymbol{A}(\boldsymbol{r},t)\,, \tag{3.6}$$

with the gauge condition:

$$\boldsymbol{\nabla}\cdot\boldsymbol{A}(\boldsymbol{r},t) = 0\,. \tag{3.7}$$

Combining Eq. (3.1) with Eq. (3.5) it is possible to prove that the vector potential fulfills the following wave equation:

$$\nabla^2\boldsymbol{A}(\boldsymbol{r},t) = \frac{1}{c^2}\frac{\partial^2\boldsymbol{A}(\boldsymbol{r},t)}{\partial t^2}\,. \tag{3.8}$$

Eq. (3.8) is a linear differential equation, its solutions can be expanded in normal modes. The functional form of such normal modes depends, in general, on boundary conditions.

Hence, we study the specific case of a cubical volume of side L, $V = L^3$. While sending $V \to \infty$ we will recover electrodynamics in free space, keeping V finite is the appropriate description of cavity electrodynamics, where light is confined inside a reflective cavity. A generic solution of Eq. (3.8) reads[76]:

$$\boldsymbol{A}(\boldsymbol{r},t) \;=\; \sum_{\boldsymbol{q},\sigma} A_{\boldsymbol{q}}\left[\boldsymbol{u}_{\boldsymbol{q},\sigma}(\boldsymbol{r})a_{\boldsymbol{q},\sigma}e^{-i\omega_{\boldsymbol{q}}t} + \text{c.c.}\right] , \tag{3.9}$$

where $A_{\boldsymbol{q}} = \sqrt{2\pi\hbar c^2/(V\omega_{\boldsymbol{q}})}$, $\omega_{\boldsymbol{q}} = cq$, $a_{\boldsymbol{q},\sigma}$ are expansion coefficients and $\boldsymbol{u}_{\boldsymbol{q},\sigma}(\boldsymbol{r})$ are mode functions. In the chosen cubic geometry, $\boldsymbol{u}_{\boldsymbol{q},\sigma}(\boldsymbol{r})$ reads:

$$\boldsymbol{u}_{\boldsymbol{q},\sigma}(\boldsymbol{r}) \;=\; \boldsymbol{u}_{\boldsymbol{q},\sigma}e^{i\boldsymbol{q}\cdot\boldsymbol{r}} , \tag{3.10}$$

where $\boldsymbol{q} = (2\pi n_x/L, 2\pi n_y/L, 2\pi n_z/L)$ with (n_x, n_y, n_z) relative integers, $\sigma = 1, 2$ is the polarization index, $\boldsymbol{u}_{\boldsymbol{q},\sigma}$ is the linear polarization vector. Normalization factors have been chosen such that the amplitudes $a_{\boldsymbol{q},\sigma}$ and $a^*_{\boldsymbol{q},\sigma}$ are dimensionless. In classical electrodynamics, $a_{\boldsymbol{q},\sigma}$ and $a^*_{\boldsymbol{q},\sigma}$ are complex amplitudes. The quantization of the electromagnetic field can be done by promoting these amplitudes to be operators, $a_{\boldsymbol{q},\sigma} \to \hat{a}_{\boldsymbol{q},\sigma}$ and $a^*_{\boldsymbol{q},\sigma} \to \hat{a}^\dagger_{\boldsymbol{q},\sigma}$, fulfilling suitable bosonic commutation relations:

$$\left[\hat{a}_{\boldsymbol{q},\sigma}, \hat{a}^\dagger_{\boldsymbol{q}',\sigma'}\right] \;=\; \delta_{\boldsymbol{q},\boldsymbol{q}'}\delta_{\sigma,\sigma'} , \tag{3.11}$$

$$\left[\hat{a}_{\boldsymbol{q},\sigma}, \hat{a}_{\boldsymbol{q}',\sigma'}\right] \;=\; \left[\hat{a}^\dagger_{\boldsymbol{q},\sigma}, \hat{a}^\dagger_{\boldsymbol{q}',\sigma'}\right] = 0 . \tag{3.12}$$

In general, the quantum electromagnetic field can be described by a collection of independent harmonic oscillators obeying the above commutation relations. Such ladder operator, $\hat{a}^\dagger_{\boldsymbol{q},\sigma}$ can be interpreted as an operator which creates a photon with momentum $\boldsymbol{q}$ and polarization σ.

The Hamiltonian of the electromagnetic field is given by:

$$\hat{\mathcal{H}}_{\text{ph}} = \frac{1}{8\pi}\int d\boldsymbol{r}\left[\hat{\boldsymbol{E}}^2(\boldsymbol{r}) + \hat{\boldsymbol{B}}^2(\boldsymbol{r})\right] . \tag{3.13}$$

The Hamiltonian in Eq. (3.13) can be expressed in term of creation and annihilation operators as follows

$$\hat{\mathcal{H}}_{\text{ph}} = \sum_{\boldsymbol{q},\sigma}\hbar\omega_{\boldsymbol{q}}\left[\hat{a}^\dagger_{\boldsymbol{q},\sigma}\hat{a}_{\boldsymbol{q},\sigma} + \frac{1}{2}\right] . \tag{3.14}$$

In this expression, the Hamiltonian is the sum of photon number $\hat{a}^\dagger_{\boldsymbol{q},\sigma}\hat{a}_{\boldsymbol{q},\sigma}$ multiplied by the correspondent photonic energy $\hbar\omega_{\boldsymbol{q}}$. The additional term $\hbar\omega_{\boldsymbol{q}}/2$ represents the zero-point-energy of each mode. Finally, in the Schrodinger picture the quantized version of the vector potential in Eq.(3.9) reads [76]:

$$\hat{\boldsymbol{A}}(\boldsymbol{r}) = \sum_{\boldsymbol{q},\sigma} A_{\boldsymbol{q}}\boldsymbol{u}_{\boldsymbol{q},\sigma}(\hat{a}_{\boldsymbol{q},\sigma}e^{i\boldsymbol{q}\cdot\boldsymbol{r}} + \hat{a}^\dagger_{\boldsymbol{q},\sigma}e^{-i\boldsymbol{q}\cdot\boldsymbol{r}}) . \tag{3.15}$$

This is the first fundamental ingredient of the Dicke model, photons can be described as a collection of quantum harmonic oscillators.

3.1.2 Atoms as two-level systems

In this Subsection we will show that a collection of independent atoms can be treated, under suitable assumptions, as a collection of independent two-level systems (TLSs). Here we follow Refs. [40, 77]. We consider an atomic gas composed by N identical atoms. We focus on the electronic degree of freedom, disregarding ionic and center-of-mass motion. Such system, composed by N electrons (each one bounded to a different atom) is described by a non-relativistic Hamiltonian of the form

$$\hat{\mathcal{H}} = \sum_{i=1}^{N} \hat{h}_i \ , \tag{3.16}$$

$$\hat{h}_i = \frac{\hat{\boldsymbol{p}}_i^2}{2m} + V(\hat{\boldsymbol{r}}_i) \ . \tag{3.17}$$

Here, m is the electron mass, $\hat{\boldsymbol{p}}_i, \hat{\boldsymbol{r}}_i$ are momentum and position of the i-th electron and $V(\boldsymbol{r})$ is the generic atomic potential dependent on the position coordinate. We assume that each electron is well localized on a different atom. Atoms are supposed to be well separated and thus we can neglect Coulomb repulsion between electrons.

We now focus on the Hamiltonian of the i-th electron, $\hat{h}_i$. We denote the ground state (first excited state) as $|\mathrm{g}\rangle_i$ ($|\mathrm{e}\rangle_i$) and as $\hbar\omega_{\mathrm{eg}}$ the energy gap between these two states. If we are interested only in phenomena occurring at an energy scale ϵ nearly resonant with the energy gap $\hbar\omega_{\mathrm{eg}}$ and we further assume that two lowest energy levels are well separated by the higher energy levels, we can truncate the Hibert space of each electron, by considering as local basis only the two lowest energy levels. In this case, we can consider each electron as a TLS. We define $\hat{\sigma}_i^z$ such that $\hat{\sigma}_i^z |\mathrm{g}\rangle_i = -|\mathrm{g}\rangle_i$ and $\hat{\sigma}_i^z |\mathrm{e}\rangle_i = |\mathrm{e}\rangle_i$. Other Pauli matrices $(\hat{\sigma}_i^+, \hat{\sigma}_i^-)$ are defined accordingly. The Hamiltonian in Eq. (3.16) projected on the two lowest energy levels reads

$$\hat{\mathcal{H}}_{\mathrm{TLS}} = \sum_{i=1}^{N} \frac{\hbar\omega_{\mathrm{eg}}}{2} \hat{\sigma}_i^z \ . \tag{3.18}$$

This is the second fundamental ingredient of the Dicke model [25, 40, 77], atoms can be described as a collection of identical TLSs. As an important remark, such Hilbert space truncation is often critical and can be a source of many mistakes. For example, it is known [75, 78] that a Hamiltonian obtained by Hilbert space truncation can violate the gauge principle. For future reference we define collective atomic operators as:

$$\hat{J}^z = \sum_{i=1}^{N} \frac{\hat{\sigma}_i^z}{2} \ , \tag{3.19}$$

$$\hat{J}^{\pm} = \sum_{i=1}^{N} \hat{\sigma}_i^{\pm} \ . \tag{3.20}$$

It is worth notice that these operators fulfill the algebra of the angular momentum [84]. Other components of this pseudo-spin $\hat{J}^x, \hat{J}^y$ and its magnitude $\hat{\boldsymbol{J}}^2$ are defined accordingly. In the following, it will be useful to consider the basis formed by the so-called Dicke states $|J, M\rangle$, which are the eigenvectors of the operators $\hat{\boldsymbol{J}}^2$ and $\hat{J}^z$, such that $J(J+1)$ is the eigenvalue of $\hat{\boldsymbol{J}}^2$ and M denotes the eigenvalue of $\hat{J}^z$. By basic rules of angular momentum composition [84], it is possible to show that the maximum value of J is $N/2$. M assumes the

possible values $M = J, J-1, ..., -J$. For sake of simplicity, in this Section we assume the number of TLSs N to be even. Similar considerations hold for odd numbers.

In this basis, the Hamiltonian in Eq. (3.18) reads:

$$\hat{\mathcal{H}}_{\rm TLS} = \hbar\omega_{\rm eg}\hat{J}^z \ . \tag{3.21}$$

Important features can be already observed in this simple Hamiltonian. Firstly, Dicke states $|J, M\rangle$ are eigenvectors of Eq. (3.21) with eigenenergies $\epsilon_M \equiv \hbar\omega_{\rm eg}M/2$. The ground state is therefore the non-degenerate state $|N/2, -N/2\rangle$ which has energy $-\hbar\omega_{\rm eg}N/2$. Secondly, each level $\hbar\omega_{\rm eg}M/2$ is $\binom{N}{M}$ times degenerate, since the same M can correspond to different values of J. Such degeneracy takes into account the fact that in total there are 2^N possible states, as we can easily verify from simple combinatorial arguments. The full spectrum of $\hat{\mathcal{H}}_{\rm TLS}$ is sketched in Fig. 3.1.

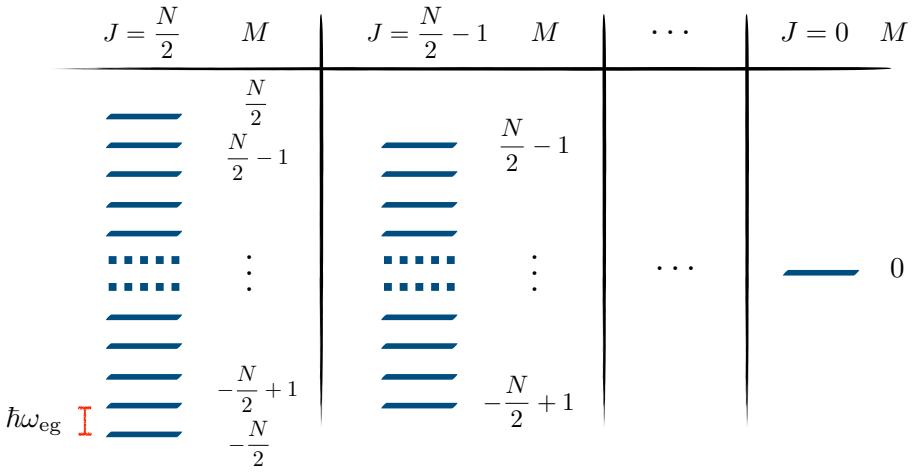

FIGURE 3.1: A sketch of the full spectrum of $\hat{\mathcal{H}}_{\rm TLS}$. Different columns correspond to different sectors of the Hilbert space with different J, with $J \leq N/2$. Once the quantum number J (the column) is fixed, M varies accordingly assuming the values $M = J, J-1, \ldots, -J$, corresponding to different rows. The value of M determines the energy according to the relation, $\epsilon_M \equiv \hbar\omega_{\rm eg}M/2$.

Let us analyze in detail the case of two atoms. The pseudo-spin basis $|J, M\rangle$ can be expressed in terms of the local basis as follows: $|1,1\rangle = |{\rm e}\rangle_1 |{\rm e}\rangle_2$; $|1,0\rangle = \big(|{\rm g}\rangle_1 |{\rm e}\rangle_2 + |{\rm e}\rangle_1 |{\rm g}\rangle_2\big)/\sqrt{2}$; $|1,-1\rangle = |{\rm g}\rangle_1 |{\rm g}\rangle_2$; $|0,0\rangle = \big(|{\rm g}\rangle_1 |{\rm e}\rangle_2 - |{\rm e}\rangle_1 |{\rm g}\rangle_2\big)/\sqrt{2}$.

3.1.3 The Dicke model

In this Subsection we finally derive the Dicke model by coupling the atoms, described by $\hat{\mathcal{H}}_{\rm TLS}$ (Eq.(3.18), with photons [40]. Hence, we begin by discussing light-matter coupling.

In the Coulomb gauge, the light-matter interaction is correctly obtained trough the *minimal coupling*, i.e. the substitution $\hat{\boldsymbol{p}}_i \to \hat{\boldsymbol{p}}_i + e\hat{\boldsymbol{A}}(\hat{\boldsymbol{r}}_i)/c$, where $-e < 0$ is the electron charge [79–82]. The full Hamiltonian is therefore given by

$$\hat{\mathcal{H}}_{\boldsymbol{A}} = \hat{\mathcal{H}} + \hat{\mathcal{H}}_{\rm ph} + \sum_{i=1}^{N} \frac{e}{mc}\hat{\boldsymbol{A}}(\boldsymbol{r}_i)\cdot\hat{\boldsymbol{p}}_i + \sum_{i=1}^{N}\frac{e^2}{2mc^2}\hat{\boldsymbol{A}}^2(\boldsymbol{r}_i) \ , \tag{3.22}$$

where $\hat{\boldsymbol{A}}^2(\boldsymbol{r}_i)$ is the vector potential defined in Eq. (3.15). The third and fourth terms in Eq. (3.22) are often referred to respectively as the paramagnetic and diamagnetic contributions to the light-matter coupling Hamiltonian. Let us assume that only a single mode $\hat{a}$, whose frequency $\omega_{\rm c}$ is resonant with that of TLSs $\omega_{\rm c} \simeq \omega_{\rm eg}$, is relevant. All other off-resonant modes are neglected. Furthermore, we neglect the spatial dependence of the vector potential, taking the limit $\boldsymbol{q} \to 0$ to begin with, [1] i.e. $\hat{\boldsymbol{A}} = A_0 \boldsymbol{u}(\hat{a}+\hat{a}^\dagger)$, where we have renamed the polarization as $\boldsymbol{u}$, $A_0 = \sqrt{2\pi\hbar c^2/(V\omega_{\rm c})}$, V is the volume of the cavity, and the single photon Hamiltonian reads $\hat{\mathcal{H}}_{1-\rm ph} = \hbar\omega_{\rm c}\hat{a}^\dagger\hat{a}$. The full Hamiltonian reads

$$\hat{\mathcal{H}}_{\boldsymbol{A}_0} \;=\; \hat{\mathcal{H}} + \hbar\omega_{\rm c}\hat{a}^\dagger\hat{a} + \sum_{i=1}^{N}\frac{e}{mc}\hat{\boldsymbol{p}}_i\cdot\boldsymbol{A}_0(\hat{a}+\hat{a}^\dagger) + \sum_{i=1}^{N}\frac{e^2A_0^2}{2mc^2}(\hat{a}+\hat{a}^\dagger)^2 \;, \tag{3.23}$$

where $\boldsymbol{A}_0 \equiv A_0\boldsymbol{u}$. For future reference we define $\Delta \equiv Ne^2A_0^2/(2mc^2)$. As in the previous Subsection 3.1.2, we project on the local basis consisting of the two lowest energy levels, $|{\rm g}\rangle_i$ and $|{\rm e}\rangle_i$. This approximation is well justified only if we assume that $\hbar\omega_{\rm eg}$ is the only energy-transition in resonance with a cavity mode. By using the fundamental commutation relation $i\hbar\hat{\boldsymbol{p}}_i/m = [\hat{\boldsymbol{r}}_i, \hat{\mathcal{H}}]$ we get a Hopfield-like [83] model:

$$\hat{\mathcal{H}}_{\rm Hopf} = \hbar\omega_{\rm eg}\hat{J}^z + \hbar\omega_{\rm c}\hat{a}^\dagger\hat{a} + \Big[g\hat{J}^+(\hat{a}+\hat{a}^\dagger) + {\rm h.c.}\Big] + \Delta(\hat{a}+\hat{a}^\dagger)^2 \;, \tag{3.24}$$

where $g \equiv ie\omega_{\rm eg}\langle{\rm e}|\hat{\boldsymbol{r}}\cdot\boldsymbol{A}_0|{\rm g}\rangle/c$. Notice that we have dropped the index i, since all atoms are considered to be identical. On top of all the approximations discussed in the present Section, in order to get the Dicke model, we have to artificially neglect the diamagnetic term (i.e. setting $\Delta = 0$), obtaining

$$\boxed{\hat{\mathcal{H}}_{\rm Dicke} = \hbar\omega_{\rm eg}\hat{J}^z + \hbar\omega_{\rm c}\hat{a}^\dagger\hat{a} + \Big[g\hat{J}^+(\hat{a}+\hat{a}^\dagger) + {\rm h.c.}\Big] \;.} \tag{3.25}$$

The Dicke model [25] describes N TLSs coupled to a single spatially-uniform cavity mode (for a cartoon, see Fig. 3.2). Dicke introduced it in order to describe the coherent spontaneous radiation, known as superradiance, that occurs in a ensemble of atoms cooperatively coupled with a privileged radiation mode. The Dicke model also displays a quantum phase transition, known as superradiant phase-transition. We will discuss the main properties of these "superradiances" in the next two Sections, Sect. 3.2 and Sect. 3.3.

Few comments are in order. Following a microscopic derivation, we obtain an Hopfield-like model in Eq.(3.24) rather then the Dicke model in Eq.(3.25). Afterwards, we obtained the Dicke model from the Hopfield-like Hamiltonian artificially neglecting the diamagnetic term $\Delta(\hat{a}+\hat{a}^\dagger)^2$. We show here that the coupling strength g and Δ are not independent.

Both these terms are obtained though *minimal coupling* and they have to fulfill a precise relation, known as Thomas-Reiche-Kuhn (TRK) sum rule [84], in order to preserve gauge invariance. We explicitly derive and comment this relation. For future reference, we denote by $|k\rangle$ and ϵ_k the eigenstates and eigenvalues of $\hat{h}$ [85, 86] in Eq.(3.16), with $|{\rm g}\rangle$ and $|{\rm e}\rangle$ being the first two lowest energy levels.

[1] This approximation is well justified in standard atomic setup, where the characteristic size ℓ of the electronic wavefunction is of the order of the Bohr radius $\ell \sim a_{\rm B} = 5\ 10^{-2}nm$, while the characteristic energy gap is of the order of the electronvolt $\hbar\omega_{\rm eg} \sim 1eV$. Assuming the photon energy $\hbar\omega_{\boldsymbol{q}}$ to be in resonance with this transition, we obtain a photon wavelength $\lambda = 2\pi/q \simeq 10^2nm$. Hence, the limit $\lambda/\ell \gg 1$ (or, equivalently, $\boldsymbol{q} \to 0$) is well satisfied.

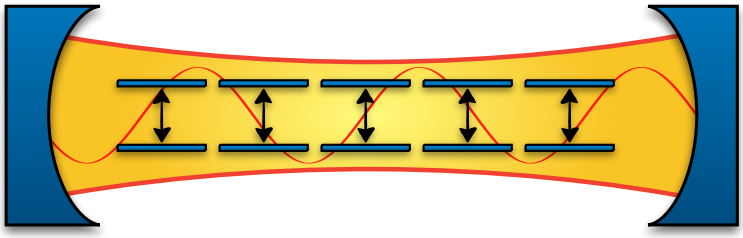

Figure 3.2: A skecth of the Dicke model. A collection of TLSs (modelling an atomic ensamble) are inside an electromagnetic cavity.

We start by noticing that

$$\frac{|g|^2}{\hbar\omega_{\rm eg}} = \frac{e^2}{\hbar c^2}\omega_{\rm eg}|\left\langle {\rm e}|\hat{\boldsymbol{r}}\cdot\boldsymbol{A}_0|{\rm g}\right\rangle|^2 \tag{3.26}$$

$$\leq \frac{e^2}{\hbar^2 c^2}\sum_{k\neq {\rm g}}(\epsilon_k-\epsilon_0)|\left\langle k|\hat{\boldsymbol{r}}\cdot\boldsymbol{A}_0|{\rm g}\right\rangle|^2 . \tag{3.27}$$

Exploiting the identity [40],

$$\Delta = \frac{e^2}{\hbar^2 c^2}\sum_{k\neq {\rm g}}(\epsilon_k-\epsilon_0)|\left\langle k|\hat{\boldsymbol{r}}\cdot\boldsymbol{A}_0|{\rm g}\right\rangle|^2 , \tag{3.28}$$

we get the TRK sum-rule [84]

$$\frac{N|g|^2}{\hbar\omega_{\rm eg}} \leq \Delta . \tag{3.29}$$

Eq. (3.29) is a manifestation of the TRK sum rule [84] which expresses the fact that the paramagnetic and diamagnetic contributions to the physical current-current response function cancel out in the uniform static limit, namely when the electromagnetic field is a purely gauge field. As we can see from Eq. (3.29), requiring Δ to be strictly zero implies that the TLSs are totally decoupled from photons, i.e. $g = 0$. Since Δ scales like g^2, we can approximately neglect the diamagnetic term in the weak coupling regime ($g \ll \{\hbar\omega_{\rm c}, \hbar\omega_{\rm eg}\}$). Conversely, in the strong coupling regime ($g \sim \{\hbar\omega_{\rm c}, \hbar\omega_{\rm eg}\}$) the paramagnetic and the diamagnetic terms have the same importance. In this case, neglecting Δ can lead to gross mistakes. The inequality in Eq. (3.29) and the above considerations will be crucial in order to discuss the superradiant phase transition and its impossibility when gauge invariance is properly taken into account (see Sect. 3.3 below).

3.2 Superradiant emission

The term superradiance was coined in 1954 by Dicke [25]. It is a collective phenomenon [87, 88] that occurs when an ensemble of N excited atoms interact coherently with a common

electromagnetic mode. If each atom emits independently, the total intensity of the emitted light I would be the incoherent sum of each atomic contribution, i.e. $I \sim N$. This effect goes under the name of fluorescence. Conversely, if the atoms are coherently coupled with the same mode, a collective effect arises. The collective emission is started when an excited electronic state decays to the ground state by emitting a photon. This photon, which does not immediately escape the cavity, populates the electromagnetic mode, where it can interact with all atoms and stimulates further emissions. This induces a chain reaction where all atomic excitations are fast released in a bright flash. In this case, the total intensity scales quadratically in the number of atoms, i.e. $I \sim N^2$, due to this constructive interference. This enhancement by a factor N in comparison with ordinary fluorescence has led to the name "superradiance".

Let us discuss in detail this effect. We consider the Dicke model in Eq. (3.25) in presence of strong dissipation due to imperfect leaky cavity mirrors. The cavity losses are parametrized by the decay rate κ. We set ourselves in the so-called weak coupling regime, i.e. $\kappa \gg g$ meaning that the probability that an atom adsorbs back an emitted photon is negligible. At initial time, all the N atoms are considered to be in its own excited state, namely

$$|\psi(0)\rangle = \underbrace{|\mathrm{e},\mathrm{e},\ldots,\mathrm{e}\rangle}_{N} \ . \tag{3.30}$$

Let us first consider the case where all atoms interact independently with the electromagnetic modes. Physically this means that the mean distance between the atoms r is large compared to the photon wavelength λ, $r \gg \lambda$. Tracing out the cavity and employing the Born-Markov approximation [87] we obtain a Lindblad master equation which describes the dynamics of the atomic ensemble,

$$\frac{d}{dt}\rho_N(t) = \sum_i \frac{\gamma}{\hbar}\Big[\hat{\sigma}_i^+ \rho_N(t)\hat{\sigma}_i^- - \frac{1}{2}\big\{\hat{\sigma}_i^+\hat{\sigma}_i^-, \rho_N(t)\big\}\Big] \ , \tag{3.31}$$

where $\rho_N(t)$ is the atoms density matrix, $\{.,.\}$ is the anticommutator and the decay rate γ is given by $\gamma = g^2/\kappa$. In writing Eq. (3.31) we are considering the cavity to be in contact with a bosonic bath at zero temperature. This means that we are neglecting thermal photons that might come from outside the cavity and excite the atoms. Eq. (3.31) induces an independent dynamics for each atom. Let us denote the probability to find the atoms in its own excited state $|\mathrm{e}\rangle$ at time t as $p(t)$. From Eq. (3.31) we get as a solution $p(t) = p(0)e^{-\frac{\gamma}{\hbar}t}$, where $p(0)$ is the initial probability to find the atom in its excited state. Due to the initial condition, Eq. (3.30), $p(0) = 1$. As expected, the decay time scale $\tau_\parallel$ is given by $\tau_\parallel = \hbar/\gamma$. We have used the same notation of Sect. 2.2 for the parallel time, since similarly to the parallel protocol described there, all atoms are independently coupled with a different electromagnetic mode.

We now consider the case where all atoms interact coherently with the same mode, i.e. $r \ll \lambda$. In this case, the evolution of the atomic density matrix is dictated by the following master equation [87, 88]

$$\frac{d}{dt}\rho_N(t) = \frac{\gamma}{\hbar}\Big[\hat{J}^+ \rho_N(t)\hat{J}^- - \frac{1}{2}\big\{\hat{J}^+\hat{J}^-, \rho_N(t)\big\}\Big] \ . \tag{3.32}$$

Unfortunately, there is not any known analytic solution to Eq. (3.32). Anyway, it is possible to find a mean field solution [88], factorizing all operators products (e.g. $\langle \hat{J}^+\hat{J}^-\rangle \to \langle \hat{J}^+\rangle \langle \hat{J}^-\rangle$). We parametrize the expectation values of $\hat{J}^z$ and $\hat{J}^\pm$ in terms of the polar coordinates θ, ϕ, namely $\langle \hat{J}^z\rangle = J\cos(\theta)$ and $\langle \hat{J}^\pm\rangle = J\sin(\theta)e^{\pm i\phi}$. Once the mean field

approximation is taken, the pseudo-spin behaves classicaly, obeying the equations of motion of an over-dumped pendulum [88],

$$\dot{\theta} = \frac{N\gamma}{\hbar}\sin(\theta)\ , \tag{3.33}$$

$$\dot{\phi} = 0\ . \tag{3.34}$$

The probability to find a single atom in its excited state p can be expressed as a function of the polar coordinates, $p = \cos(\theta)$. The implicit solution of Eq. (3.33) is given by

$$\boxed{t = \frac{\hbar}{2N\gamma}\log\left\{\frac{\big[1-p(t)\big]\ p(0)}{\big[1-p(0)\big]\ p(t)}\right\}\ ,} \tag{3.35}$$

while $\phi(t) = \phi(0)$. This equation reveals that decay time $\tau_\sharp$ scales with $1/N$, $\tau_\sharp \sim \hbar/(N\gamma)$. Again, we used the same notation of Sect. 2.2 for the collective time to underline a connection with the power advantage defined there in Eq. (2.13).

It is possible to invert Eq. (3.32) to obtain the explicit form of $p(t)$,

$$p(t) = \left\{\frac{p(0)\big[1-\tanh(\frac{N\gamma t}{\hbar})\big]}{1+\tanh(\frac{N\gamma t}{\hbar})\big[1-2p(0)\big]}\right\}\ . \tag{3.36}$$

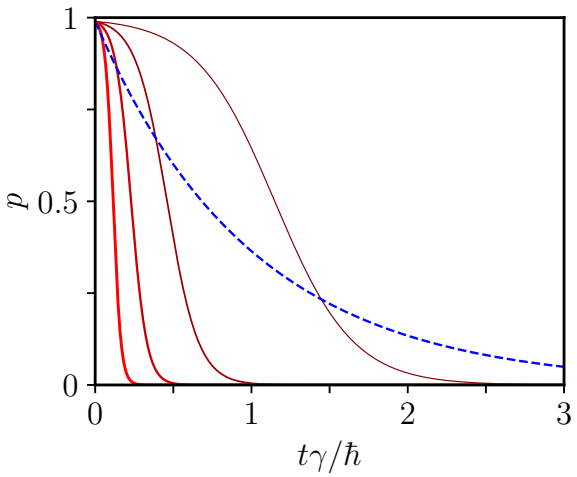

FIGURE 3.3: The probability $p(t)$ to find an atom in its own excited state as a function of time (in units of $\hbar/\gamma$). $p(t)$ for independent (coherent) emission is plotted as a blu dashed (red thick) line. The various solid red lines correspond to different values of the number N of atoms: $N = 2, 5, 10, 20$. The lines thicken and brighten with increasing N. The initial probabilty is set to be $p(0) = 0.99$.

We can see by inspection that the initial condition $p(0) = 1$, corresponding to the initial state in Eq. (3.30), gives a constant solution $p(t) = p(0) = 1$ (while the corresponding time t in Eq. (3.35) is ill-defined). This is due to the fact that the correspondent initial angle $\theta(0) = 0$ is an unstable equilibrium point, meaning that any small perturbation gives rise to a departure from the equilibrium solution. As a matter of fact, this equilibrium point is an artifact of the classical solutions, since taking into account quantum fluctuation drives the trajectory away from this point. In the quantum case, the only equilibrium point (or fixed-point of the dynamical map) lies at $p = 0$.

In summary, we studied the emission of an ensemble of N excited atoms enclosed in a dissipative cavity. Fig. 3.3 shows the probability to find an atom in its own excited state $p(t)$ as a function of time comparing the case of independent emission (blue dashed line) and collective superradiant emission (red thick lines).

If each atom emits independently, the time-scale of the process is given by $\tau_{\parallel} = \hbar/\gamma$. Conversely, if the atoms lose their energy through the same mode, the speed of the emission process (or discharging process in the QB jargon) is enhanced by a factor N, $\tau_{\sharp} \sim \tau_{\parallel}/N$. This can be put in a strong analogy with the charging protocol proposed by Ref. [22] (and discussed in Sect. 2.2), where a Hamiltonian that acts on all the qubits simultaneusly provide a speed-up in the charging time. This connection is further investigated in Chap. 4, where a high-power battery based on the Dicke model is proposed. As we will see there, the superradiant emission, proposed by Dicke [25], is at the core of the collective advantage found in a Dicke QB [24].

3.3 Superradiant phase transition or photon condensation

The Dicke model, discussed in detail in Sect. 3.1, displays a phase transition, named "superradiant" phase transition in the Literature. In 1973 Hepp and Lieb [31] and Wang and Hioe [38] have shown that for sufficiently strong light-matter coupling the Dicke model in the thermodynamic limit has a finite temperature second-order equilibrium phase transition between a normal and "superradiant" state. In the superradiant phase, the ground state exhibits a macroscopic number of photons, *i.e.* $\langle \hat{a} \rangle \propto \sqrt{N}$. Due to this fact, we dubbed this exotic phase as "photon condensate" to avoid confusion with the already mentioned superradiant emission phenomena. Later, it was shown that the inclusion of the diamagnetic term proportional to $(\hat{a} + \hat{a}^{\dagger})^2$ (Ref. 39), which is naturally generated by the minimal coupling procedure $\hat{\boldsymbol{p}} \to \hat{\boldsymbol{p}} + e\boldsymbol{A}/c$, forbids the phase transition, if the TRK sum-rule [84] is taken into account. Recently, it has been proved [37] that the Dicke model displays also a quantum phase transition at zero temperature, tuned by the light-matter coupling. Again, the addition of the diamagnetic term fulfilling the TRK sum-rule prevents the occurrence of photon condensation [40]. In has been argued [40] that this sum-rule can be violated in circuit QED setups, due to the peculiar topology of the wave-function in these systems, opening a path to realize the superradiant phase transition. Nevertheless, this question is still open and debated [73].

The rest of this Section is organized as follows. In Subsect. 3.3.1 we discuss the photon condensation in the Dicke model. This Subsection is based on the results of Ref.[37]. In Subsect. 3.3.2 we show that the addition of a diamagetic term fulfilling the TRK sum-rule to the Dicke model forbids the occurrence of photon condensation. In this Subsection the no-go theorem is presented following the line of reasoning of Ref.[40]. The content of the present Section is preliminary to the contents of Chap. 8, where the no-go theorem is generalized and to Chap. 9 where a possible path to overcome this theorem is presented.

3.3.1 Photon condensation in the Dicke model

We here discuss the occurrence of a quantum phase transition [37], named photon condensation, in the Dicke model in Eq. (3.25). Contrary to classical phase transitions, which are driven by temperature, quantum phase transitions are controlled by a Hamiltonian parameter. In this case, photon condensation is controlled by the light-matter coupling g. Moreover, phase transitions can occur only in the thermodynamic limit [89], namely $N \to \infty$, $V \to \infty$ with $N/V \to$ const. Looking at the microscopic expression for $g \equiv ie\omega_{\mathrm{eg}} \langle \mathrm{e}|\hat{\boldsymbol{r}} \cdot \boldsymbol{A}_0|\mathrm{g}\rangle /c$ (see below Eq.(3.24)) with $A_0 = \sqrt{2\pi\hbar c^2/(V\omega_{\mathrm{c}})} \sim 1/\sqrt{N}$, we can see that the coupling is not an

intensive quantity, i.e. $g \sim 1/\sqrt{N}$, in the thermodynamic limit. Hence, we decide to work with a rescaled intensive coupling g_0 defined as $g_0 \equiv \sqrt{N}g$. [2] Without any loss of generality, we assume g_0 to be real.

With this choice, the Dicke model in Eq. (3.25) reads

$$\hat{\mathcal{H}}_{\text{Dicke}} = \hbar\omega_{\text{eg}}\hat{J}^z + \hbar\omega_{\text{c}}\hat{a}^\dagger\hat{a} + \frac{g_0}{\sqrt{N}}\big(\hat{J}^+ + \hat{J}^-\big)\big(\hat{a} + \hat{a}^\dagger\big) \ . \tag{3.37}$$

By means of the Holstein-Primakoff transformations [90] it is possible to express collective pseudo-spin operators in terms of the bosonic operators $\hat{b}, \hat{b}^\dagger$, namely

$$\hat{J}^z = \hat{b}^\dagger\hat{b} - \frac{N}{2} \ , \tag{3.38}$$

$$\hat{J}^+ = (\hat{J}^-)^\dagger = \hat{b}^\dagger\sqrt{N}\sqrt{1 - \frac{\hat{b}^\dagger\hat{b}}{N}} \ . \tag{3.39}$$

In the normal phase, we note that the ratio $\langle\hat{b}^\dagger\hat{b}\rangle/N$ goes to zero in the thermodynamic limit $N \to \infty$, meaning that the atom is not macroscopically excited. In this case, we can legitimately approximate ladder pseudo-spin operator with bosonic ladder operators, $\hat{J}^+ \to \sqrt{N}\hat{b}^\dagger, \hat{J}^- \to \sqrt{N}\hat{b}$. The Dicke Hamiltonian is then approximated by two-modes bosonic Hamiltonian

$$\hat{\mathcal{H}}_{\text{Dicke}} = \hbar\omega_{\text{eg}}\hat{b}^\dagger\hat{b} + \hbar\omega_{\text{c}}\hat{a}^\dagger\hat{a} + g_0\big(\hat{b}^\dagger + \hat{b}\big)\big(\hat{a}^\dagger + \hat{a}\big) \ . \tag{3.40}$$

This Hamiltonian is quadratic in the bosonic operators and can be diagonalized in terms of the Bogoliubov eigenmodes $\hat{\gamma}_+$ and $\hat{\gamma}_-$ as follows

$$\hat{\mathcal{H}}^< = \sum_{i=\pm}\epsilon_i^<\hat{\gamma}_i^\dagger\hat{\gamma}_i + E_{\text{G}} \ , \tag{3.41}$$

where E_{G} is the ground state energy and $\epsilon_i^<$ are the energies of the Bogoliubov eigenmodes, which read explicitly

$$(\epsilon_\pm^<)^2 = \frac{1}{2}\Big[(\hbar\omega_{\text{c}})^2 + (\hbar\omega_{\text{eg}})^2 \pm \sqrt{\big[(\hbar\omega_{\text{c}})^2 - (\hbar\omega_{\text{eg}})^2\big]^2 + 16g_0^2\hbar\omega_{\text{c}}\hbar\omega_{\text{eg}}}\Big] \ . \tag{3.42}$$

For $g_0 = g_0^{\text{c}} \equiv \sqrt{\hbar\omega_{\text{c}}\hbar\omega_{\text{eg}}}/2$, the lowest mode becomes soft $\epsilon_-^< = 0$, signaling a quantum phase transition. For $g_0 > g_0^{\text{c}}$, the energy $\epsilon_-^<$ is imaginary, meaning that the model in Eq. (3.40) becomes unphysical. In this case, a different path has to be taken to solve the Dicke model. To do so, we consider the Holstein-Primakoff transformed Hamiltonian of Eq. (3.37) and displace the bosonic modes in the following way

$$\hat{A} \equiv \hat{a} + \alpha \ , \tag{3.43}$$

$$\hat{B} \equiv \hat{b} + \beta \ . \tag{3.44}$$

[2] One may note that this choice is somehow crucial also in the context of superradiant emission. If in Sect. 3.2 the intensive coupling constant g_0 were used instead of $g = g_0/\sqrt{N}$ the coherent speed-up would have been completely reabsorbed. The decay time scale $\tau_\sharp$ (defined by Eq.(3.35)) reads in terms of microscopic parameter $\tau_\sharp \sim \hbar\kappa/(Ng^2)$ or, in terms of g_0, $\tau_\sharp \sim \hbar\kappa/(g_0^2)$, which does not scale with N. Whether g or g_0 is the correct *physical* parameter ultimately depends on the experimental setup. In Haroche emission experiments [33], for example, the number of atoms N is varied without altering the volume of the cavity, and therefore the description with g is more appropriate. In the present discussion of phase transitions, where the thermodynamic limit is involved ($N \to \infty$, $V \to \infty$ with $N/V \to$ const) we chose to use g_0 as the *physical* parameter.

Neglecting terms such $\langle \hat{B}^\dagger \hat{B} \rangle / N$ and choosing the suitable α and β in order to set to zero terms linear in the bosonic operator, we obtain an Hamiltonian quadratic in the bosonic operators $\hat{A}$ and $\hat{B}$. This can be diagonalized via a Bogoliubov transformation: $\hat{\mathcal{H}}^{>} = \sum_{i=\pm} \epsilon_i^{>} \hat{\gamma}_i^\dagger \hat{\gamma}_i + E_{\rm G}$, where

$$(\epsilon_\pm^{>})^2 = \frac{1}{2}\Big[(\hbar\omega_{\rm c})^2 + \Big(\frac{g\hbar\omega_{\rm eg}}{g_{\rm c}}\Big)^2 \pm \sqrt{\Big[(\hbar\omega_{\rm c})^2 - \Big(\frac{g\hbar\omega_{\rm eg}}{g_{\rm c}}\Big)^2\Big]^2 + 4\big(\hbar\omega_{\rm c}\hbar\omega_{\rm eg}\big)^2}\Big] \ . \tag{3.45}$$

It is worth to notice that this Hamiltonian is well defined only for $g_0 \geq g_0^{\rm c}$ since otherwise $\epsilon_-^{>}$ would be an imaginary number. The spectrum of the lowest excitation of the Dicke model is shown in Fig. 3.4, (a).

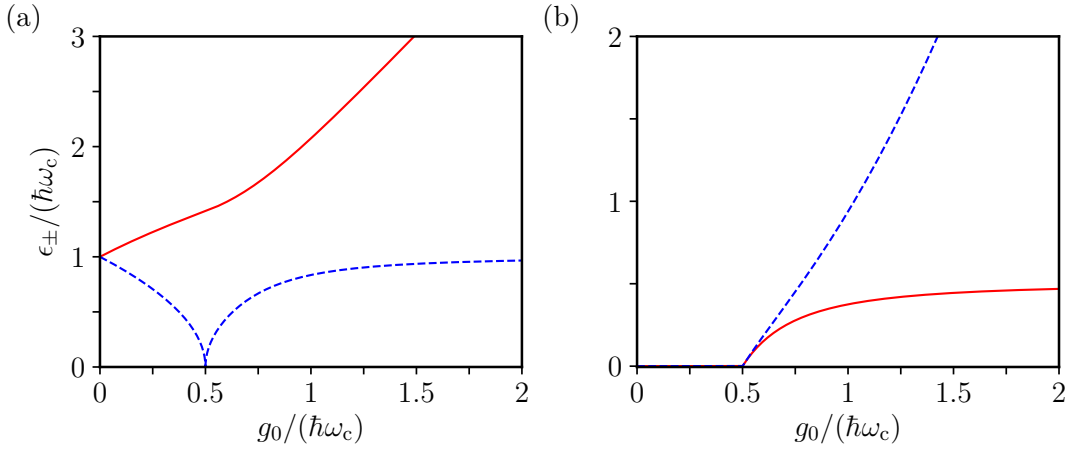

FIGURE 3.4: Panel (a) shows the upper ϵ_+ (red solid line) and lower energy-branch ϵ_- (blue dashed line) of $\hat{\mathcal{H}}_{\rm Dicke}$ (in units of $\hbar\omega_{\rm c}$) as a function of g_0 (in units of $\hbar\omega_{\rm c}$). Panel (b) shows the ground state number of photons (blue dashed line), $\langle \hat{a}^\dagger \hat{a} \rangle / N$ and the ground state probability (red solid line) to find an atom in its own excited state, $p \equiv \langle \hat{J}^z \rangle / N + 1/2$. In both panels, the resonant condition $\omega_{\rm c} = \omega_{\rm eg}$ is assumed.

We now show that the phase transition has an observable manifestation in the atomic inversion $\langle \hat{J}^z \rangle$ and in the photon occupation number $\langle \hat{a}^\dagger \hat{a} \rangle$, where $\langle \ldots \rangle$ denotes ground state expectation values. For $g_0 < g_0^{\rm c}$, these two quantities (shown in Fig. 3.4,(b)) read

$$\langle \hat{J}^z \rangle = -\frac{N}{2} \ , \tag{3.46}$$

$$\langle \hat{a}^\dagger \hat{a} \rangle = 0 \ , \tag{3.47}$$

while for $g_0 > g_0^{\rm c}$,

$$\langle \hat{J}^z \rangle = -\frac{N}{2}\Big(\frac{g_0^{\rm c}}{g_0}\Big)^2 \ , \tag{3.48}$$

$$\langle \hat{a}^\dagger \hat{a} \rangle = N\frac{[g_0^4 - (g_0^{\rm c})^4]}{(\hbar\omega_{\rm eg} g_0)^2} \ . \tag{3.49}$$

In the normal phase, $g_0 < g_0^{\rm c}$, all atoms are in its own local ground state $|{\rm g}\rangle_i$, i.e. $\langle \hat{J}^z \rangle = -N/2$, while there are no photons in the system, $\langle \hat{a}^\dagger \hat{a} \rangle = 0$. In the photon condensate phase,

$g_0 > g_0^c$, both atoms and photons acquire a macroscopic number of excitations (see also Fig. 3.4,(b)). The photon condensate phase owes its name to this fact, the ground state has a macroscopic number of photons.

3.3.2 No-go theorem: the Hopfield model

We finally comment on the inclusion of the diamagnetic term in Eq. (3.24). For sake of simplicity, we assume the cavity frequency and the atomic transition frequency to be equal, $\omega_c = \omega_{eg}$. In the normal phase, we can safely perform the Holdstein-Primakoff transformations [90] and neglect terms like $\langle \hat{b}^\dagger \hat{b} \rangle / N$ in the thermodynamic limit. The Hopfield Hamiltonian reads [40, 83]

$$\hat{\mathcal{H}}_{\text{Hopf}} = \hbar\omega_{eg}\hat{b}^\dagger\hat{b} + \hbar\omega_c\hat{a}^\dagger\hat{a} + g_0\left(\hat{b}^\dagger + \hat{b}\right)\left(\hat{a}^\dagger + \hat{a}\right) + \Delta\left(\hat{a}^\dagger + \hat{a}\right)^2 . \tag{3.50}$$

This quadratic Hamiltonian can be diagonalized by means of Bogoliubov transformations. Energies of the Bogoliubov modes are given by

$$(\epsilon_\pm^<)^2 = (\hbar\omega_c)^2 + 2\hbar\omega_c\left(\Delta \pm \sqrt{\Delta^2 + g_0^2}\right) . \tag{3.51}$$

This spectrum is shown in Fig. 3.5.

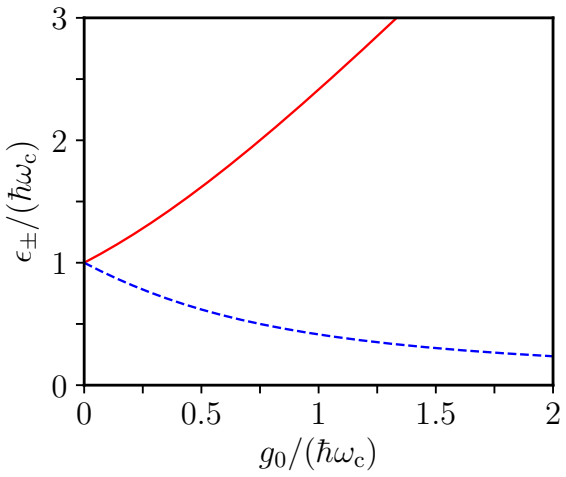

Figure 3.5: The upper ϵ_+ (red solid line) and lower energy-branch ϵ_- (blue dashed line) of $\hat{\mathcal{H}}_{\text{Hopf}}$ (in units of $\hbar\omega_c$) as a function of g_0 (in units of $\hbar\omega_c$). The condition $\xi = 1$ is taken.

As previously discussed in Sect. 3.1, a precise relation [40] between g_0 and Δ exists due to the TRK sum rule. Eq. (3.29) can be recast in terms of g_0 as

$$\Delta = \xi\frac{g_0^2}{\hbar\omega_c} , \tag{3.52}$$

where ξ is a free parameter, fulfilling $\xi \geq 1$. The critical coupling g_0^c at which the phase transition occurs is given by the softening of the lowest mode, i.e. $\epsilon_-^< = 0$. The critical coupling reads

$$\boxed{(g_0^c)^2 = \frac{(\hbar\omega_c)^2}{4(1-\xi)}} . \tag{3.53}$$

This equation does not admit a real solution for $\xi \geq 1$ and, as shown in Fiq. 3.5, there is always a finite energy gap between the ground state and the first excited state, meaning that no phase transition occurs. Since ξ is indeed constrained to be greater or equal to one by Eq. (3.52), *physical* models do not display any photon condensation.

Physically, the Dicke model describes an ensemble of atoms coupled with a single spatially-uniform electromagnetic mode. Since we are looking to equilibrium properties this mode displays no time-dependence. Such a constant and uniform vector potential corresponds to a purely gauge field and therefore it cannot have any physical effect. Thanks to Eq. (3.52), paramagnetic and diamagnetic currents cancel out in response to a such fictitious field. This is a so-called no-go theorem [40] for photon condensation.

While the present analysis is restricted to the Dicke model, it is possible to show that an arbitrary non-relativistic electronic system coupled to a single bosonic mode does not display photon condensation, even in presence of strong electron-electron interactions, as we show in Chap. 8. Since the root of this no-go theorem resides in the fact that a spatially-uniform electromagnetic mode corresponds to a purely gauge field, a natural way to circumvent the theorem is to consider a spatially-varying mode. Following this path, as we show in Chap. 9, it is possible to derive a criterion for the occurrence of photon condensation.

Part II

Dicke Quantum Batteries

4

High-power collective charging of a solid-state quantum battery

In this Chapter we present our work on a Dicke quantum battery, a solid state implementation of the quantum thermodynamics concepts exposed in Chap.2. The results of this work have been published in Ref. [24] and this chapter is largely based upon it.

We start this Chapter with a synopsis, Sect. 4.1, of the current state of the field. In Sect. 4.2 we introduce our model and the charging protocol. Sect. 4.3 discusses the parallel protocol, where each battery cell is charged independently, while Sect. 4.4 describes the collective charging, where all cells are charged by the same energy source. Storage and discharging are presented in Sect. 4.5 and few experimental considerations are given in Sect. 4.6. We end with a discussion of our findings in Sect. 4.7. Further technical details are reported in App. A.

4.1 Synopsis

In the last few decades, batteries [91, 92] have been the driving force behind the revolution in personal electronics and are steadily gaining tremendous importance also in the automotive sector [93]. Currently, there is also an ever increasing demand on energy storage systems able to manage large power densities [94], an issue that has been so far partially addressed by the use of supercapacitors [95, 96]. Batteries and supercapacitors essentially operate on the basis of extremely robust electrochemical principles that have been developed between the Eighteenth and Nineteenth centuries [91, 92]. While it is pivotal to continue research on advanced materials (see, e.g., Ref. 97) to optimize the performance of available energy storage devices, it seems timely and very natural to ask ourselves whether it is useful to transcend conventional electrochemistry to create an entirely new class of powerful batteries.

Quantum phenomena, such as phase coherence and entanglement, constitute remarkable resources that, when properly manipulated and engineered, may enable superior performance of technological devices of various sorts. The prime example is quantum computing performed with quantum bits (realized, e.g., with superconducting circuitry [98, 99]) as compared to classical computing performed with classical bits [100]. While in quantum computing quantum

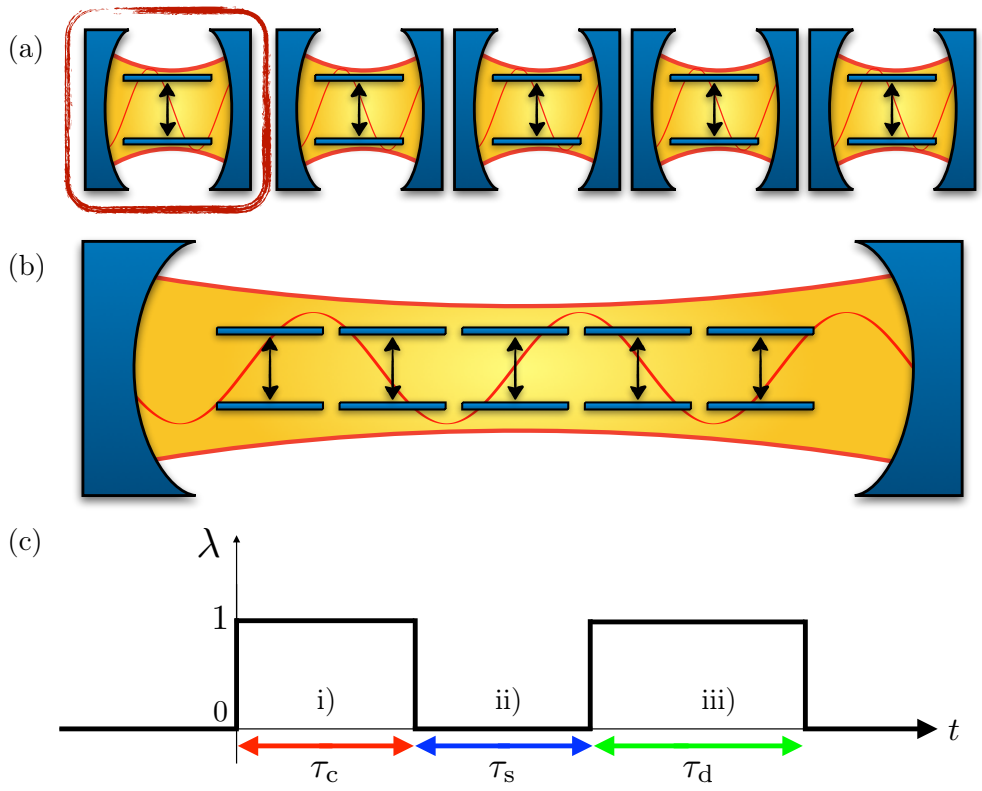

FIGURE 4.1: a) An array of identical Rabi quantum batteries operating in parallel. The elementary building block, enclosed in a red box, consists of a two-level system with an energy separation ω_{eg} between the ground $|g\rangle$ and excited state $|e\rangle$. Each two-level system is coupled to a separate cavity hosting a single photonic mode. The red arrow indicates a particle-hole transition induced by the photon field. b) A Dicke quantum battery, where the same array of two-level systems is now embedded into a single cavity and interacting with a common photonic mode. c) Time evolution of the dimensionless coupling constant $\lambda(t)$ introduced in Eq. (4.2). i) After initializing the system in the state $|\psi(0)\rangle$ defined in Eq. (4.1), one turns on the coupling $\lambda(t)$ bringing it to one and keeping it on for a time τ_c in order to charge the array (charging phase, red arrow). ii) The coupling is then switched off for a time τ_s (storage phase, blue arrow). iii) Finally, the coupling is again turned on for a time τ_d to discharge the array (discharging phase, green arrow).

phenomena are employed to achieve efficient manipulation and processing of information, an emerging theoretical research activity is currently focused on utilizing genuine quantum resources to achieve superior performances in the manipulation and processing of energy [101]. Specifically, whether and how quantum correlations may be harnessed to achieve high thermodynamic efficiency in the transduction of heat into work in quantum-mechanical thermal machines is something that is currently being actively investigated [11–19].

Given this context, we are naturally led to consider whether quantum resources such as entanglement may be usefully employed to improve the performance (e.g. by speeding up the charging time) of "quantum batteries" (QBs). To this end we consider a quantum system—see red box in Fig. 4.1(a)—having a discrete energy spectrum, which can be kept well isolated from its environment so as to hold its energy for a sufficiently long time relative to the intended use. Many of such systems can be considered together, making a QB. In Figs. 4.1(a) and (b) we see two examples. In panel (a), each quantum system—in this case a two-level system

(TLS)—is coupled to a separate cavity, each hosting a single photonic mode. In panel (b), an ensemble of many TLSs is embedded in a single cavity and interacting with a common photonic mode. Charging of a QB requires a protocol of "interaction" of the QB itself with some external body or field (the "energy source", namely the cavity field in our example), which raises its energy over a time span that is much shorter than the QB lifetime.

Early pioneering works [20–23] have considered a special subclass of charging protocols, namely those that can be described by unitary quantum gates acting on arrays of QBs. The main finding of these works is that addressing N QBs at once, by means of a *global entangling operation*, can result in a speed-up of the averaged charging power (stored energy over charging time) as compared to charging them individually, in a parallel fashion. As noted in Ref. 23, however, such global entangling operations involve highly non-local interactions, which may be difficult to realize in practice.

In this Chapter, we propose a practical architecture for a QB constituted by an array of N TLSs (see Fig. 4.1). We fully relax the constraint on the unitary evolution of the QB employed in previous theoretical works. Such unitary evolution regime occurs only when the dynamics of the energy source is very slow compared to the QB dynamics (i.e. in the Born-Oppenheimer limit). This, although certainly interesting, is motivated more by mathematical convenience than adherence to reality. Here, we consider the more realistic situation in which no time scale separation exists between the QB and energy source subsystems. Accordingly, we treat the system "QB+energy source" in a fully quantum mechanical fashion, which generally results in a non-unitary reduced dynamics of the QB alone. In the proposed architecture, the non-local interaction among the N TLSs is achieved by coupling all of them to the very same quantum energy source, which effectively results in a highly non-local interaction.

More specifically, our analysis relies on modelling the array of TLSs, entangled by a common quantized electromagnetic energy source, through the Dicke model [25], see Fig. 4.1(b). Interestingly, we find a collective enhancement of the charging power of a factor $\sqrt{N}$, independent of the strength of the TLS-cavity coupling.

The solid-state Dicke QBs proposed here can be realized, e.g., by utilizing superconducting qubits [102–105] or nanofabricated semiconductor quantum dots [106–113], the former having relaxation and coherence times of the order of microseconds, with ultrafast (e.g. nanosecond) charging time scales enabled by π pulses. Another intriguing realization could rely on deterministically placing individual core-shell colloidal quantum dots [114, 115] in an optical microcavity. Such systems may enable to run the charging protocol via visible photons, thus facilitating the experimental realization and increasing the stored energy density.

4.2 Model and charging/discharging protocol

We consider the charging process of N TLSs prepared in their ground state $|\mathrm{g}\rangle$, via coupling to a single cavity mode residing in the N photon Fock state[1] $|N\rangle$. The initial state of the total system therefore reads:

$$|\psi(0)\rangle = |N\rangle \otimes \underbrace{|\mathrm{g},\mathrm{g},\ldots,\mathrm{g}\rangle}_{N} \ . \tag{4.1}$$

[1]Experimentally, the preparation of quantum systems in Fock states for small N has been demonstrated e.g. in Refs. 116–120. We have checked in a number of exactly solvable models of QBs—not shown here—that the quantum collective enhancement of the maximum charging power, scaling like $\sqrt{N}$ for $N \gg 1$, does not depend on the choice of the initial state for the cavity photons and does not occur only for Fock states, but also for coherent as well as thermal states.

We model the quantum dynamics of the N TLSs coupled to a single cavity mode via the following time-dependent Dicke Hamiltonian [25]($\hbar = 1$ throughout this Chapter):

$$\hat{\mathcal{H}}^{\sharp}(t) = \omega_{\rm c}\hat{a}^{\dagger}\hat{a} + \omega_{\rm eg}\hat{J}^{z} + 2g\lambda(t)\hat{J}^{x}\left(\hat{a}^{\dagger} + \hat{a}\right) \ . \tag{4.2}$$

Here, $\hat{a}$ ($\hat{a}^{\dagger}$) annihilates (creates) a cavity photon with frequency $\omega_{\rm eg}$ and $\hat{J}^{\alpha} = (1/2)\sum_{i}^{N}\hat{\sigma}_{i}^{\alpha}$ with $\alpha = x, y, z$ are the components of a collective spin operator expressed in terms of the Pauli operators $\hat{\sigma}_{i}^{\alpha}$ of the i-th TLS. The quantity $\omega_{\rm eg}$ is the energy splitting between the ground $|{\rm g}\rangle$ and excited state $|{\rm e}\rangle$ of each TLS. Below, we focus on the resonant regime, $\omega_{\rm eg} = \omega_{\rm c}$. The strength of the TLS-cavity coupling is given by the dimensionless parameter g. $\lambda(t)$ is a classical control parameter whose explicit dependence on time t specifies the charging/discharging protocol. For the sake of definiteness, we consider the protocol sketched in Fig. 4.1(c). i) The interaction between the TLSs and the cavity is turned on at time $t = 0^{+}$, $\lambda_{0^{+}} = 1$, and kept it at this value for $0 < t \leq \tau_{\rm c}$. During this charging step, energy transfer occurs from the cavity to the array of TLSs. ii) The interaction is then turned off at time $\tau_{\rm c}^{+}$, i.e. $\lambda(\tau_{\rm c}^{+}) = 0$, and kept it off for $\tau_{\rm c} < t \leq \tau_{\rm c} + \tau_{\rm s}$. During this storage step, the TLSs are assumed to be isolated from the environment, and hence keep their energy. Finally, iii) the interaction is again turned on for a time $\tau_{\rm d}$, $\lambda(t) = 1$ for $\tau_{\rm c} + \tau_{\rm s} < t \leq \tau_{\rm c} + \tau_{\rm s} + \tau_{\rm d}$. During this discharging step, energy is transferred from the TLSs to the cavity. An alternative charging/discharging protocol, which is fully feasible experimentally [104, 116], may rely on a time-independent $\lambda(t) \equiv 1$ coupling and a non-zero time-dependent $\Delta(t) = \omega_{\rm eg}(t) - \omega_{\rm c}$ detuning. This is discussed in Appendix A.1, where the equivalence of these two alternative protocols is shown.

4.3 Parallel charging

We begin by considering the case in which charging occurs in a parallel fashion, see Fig. 4.1(a). Namely, we consider N copies of TLSs, each coupled to a distinct cavity. In the case of a single TLS, the Dicke Hamiltonian (4.2) reduces to the Rabi Hamiltonian [121, 122]. In this case, the total parallel Hamiltonian is a sum of N independent Rabi Hamiltonians, $\hat{\mathcal{H}}^{\parallel}(t) = \sum_{i=1}^{N}\hat{h}_{i}^{\parallel}(t)$, where $\hat{h}_{i}^{\parallel}(t) = \omega_{\rm c}\hat{a}_{i}^{\dagger}\hat{a}_{i} + \omega_{\rm eg}\hat{\sigma}_{i}^{z} + 2g\lambda(t)\hat{\sigma}_{i}^{x}\left(\hat{a}_{i}^{\dagger} + \hat{a}_{i}\right)$. At each TLS is associate a different cavity mode $\hat{a}_{i}$. The energy $E_{\parallel}^{(N)}(\tau_{\rm c})$ stored at time $\tau_{\rm c}$ in a parallel fashion by N copies of such resonant (i.e. $\omega_{\rm eg} = \omega_{\rm c}$) Rabi QBs is N times the energy $\epsilon(\tau_{\rm c})$ stored in a single Rabi QB:

$$E_{\parallel}^{(N)}(\tau_{\rm c}) = N\epsilon(\tau_{\rm c}) \equiv \frac{N\omega_{\rm c}}{2}\Big[\langle\phi(\tau_{\rm c})|\hat{\sigma}^{z}|\phi(\tau_{\rm c})\rangle - \langle\phi(0)|\hat{\sigma}^{z}|\phi(0)\rangle\Big] \ . \tag{4.3}$$

The symbol $|\phi(\tau_{\rm c})\rangle$ stands for the evolved initial state $|\phi(0)\rangle$, according to $\hat{h}(t)$ for a time $\tau_{\rm c}$, i.e., $|\phi(\tau_{\rm c})\rangle = \exp\big[-i\int_{0}^{\tau_{\rm c}} dt\hat{h}^{\parallel}(t)\big]|\psi(0)\rangle$. We now introduce the maximum stored energy (i.e. the "capacity") and the maximum charging power in the parallel-charging operation mode: $\tilde{E}_{\parallel}^{(N)} = \max_{\tau_{\rm c}}[E_{\parallel}^{(N)}(\tau_{\rm c})]$ and $\bar{P}_{\parallel}^{(N)} = \max_{\tau_{\rm c}}[P_{\parallel}^{(N)}(\tau_{\rm c})]$, where the charging power [22, 23] after a time $\tau_{\rm c}$ is defined as $P_{\parallel}^{(N)}(\tau_{\rm c}) \equiv E_{\parallel}^{(N)}(\tau_{\rm c})/\tau_{\rm c}$. Both $\tilde{E}_{\parallel}^{(N)}$ and $\bar{P}_{\parallel}^{(N)}$ scale linearly with N (yielding a constant energy and power per QB):

$$\tilde{E}_{\parallel}^{(N)} = \omega_{\rm c}N\mathcal{F}_{\rm E}\Big(\frac{g}{\omega_{\rm c}}\Big) \propto N \ , \tag{4.4}$$

and

$$\bar{P}_{\parallel}^{(N)} = \omega_{\rm c}gN\mathcal{F}_{\rm P}\Big(\frac{g}{\omega_{\rm c}}\Big) \propto N \ , \tag{4.5}$$

where $\mathcal{F}_{\rm E}$ and $\mathcal{F}_{\rm P}$ are dimensionless functions of $g/\omega_{\rm c}$, which can be calculated exactly [123]. Their expression greatly simplifies in the weak-coupling $g/\omega_{\rm c} \ll 1$ limit, where the Rabi Hamiltonian can be approximated by the Jaynes-Cummings one [124]. In such a limit, the stored energy takes the form $E_{\parallel}^{(N)}(\tau_{\rm c}) = N\omega_{\rm c}\sin^2(g\tau_{\rm c})$, and hence [2] $\mathcal{F}_{\rm E}(g/\omega_{\rm c}) \to 1$ and $\mathcal{F}_{\rm P}(g/\omega_{\rm c}) \to 0.724$. Since we are interested in the collective charging case and in scalings with N, we will not dwell upon deriving exact expressions for $\mathcal{F}_{\rm E}$ and $\mathcal{F}_{\rm P}$.

4.4 Collective charging

We now investigate the maximum stored energy and maximum charging power when the N TLSs are coupled to one and the same cavity—see Fig. 4.1(b)—as described by the Dicke Hamiltonian (4.2). The latter has a conserved quantity given by the so-called cooperation number [125, 126] $\hat{J}^2 = \sum_{\alpha=x,y,z}\left(\hat{J}^{\alpha}\right)^2$. A convenient basis set for representing the Hamiltonian (4.2) is $|n, J, M\rangle$, where n indicates the number of photons, $J(J+1)$ is the eigenvalue of $\hat{J}^2$, and M denotes the eigenvalue of $\hat{J}_z$. With this notation, the initial state (4.1) reads $|\psi(0)\rangle = |N, \frac{N}{2}, -\frac{N}{2}\rangle$ and the matrix elements of the Dicke Hamiltonian read [127]

$$\begin{aligned}\langle n', \frac{N}{2}, \frac{N}{2}-q'|\hat{\mathcal{H}}_{\lambda_t}^{(N)}|n, \frac{N}{2}, \frac{N}{2}-q\rangle = \omega_{\rm c}\Bigg\{\left(n+\frac{N}{2}-q\right)\delta_{n',n}\delta_{q',q} \\ +\lambda\Big[f^{(1)}_{n,\frac{N}{2},\frac{N}{2}-q}\delta_{n',n+1}\delta_{q',q+1} + f^{(2)}_{n,\frac{N}{2},\frac{N}{2}-q}\delta_{n',n+1}\delta_{q',q-1} \\ + f^{(3)}_{n,\frac{N}{2},\frac{N}{2}-q}\delta_{n',n-1}\delta_{q',q+1} + f^{(4)}_{n,\frac{N}{2},\frac{N}{2}-q}\delta_{n',n-1}\delta_{q',q-1}\Big]\Bigg\}\,,\end{aligned} \tag{4.6}$$

with

$$f^{(1)}_{k,J,M} = \sqrt{(k+1)\left[J(J+1)-M(M-1)\right]}\,, \tag{4.7}$$

$$f^{(2)}_{k,J,M} = \sqrt{(k+1)\left[J(J+1)-M(M+1)\right]}\,, \tag{4.8}$$

$$f^{(3)}_{k,J,M} = \sqrt{k\left[J(J+1)-M(M-1)\right]}\,, \tag{4.9}$$

$$f^{(4)}_{k,J,M} = \sqrt{k\left[J(J+1)-M(M+1)\right]}\,. \tag{4.10}$$

We remark that the number of photons is not conserved by the Dicke Hamiltonian nor it is bounded from above, hence taking, in principle, any integer value. Accordingly, the matrix (4.6) is infinite-dimensional. In practice, we need to truncate it by introducing a cutoff $N_{\rm ph} > N$ given by the maximum number $N_{\rm ph}$ of photons. This is chosen in such a way that a larger value of it, $N'_{\rm ph} > N_{\rm ph}$, would not produce any noticeable difference in the computed eigenvalues and eigenvectors. In the following, we show numerical results obtained from the exact diagonalization of the matrix (4.6) for $N = 2, \ldots, 20$. We have checked that excellent numerical convergence is achieved by choosing $N_{\rm ph} = 4N$. (A linear scaling of $N_{\rm ph}$ with N has also been found in Ref. 127.)

[2] The prefactors can be understood considering the fact that $y = 1-\cos x$ has absolute maximum $y_{\max} = 2$ at $x_{\max} = \pi \pmod{[2\pi]}$, while $y = (1-\cos x)/x$ has the absolute maximum $y_{\max} \approx 0.724$ at $x_{\max} \approx 2.331$ as can be easily achieved by numerical investigation.

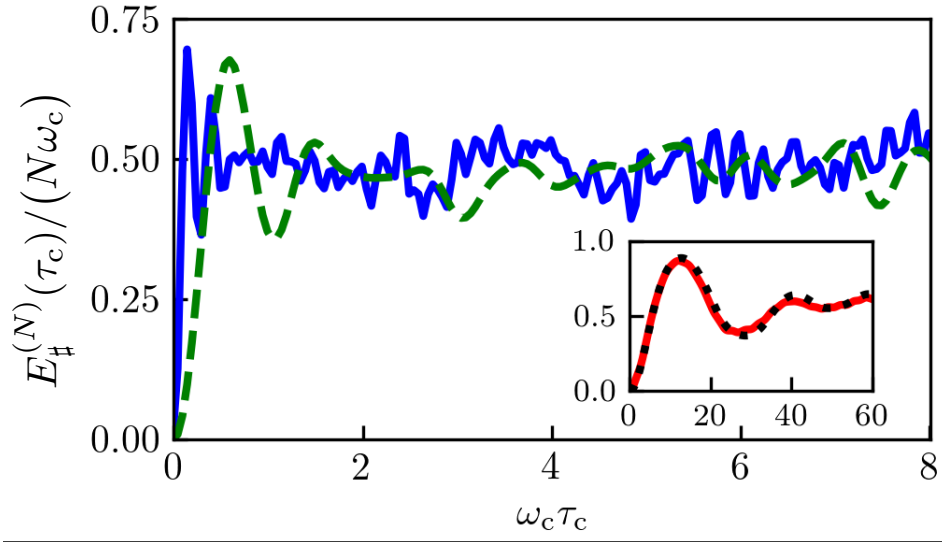

FIGURE 4.2: The dependence of the stored energy $E_\sharp^{(N)}(\tau_c)$ (in units of $N\omega_c$) on τ_c (in units of $1/\omega_c$) for $g/\omega_c = 0.5$ (green dashed line) and $g/\omega_c = 2.0$ (blue solid line). Inset: same as in the main panel but for $g/\omega_c = 0.05$ (red solid line), i.e. in the weak-coupling limit, is compared to results for the Tavis-Cummings model (black dotted line). All data in this figure have been computed by setting $N = 10$.

The energy $E_\sharp^{(N)}(\tau_c)$ stored collectively at time τ_c by the N TLSs is given by

$$E_\sharp^{(N)}(\tau_c) = \omega_c \Big[\langle\psi(\tau_c)|\hat{J}_z|\psi(\tau_c)\rangle - \langle\psi(0)|\hat{J}_z|\psi(0)\rangle \Big] , \tag{4.11}$$

where $|\psi(\tau_c)\rangle = \exp\big[-i\int_0^{\tau_c} dt\hat{\mathcal{H}}^\sharp(t)\big]|\psi^{(N)}(0)\rangle$. The dependence of $E_\sharp^{(N)}(\tau_c)$ on τ_c is reported in Fig. 4.2 for a few values of g/ω_c. We observe smooth oscillations for $g/\omega_c \ll 1$ (red solid line in the inset of Fig. 4.2), which are in full agreement with results obtained for the Tavis-Cummings model [125, 126] (black dotted line in the inset of Fig. 4.2). In the latter, counter-rotating terms are absent, leading to the conservation of the number of excitations and the further constraint $n = q$ ($n' = q'$) in Eq. (4.6). A more complicated oscillatory pattern showing beating appears for increasing g/ω_c (green dashed and blue solid lines in Fig. 4.2).

Figures 4.3(a) and (c) show the maximum stored energy $\tilde{E}_\sharp^{(N)} \equiv \max_{\tau_c}[E_\sharp^{(N)}(\tau_c)]$ and maximum charging power $\bar{P}_\sharp^{(N)} \equiv \max_{\tau_c}[P_\sharp^{(N)}(\tau_c)/\tau_c]$ in the collective case, as functions of N, for various values of g/ω_c. Note that the vertical axes of Figs. 4.3(a) and (c) are rescaled by $N\omega_c$ and $g\omega_c N\sqrt{N}$, respectively. We clearly see that such rescaled quantities rapidly converge to a certain asymptotic value as N increases. This implies that, for sufficiently large values of N, $\tilde{E}_\sharp^{(N)}$ and $\bar{P}_\sharp^{(N)}$ reach asymptotic values characterized by the following scaling laws

$$\tilde{E}_\sharp^{(N)} \propto N , \tag{4.12}$$

and

$$\boxed{\bar{P}_\sharp^{(N)} \propto N^{3/2} .} \tag{4.13}$$

The super-linear scaling of the maximum charging power in Eq. (4.13) constitutes direct evidence of a $\sqrt{N}$ advantage associated to collective charging as compared to parallel charging, Eq. (4.5). Such advantage is related to a scaling law of the time required to reach the maximum power, $\tau_c \propto 1/\sqrt{N}$, and has a collective origin. Finally, Figs. 4.3(b) and (d) illustrate the dependencies of the maximum stored energy and charging power of Dicke QBs on the coupling constant g/ω_c, for various values of N. Plotting the same rescaled quantities, $\tilde{E}_\sharp^{(N)}/(N\omega_c)$ and $\bar{P}_\sharp^{(N)}/(g\omega_c N\sqrt{N})$, versus the effective coupling parameter [37] $g_N \equiv g\sqrt{N}$, one notices a collapse onto universal curves, as shown in Appendix A.2. We remind the reader that the ground state of the Dicke model displays a superradiant quantum phase transition (SQPT) at $g_N = \omega_c/2$. A feeble reminiscence of such SQPT is also seen in the maximum charging energy of Dicke QBs, as illustrated in Appendix A.2.[3]

[3]We note that the possibility to achieve a SQPT in a real solid-state device has been debated at length [40, 69, 70, 73–75]. This is due to the detrimental effect of a term quadratic in the bosonic field, i.e. $\propto (\hat{a}^\dagger + \hat{a})^2$, which is missing in Eq. (4.2) and typically emerges from the minimal coupling of matter with the cavity radiation field. The authors of Refs. 70, 73 have argued, however, that this term does not prevent the emergence of SQPTs in alternative artificial TLSs such as phase qubits. We have investigated the role of the $(\hat{a}^\dagger + \hat{a})^2$ term and found it to be irrelevant with respect to our main findings above. For details, see Appendix A.3.

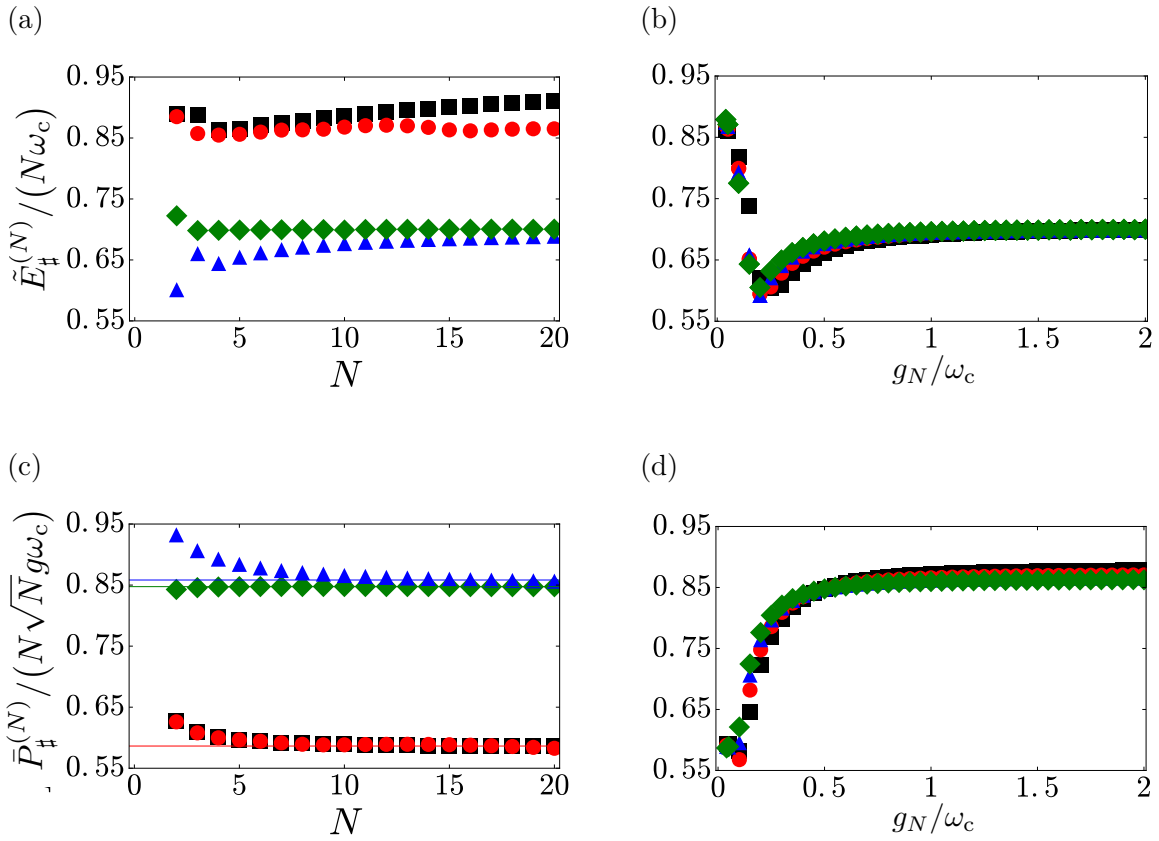

FIGURE 4.3: Panel (a) The maximum stored energy $E_\lambda^{(\sharp)}$ (in units of $N\omega_c$) is plotted as a function of N. Black squares denote the results for the Tavis-Cummings model at $g/\omega_c = 0.05$. Results for Dicke QBs refer to $g/\omega_c = 0.05$ (red circles), $g/\omega_c = 0.5$ (blue triangles), and $g/\omega_c = 2.0$ (green diamonds). Panel (b) Same as in panel (a) but as a function of g/ω_c for $N = 6$ (black squares), $N = 8$ (red circles), $N = 10$ (blue triangles), and $N = 12$ (green diamonds). Panel (c) The maximum charging power $\bar{P}_\sharp^{(N)}$ (in units of $N\sqrt{N}g\omega_c$) is plotted as a function of N. Color coding and labeling is the same as in panel (a). The thin horizontal lines are best fits to the numerical results, indicating the asymptotic values of the maximum power at large N: $\lim_{N\gg 1} \bar{P}_\sharp^{(N)}/(N\sqrt{N}g\omega_c) = 0.586$ for $g/\omega_c = 0.05$ (red), 0.858 for $g/\omega_c = 0.5$ (blue), and 0.847 for $g/\omega_c = 2$ (green). Panel (d) Same as in panel (c) but as function of g/ω_c for $N = 6$ (black squares), $N = 8$ (red circles), $N = 10$ (blue triangles), and $N = 12$ (green diamonds).

4.5 Storage and discharging

We now briefly comment upon storage and discharging phases of our Dicke QBs. We assume the storage time $\tau_{\rm s}$ is much shorter than any decoherence/relaxation time scale in a real solid-state implementation. Under this assumption, the Dicke QB retains its energy during the storage step. In the parallel case, and when $g/\omega_{\rm c} \ll 1$ (in which case the rotating wave approximation holds), independent of the duration of the storage time $\tau_{\rm s}$, the initial state (4.1) is recovered at the end of the discharging phase if the condition $\tau_{\rm c} + \tau_{\rm d} = \pi/g$ is met. In the collective case, as either N or $g/\omega_{\rm c}$ increases, such recoverability is lost. Accordingly, the smaller $g/\omega_{\rm c}$ the higher $\tilde{E}_\sharp^{(N)}$, the higher the recoverability (not shown). This is a signature of energy injection incurred when turning the coupling on and off, namely that $\delta E^{\rm on} = \langle\psi(0)|\hat{\mathcal{H}}^\sharp(0^+) - \hat{\mathcal{H}}^\sharp(0^-)|\psi(0)\rangle$ and $\delta E^{\rm off} = \langle\psi(\tau_{\rm c})|\hat{\mathcal{H}}^\sharp(\tau_{\rm c}^+) - \hat{\mathcal{H}}^\sharp(\tau_{\rm c}^-)|\psi(\tau_{\rm c})\rangle$ are generally non-vanishing.

4.6 Experimental considerations

The TLS+cavity system may be realized with state-of-the-art solid-state technology, by using e.g. superconducting qubits coupled to superconducting line resonators [102–104] or nanofabricated quantum dots (see e.g. Refs. 107, 108) combined with superconductive microwave circuits [108, 113], photonic crystals [106], or THz planar microcavities [128]. Concerning the typical values of the relevant physical parameters discussed in this Chapter, the implementations of Rabi and Dicke Hamiltonians in such solid-state devices [104, 113, 116] have a resonant frequency $\omega_{\rm c} \approx \omega_{\rm a}$ ranging from GHz to THz values and an individual interaction parameter g typically taking values in the range 10-100 MHz. This leads to $g/\omega_{\rm c} \approx 10^{-3}$-$10^{-2}$, fully justifies the rotating wave approximation discussed for the Rabi model. Moreover, the relevant time scales of relaxation and decoherence processes have to be compared with g^{-1}. In particular, one can introduce the decoherence rate Γ_ϕ and the electron relaxation rate $\Gamma_{\rm e}$ [98, 129]. The proposed charging/discharging protocol—together with all other possible quantum-computing implementations—is meaningful under the condition $\Gamma_\phi \lesssim \Gamma_{\rm e} < g$, which is satisfied in the experiments discussed in Refs. 104, 113, 116. This condition is even further justified in the Dicke model where the global coupling scales as $g_N = g\sqrt{N}$. Recent experimental work has also demonstrated that the strong-coupling $g/\omega_{\rm c} \approx 1$ limit can also be reached [130–132]. Colloidal quantum dots such as core-shell CdSe dots [114, 115] may offer another possible solution for implementing Dicke QBs, bringing the resonant frequency to hundreds of THz. This could facilitate the coupling of the dots with the photonic (micro)cavity mode and also yield an improved stored energy density.

4.7 Summary and conclusions

We have introduced the concept of a "Dicke quantum battery", consisting of an array of entangled two-level systems. Our aim is to put on concrete and experimentally feasible grounds the intriguing abstract ideas previously presented in Refs. 22, 23. The main physics is captured by the toy model in Eq. (4.2), which can in principle be engineered in a solid-state platform and displays collective powerful charging, Eq. (4.13) and Fig. 4.3(c). In particular, the interaction of an array of two-level systems with a common quantized electromagnetic mode in a cavity automatically creates entanglement among the N two-level systems. This is ultimately due to an effective long-range interaction between the two-level systems mediated by the cavity

photons. We observe an enhanced scaling of the maximum charging power, as envisaged in Refs. 22, 23, with a $\sqrt{N}$-fold enhancement with respect to the parallel case, independent of the value of the coupling strength g—see Eq. (4.13). We further note an interesting trade-off between power and reversibility of the charging process. Highest values of the maximum power are achieved at strong coupling. These come, however, at the cost of a lower stored energy, accompanied by a decrease in the efficiency of energy transfer from the quantum batteries to the cavity in the discharging phase. On the other hand, at weak coupling, one finds larger values of the maximum stored energy and a higher efficiency of energy transfer in the discharging step, at the cost of lower values of the maximum power.

5

Extractable work, the role of correlations, and asymptotic freedom in quantum batteries

In this Chapter we present our work the extractable work, the role of correlations and asymptotic freedom in quantum batteries. The results of this work have been published in Ref. [26] and this Chapter is largely based upon it.

We start this chapter with a synopsis, Sect. 5.1, of the current state of the field and our contribution. In Sect. 5.2 we introduce the charging protocol of the quantum battery and make the distinction between the average mean energy and the extractable work. Sect. 5.3 presents the results: the dependence of the extractable work on the initial state, the optimality of the coherent state as initial state due to minimal locking correlations and the asymptotic freedom of such correlations for the $N \to \infty$ limit. An extensive discussion and summary is provided in Sect. 5.4. Some technical details of the calculations are reported in App. B.

5.1 Synopsis

The possibility of using quantum phenomena for technological purposes is currently a very active research field. In this context, an interesting research topic is that of "quantum batteries" (QBs) [20–24, 48, 49, 135, 136], i.e. quantum mechanical systems which behave as efficient energy storage devices. This is motivated by the fact that genuine quantum effects, such as entanglement or squeezing, can typically boost the performances of classical protocols, e.g. by speeding up the underlying dynamics [137, 138]. The advantage provided by quantum correlations in the charging (or discharging) process of a QB has been discussed in a fully abstract fashion [20–23] and, more recently, for concrete models that could be implemented in the laboratory [24, 48, 49]. Up to now, research efforts have been mostly focused on maximizing the stored energy, minimizing the charging time or maximizing the average charging power [22–24, 48, 49]. A "good" QB, however, should not only store a relevant amount of energy, but also have the capability to fully deliver such energy in a useful way which, said in thermodynamic terms, is the capability of performing work. This observation is not a negligible subtlety, since in quantum information theory it is well known that correlations

and entanglement may induce limitations on the task of energy extraction [16, 20, 139–142]. We are therefore naturally led to face a somewhat frustrating situation in which quantum correlations have simultaneously both a positive and a negative effect in the process of energy storage. On one hand, they can speed up the charging time of QBs, while, on the other hand, they can pose a severe limit on the work that can be actually extracted from it.

In this work we shed some light on the competition between the aforementioned positive and negative aspects of quantum correlations, by analyzing the case of N two-level systems (qubits) charged via a single optical mode, the so-called Tavis-Cummings model [125, 126], which is known to provide an effective description of experimentally feasible many-body systems in circuit-QED [104, 143–145]. Our findings show that in the case of QBs involving a small number of qubits the energy locked by correlations can be large and must be taken into account for a rigorous and fair analysis of the performance of the QB itself. Luckily, however, this negative effect can be strongly reduced by an optimization over the initial state of the charging system, i.e. by properly preparing the initial state of the charger. Moreover, in the thermodynamic $N \to \infty$ limit of many qubits, the fraction of locked energy becomes negligible, independent of the initial state of the charger. We argue that this is a general property of quantum charging processes of closed Hamiltonian systems, which can be applied to other schemes (e.g. those analyzed in Ref. [49]) beyond the specific setup presented here, being ultimately linked to the integrability of the dynamics and not depending on the details of the latter.

By analysing a prototypical model made of N two-level systems (qubits) charged by a single optical mode, in this work we shed some light on the competition between the aforementioned positive and negative aspects of quantum correlations. Our findings show that in the case of QBs involving a small number of qubits the energy locked by correlations can be large and must be taken into account for a rigorous and fair analysis of the performance of the QB itself. Luckily, however, this negative effect can be strongly reduced by an optimization over the initial state of the charging system, i.e. by properly preparing the initial state of the charger. Moreover, in the thermodynamic $N \to \infty$ limit of many qubits, the fraction of locked energy becomes negligible, independent of the initial state of the charger. We argue that this is a general property of quantum charging processes of closed Hamiltonian systems, which is ultimately linked to the integrability of the dynamics and does not depend on the details of the underlying microscopic model.

5.2 Mean Energy versus Extractable work

We start by defining a general model for the charging process of a QB, schematically represented in Fig. 5.1(a). Here a first quantum system A acts as the energy "charger" for a second quantum system B that instead acts as the battery of the model. They are characterized by local Hamiltonians $\hat{\mathcal{H}}_{\rm A}$ and $\hat{\mathcal{H}}_{\rm B}$ respectively, that for the sake of convenience are selected to have both zero ground-state energy. Later on we shall also assume B to be composed by N non-mutually interacting elements: for the moment however this assumption is not relevant, and we do not invoke it yet. At time $t = 0$ the system starts in a pure factorized state $|\psi\rangle_{\rm A} \otimes |{\rm G}\rangle_{\rm B}$, with $|{\rm G}\rangle_{\rm B}$ being the ground state of $\hat{\mathcal{H}}_{\rm B}$, and $|\psi\rangle_{\rm A}$ having mean local energy $E_{\rm A}(0) \equiv {}_{\rm A}\langle\psi|\hat{\mathcal{H}}_{\rm A}|\psi\rangle_{\rm A} > 0$. By switching on a coupling Hamiltonian $\hat{\mathcal{H}}_1$ between the two systems, our aim is to transfer as much energy as possible from A to B, in some finite amount of time τ, the charging time of the protocol. For this purpose we write the global Hamiltonian

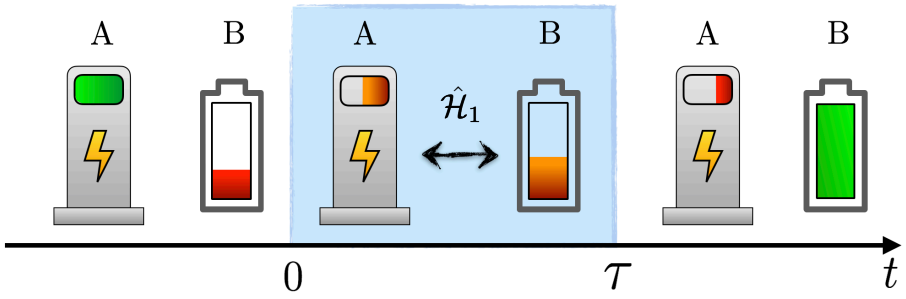

Figure 5.1: Panel (a) The charging protocol of a quantum battery. At time $t < 0$ the two systems A (i.e. the charger) and B (i.e. the battery) do not interact and cannot exchange energy. In the time interval $0 < t < \tau$, the coupling Hamiltonian $\hat{\mathcal{H}}_1$ is switched on and the two subsystems interact with a coupling strength g. Finally, the interaction is switched off at time τ and, after that, the energy stored in the battery B, $E_{\rm B}(\tau)$, is conserved.

of the model as

$$\hat{\mathcal{H}}(t) \equiv \hat{\mathcal{H}}_{\rm A} + \hat{\mathcal{H}}_{\rm B} + \lambda(t)\hat{\mathcal{H}}_1, \tag{5.1}$$

where $\lambda(t)$ is a classical parameter that represents the external control we exert on the system, and which we assume to be given by a step function equal to 1 for $t \in [0, \tau]$ and zero elsewhere. Accordingly, indicating with $|\psi(t)\rangle_{\rm AB}$ the evolved state of the system at time t, its total energy $E(t) \equiv {}_{\rm AB}\langle\psi(t)|\hat{\mathcal{H}}(t)|\psi(t)\rangle_{\rm AB}$ is constant at all times with the exception of the switching points, $t = 0$ and $t = \tau$, where some non-zero energy can be passed on AB by the external control (see Ref. [49] for a detailed analysis on the energy cost of modulating the interaction). For the sake of simplicity we set these contributions equal to zero by assuming $\hat{\mathcal{H}}_1$ to commute with the local terms $\hat{\mathcal{H}}_{\rm A} + \hat{\mathcal{H}}_{\rm B}$ [146]. Under this condition, the energy that moves from A to B can be expressed in terms of the mean local energy of the battery at the end of the protocol, i.e. the quantity

$$E_{\rm B}(\tau) \equiv {\rm tr}[\hat{\mathcal{H}}_{\rm B}\rho_{\rm B}(\tau)], \tag{5.2}$$

$\rho_{\rm B}(\tau)$ being the reduced density matrix of the battery at time τ. The next question to ask is which part of $E_{\rm B}(\tau)$ can be extracted from B without having access to the charger (a reasonable scenario in any relevant practical applications where the charger A is not available to the end user), and what is instead locked by the correlations AB have established during the charging process. We recall that a proper measure for this quantity is provided by the ergotropy [43] of the state $\rho_{\rm B}(\tau)$, already introduced in Sect. [**?**]. We remind that given a quantum system X characterized by a local Hamiltonian $\hat{\mathcal{H}}$, the ergotropy $\mathcal{E}(\rho, \hat{\mathcal{H}})$ is a functional which measures the maximum amount of energy that can be extracted from a density matrix ρ of X without wasting into heat. A closed expression for this quantity can be obtained in terms of the difference

$$\mathcal{E}(\rho, \hat{\mathcal{H}}) = E(\rho) - E(\tilde{\rho}), \tag{5.3}$$

between the mean energy $E(\rho) = {\rm tr}[\hat{\mathcal{H}}\rho]$ of the state ρ and of the mean energy $E(\tilde{\rho}) = {\rm tr}[\hat{\mathcal{H}}\tilde{\rho}]$ of the passive counterpart $\tilde{\rho}$ of ρ [43–45, 147–150]. The latter is defined as the density matrix

of X which is diagonal on the eigenbasis of $\hat{\mathcal{H}}$ and whose eigenvalues correspond to a proper reordering of those of ρ, i.e. $\tilde{\rho} = \sum_n r_n |\epsilon_n\rangle \langle\epsilon_n|$ with $\rho = \sum_n r_n |r_n\rangle \langle r_n|$, $\hat{\mathcal{H}} = \sum_n \epsilon_n |\epsilon_n\rangle \langle\epsilon_n|$, with $r_0 \geq r_1 \geq \cdots$ and $\epsilon_0 \leq \epsilon_1 \leq \cdots$, yielding

$$E(\tilde{\rho}) = \sum_n r_n \epsilon_n. \tag{5.4}$$

Notice that, if we set the ground-state energy to zero ($\epsilon_0 = 0$) and if the state is pure then $E(\tilde{\rho}) = 0$ and the ergotropy coincides with the mean energy of ρ, i.e. $\mathcal{E}(\rho, \hat{\mathcal{H}}) = E(\rho)$. On the contrary, if the state is mixed, the extractable work is in general smaller than the mean energy, i.e. $\mathcal{E}(\rho, \hat{\mathcal{H}}) < E(\rho)$. For the problem we are considering since the global system dynamics of AB is unitary and the initial state of the charger-battery system is pure, it remains pure at all times. However, the local state of the battery $\rho_{\rm B}(\tau)$ will be in general mixed because of its entanglement with the charger introducing a non trivial gap between its ergotropy

$$\mathcal{E}_{\rm B}(\tau) \equiv \mathcal{E}(\rho_{\rm B}(\tau), \hat{\mathcal{H}}_{\rm B}), \tag{5.5}$$

and the energy $E_{\rm B}(\tau)$ of Eq. (5.2) it stores at the end of the charging process. As we will show below, the former can be much smaller than the latter for the experimentally relevant case of a system composed by a small number of battery elements [113, 151].

5.3 Results

For the sake of concreteness and the feasibility of its experimental realization, in the remaining of the chapter we focus on a definite model in which the charger A is a photonic cavity coupled to a array of N non-mutually interacting qubits that acts as the battery B [24]. The microscopic Hamiltonian is therefore the one of the Tavis-Cummings model [125, 126]:

$$\hat{\mathcal{H}}_{\rm A} = \omega_0 \hat{a}^\dagger \hat{a} \ , \tag{5.6}$$

$$\hat{\mathcal{H}}_{\rm B} = \omega_0 \sum_{i=1}^{N} \hat{\sigma}_i^+ \hat{\sigma}_i^- \ , \tag{5.7}$$

$$\hat{\mathcal{H}}_1 = g \sum_{i=1}^{N} (\hat{a}\hat{\sigma}_i^+ + \hat{a}^\dagger \hat{\sigma}_i^-) \ , \tag{5.8}$$

where $\hat{a}\,(\hat{a}^\dagger)$ is a bosonic annihilation (creation) operator, $\hat{\sigma}_i^\pm$ are raising/lowering spin operators for the i-th qubit, ω_0 is the characteristic frequency of both subsystems, and g the coupling strength ($\hbar = 1$ throughout this chapter). In this setting we compare the final maximum extractable work measured by the ergotropy $\mathcal{E}_{\rm B}^{(N)}(\tau)$ and the mean energy $E_{\rm B}^{(N)}(\tau)$ of the battery with respect to different initial states $|\psi\rangle_{\rm A}$ of the charger (the label N being added to put emphasis on the size of the B system). We restricting ourselves to three typical quantum optical states [76]: a Fock state, a coherent state, and a squeezed vacuum state, all having the same input energy $E_{\rm A}^{(N)}(0)$ that we set equal to $N\omega_0$ in order to ensure that it matches the full energy capacity of the battery. In Fig. 5.2 we show the stored energy $E_{\rm B}^{(N)}(\tau)$, the energy of the charger $E_{\rm A}^{(N)}(\tau) \equiv {\rm tr}[\hat{\mathcal{H}}_{\rm A}\rho_{\rm A}(\tau)]$ and ergotropy $\mathcal{E}_{\rm B}^{(N)}(\tau)$ as functions of the duration of the charging protocol τ for the case of the input coherent state. We clearly see

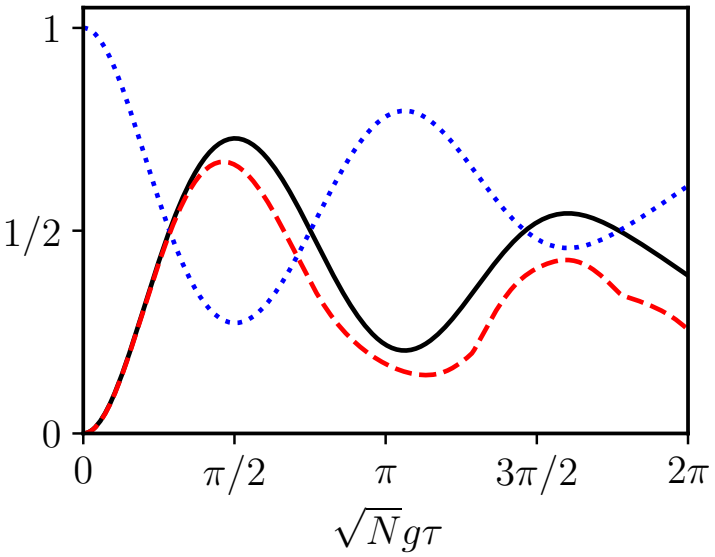

Figure 5.2: The energy $E_{\rm B}^{(N)}(\tau)$ (solid black line), the ergotropy $\mathcal{E}_{\rm B}^{(N)}(\tau)$ (dashed red line), and the energy $E_{\rm A}^{(N)}(\tau)$ (dotted blue line) are shown as functions of $\sqrt{N}g\tau$. All quantities are measured in units of $N\omega_0$. Numerical results in this figure have been obtained by choosing a coherent state for $N = 8$.

that for $\sqrt{N}g\tau \lesssim \pi/4$ the difference between ergotropy and energy is relatively small. Conversely, at large times, correlations between A and B are developed and energy and ergotropy are significantly different.

We now focus on the main point of this work, i.e. a comparison between the fraction of extractable work with respect to the total mean energy of the battery. Consistently with previous approaches already used in the literature [22, 24], we fix the duration of the protocol to the value $\tau = \bar{\tau}$ which ensures the maximum value for the average charging power $P_{\rm B}^{(N)}(\tau) \equiv E_{\rm B}^{(N)}(\tau)/\tau$, i.e. $P_{\rm B}^{(N)}(\tau) \leq P_{\rm B}^{(N)}(\bar{\tau})$.

We start by observing that, as explicitly discussed in App. B, *all* initial states exhibit the same $P_{\rm B}^{(N)}(\bar{\tau}) \propto N^{3/2}$ scaling reported in Ref. [24], where only Fock states were considered. This corresponds to a $\bar{\tau} \propto 1/\sqrt{N}$ collective speed-up of the charging time which is independent of the initial state of A, and valid in particular for a semi-classical coherent state: highly non-classical initial states are therefore not necessary for optimizing the charging part of the protocol.

Next, in Fig. 5.3(a) we illustrate the dependence of the ratio $\mathcal{E}_{\rm B}^{(N)}(\bar{\tau})/E_{\rm B}^{(N)}(\bar{\tau})$ between the extractable work and the mean energy of the battery on the number N of qubits and for the three selected initial states. We clearly see two important facts: (i) for small N, the extractable work can be much smaller than the mean energy of the battery and coherent input states appear to be optimal; (ii) for large values of N, almost all the mean energy of the battery becomes extractable. The latter result justifies a posteriori previous asymptotic approaches [22, 24] to QBs in which only the mean energy was considered as a figure of merit.

Fig. 5.3(b) shows the amount of energy that can be extracted from a fraction of $M \leq N$

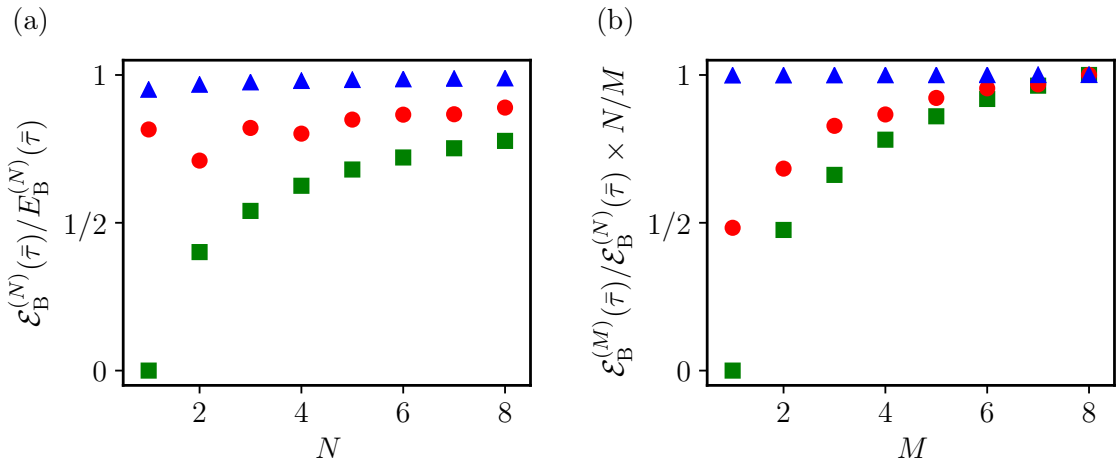

FIGURE 5.3: Panel (a) The ratio $\mathcal{E}_{\rm B}^{(N)}(\bar{\tau})/E_{\rm B}^{(N)}(\bar{\tau})$ as a function of N for three initial states of the charger: a Fock state (red circles), a coherent state (blue triangles), and a squeezed state (green squares). Panel (b) The quantity $\left[\mathcal{E}_{\rm B}^{(M)}(\bar{\tau})/M\right]/\left[E_{\rm B}^{(N)}(\bar{\tau})/N\right]$ as a function of $M \leq N$. Colour coding as in panel (a). Data in panel (b) have been obtained by setting $N = 8$.

qubits (and normalized by M) divided by the same quantity evaluated for all N qubits (and normalized by N), i.e. $\left[\mathcal{E}_{\rm B}^{(M)}(\bar{\tau})/M\right]/\left[\mathcal{E}_{\rm B}^{(N)}(\bar{\tau})/N\right]$. This ratio describes the fraction of energy that can be extracted when only operations on a subset of M qubits are allowed. This is of interest because performing operations on all qubits may be experimentally challenging. Our results show, however, that this is in general not necessary. Indeed, our illustrative results for $N = 8$ demonstrate that operating on a subset of just $M = 4$ is already sufficient to extract $\gtrsim 3/4$ of all the available work. We further note that also in this case the coherent states are optimal. The fraction of extractable work from these initial states is weakly affected by the limitation to local operations on $M \leq N$ qubits, and is practically constant and ≈ 1. These makes coherent states ideal initial charging states for QBs. In App. B, we further elaborate on the fact that coherent states are the optimal choice for work extraction.

5.4 Summary and conclusions

We now discuss on more qualitative grounds the physics behind the two main results emerging from our numerical analysis, i.e. the optimality of coherent states for small N and the asymptotic freedom of the charger-battery system from locking correlations in the $N \gg 1$ limit.

From the definition of ergotropy in Eq. (5.3), it is clear that the more mixed a state is, the more difficult it is to extract its energy, a fact which is analogous to the difficulty of extracting work from a classical thermodynamic system with large entropy. Since the state of the charger-battery is pure, in our quantum model the entropy of the reduced state of the battery is a consequence of its entanglement with the charger. We can therefore say that, for what concerns the capability of work extraction, it is convenient to produce as little entanglement as possible between the charger and the battery. From this argument, we naturally conclude that highly non-classical initial states of the charger (such as Fock or squeezed states), which induce a complex and entangling dynamics, are not optimal for

work extraction. On the contrary, we expect semi-classical states like coherent states, which are well known in quantum optics for producing small entanglement under energy-conserving interactions, to be optimal for maximizing the final ergotropy of the battery (while maintaining the collective speed-up of the charging time). This argument provides a simple yet natural qualitative explanation of our numerical results.

For what concerns instead the asymptotic freedom from locking correlations in the $N \to \infty$ limit, we argue that this is not a peculiar feature of our model but rather a much more universal fact that applies to all those systems whose dynamics is restricted to a small part of the Hilbert space, a phenomenon intrinsically connected with the integrability of the model. In order to understand this point we start again from our previous observation that the charger-battery entanglement is the main limiting factor for the task of work extraction. It is well known that the entanglement entropy of the subsystems of an integrable system usually fails to scale with their size. This phenomenon is also known under the name of *area law* [152–154]. On the contrary, the energy is an extensive quantity, which grows linearly with the size of our battery. For this reason, we expect that the relative ratio between the locked and the extractable energy is negligible in the $N \to \infty$ limit. A way to put this observation on a more rigorous ground is via a result we prove in App. B.4 namely that if the system B is composed of N resonant qubits and the number of non-null eigenvalues of the density matrix ρ_{B} scales polynomially in N, than all its energy is accessible in the thermodynamic limit, i.e.

$$\boxed{\lim_{N\to\infty} \mathcal{E}_{\mathrm{B}}^{(N)}/E_{\mathrm{B}}^{(N)} = 1 \ ,} \tag{5.9}$$

the limit being achieved with a finite-size $1/N$ scaling, as in Fig. 5.3(a).

Now, one can identify at least two relevant classes of models which fulfil the requirements listed above. The first is represented by systems which, as our integrable [155] Tavis-Cummings QB model, are characterized by energy preserving interactions, i.e. $[\hat{\mathcal{H}}_1, \hat{\mathcal{H}}_0] = 0$, and which have a single charger A with a not highly degenerate spectrum and initialized into an input configuration with a sufficiently well behaved energy distribution (e.g. a Fock or a coherent state). In this case, assuming as usual the initial mean energy of A to be proportional to N, the number of relevant eigenvalues of its density matrix $\rho_{\mathrm{A}}(\tau)$ at the end of the charging process will be upper bounded by a quantity d that scales at most polynomially with N. (As a matter of fact, for the Tavis-Cummings QB model the scaling of d is indeed linear with N, see e.g. Refs. [24, 156].) This is a simple consequence of the fact that the energy of A can only be reduced by the interaction with the battery, initially in its ground state. Since the global state of the complete system is pure, the spectrum of $\rho_{\mathrm{A}}(\tau)$ will be equal to the spectrum of $\rho_{\mathrm{B}}(\tau)$ [3] making the number of its non-negligible eigenvalues also equal to d, and hence ultimately leading to Eq. (5.9).

The second class of models for which we expect Eq. (5.9) to hold, are those where the dynamics of the QB is restricted to a small subspace of the entire exponentially large Hilbert space due to the conservation of some operator and the form of the initial state. A notable example is the Dicke model [25], which exhibits conservation of $\hat{J}^2$. In this case, the initial state for the battery has a definite eigenvalue for $\hat{J}^2$, namely $J = N/2$, and hence all the dynamics of B lies in the subspace with a definite J leading once more to Eq. (5.9), as we explicitly show, via numerical analysis in App. B.5.

In summary, by studying a physically well motived QB model, we found that, for a small number of batteries (as in current state-of-the-art solid-state technology [104, 143–145]), the extractable energy can be significantly smaller than the mean energy stored in the devices. This negative effect strongly depends on the choice of the initial state of the charger and we

found that coherent states are optimal for mitigating this phenomenon. For a large number of the batteries, instead, we found that the extractable energy converges to the stored energy. We also argued that this a rather universal phenomenon characterizing all charger-battery systems in which the amount of entanglement is not extensive with respect to the size N of the battery.

6

Quantum versus classical many-body batteries

In this Chapter we compare quantum and classical many-body batteries by studying a series of quantum models which possess a well-defined classical analogue. The results of this work have been published in Ref. [27] and this chapter is largely based upon it.

This Chapter is organized as following. We start this Chapter giving a synopsis (Sect.6.1), then, in Sect. 6.2 we explain how the classical versus quantum comparison is actually carried out in this Chapter, briefly reviewing the correspondence between quantum commutators and classical Poisson brackets. In Sect. 6.3 we recap the charging protocol first introduced in Refs. 24, 49 and introduce the figures of merit needed to evaluate the performance of classical and quantum many-body batteries. In Sect. 6.4 we discuss the first model (single bosonic mode coupled to N harmonic oscillators). We demonstrate analytically that in this case classical and quantum versions of the model display fast charging with the same time scale. In Sect. 6.5 we introduce the second model (N qubits coupled to N qubits) and demonstrate how the classical version of the model outperforms the quantum one. In Sect. 6.6 we compare the Dicke QB model introduced in Ref. 24 (and discussed in Chap. 4) with the corresponding classical analogue, showing numerically that the relative performance depends on the charger-matter coupling g. Finally, in Sect. 6.7 we report a summary of our main findings and our conclusions.

6.1 Synopsis

As we have seen in the previous Chapters, quantum batteries (QBs) [20–24, 26, 46, 48–50, 63, 135] are quantum mechanical systems that are able to store energy. These works have a key common thread in trying to understand whether quantumness yields a temporal speed-up of the charging process. A first, abstract approach [22, 23] studied the possibility to charge N systems via unitary operations. The authors introduced a parallel charging scheme, in which each of the subsystems is acted upon independently of the others, and a collective charging scheme, where global unitary operations acting on the full Hilbert space of all subsystems are allowed. In these works it was shown that the charging time scales with N, decreasing for increasing N. In the collective charging case and for large N, the

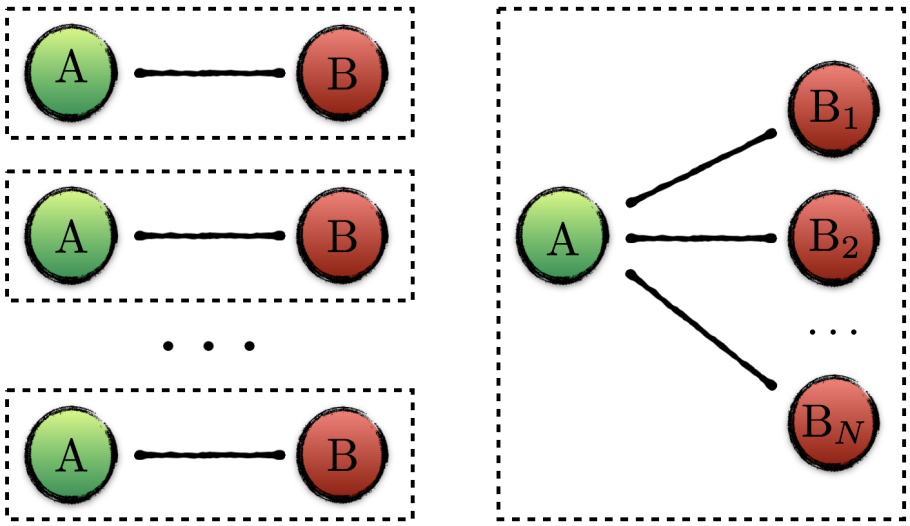

FIGURE 6.1: A sketch of the parallel (left) versus collective (right) charging schemes introduced in the main text.

power delivered by a QB is much larger than the one delivered by the parallel scheme. This speed-up was dubbed "quantum advantage" [22–24, 48]. Furthermore, in Ref. 23 it was shown that entanglement is not required to speed-up the evolution of a QB, since states which are confined in the sphere of separable states share an identical speed-up. However, the authors of Ref. 23 pointed out that such highly mixed states host only a vanishing amount of energy, yielding therefore a highly non-optimal result from the point of view of energy storage and delivery.

In the same spirit, the authors of Refs. 24, 26, 46, 48, 49 studied similar issues but in realistic setups which can be implemented in a laboratory, such as arrays of qubits in cavities [24, 26, 46, 49] and spin chains in external magnetic fields [48]. In Refs. 24, 26, 46, 49, the battery units are not charged via abstract unitaries but, rather, by other quantum mechanical systems dubbed "chargers". In this framework, the parallel scheme is the one in which each battery is charged by its own charger, independently of the others—see Fig. 6.1. On the contrary, the collective scheme is the one in which all batteries are charged by the very same charger. Also in this context, the collective scheme outperforms the parallel one in terms of speed of the charging process. Finally, the authors of Ref. 48 demonstrated that quantum batteries have the potential for faster charging over their classical counterparts. As they noticed, however, the classical counterparts were assumed to be composed of non-interacting units.

In this Chapter we compare the performance of QBs with that of their appropriate classical versions. Such comparison is clearly of great interest for foundational reasons but may have also implications on the development of scalable solid-state systems where energy transfer processes and their time scales can be studied experimentally. Indeed, despite any solid-state QB device is going to operate on the basis of electrons, photons, spins, etc, which are microscopically ruled by the laws of quantum mechanics, often classical descriptions of their collective behavior may be applied. An example is provided by the elementary charged collective excitations in metals and semiconductors, i.e. plasmons, which are almost always well

captured by the random phase approximation and behave classically in the long-wavelength limit [85, 86]. We focus on three models. In the first one, a single bosonic mode (the charger) is coupled to N harmonic oscillators (the proper battery composed of N subunits). In the second one, N qubits playing the role of charging units are coupled to another set of N qubits playing the role of the proper battery. Finally, the third one is the Dicke QB introduced in Ref. 24. In the first case, the performance of classical and quantum versions of the model is identical. In the second case, the classical version outperforms the quantum one. In the third case, there is a range of values of the charger-matter coupling parameter g for which the quantum (classical) model performs better than the classical (quantum) one.

6.2 Comparison between quantum and classical mechanics

In quantum mechanics, the evolution of an operator $\hat{O}$ in time t is described by the Heisenberg equation of motion $\hbar\, d\hat{O}(t)/dt = i[\mathcal{H}, \hat{O}(t)]$, where $\hat{\mathcal{H}}$ is the Hamiltonian. Moreover, canonically conjugate variables, such as position $\hat{q}_i$ and momentum $\hat{p}_j$, fulfill the commutation relation $[\hat{q}_i, \hat{p}_j] = i\hbar\delta_{i,j}$. In the case of angular momentum $\hat{\boldsymbol{J}}$, a similar relation holds between different components: $[\hat{J}_i, \hat{J}_j] = \sum_k i\hbar\epsilon_{ijk}\hat{J}_k$, where ϵ_{ijk} is the Levi-Civita tensor.

In Hamiltonian mechanics, a classical physical system is uniquely described by a set of canonical coordinates $\boldsymbol{x}^{\mathrm{T}} = (\boldsymbol{p}, \boldsymbol{q})$, where the components q_i, p_i are conjugate variables obeying $\{q_i, p_j\} = \delta_{i,j}$. Here, $\{u, v\} \equiv \sum_i (\partial_{q_i} u\ \partial_{p_i} v - \partial_{p_i} u\ \partial_{q_i} v)$ denotes the Poisson brackets.

The time evolution of the system is uniquely defined by Hamilton's equations:

$$\begin{aligned} \frac{dq_i}{dt} &= \partial_{p_i}\mathcal{H}^{\mathrm{cl}}(\boldsymbol{x}) \ , \\ \frac{dp_i}{dt} &= -\partial_{q_i}\mathcal{H}^{\mathrm{cl}}(\boldsymbol{x}) \ . \end{aligned} \tag{6.1}$$

A proper comparison between quantum and classical systems can be made by following the canonical quantization procedure [157]. Once the Hamilton's function $\mathcal{H}^{\mathrm{cl}}(\boldsymbol{x})$ of a classical system is written in terms of conjugate variables with Poisson brackets $\{q_i, p_j\} = \delta_{i,j}$, quantization is carried out by replacing classical coordinates by operators and enforcing canonical commutation relations instead of canonical Poisson brackets.

While finding the classical analog of a quantum system with degrees of freedom that are position and momentum is straightforward and consists in making the replacements $\hat{q}_i \to q_i$ and $\hat{p}_j \to p_j$, the classical version of quantum mechanical angular momentum is more subtle. It turns out [88, 158] that the right choice is to replace the components $\hat{J}^i$ of the angular momentum operator $\hat{\boldsymbol{J}}$, with $\hat{\boldsymbol{J}}^2 = \hbar^2 J(J+1)$, with the classical canonical coordinates $J^z = J\cos(\theta)$ and $\phi = \arctan(J^y/J^x)$, so that $\{J\cos(\theta), \phi\} = 1$, i.e. $\hat{J}^z \to J\cos(\theta)$, $\hat{J}^x \to J\sin(\theta)\cos(\phi)$, and $\hat{J}^y \to J\sin(\theta)\sin(\phi)$.

In the remainder of this Chapter we set $\hbar = 1$.

6.3 Charging protocol and figures of merit

We start by reviewing a model for the charging process of a QB [24, 26, 46, 49]. As stated above, the classical and quantum cases are both described by a Hamiltonian formalism. We can therefore introduce the charging protocol in terms of a general Hamiltonian, without specifying *a priori* whether we treat the classical or quantum case. As such, we will describe the protocol in general, commenting explicitly on the classical and quantum cases only when it is needed.

As already discussed in Chaps.**??**,in our charging protocol [24, 26, 46, 49], a first system A acts as the energy "charger" for a second system B, which instead acts as the proper battery. They are characterized by local Hamiltonians $\hat{\mathcal{H}}_{\rm A}$ and $\hat{\mathcal{H}}_{\rm B}$, respectively, which, for the sake of convenience, are both chosen to have zero ground-state energy. We also assume B to be composed of N non-mutually interacting elements. (Effective interactions between these elements are induced by the charger. In the Dicke QB case, for example, the cavity mode induces effective interactions between all the qubits.) In the quantum case, the system at time $t = 0$ is in a pure factorized state $|\psi(0)\rangle_{\rm AB} = |\psi\rangle_{\rm A} \otimes |{\rm G}\rangle_{\rm B}$, $|{\rm G}\rangle_{\rm B}$ being the ground state of $\hat{\mathcal{H}}_{\rm B}$ and $|\psi\rangle_{\rm A}$ having mean local energy $E_{\rm A}^{(N)}(0) \equiv {}_{\rm A}\langle\psi|\hat{\mathcal{H}}_{\rm A}|\psi\rangle_{\rm A} > 0$, where N is the number of elements which compose the battery. Analogously, in the classical case we impose that the system B at time $t = 0$ is in the configuration with the lowest energy and we fix the energy in the charger A to be $E_{\rm A}^{(N)}(0) > 0$.

By switching on a coupling Hamiltonian $\hat{\mathcal{H}}_1$ between A and B, our aim is to provide as much energy as possible to B, in some finite amount of time τ, the charging time of the protocol. For this purpose, we write the global Hamiltonian of the AB system as

$$\hat{\mathcal{H}}(t) \equiv \hat{\mathcal{H}}_{\rm A} + \hat{\mathcal{H}}_{\rm B} + \lambda(t)\hat{\mathcal{H}}_1 \ , \tag{6.2}$$

where $\lambda(t)$ is a time-dependent parameter that represents the external control we exert on the system, and which we assume to be given by a step function equal to 1 for $t \in [0, \tau]$ and zero elsewhere. Accordingly, in the quantum case, we denote by $|\psi(t)\rangle_{\rm AB} = \exp\big[-i\hat{\mathcal{H}}(t)t\big]|\psi(0)\rangle_{\rm AB}$ the evolved state of the AB system at time t, $\hat{\mathcal{H}}(t)$ being constant at all times with the exception of the switching points, $t = 0$ and $t = \tau$, and by $E(t) \equiv {}_{\rm AB}\langle\psi(t)|\hat{\mathcal{H}}(t)|\psi(t)\rangle_{\rm AB}$ its total energy. We note that the total energy is a constant of the motion, i.e. $-idE(t)/dt = {}_{\rm AB}\langle\psi(t)|\big\{\big[\hat{\mathcal{H}}(t), \hat{\mathcal{H}}(t)\big] - i\partial\hat{\mathcal{H}}(t)/(\partial t)\big\}|\psi(t)\rangle_{\rm AB} = 0$, with the exception of the switching points, in which $\partial\hat{\mathcal{H}}(t)/\partial t \neq 0$. At the two time instants $t = 0$ and $t = \tau$ a non-zero energy can be transferred to AB by the external control. (See Ref. 49 for a detailed analysis of the energy cost of modulating the interaction.)

The same conditions hold in the classical case where we denote by $\boldsymbol{x}^{\rm T}(t) = (\boldsymbol{p}(t), \boldsymbol{q}(t))$ and $E(t) = \mathcal{H}^{\rm cl}\big(\boldsymbol{x}(t)\big)$ the solution of Hamilton's equations of motion and the total energy at time t, respectively. Here, $\boldsymbol{p}$ and $\boldsymbol{q}$ are classical conjugate variables. It is also useful to define the vector $\boldsymbol{x}_{\rm B}^{\rm T}(t) = (\boldsymbol{p}_{\rm B}(t), \boldsymbol{q}_{\rm B}(t))$, denoting the position in phase space of B at time t.

In the quantum case, we are mainly interested in the mean local energy of the battery at the end of the protocol, already defined in Eq.(5.2), i.e.

$$E_{\rm B}^{(N)}(\tau) \equiv {\rm tr}[\hat{\mathcal{H}}_{\rm B}\rho_{\rm B}(\tau)] \ , \tag{6.3}$$

$\rho_{\rm B}(\tau)$ being the reduced density matrix of the battery at time τ. It is worth noticing that while $E_{\rm B}^{(N)}(\tau)$ does not necessarily represent the amount of energy that one can recover from the battery after charging, it has been shown that for large enough N this is not a relevant issue [26]. In the classical case, the corresponding quantity is the energy in B, $E_{\rm B}^{(N)}(\tau) = \mathcal{H}_{\rm B}^{\rm cl}(\boldsymbol{x}_{\rm B}(\tau))$.

The performance of the charger-battery set-up can be studied by analyzing the average storing power $P_{\rm B}^{(N)}(\tau) \equiv E_{\rm B}^{(N)}(\tau)/\tau$. Specifically, we define the maximum average power as $\bar{P}_{\rm B}^{(N)} \equiv \max_\tau[P_{\rm B}^{(N)}(\tau)]$. Finally, we introduce the optimal charging time $\bar{\tau}$, $\bar{P}_{\rm B}^{(N)} = P_{\rm B}^{(N)}(\bar{\tau})$, and the energy at the maximum power, $\bar{E}_{\rm B}^{(N)} \equiv E_{\rm B}^{(N)}(\bar{\tau})$.

Our aim is to compare the parallel charging scenario against the collective one [22–24]. As mentioned above, we define as a parallel charging, the protocol in which N batteries are

independently charged by N chargers. Each charger has an energy $E_{\rm A}^{(1)}(0)$. Conversely, the collective charging case is the one in which all N batteries are charged by the same charger. In order to do a clear comparison, in the collective charging case we impose that the charger has total energy equal to the sum of the energies of all the chargers of the parallel charging scheme, i.e. $E_{\rm A}^{(N)}(0) = NE_{\rm A}^{(1)}(0)$.

Since we are interested in comparing the power of the protocols, we denote by the symbol $\bar{P}_\sharp$ ($\bar{P}_\parallel$) the maximum power in the collective (parallel) protocol. Following Ref. 23, we introduce the so-called collective advantage:

$$\Gamma \equiv \frac{\bar{P}_\sharp}{\bar{P}_\parallel} \ . \tag{6.4}$$

We have $\bar{P}_\sharp = \bar{P}_{\rm B}^{(N)}$ and $\bar{P}_\parallel = N\bar{P}_{\rm B}^{(1)}$. The latter property follows from the fact that the power in the parallel charging scheme is trivially extensive.

The figure of merit in Eq. (6.4) quantifies how convenient is to charge a battery in a collective fashion rather than in a parallel way. While in Refs. 23, 24 this quantity is named "quantum advantage", it is possible to define Γ also in the classical case. Since our main goal is to compare quantum and classical batteries, we will denote by $\Gamma_{\rm qu}$ the collective advantage produced by a quantum Hamiltonian and by $\Gamma_{\rm cl}$ the collective advantage produced by the analog classical Hamiltonian. What matters is therefore the ratio

$$R \equiv \frac{\Gamma_{\rm qu}}{\Gamma_{\rm cl}} \ . \tag{6.5}$$

If $R = 1$, the QB and its classical analog share the same collective boost in the charging process. Conversely, having $R > 1$ means that there is a genuine quantum advantage. Finally, $R < 1$ means that the collective dynamics in the classical model is more beneficial.

The quantity R will be crucial below in determining if fast charging is due to exquisitely quantum resources or, rather, if it has a collective (i.e. many-body) origin due to effective interactions between the battery subunits, which is present also in the classical case. It is important to stress that we only considered QBs charged via another quantum system. Another possibility it is to consider a battery charged via a classical external source [46] or a quench in the Hamiltonian [22, 23].

6.4 Harmonic oscillator batteries

In this Section we study a system composed by $N + 1$ harmonic oscillators, one acting as a charger while the remaining N playing the role of the proper battery. This system is described by the following Hamiltonian,

$$\begin{aligned} \hat{\mathcal{H}}_{\rm A} &= \omega_0 \hat{a}^\dagger \hat{a} \ , \\ \hat{\mathcal{H}}_{\rm B} &= \omega_0 \sum_i \hat{b}_i^\dagger \hat{b}_i \ , \\ \hat{\mathcal{H}}_1 &= g \sum_i \left(\hat{a}\hat{b}_i^\dagger + \hat{a}^\dagger \hat{b}_i \right) \ , \end{aligned} \tag{6.6}$$

where a (b_i) is the destruction bosonic operator acting on A (on the i-th unit of the battery B), and ω_0 and g are the characteristic frequency of both systems and the charger-battery coupling parameter, respectively. For simplicity, we choose $E_{\rm A}^{(1)}(0) = \omega_0$.

It is useful to introduce the bright mode [159] $\hat{B} = \sum_i \hat{b}_i/\sqrt{N}$, which is a bosonic mode fulfilling $[\hat{B}, \hat{B}^\dagger] = 1$. Expressing the Hamiltonian in terms of the bright mode, we obtain:

$$\begin{aligned} \hat{\mathcal{H}}_{\rm B} &= \omega_0 \hat{B}^\dagger \hat{B} \ , \\ \hat{\mathcal{H}}_1 &= g_N \left(\hat{a}\hat{B}^\dagger + \hat{a}^\dagger \hat{B} \right) \ , \end{aligned} \tag{6.7}$$

where

$$g_N \equiv \sqrt{N} g \ . \tag{6.8}$$

Hence, the AB system is equivalent to two harmonic oscillators with a renormalized coupling g_N. It is straightforward to obtain the dynamics of the energy of B, which is independent of the initial state $|\psi\rangle_{\rm A}$ in A, once we fix the condition $E_{\rm A}^{(N)}(0) = N\omega_0$. In order to calculate the stored energy (5.2) we find then useful to adopt the Heisenberg representation, writing $E_{\rm B}^{(N)}(\tau) = {\rm tr}[\rho_{\rm AB}(0)\hat{\mathcal{H}}_{\rm B}(\tau)]$, where $\rho_{\rm AB}(0)$ is the density matrix of the full system at the initial time, with $\hat{\mathcal{H}}_{\rm B}(\tau) \equiv e^{i\hat{\mathcal{H}}\tau}\hat{\mathcal{H}}_{\rm B}e^{-i\hat{\mathcal{H}}\tau}$. Expressing $\hat{a}$ and $\hat{b}$ as functions of the normal operators $\hat{\gamma}_\pm = (\hat{a} \pm \hat{B})\sqrt{2}$ and using that the latter evolve simply as $\hat{\gamma}_\pm(t) = e^{-i\omega_\pm t}\hat{\gamma}_\pm$ with $\omega_\pm = \omega_0 \pm g_N$, we obtain

$$\hat{\mathcal{H}}_{\rm B}(\tau) = \frac{\omega_0}{2}\left\{ \hat{a}^\dagger\hat{a} + \hat{B}^\dagger\hat{B} - \left[\frac{e^{-i2g_N\tau}}{2}(\hat{a}^\dagger\hat{a} - \hat{B}^\dagger\hat{B} + \hat{B}^\dagger\hat{a} - \hat{a}^\dagger\hat{B}) + {\rm H.c.} \right] \right\} ,$$

and, finally:

$$E_{\rm B}^{(N)}(\tau) = N\omega_0 \sin^2(g\sqrt{N}\tau) \ . \tag{6.9}$$

Defining $Y = \max_x[\sin^2(x)/x]$, the maximum power reads $\bar{P}_{\rm B}^{(N)} = N\sqrt{N}g\omega_0 Y$. Accordingly, we have:

$$\Gamma_{\rm qu} = \sqrt{N} \ . \tag{6.10}$$

We note that if $|\psi\rangle_{\rm A}$ is a coherent state, the evolved state $|\psi(t)\rangle_{\rm AB}$ remains factorized at all times [49, 76]. This is an example where the advantage is present, despite the total absence of correlations.

Now we study the classical analog of the quantum model in Eq. (6.6), which can be simply obtained by reversing the quantization procedure and substituting quantum commutators with classical Poisson brackets. The corresponding classical Hamiltonian describes a set of coupled springs:

$$\begin{aligned} \mathcal{H}_{\rm A}^{\rm cl} &= \frac{\omega_0}{2}\left(p_a^2 + q_a^2\right) , \\ \mathcal{H}_{\rm B}^{\rm cl} &= \frac{\omega_0}{2}\sum_i \left(p_{b_i}^2 + q_{b_i}^2\right) \ , \\ \mathcal{H}_1^{\rm cl} &= g\sum_i \left(q_a q_{b_i} + p_a p_{b_i}\right) \ , \end{aligned} \tag{6.11}$$

where (p_a, q_a) are conjugate variables of the charger and $(\boldsymbol{p}_{b_i}, \boldsymbol{q}_{b_i})$ are conjugate variables of the i-th battery. As earlier, we choose $E_{\rm A}^{(1)}(0) = \omega_0$. We now introduce $Q_b = \sum_i q_{b_i}/\sqrt{N}$ and $P_b = \sum_i p_{b_i}/\sqrt{N}$. The classical Hamiltonian becomes

$$\begin{aligned} \mathcal{H}_{\rm B}^{\rm cl} &= \frac{\omega_0}{2}\left(P_b^2 + Q_b^2\right) \ , \\ \mathcal{H}_1^{\rm cl} &= g_N\left(q_a Q_b + p_a P_b\right) \ . \end{aligned} \tag{6.12}$$

We conclude that also in the classical case the model maps into that of two coupled oscillators with a renormalized coupling g_N.

Hamilton's equations of motion follow from Eqs. (6.1), (6.11), and (6.12):

$$\begin{aligned}
\frac{dp_a}{dt} &= -\omega_0 q_a - g_N Q_b \ , \\
\frac{dq_a}{dt} &= \omega_0 p_a + g_N P_b \ , \\
\frac{dP_b}{dt} &= -\omega_0 Q_b - g_N q_a \ , \\
\frac{dQ_a}{dt} &= \omega_0 P_b + g_N p_a \ .
\end{aligned} \tag{6.13}$$

Solving these equations we find that, irrespective of the particular initial condition, given the constraint $E_{\rm A}^{(N)}(0) = N\omega_0$, the stored energy reads $E_{\rm B}^{(N)}(\tau) = N\omega_0 \sin^2(g\sqrt{N}\tau)$. This implies

$$\Gamma_{\rm cl} = \sqrt{N} \ , \tag{6.14}$$

and $R = 1$. This is the main result of this Section. For the case of harmonic oscillator batteries defined in (6.6), fast charging, i.e. $\Gamma \propto \sqrt{N}$, is solely due to the collective behavior of the underlying many-particle system, and does not have its roots in the quantumness of its Hamiltonian.

6.5 Spin batteries

In this Section we study a system composed by N qubits, acting as charger, coupled to another set of N qubits, which play the role of the battery. The quantum Hamiltonian is

$$\begin{aligned}
\hat{\mathcal{H}}_{\rm A} &= \omega_0 \left(\hat{J}^z_{(a)} + \frac{N}{2} \right) \ , \\
\hat{\mathcal{H}}_{\rm B} &= \omega_0 \left(\hat{J}^z_{(b)} + \frac{N}{2} \right) \ , \\
\hat{\mathcal{H}}_1 &= 4g \left(\hat{J}^x_{(a)} \hat{J}^x_{(b)} + \hat{J}^y_{(a)} \hat{J}^y_{(b)} \right) \ ,
\end{aligned} \tag{6.15}$$

where $\hat{J}^\alpha_{(a)}$ ($\hat{J}^\alpha_{(b)}$) with $\alpha = x, y, z$ are the components of a collective spin operator of length $J = N/2$ acting on the Hilbert space of the charger A (battery B), while all the other parameters have the same meaning as in Eq. (6.6).

Defining $\hat{\mathcal{H}}_0 = \hat{\mathcal{H}}_{\rm A} + \hat{\mathcal{H}}_{\rm B}$, the propagator in the interaction picture simply reads $\tilde{U}_t = e^{i\hat{\mathcal{H}}_0 t} e^{-i\hat{\mathcal{H}} t} = e^{-i\hat{\mathcal{H}}_1 t}$. Hence, in this model there is no dependence of the dynamics on the energy scale ω_0, and $\tilde{U}_t$ depends only on the product gt. As in the case of Eq. (6.10), this scaling implies that the collective advantage $\Gamma_{\rm qu}$ for this model does not depend on the value of g but only on N. In Fig. 6.2(a) we report the log-log plot of the collective advantage $\Gamma_{\rm qu}$ as a function of N. Fits to the numerical data (not shown) indicate a quasi-linear dependence on N for large N of the form

$$\Gamma_{\rm qu} \propto N^\alpha \ , \tag{6.16}$$

with $\alpha \sim 1$ and a proportionality constant ~ 0.25.

We now move on to analyze the classical case. Following the discussion of Sect. 6.2, we model the analog classical Hamiltonian as

$$\begin{aligned}\mathcal{H}_{\rm A}^{\rm cl} &= N\omega_0\frac{\big[\cos(\theta_a)+1\big]}{2},\\ \mathcal{H}_{\rm B}^{\rm cl} &= N\omega_0\frac{\big[\cos(\theta_b)+1\big]}{2}\ ,\\ \mathcal{H}_{1}^{\rm cl} &= gN^2\sin(\theta_a)\sin(\theta_b)\cos(\phi_a-\phi_b)\ ,\end{aligned} \tag{6.17}$$

where $(N\cos(\theta_a)/2,\phi_a)$ and $(N\cos(\theta_b)/2,\phi_b)$ are conjugate variables [88, 158].

Hamilton's equations of motion follow from Eqs. (6.1) and (6.17). We find

$$\begin{aligned}\frac{d\cos(\theta_a)}{dt} &= 2gN\sin(\theta_a)\sin(\theta_b)\sin(\phi_a-\phi_b),\\ \frac{d\phi_a}{dt} &= \omega_0-2gN\cot(\theta_a)\sin(\theta_b)\cos(\phi_a-\phi_b)\ .\end{aligned} \tag{6.18}$$

Since the Hamiltonian is invariant under the exchange of variables $a\leftrightarrow b$, the equations of motion for $\cos(\theta_b)$ and ϕ_b can be simply obtained by exchanging $a\leftrightarrow b$.

It is now useful to define $\varphi_a=\phi_a+\omega_0 t$ and $\varphi_b=\phi_b+\omega_0 t$, which allow us to write Eq. (6.18) as follows:

$$\begin{aligned}\frac{d\cos(\theta_a)}{dt} &= 2gN\sin(\theta_a)\sin(\theta_b)\sin(\varphi_a-\varphi_b),\\ \frac{d\varphi_a}{dt} &= -2gN\cot(\theta_a)\sin(\theta_b)\cos(\varphi_a-\varphi_b)\ .\end{aligned} \tag{6.19}$$

These equations show that the only energy scale in the problem is gN. On the basis of simple dimensional analysis we therefore expect $\bar{\tau}\propto 1/(gN)$. Accordingly, since the energy of the system is always extensive, the power scales like $\bar{P}\propto N/\bar{\tau}$. This will yield $\bar{P}_{\parallel}\propto N$ while $\bar{P}_{\sharp}\propto N^2$ leading to $\Gamma_{\rm cl}\propto N$. This argument is not asymptotic, i.e. does not only apply for $N\gg 1$. In Fig. 6.2(b) we plot the classical collective advantage obtained by solving numerically Hamilton's equation of motion. Indeed, we clearly see a linear growth in N, also for small values of N, perfectly consistent with the dimensional argument.

Finally, in Fig. 6.2(c) we show the ratio R defined as in Eq. (6.5), for the case of our spin batteries. We conclude that, for this model, quantum mechanical dynamics yields a *disadvantage* rather than an advantage, as $R<1$ for all N. This is the second main result of this Chapter.

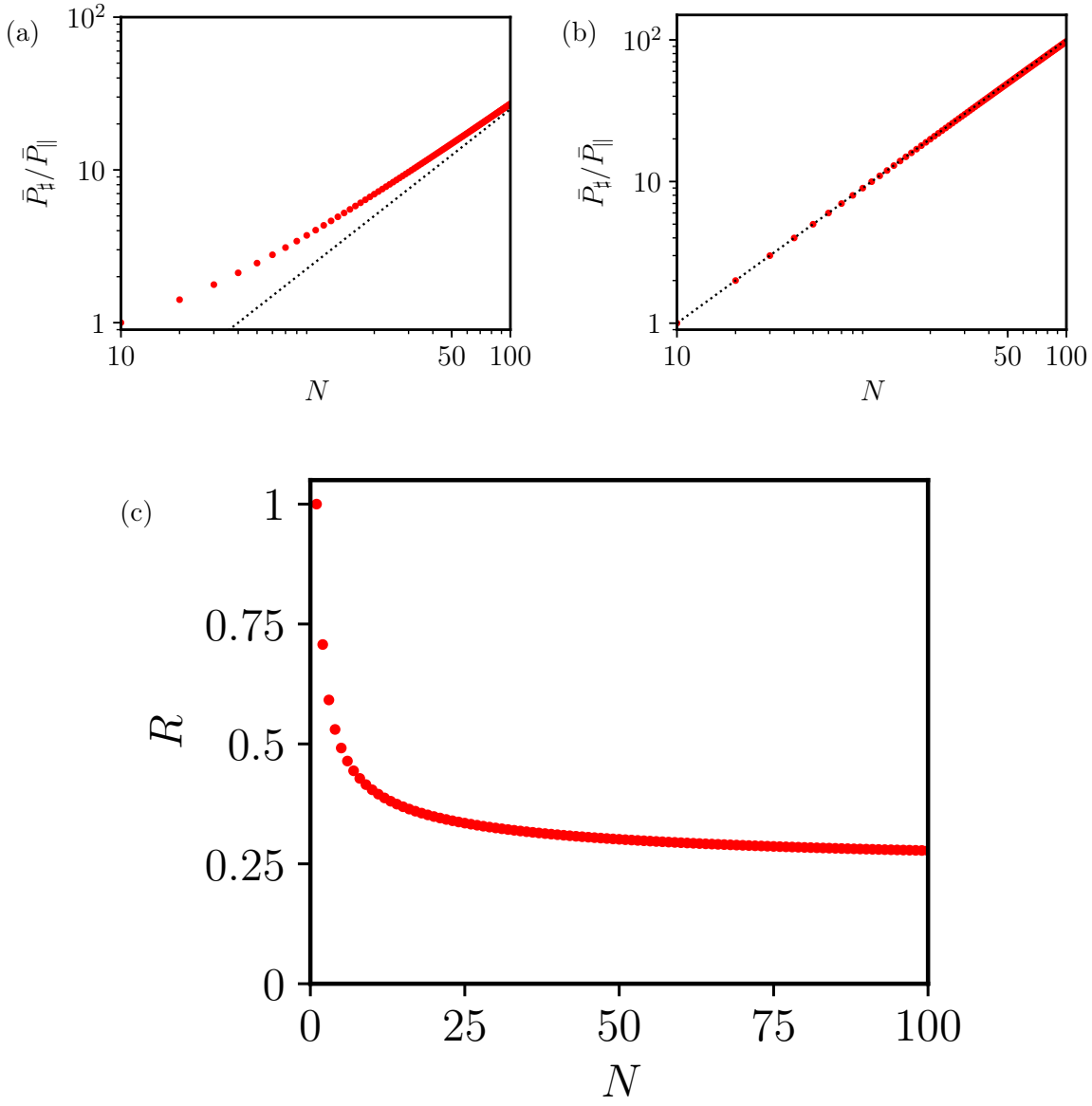

Figure 6.2: Performance of quantum and classical spin batteries—see Sect. 6.5. Panel (a) shows the advantage $\Gamma_{\rm qu}$ in the quantum case, plotted as a function of N, in a log-log scale. The black dashed line represents perfectly linear scaling in N, i.e. $\alpha = 1$ in Eq. (6.16), with a proportionality constant on the order of ~ 0.25. Panel (b) Same as in panel (a), but for the classical case. In this case the scaling is again linear in N with proportionality constant that is, however, equal to 1. Panel (c) shows the ratio $R = \Gamma_{\rm qu}/\Gamma_{\rm cl}$ as a function of N. Notice that, for large enough N, R approaches ~ 0.25, i.e. the ratio between the prefactors of the linear scaling with N of the quantum and classical advantages. Results in this figure do not depend on g.

6.6 Dicke batteries

In this Section we study the case of Dicke batteries [24, 26]. In a Dicke QB, one cavity mode, acting as charger, is coupled to N qubits, which play the role of the battery. The quantum Hamiltonian is [24] (see also Refs. 25 [1].)

$$\begin{aligned} \hat{\mathcal{H}}_{\rm A} &= \omega_0\, \hat{a}^\dagger \hat{a}\ , \\ \hat{\mathcal{H}}_{\rm B} &= \omega_0 \left(\hat{J}^z + \frac{N}{2} \right)\ , \\ \hat{\mathcal{H}}_1 &= 2g \left(\hat{a}^\dagger + \hat{a} \right) \hat{J}^x\ , \end{aligned} \tag{6.20}$$

where $\hat{J}^\alpha$ with $\alpha = x, y, z$ are the components of a collective spin operator of length $J = N/2$, while all the other parameters have the same meaning as in Eq. (6.6). As in the other models introduced in previous Sections, we choose $E_{\rm A}^{(1)}(0) = \omega_0$. Moreover, for the sake of simplicity, we fix $|\psi\rangle_{\rm A}$ to be a Fock state. In Refs. 26, 49 it was shown that the particular choice of the initial state does not change qualitatively the collective advantage. While a detailed analysis of Dicke QBs is reported in Ref. 24, here we summarize the main findings—Fig. 6.3(a)—and compare them with those obtained for the classical analog of a Dicke QB.

In Fig. 6.3(a) we plot the collective advantage $\Gamma_{\rm qu}$ of a Dicke QB for different choices of the coupling parameter g. In agreement with Ref. 24, fits to the numerical data (not shown) suggest the following power-law scaling in the limit of large N

$$\Gamma_{\rm qu} \propto \sqrt{N}\ . \tag{6.21}$$

We now analyze the classical case. In the literature there is a well-established classical analog of the Dicke model [158, 160, 161], which reads as follow

$$\begin{aligned} \mathcal{H}_{\rm A}^{\rm cl} &= \frac{\omega_0}{2} \left(p_a^2 + q_a^2 \right), \\ \mathcal{H}_{\rm B}^{\rm cl} &= N\omega_0 \frac{\big[\cos(\theta) + 1 \big]}{2}\ , \\ \mathcal{H}_1^{\rm cl} &= g\sqrt{2} N q_a \sin(\theta) \cos(\phi)\ , \end{aligned} \tag{6.22}$$

where (p_a, q_a) and $(N\cos(\theta)/2, \phi)$ are classical conjugate variables [88, 158]. We remind the reader that this procedure is carefully discussed in Section 6.2. This Hamiltonian describes a spring coupled to a nonlinear pendulum of length N.

We would like to stress that the model defined by Eq. (6.22) is not a semi-classical approximation of the quantum Hamiltonian in Eq. (6.20), but represents instead an intrinsically

[1] The Hamiltonian in Eq. (6.20) has been widely used in the literature [63, 158] with a different normalization of the coupling constant, namely with the replacement $g \to g/\sqrt{N}$. This different choice guarantees well-defined results [63] if one works in the thermodynamic limit defined by $N \to \infty$, $L \to \infty$ with $n \equiv N/L = \text{const}$, where L is the length of the cavity. In this limit, the length of the cavity scales with the number N of qubits in order to keep the density n of qubits constant. Whether one uses Eq. (6.20) or Eq. (6.20) with the replacement $g \to g/\sqrt{N}$ ultimately depends on the experimental setup. For example, in circuit-QED setups like the one realized in Ref. 104, the length of the photonic cavity (i.e. the length of the transmission line resonator) does not scale with the number of qubits (i.e. the number of transmons). Indeed, in Ref. 104 the resonator is ~ 20 mm long, while a transmon has a linear size which is on the order of 300 μm. This implies that the resonator used in the setup of Ref. 104 can host something like $N = 40$-50 qubits, without any need to scale its length with N for their accommodation. The authors of Ref. 104 used the same Hamiltonian as in Eq. (6.20) and Ref. 24 to explain their data

classical description of a classical spin coupled to a cavity, directly obtainable from classical Hamiltonian mechanics. Our aim is indeed not to approximate the quantum model, but to understand the differences between the quantum and the classical batteries.

As in all previous cases, we choose $E_{\rm A}^{(1)}(0) = \omega_0$. We still have the freedom to choose initial conditions, since the previous condition imposes only the constraint $p_a^2(0)+q_a^2(0) = 2N\omega_0$. For the sake of simplicity, we choose $p_a(0) = q_a(0)$. We have checked that other initial conditions do not alter our main conclusions.

From Eqs. (6.1) and (6.22) we find Hamilton's equations of motion for the classical Dicke battery:

$$\begin{aligned}
\frac{dp_a}{dt} &= -\omega_0 q_a - \sqrt{2}Ngq_a \sin(\theta)\cos(\phi) \ , \\
\frac{dq_a}{dt} &= \omega_0 p_a \ , \\
\frac{d\cos(\theta)}{dt} &= 2\sqrt{2}gq_a \sin(\theta)\sin(\phi), \\
\frac{d\phi}{dt} &= \omega_0 - 2\sqrt{2}gq_a \cos(\phi)\cot(\theta) \ .
\end{aligned} \tag{6.23}$$

We can rescale these equations in such a way to have $P_a^2(0) + Q_a^2(0) = 2$, i.e. $P_a = \sqrt{N}p_a$ and $Q_a = \sqrt{N}q_a$. We obtain:

$$\begin{aligned}
\frac{dP_a}{dt} &= -\omega_0 Q_a - \sqrt{2}g_N Q_a \sin(\theta)\cos(\phi) \ , \\
\frac{dQ_a}{dt} &= \omega_0 P_a \ , \\
\frac{d\cos(\theta)}{dt} &= 2\sqrt{2}g_N Q_a \sin(\theta)\sin(\phi), \\
\frac{d\phi}{dt} &= \omega_0 - 2\sqrt{2}g_N Q_a \cos(\phi)\cot(\theta) \ ,
\end{aligned} \tag{6.24}$$

where $g_N \equiv \sqrt{N}g$ has been defined in Eq. (6.8). We note that, in these equations, the only parameters with physical dimensions (of energy) are ω_0 and g_N. Since $\bar{\tau}$ has physical dimensions of inverse energy (in our units), the optimal charging time must have the following form:

$$\bar{\tau} = \frac{1}{g_N} F(\omega_0/g_N) \ , \tag{6.25}$$

where $F(x)$ is an unknown dimensionless function. From this expression we can conclude that, as long as $F(x)$ does not reach zero for $x = 0$, also in the classical scenario the collective advantange parameter will exhibit a $\sqrt{N}$ scaling similar to the one in Eq. (6.21) observed for the quantum counterpart, i.e. $\Gamma_{\rm cl} \propto \sqrt{N}$. Indeed, assuming $F(0) \neq 0$, from (6.25) it follows that for large enough N the charging time can be approximated as $\bar{\tau} \simeq F(0)/g_N$ with a $1/\sqrt{N}$ scaling. Accordingly, since the energy is an extensive quantity, we will have $\bar{P} \propto N/\bar{\tau}$. This relation yields, asymptotically, $\bar{P}_{\rm B}^{(N)} \propto N\sqrt{N}$, which implies $\Gamma_{\rm cl} \propto \sqrt{N}$ as anticipated. To put this observation on a firmer ground, we resort to numerical integration of Eqs. (6.23). In Fig. 6.3(b) we plot the collective advantage $\Gamma_{\rm cl}$ as a function of N, for different values of g. A comparison with the expected $\sqrt{N}$ scaling of $\Gamma_{\rm cl}$ in the large-N limit is also shown. (The expected saturation to the $\sqrt{N}$ scaling law requires $g_N/\omega_0 \gg 1$ and is therefore difficult to reach numerically for small values of g/ω_0.)

We now proceed with a more quantitative comparison between $\Gamma_{\rm qu}$ and $\Gamma_{\rm cl}$. In Fig. 6.3(c) we report the plot of the quantity R of Eq. (6.5) as a function of N, for different values of g. We clearly see that the ratio R can be smaller or larger than unity depending on the value of g. This is emphasized in Fig. 6.3(d), where we show R as a function of g for $N = 50$. This is the third main result of this Chapter. The quantum advantage shown by a Dicke QB in a window of values of g is on the order of 10% and therefore not spectacular but clearly indicates the possibility to engineer more complex quantum Hamiltonians to achieve much better quantum performances. These will be the subject of future work.

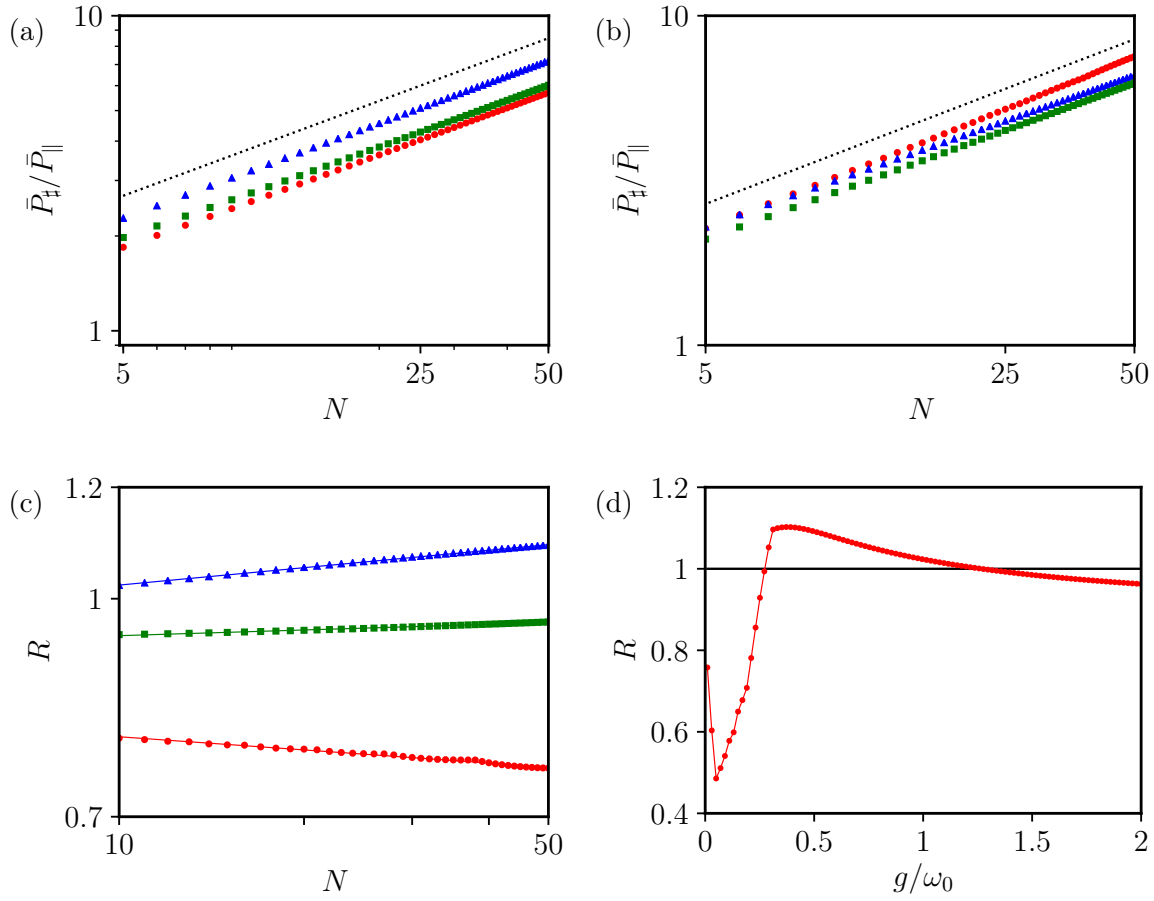

FIGURE 6.3: Performance of quantum and classical Dicke batteries—see Sect. 6.6. Panel (a) shows the advantage Γ in the quantum case, plotted as a function of N in a log-log scale. Different symbols refer to different values of the charger-battery coupling parameter g: $g = 0.01\omega_0$ (red circles), $g = 0.5\omega_0$ (blue triangles), and $g = 2\omega_0$ (green squares). The black dashed line represents a scaling of the form $\Gamma_{\rm qu} \propto \sqrt{N}$, i.e. $\alpha = 0$ in Eq. (6.21). Panel (b) Same as in panel (a), but for the classical case. Panel (c) shows the ratio R plotted as a function of N, for the same values of g reported in panels (a) and (b). Panel (d) shows the ratio R plotted as a function of g, for $N = 50$. A quantum advantage on the order of 10% can be observed in a small interval around $g \simeq 0.5\omega_0$.

6.7 Summary and conclusions

In this Chapter we have compared three quantum battery models against their rigorous classical versions in order to better understand the origin of the fast charging phenomenon discussed in previous literature.

In particular, we have defined a genuine *quantum advantage* (i.e. $R > 1$) via the ratio R in Eq. (6.5) between the collective advantages in the quantum and classical cases, $\Gamma_{\rm cl}$ and $\Gamma_{\rm qu}$, respectively.

In the case of harmonic oscillator batteries—see Sect. 6.4—$R = 1$ for all values of N and g. Quantum harmonic oscillator batteries defined as in Eq. (6.6) do not therefore display any quantum advantage. The case of spin batteries, discussed in Sect. 6.5, is even worse. In this model, indeed, $R < 1$ for all values of N and g.

We can safely conclude that, in these two cases, fast charging in the quantum case (i.e. the fact that $\Gamma_{\rm qu}$ increases for increasing N) is solely due to the collective behavior of the many-body systems described by the quantum Hamiltonians in Eqs. (6.6) and (6.15), which is also present in the corresponding classical Hamiltonians.

The case of Dicke batteries, discussed in Sect. 6.6, is far more richer. In this case, the ratio R depends on the charger-battery coupling parameter g and, for each fixed N, can be larger than unity in a range of values of g. As evident from Figs. 6.3(c) and (d), the quantum advantage displayed by a Dicke quantum battery at optimal coupling is on the order of 10%. More work is needed to discover quantum models of batteries with larger values of R.

For the sake of completeness, we note that the authors of Ref. 63 have proposed to study the evolution of the battery state in the energy eigenspace of the battery Hamiltonian. Combining this geometric approach with bounds on the power, they are able to distinguish whether the quantum advantage in a charging process stems either from the speed of evolution or the non-local character of the battery state.

7

Quantum advantage in the charging process of Sachdev-Ye-Kitaev batteries

In this Chapter we present our work on a Sachdev-Ye-Kitaev quantum battery, a charging protocol which directly realizes the quantum speed-up foreseen in Chap.2. The results of this work have been published in Ref. [28] and this chapter is largely based upon it.

We start this Chapter with a synopsis, Sect. 7.1, of the current state of the field. In Sec. 7.2 we generally introduce the charging protocol. In Sect. 7.3 we discuss how we employ the SYK model in the context of charging. Sect. 7.4 shows that this model realizes the energy non-local charging dynamics envisioned in Ref. [22]. Sect. 7.5 analyzes the charging dynamics with the bound derived in Ref. [63] showing that the charging speed-up is rooted in the quantum correlations established during the protocol. A final discussion and summary is provided in Sect. 7.6. Further technical details are reported in App. C.

7.1 Synopsis

In the era of quantum supremacy for quantum computing [3, 5], research on the potential usefulness of quantum mechanical resources (such as entanglement) in energy science has led a consistent number of authors to introduce and study "quantum batteries" (QBs). A QB [20, 135] is a system composed of N identical *quantum cells*, where energy is stored and from which work can be extracted.

In 2013, Alicki and Fannes [20] suggested that "entangling unitary controls", i.e. unitary operations acting globally on the state of the N quantum cells, lead to better work extraction capabilities from a QB, when compared to unitary operations acting on each quantum cell separately. Hovhannisyan et al. [21] were the first to demonstrate that entanglement generation leads to a speed-up in the process of work extraction, thereby leading to larger delivered power. Later on, the authors of Refs. [22, 23] focussed on the charging (rather than the discharging) procedure and identified two types of charging schemes: i) the *parallel* charging scheme in which each of the N quantum cells is acted upon independently of the others; and ii) the *collective* charging scheme, where global unitary operations (i.e. the entangling unitary

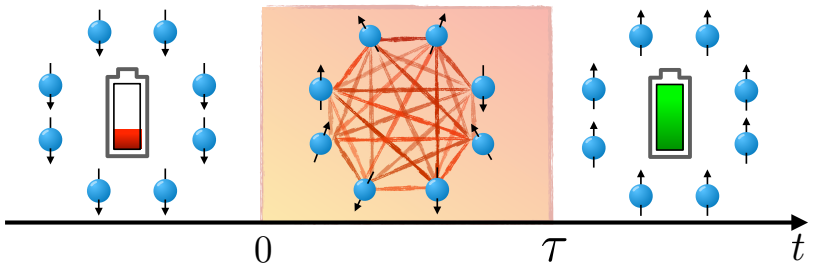

FIGURE 7.1: The charging protocol of a QB made of N spin-1/2 units, described by the $\hat{\mathcal{H}}_0$ in Eq. (7.1). At time $t < 0$, the battery is fully discharged. In the time interval $0 < t < \tau$, the interacting charging Hamiltonian $\hat{\mathcal{H}}_1$ is switched on, and energy is injected via the quench. Finally, at time τ, interactions are switched off and $\hat{\mathcal{H}}_0$ is switched back on, so that the stored energy $E^N(\tau)$ is conserved thereafter.

controls of Ref. [20]) acting on the full Hilbert space of the N quantum cells are allowed. They were able to show that, in the collective charging case and for $N \geq 2$, the charging power of a QB is larger than in the parallel scheme. This collective speed-up (stemming from entangling operations) during the charging procedure of a QB has been named "quantum advantage".

In the quest for such quantum advantage and potential laboratory implementations of QBs—based, e.g., on circuit quantum electrodynamics and trapped-ion setups—the abstract concepts of "quantum cell" and "entangling operations" have been recently spelled out more explicitly [24, 26, 27, 46, 48–63]. Different prototypes of QBs have been devised: i) Dicke models, where arrays of N qubits (i.e. the proper battery) are coupled to a harmonic energy source [24, 26, 46, 49–51]; ii) deterministic spin chains [27, 48, 63]; and iii) disordered spin chains [53, 54]. These quantum cells can be charged by switching on either direct [48, 53, 54] or effective [24, 26, 46, 49–51] interactions between them.

The authors of Refs. [24, 48] proposed two concrete implementations of the collective charging scheme, and claimed the existence of a quantum advantage over the parallel charging procedure. However, Julià-Farré et al. [63] noticed that the Hamiltonians adopted in Refs. [24, 48] were not properly defined in the thermodynamic limit, in the sense that their average values did not display extensivity with N, but, rather, displayed a super-linear growth with N. Moreover, the same authors were able to derive a rigorous bound for the charging power, allowing to distinguish between a genuine entanglement-induced speed-up and spurious effects, given e.g. by the lack of a well-defined thermodynamic limit. In agreement with Ref. [27], the conclusion of Ref. [63] is that *all* the many-body QB models proposed in the literature so far do not feature any genuine quantum advantage.

Motivated by this literature, we propose a model of a QB which i) is properly defined in the thermodynamic limit and ii) unequivocally presents a genuine quantum advantage. Our implementation relies on the Sachdev-Ye-Kitaev (SYK) model [29, 30, 162, 163], which has recently attracted a great deal of attention for its exact solvability and profound properties. The SYK model describes quantum matter with no quasiparticles. It displays fast scrambling [164, 165], has a nonzero entropy density at vanishing temperature [166, 167], all its eigenstates exhibit volume-law entanglement entropy [168, 169], and is holographically connected to the dynamics of AdS_2 horizons of quantum black holes [30, 162, 170, 171]. Proposals to realize the SYK Hamiltonian have been recently put forward and rely on ultra-cold

atoms [172], graphene flakes with irregular boundaries [173], and topological superconductors [174, 175].

7.2 Many-body QBs and figures of merit.

Consider a QB made of N identical quantum cells (for a cartoon, see Fig. 2.1), which are governed by the following free and local Hamiltonian ($\hbar = 1$):

$$\hat{\mathcal{H}}_0 = \sum_{j=1}^{N} \hat{h}_j \ . \tag{7.1}$$

At time $t = 0$, the system is prepared in its ground state $|0\rangle$, physically representing the discharged battery. By suddenly switching on a suitable interaction Hamiltonian $\hat{\mathcal{H}}_1$ for a finite amount of time τ (and switching off $\hat{\mathcal{H}}_0$), one aims at injecting as much energy as possible into the quantum cells [22, 23, 48]. The time interval τ is called the *charging time* of the protocol. As already seen in Sect.2.1 in Eq. 2.2, the full model Hamiltonian can be thus written as

$$\hat{\mathcal{H}}(t) = \hat{\mathcal{H}}_0 + \lambda(t)\big(\hat{\mathcal{H}}_1 - \hat{\mathcal{H}}_0\big) \ , \tag{7.2}$$

where $\lambda(t)$ is a classical parameter that represents the external control exerted on the system, and which is assumed to be given by a step function equal to 1 for $t \in [0, \tau]$ and zero elsewhere. Such charging protocol is experimentally feasible, e.g. in cold-atom setups [176], where implementing sudden quenches is a standard procedure. Accordingly, denoting by $|\psi(t)\rangle$ the state of the system at time t, its total energy $E^{(N)}_{\rm tot}(t) = \langle\psi(t)|\hat{\mathcal{H}}(t)|\psi(t)\rangle$ is constant for all values of t but $t = 0$ and $t = \tau$ (the switching points).

The energy injected into the N quantum cells can be expressed in terms of the mean local energy at the end of the protocol, $E^{(N)}(\tau) = \langle\psi(\tau)|\hat{\mathcal{H}}_0|\psi(\tau)\rangle$. In writing the previous equation, we have set to zero the ground-state energy $\langle \mathrm{G}|\hat{\mathcal{H}}_0|\mathrm{G}\rangle$. Other crucial figures of merit are the average charging power $P^{(N)}(\tau) = E^{(N)}(\tau)/\tau$ and its optimal value

$$P^{(N)}(\bar{\tau}) = \max_{\tau>0} P^{(N)}(\tau) \ , \tag{7.3}$$

obtained at time $\bar{\tau}$. In the following, we will be mainly interested in the scaling of the optimal charging power $P^{(N)}(\bar{\tau})$ with the number N of quantum cells.

7.3 SYK-based charging protocols.

We assume each quantum cell to be a spin-1/2 system. In the absence of charging operations, the system is described by the non-interacting Hamiltonian (7.1), with $\hat{h}_j = \omega_0 \hat{\sigma}^y_j/2$. Here, $\omega_0 > 0$ represents a magnetic field strength (with units of energy) and $\hat{\sigma}^\alpha_j$ ($\alpha = x, y, z$) are the Pauli matrices. The battery energy $E^{(N)}(\tau)$ will be measured in units of the energy scale ω_0. At time $t = 0$, the quantum cells are initialized in the ground state of $\hat{\mathcal{H}}_0$, $|0\rangle = \bigotimes_{j=1}^{N} |{\downarrow^{(y)}}\rangle_j$, where $\hat{\sigma}^y_j |{\downarrow^{(y)}}\rangle_j = -|{\downarrow^{(y)}}\rangle_j$.

For the charging Hamiltonian $\hat{\mathcal{H}}_1$, we use the complex SYK (c-SYK) [162, 177, 178] model Hamiltonian:

$$\hat{\mathcal{H}}_1^{\text{c-SYK}} = \sum_{i,j,k,l=1}^{N} J_{i,j,k,l} \hat{c}_i^\dagger \hat{c}_j^\dagger \hat{c}_k \hat{c}_l \ , \tag{7.4}$$

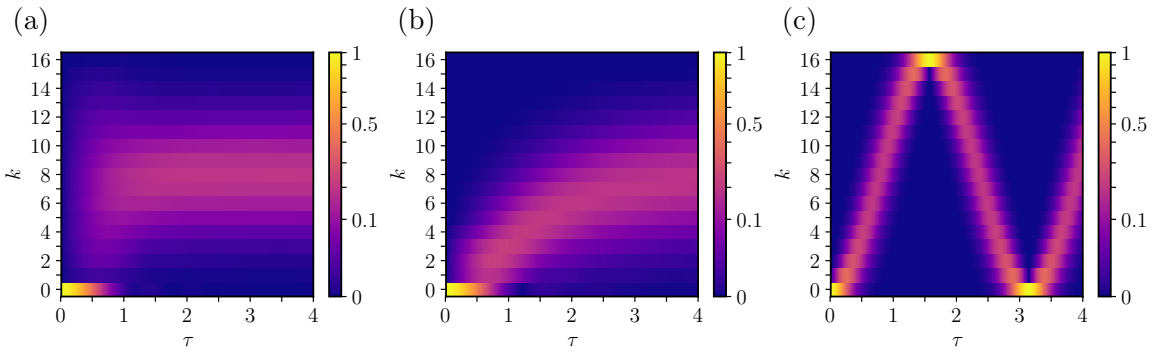

FIGURE 7.2: Dynamics of the dimensionless population $p_k(\tau)$ of the QB energy levels as a function of time τ (in units of $1/J$) and the level index k for three different charging protocols: c-SYK (a), b-SYK with $\bar{J} = J$ (b), and parallel with $K = J$ (c). Data in panels (a) and (b) correspond to a single realization of disorder in the couplings $J_{i,j,k,l}$ and $\bar{J}_{i,j,k,l}$.

where $\hat{c}_j^\dagger$ ($\hat{c}_j$) is a spinless fermionic creation (annihilation) operator [1]. This has to be understood in its spin-1/2 representation, which is obtained by the Jordan-Wigner (JW) transformation $\hat{c}_j^\dagger = \hat{\sigma}_j^+ \left(\Pi_{m=1}^{j-1} \hat{\sigma}_m^z\right)$, where $\hat{\sigma}_j^\pm \equiv (\hat{\sigma}_j^x \pm i\hat{\sigma}_j^y)/2$ (see App. C). The couplings $J_{i,j,k,l}$ are zero-mean Gaussian-distributed complex random variables, with variance $\langle\langle J_{i,j,k,l}^2 \rangle\rangle = J^2/N^3$, satisfying $J_{i,j,k,l} = J_{k,l,i,j}^*$ and $J_{i,j,k,l} = -J_{j,i,k,l} = -J_{i,j,l,k}$. In the following, we average any quantity of interest $\mathcal{O}$ over the distribution of $\{J_{i,j,k,l}\}$, and denote by $\langle\langle \mathcal{O} \rangle\rangle$ the averaged value, i.e. $\langle\langle \mathcal{O} \rangle\rangle \equiv \int P(\{J_{i,j,l,k}\}) \mathcal{O}(\{J_{i,j,l,k}\})\, \mathrm{d}\{J_{i,j,l,k}\}$.

We emphasize that our choice of battery and charging Hamiltonians is such that $[\hat{\mathcal{H}}_0, \hat{\mathcal{H}}_1] \neq 0$, a condition which ensures energy injection into the QB by the charging protocol (7.2). Note, finally, that the Hamiltonian in Eq. (7.4) is invariant under particle-hole symmetry (PHS) in the thermodynamic limit $N \to \infty$. Extra terms, however, need to be added to it in order to enforce PHS at any finite N [177]:

$$\hat{\mathcal{H}}_1^{\text{c-SYK (PHS)}} = \hat{\mathcal{H}}_1^{\text{c-SYK}} + \frac{1}{2} \sum_{i,j,k,l=1}^{N} J_{i,j,k,l} \times \left(\delta_{i,k} \hat{c}_j^\dagger \hat{c}_l - \delta_{i,l} \hat{c}_j^\dagger \hat{c}_k - \delta_{j,k} \hat{c}_i^\dagger \hat{c}_l + \delta_{j,l} \hat{c}_i^\dagger \hat{c}_k\right) . \tag{7.5}$$

Hereafter, we will always use this version of the c-SYK model. We have however checked that our main findings do not qualitatively change if PHS is not enforced and (7.4), rather than (7.5), is used as charging Hamiltonian.

In the following, we will also consider charging Hamiltonians based on a bosonic version of the SYK model (b-SYK) [177]:

$$\hat{\mathcal{H}}_1^{\text{b-SYK}} = \sum_{i,j,k,l=1}^{N} \bar{J}_{i,j,k,l} \hat{b}_i^\dagger \hat{b}_j^\dagger \hat{b}_k \hat{b}_l \ , \tag{7.6}$$

where $\hat{b}_j^\dagger$ ($\hat{b}_j$) creates (annihilates) an hard-core boson. The following relations are obeyed:

[1] We have decided to work with complex rather than Majorana fermions [30], since experimental realizations of the latter require complicated setups, including e.g. spin-orbit coupling, magnetic fields, and proximity superconductivity.

$\{\hat{b}_j, \hat{b}_j^\dagger\} = 1$ and $[\hat{b}_i, \hat{b}_j] = 0$ for $i \neq j$. Hence, $\hat{b}_j^\dagger$ can be directly written in its spin representation as $\hat{b}_j^\dagger = \sigma_j^+$. Similarly to $J_{i,j,k,l}$, the quantities $\bar{J}_{i,j,k,l}$ in Eq. (7.6) are random, Gaussian-distributed variables, with variance $\langle\langle \bar{J}^2_{i,j,k,l} \rangle\rangle = J^2/N^3$, satisfying $\bar{J}_{i,j,k,l} = \bar{J}^*_{k,l,i,j}$ and $\bar{J}_{i,j,k,l} = \bar{J}_{j,i,k,l} = \bar{J}_{i,j,l,k}$ (in order to comply with the bosonic commutation rules of the model). For PHS to hold, we enforce the site indices i, j, k, l in Eq. (7.6) to be all different [177]. Note that the dependence of the variance of the couplings $J_{i,j,k,l}$ and $\bar{J}_{i,j,k,l}$ on the inverse third power of N ensures that all our SYK charging Hamiltonians are well-defined in the thermodynamic limit. Indeed, their average values scale extensively with N [179].

Finally, we will also examine a parallel charging protocol [22, 23] based on the following Hamiltonian

$$\hat{\mathcal{H}}_1^{\parallel} = K \sum_{j=1}^{N} \hat{\sigma}_j^x \ . \tag{7.7}$$

In this case, each of the N quantum cells is acted upon independently of the others and no entanglement is generated [63]. The charging protocol based on $\hat{\mathcal{H}}_1^{\parallel}$ will therefore serve as reference model, to be compared against c-SYK and b-SYK charging models.

7.4 Microscopy of the charging dynamics in energy space.

As an indicator of the speed of the dynamics, we start by looking at the time evolution of the energy-level occupations. Consider the spectral decomposition of Hamiltonian (7.1): $\hat{\mathcal{H}}_0 = \sum_{k=0}^{N} \epsilon_k \sum_i |k,i\rangle \langle k,i|$, where $\epsilon_k = k\omega_0$ denote its eigenvalues and the index i accounts for the degenerate eigenvectors. We are interested in the dynamics of the populations:

$$p_k(\tau) = \sum_i |\langle k,i|\psi(\tau)\rangle|^2 \ . \tag{7.8}$$

Figure 7.2 displays $p_k(\tau)$ for the three charging Hamiltonians mentioned above: c-SYK (a), b-SYK (b), and parallel (c). While in the latter two cases the charging protocol generates a dynamics that is clearly local in energy space, this is not the case for the c-SYK model. This charging model generates a non-local population dynamics in energy space, which manifests as a sudden macroscopic population of excited levels. Indeed, after an ultrashort "thermalization" time [180] , a central band of excited energy levels appears uniformly populated. (Further details on the thermalization properties of c-SYK QBs are provided in App. C). This non-locality is a direct realization of the global charging dynamics envisioned by the authors of Ref. [22]. Recurrences appearing in the charging dynamics highlighted in panel (c) witness the integrability of the parallel Hamiltonian in Eq. (7.7), which is absent in the SYK models.

7.5 Power, bounds, and quantum advantage.

Quantitative conclusions on the charging performances of SYK QBs, compared to those of other reference many-body QBs, can be drawn from the analysis of the optimal power $P^{(N)}(\bar{\tau})$ in Eq. (7.3) and its scaling with N. Specifically, a rigorous certification of the quantum origin of the charging advantage of the c-SYK model can be achieved by considering the following bound [63]:

$$P^{(N)}(\tau) \leq 2\sqrt{\Delta_\tau \hat{\mathcal{H}}_0^2 \ \Delta_\tau \hat{\mathcal{H}}_1^2} \ , \tag{7.9}$$

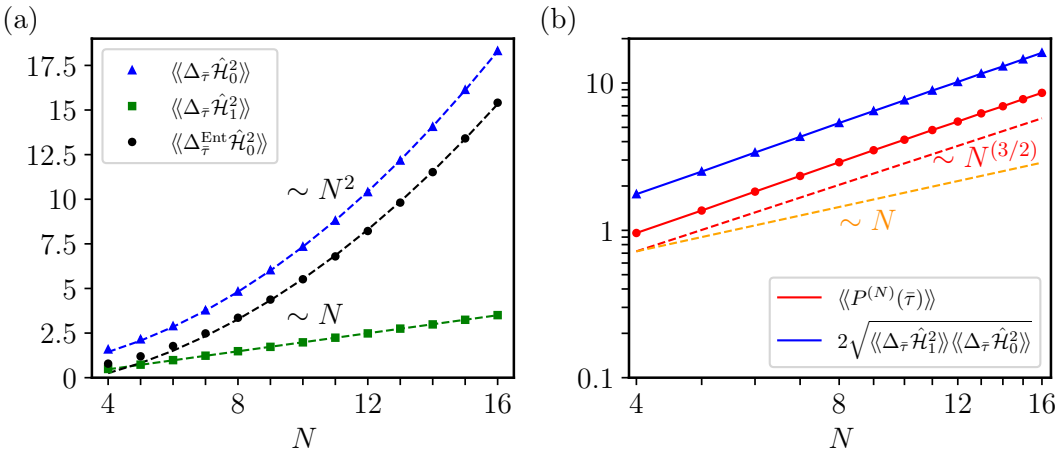

FIGURE 7.3: Panel (a) The relevant quantities for the bound (7.12), evaluated at the optimal time $\bar\tau$, and averaged over disorder: time-averaged variances $\langle\langle\Delta_{\bar\tau}\hat{\mathcal{H}}_0^2\rangle\rangle$ (blue triangles, in units of ω_0^2), $\langle\langle\Delta_{\bar\tau}\hat{\mathcal{H}}_1^2\rangle\rangle$ (green squares, in units of J^2), $\langle\langle\Delta_{\bar\tau}^{\rm Ent}\hat{\mathcal{H}}_0^2\rangle\rangle$ (black circles, in units of ω_0^2), as functions of N. Dashed curves denote linear (green) and quadratic (blue, black) fits to the numerical results. The four data points corresponding to the smallest N have been discarded from the fits. Panel (b) The optimal power (red) $\langle\langle P^{(N)}(\bar\tau)\rangle\rangle$ and the quantity in the right-hand-side of Eq. (7.12) (blue) are plotted as functions of N, in a log-log scale and in units of $\omega_0 J$. Dashed lines correspond to power laws $\sim N^{1+k}$ ($k=0.5$: red; $k=0$: orange) and are plotted as guides to the eye. Data in this figure refer to the c-SYK QB model, and have been obtained after averaging over $N_{\rm dis}=10^3$ (for $N=4,\dots,10$), 5×10^2 (for $N=11,12$), and 10^2 (for $N=13,\dots,16$) instances of disorder in the couplings $\{J_{i,j,k,l}\}$.

where $\Delta_\tau\hat{\mathcal{H}}^2\equiv(1/\tau)\int_0^\tau dt[\langle\hat{\mathcal{H}}^2\rangle_t-(\langle\hat{\mathcal{H}}\rangle_t)^2]$ and $\langle\hat{\mathcal{O}}\rangle_t\equiv\langle\psi(t)|\hat{\mathcal{O}}|\psi(t)\rangle$. Here, $\Delta_\tau\hat{\mathcal{H}}_1^2$ represents the charging speed in the Hilbert space: larger values of such quantity correspond to trivial increases of the charging speed. In contrast, $\Delta_\tau\hat{\mathcal{H}}_0^2$ is connected with the distance traveled in the Hilbert space. An enhancement of it can be linked to shortcuts in the Hilbert space: starting from a pure state and going through highly entangled states, it is possible to reduce the length of the trajectory in such space, consequently enhancing the charging power [63]. This is a genuine quantum effect, with no classical analogue. Any increase of the average optimal power linked to $\Delta_\tau\hat{\mathcal{H}}_0^2$ can be considered as the smoking gun of a genuine quantum advantage, unreproducible by classical dynamics. A detailed derivation of the bound (7.9) is provided in App. C.

If the battery Hamiltonian $\hat{\mathcal{H}}_0$ is made of a sum of local terms, as in Eq. (7.1), it is possible to write $\Delta_\tau\hat{\mathcal{H}}_0^2$ as: $\Delta_\tau\hat{\mathcal{H}}_0^2=\Delta_\tau^{\rm Loc}\hat{\mathcal{H}}_0^2+\Delta_\tau^{\rm Ent}\hat{\mathcal{H}}_0^2$, with [63]

$$\Delta_\tau^{\rm Loc}\hat{\mathcal{H}}_0^2 \equiv \frac{1}{\tau}\int_0^\tau dt\sum_i\left[\langle\hat{h}_i^2\rangle_t-\langle\hat{h}_i\rangle_t^2\right], \tag{7.10}$$

$$\Delta_\tau^{\rm Ent}\hat{\mathcal{H}}_0^2 \equiv \frac{1}{\tau}\int_0^\tau dt\sum_{i\neq j}\left[\langle\hat{h}_i\hat{h}_j\rangle_t-\langle\hat{h}_i\rangle_t\langle\hat{h}_j\rangle_t\right]. \tag{7.11}$$

The quantity (7.10), being a sum of local terms, scales linearly with N (i.e. is extensive) by construction. On the other hand, $\Delta_\tau^{\rm Ent}\hat{\mathcal{H}}_0^2$, whose explicit form can be immediately linked to correlations between sites i and j, may display a super-linear scaling with N. Due to the non-linearity of the bound (7.9), which applies to a single disorder realization, averaging over disorder is not straightforward. Through the Cauchy-Schwarz inequality, though, it is possible

to rewrite it as $\langle\!\langle P^{(N)}(\tau)\rangle\!\rangle \leq 2\left\langle\!\!\left\langle \sqrt{\Delta_\tau \hat{\mathcal{H}}_0^2\, \Delta_\tau \hat{\mathcal{H}}_1^2}\right\rangle\!\!\right\rangle \leq 2\sqrt{\langle\!\langle \Delta_\tau \hat{\mathcal{H}}_0^2\rangle\!\rangle \langle\!\langle \Delta_\tau \hat{\mathcal{H}}_1^2\rangle\!\rangle}$, meaning that one can separately study the averaged quantities $\langle\!\langle \Delta_\tau \hat{\mathcal{H}}_0^2\rangle\!\rangle$ and $\langle\!\langle \Delta_\tau \hat{\mathcal{H}}_1^2\rangle\!\rangle$. Here we are interested in the scaling at the optimal time $\bar{\tau}$, thus we focus on

$$\langle\!\langle P^{(N)}(\bar{\tau})\rangle\!\rangle \leq 2\sqrt{\langle\!\langle \Delta_{\bar{\tau}} \hat{\mathcal{H}}_0^2\rangle\!\rangle \langle\!\langle \Delta_{\bar{\tau}} \hat{\mathcal{H}}_1^2\rangle\!\rangle}\ . \tag{7.12}$$

Since the battery energy is measured in units of ω_0 and time in units of $1/J$, the averaged charging power $\langle\!\langle P^{(N)}(\bar{\tau})\rangle\!\rangle$ is measured in units of $\omega_0 J$. Given this choice, we specify the energy scales of the b-SYK and parallel-charging protocols by setting $\bar{J} = K = J$ [2].

Figure 7.3(a) shows the relevant quantities for the bound (7.12), for a c-SYK QB. While $\langle\!\langle \Delta_{\bar{\tau}} \hat{\mathcal{H}}_1^2\rangle\!\rangle$ is extensive in N, we observe that both $\langle\!\langle \Delta_{\bar{\tau}} \hat{\mathcal{H}}_0^2\rangle\!\rangle$ and $\langle\!\langle \Delta_{\bar{\tau}}^{\mathrm{Ent}} \hat{\mathcal{H}}_0^2\rangle\!\rangle$ display a super-linear scaling with N, which is compatible with a quadratic growth. This means that, during the time evolution, the c-SYK charging Hamiltonian generates the maximum possible non-locality between the quantum cells, in the form of N-partite entanglement [63]. This, together with Eq. (7.12), suggests a super-linear scaling with N of the optimal charging power,

$$\boxed{\langle\!\langle P^{(N)}(\bar{\tau})\rangle\!\rangle \sim N^{1+k}\ , \quad \text{with } k > 0\ ,} \tag{7.13}$$

where $k \approx 0.5$. For the first time in the literature on QB models [24, 26, 27, 46, 48–63], we are thus in a situation where the power enhancement is linked to $\Delta_\tau \hat{\mathcal{H}}_0^2$, a fact that hints at a quantum advantage (i.e. advantage over any classical battery) displayed by the c-SYK model with respect to the charging task. Further details on the comparison between quantum and classical many-body batteries are given in App. C.

The left- and right-hand-side members of the inequality (7.12) are displayed in Fig. 7.3(b), red and blue data, respectively. We clearly see a super-linear scaling with N ($k = 0.5$ corresponds to the red dashed straight line). We have also considered the b-SYK and parallel-charging models, showing that, in both cases, all the quantities $\langle\!\langle \Delta_{\bar{\tau}} \hat{\mathcal{H}}_0^2\rangle\!\rangle$, $\langle\!\langle \Delta_{\bar{\tau}} \hat{\mathcal{H}}_1^2\rangle\!\rangle$, and $\langle\!\langle \Delta_{\bar{\tau}}^{\mathrm{Ent}} \hat{\mathcal{H}}_0^2\rangle\!\rangle$ are extensive in N (see App. C). In agreement with the results shown in Figs. 7.2-7.3, we thus conclude that these two QB models do not display any genuine quantum advantage.

We finally recall that optimal charging powers that scale faster than N have been found in Refs. [24, 48]. Unfortunately, such super-linear scalings do not stem from $\Delta_\tau \hat{\mathcal{H}}_0^2$ but rather from $\Delta_\tau \hat{\mathcal{H}}_1^2$, and therefore have no quantum origin [63]. The fact that the Hamiltonians used in Refs. [24, 48] are not properly defined in the thermodynamic limit is ultimately at the origin of the spurious super-extensive scaling of the optimal charging power. This is *explicitly* shown in App. C for Dicke QBs. Here, we have bypassed this problem by choosing the appropriate scaling [29, 30, 162, 163, 177, 178] with N of the variance $\langle\!\langle J_{i,j,k,l}^2\rangle\!\rangle = J^2/N^3$ of the c-SYK coupling parameters.

Alternatively, another strategy to rule out any spurious effect on the optimal charging power is to use a "renormalization" approach that consists in dividing the charging Hamiltonian by its operator norm (see App. C). This procedure allows for a fair comparison between different QB models [23]. In agreement with the results illustrated above, we have found a clear increase with N of the optimal charging power only for the renormalized c-SYK Hamiltonian.

[2] This choice is not restrictive. Indeed, results for other values of parameters can be obtained through the following rescaling procedure, without the need of carrying out further simulations. A linear rescaling of the QB energy scale, $\omega_0 \to \alpha\omega_0$, reflects into a linear change of the power, i.e. $P^{(N)}(\tau) \to \alpha P^{(N)}(\tau)$. The same occurs under a linear rescaling of the charging Hamiltonian coupling constant, $J \to \alpha J$

7.6 Summary and conclusions

In summary, we have presented a numerical study of QBs where the charging Hamiltonian is based on the c- and b-SYK models [29, 30, 163]. We have used *two* independent strategies to show that fermionic SYK QBs display a genuine quantum advantange, i.e. a speed-up in the charging dynamics that stems from entanglement and is therefore unreproducible by any classical battery. This is in stark contrast with all known previous QB models [27, 63]. We used recently proposed bounds on the charging power, first demonstrated in Ref. [63]. The quantum advantage emerges as a non-zero super-linear scaling with N of the correlation-induced time-averaged variance (7.11) of the local quantum battery Hamiltonian (7.1).

In the future, it will be interesting to study SYK-type models in the context of heat engines [12, 181], where minimizing time scales is also of central importance.

Part III

Photon Condensation

8

Cavity QED of Strongly Correlated Electron Systems: A No-go Theorem for Photon Condensation

In this Chapter we display our work on no-go theorem for photon condensation, in the context of strongly correlated systems. This study lead to Ref. [41] and this Chapter is based largely on this publication.

After a synopsis of the work in Sect. 8.1, in Sect. 8.2 we prove a no-go theorem which shows that gauge invariance forbids the occurrence of photon condensation, when a spatially-uniform electromagnetic mode is considered. In Sect. 8.3 we study the strongly-interacting Falikov-Kimbal model interacting with a cavity field, showing, in accordance with the general theorem, that photon condensation does not occur. In Sect. 8.4 we give summary of our main findings and our conclusions.

8.1 Synopsis

Superradiance [25, 33, 36, 64, 65] refers to the coherent spontaneous radiation process that occurs in a dense gas when a radiation field mode mediates long-range inter-molecule interactions. Superradiance was observed first more than 40 years ago in optically pumped gases [33, 64] and has recently been identified in optically pumped electron systems in a semiconductor quantum well placed in a perpendicular magnetic field [182]. In 1973 Hepp and Lieb [31] and subsequently Wang and Hioe [38] pointed out that for sufficiently strong light-matter coupling the Dicke model, often used to describe superradiance in optical cavities, has a finite temperature second-order *equilibrium* phase transition between normal and superradiant states. To the best of our knowledge, this phase transition has never been observed [183]. In the superradiant phase the ground state contains a macroscopically large number of coherent photons, *i.e.* $\langle \hat{a} \rangle \neq 0$, where $\hat{a}$ ($\hat{a}^\dagger$) destroys (creates) a cavity photon. To avoid confusion with the phenomenon discussed in the original work by Dicke [25], we refer to the equilibrium superradiant phase as a photon condensate.

Theoretical work on photon condensation has an interesting and tortured history. Early on it was shown that photon condensation is robust against the addition of counter-rotating terms [184, 185] neglected in Refs. [31, 38]. Soon after, however, Rzażewski et al. [39] pointed out that addition of a neglected term related to the Thomas-Reiche-Kuhn (TRK) sum rule [84, 186] and proportional to $(\hat{a} + \hat{a}^\dagger)^2$ destroys the photon condensate. These quadratic terms are naturally generated by applying minimal coupling $\hat{\boldsymbol{p}} \to \hat{\boldsymbol{p}} - q\boldsymbol{A}/c$ to the electron kinetic energy $\hat{\boldsymbol{p}}^2/(2m)$. More recent research has focused on ground state properties. The quantum chaotic and entanglement properties of the Dicke model photon condensate were studied in Refs. [37, 187]. The authors of Ref. [188] criticized these studies however, pointing again to the importance of the quadratic term. The no-go theorem for photon condensation was revisited in Ref. [40], where it was claimed that it can be bypassed in a circuit quantum electrodynamics (QED) system with Cooper pair boxes capacitively coupled to a resonator. Soon after, however, Ref. [73] showed that the no-go theorem for cavity QED applies to circuit QED as well. The claims of Ref. [73] were then criticized in Ref. [189]. (See also subsequent discussions [190, 191] on light-matter interactions in circuit QED.) Later it was argued [71] that the linear band dispersion of graphene provides a route to bypass the no-go theorem, and that photon condensation could occur in graphene in the integer quantum Hall regime. This claim was later countered in Refs. [74, 75], where it was shown that a dynamically generated quadratic term again forbids photon condensation.

Recent experimental progress has created opportunities to study light matter interactions in new regimes in which direct electron-electron interactions play a prominent role. For example [192] two-dimensional (2D) electron systems can be embedded in cavities or exposed to the radiation field of metamaterials, making it possible to study strong light-matter interactions in the quantum Hall regime [193–198]. Other emerging possibilities include cavity QED with quasi-2D electron systems that exhibit exciton condensation, superconductivity, magnetism, or Mott insulating states. This Chapter is motivated by interest in strong light-matter interactions in these new regimes and by fundamental confusion on when, if ever, photon condensation is allowed.

We present a no-go theorem for photon condensation that is valid for generic non-relativistic interacting electrons at $T = 0$. This result generalizes to interacting systems existing no-go theorems for photon condensation in two-level [39, 40, 79, 80] and multi-level [73] Dicke models,which are based on the TRK sum rule. We then present a theory of cavity QED of an extended Falikov-Kimball model [199], which, in the absence of the cavity, has insulating ferroelectric and exciton condensate phases. We show through explicit microscopic calculations how the theorem is satisfied in this particular strongly correlated electron model.

8.2 Gauge invariance excludes photon condensation

We consider a system of N electrons of mass m_i described by a non-relativistic many-body Hamiltonian of the form

$$\hat{\mathcal{H}} = \sum_{i=1}^{N} \left[\frac{\hat{\boldsymbol{p}}_i^2}{2m_i} + V(\hat{\boldsymbol{r}}_i) \right] + \frac{1}{2} \sum_{i \neq j} v(\hat{\boldsymbol{r}}_i - \hat{\boldsymbol{r}}_j) \ . \tag{8.1}$$

Here, $V(\boldsymbol{r})$ is a generic function of position and $v(\boldsymbol{r})$ is a generic (non-retarded) two-body interaction, which need not even be spherically symmetric. In a solid $V(\boldsymbol{r})$ is the one-body crystal potential. Below we first exclude the possibility of a continuous transition to a condensed state, and then use this insight to exclude first-order transitions. For future reference,

we denote by $|\psi_m\rangle$ and E_m the *exact* eigenstates and eigenvalues of $\hat{\mathcal{H}}$ [85, 86], with $|\psi_0\rangle$ and E_0 denoting the ground state and ground-state energy, respectively.

We treat the cavity e.m. field in a quantum fashion, via a uniform quantum field $\hat{\boldsymbol{A}}$ corresponding to only one mode [31, 37–40, 65, 71, 73–75, 79, 185, 186, 189–191, 207, 208], i.e. $\hat{\boldsymbol{A}} = A_0\boldsymbol{u}(\hat{a}+\hat{a}^\dagger)$, where $\boldsymbol{u}$ is the polarization vector, $A_0 = \sqrt{2\pi\hbar c^2/(V\omega_{\rm c}\epsilon_{\rm r})}$, V is the volume of the cavity, $\epsilon_{\rm r}$ is its relative dielectric constant, and the photon Hamiltonian $\hat{\mathcal{H}}_{\rm ph} = \hbar\omega_{\rm c}\hat{a}^\dagger\hat{a}$, where $\omega_{\rm c}$ is the cavity frequency. The full Hamiltonian, including light-matter interactions in the Coulomb gauge [79–82] is:

$$\hat{\mathcal{H}}_{\boldsymbol{A}_0} = \hat{\mathcal{H}} + \hbar\omega_{\rm c}\hat{a}^\dagger\hat{a} + \sum_{i=1}^{N}\frac{e}{m_i c}\hat{\boldsymbol{p}}_i\cdot\boldsymbol{A}_0(\hat{a}+\hat{a}^\dagger) + \sum_{i=1}^{N}\frac{e^2A_0^2}{2m_ic^2}(\hat{a}+\hat{a}^\dagger)^2\ , \tag{8.2}$$

where $\boldsymbol{A}_0 \equiv A_0\boldsymbol{u}$ and $-e<0$ is the electron charge. The third and fourth terms in Eq. (8.2) are often referred to respectively as the paramagnetic and diamagnetic contributions to the light-matter coupling Hamiltonian. Our aim is to make general statements about the ground state $|\Psi\rangle$ of $\hat{\mathcal{H}}_{\boldsymbol{A}_0}$. For future reference we define i) the paramagnetic (number) current operator [85, 86], $\hat{\boldsymbol{j}}_{\rm p} \equiv (c/e)\delta\hat{\mathcal{H}}_{\boldsymbol{A}_0}/\delta\boldsymbol{A}_0|_{\boldsymbol{A}_0=\boldsymbol{0}} = \sum_{i=1}^{N}\hat{\boldsymbol{p}}_i/m_i$ and ii) $\Delta \equiv \sum_{i=1}^{N} e^2A_0^2/(2m_ic^2)$.

The term proportional to Δ in Eq. (8.2) can be removed by performing the transformation $\hat{b} = \cosh(x)\hat{a} + \sinh(x)\hat{a}^\dagger$, where $\cosh(x) = (\lambda+1)/(2\sqrt{\lambda})$ and $\sinh(x) = (\lambda-1)/(2\sqrt{\lambda})$ with $\lambda = \sqrt{1+4\Delta/(\hbar\omega_{\rm c})}$. The Hamiltonian (8.2) becomes: $\hat{\mathcal{H}}_{\boldsymbol{A}_0} = \hat{\mathcal{H}} + (e/c)\hat{\boldsymbol{j}}_{\rm p}\cdot\boldsymbol{A}_0\lambda^{-1/2}(\hat{b}+\hat{b}^\dagger) + \hbar\omega_{\rm c}\lambda\hat{b}^\dagger\hat{b}$. It can be shown (see App. D.1) that in the thermodynamic limit ($N\to\infty$, $V\to\infty$ limit at fixed N/V), the ground state $|\Psi\rangle$ of $\hat{\mathcal{H}}_{\boldsymbol{A}_0}$ does not contain light-matter entanglement, i.e. we can take $|\Psi\rangle = |\psi\rangle\,|\Phi\rangle$, where $|\psi\rangle$ and $|\Phi\rangle$ are matter and light wave functions. Using this property we see that in the thermodynamic limit the ground state $|\Phi\rangle$ of the effective photon Hamiltonian $\langle\psi|\,\hat{\mathcal{H}}_{\boldsymbol{A}_0}\,|\psi\rangle$ is a coherent state [47, 76] $|\beta\rangle$ satisfying $\hat{b}\,|\beta\rangle = \beta\,|\beta\rangle$. The ground-state energy is therefore given by

$$E_\psi(\beta) = \langle\psi|\hat{\mathcal{H}}|\psi\rangle + \frac{e}{c}\,\langle\psi|\hat{\boldsymbol{j}}_{\rm p}|\psi\rangle\,\cdot\boldsymbol{A}_0\frac{2{\rm Re}[\beta]}{\sqrt{\lambda}} + \hbar\omega_{\rm c}\lambda|\beta|^2\ . \tag{8.3}$$

We need to minimize $E_\psi(\beta)$ with respect to β and $|\psi\rangle$. The minimization with respect to β can be done analytically. We find that the optimal value $\bar{\beta}$ for this minimum problem is a real number given by:

$$\bar{\beta} = -\frac{1}{\hbar\omega_{\rm c}\lambda^{3/2}}\frac{e}{c}\,\langle\psi|\hat{\boldsymbol{j}}_{\rm p}|\psi\rangle\,\cdot\boldsymbol{A}_0\ . \tag{8.4}$$

We are therefore left with a *constrained* minimum problem for the matter degrees of freedom. Its solution must be sought among the normalized anti-symmetric states $|\psi\rangle$ which yield (8.4). This is the typical scenario that can be handled with the stiffness theorem [86].

For photon condensation to occur we need $E_\psi(\bar{\beta}) < E_{\psi_0}(0)$ or, equivalently,

$$\hbar\omega_{\rm c}\lambda\bar{\beta}^2 > \langle\psi|\hat{\mathcal{H}}|\psi\rangle - \langle\psi_0|\hat{\mathcal{H}}|\psi_0\rangle\ , \tag{8.5}$$

where, because of (8.4), $|\psi\rangle$ depends on $\bar{\beta}$. The dependence of $\langle\psi|\hat{\mathcal{H}}|\psi\rangle - \langle\psi_0|\hat{\mathcal{H}}|\psi_0\rangle$ on $\bar{\beta}$ can be calculated *exactly* up to order $\bar{\beta}^2$ by using the stiffness theorem [86]. We find $\langle\psi|\hat{\mathcal{H}}|\psi\rangle - \langle\psi_0|\hat{\mathcal{H}}|\psi_0\rangle = \alpha\bar{\beta}^2/2 + \mathcal{O}(\bar{\beta}^3)$, where $\alpha = -1/\chi(0) > 0$ and

$$\chi(0) \equiv -\frac{2}{\hbar^2\omega_{\rm c}^2\lambda^3}\frac{e^2}{c^2}\sum_{n\neq 0}\frac{|\langle\psi_n|\hat{\boldsymbol{j}}_{\rm p}\cdot\boldsymbol{A}_0|\psi_0\rangle|^2}{E_n-E_0} < 0 \tag{8.6}$$

is proportional to the static paramagnetic current-current response function in the Lehmann representation [85, 86]. We have used that $(e/c)\,\langle\psi_0|\hat{\boldsymbol{j}}_{\rm p}|\psi_0\rangle\cdot\boldsymbol{A}_0=0$, as proven in App. D.2. It follows that photon condensation occurs if and only if

$$4\frac{e^2}{c^2}\sum_{n\neq 0}\frac{|\langle\psi_n|\hat{\boldsymbol{j}}_{\rm p}\cdot\boldsymbol{A}_0|\psi_0\rangle|^2}{E_n-E_0}>\hbar\omega_{\rm c}+4\Delta\ . \tag{8.7}$$

However, as shown in App. D.3,

$$\frac{e^2}{c^2}\sum_{n\neq 0}\frac{|\langle\psi_n|\hat{\boldsymbol{j}}_{\rm p}\cdot\boldsymbol{A}_0|\psi_0\rangle|^2}{E_n-E_0}=\Delta\ . \tag{8.8}$$

Eq. (8.8) is the TRK sum rule [84] which expresses the fact that the paramagnetic and diamagnetic contributions to the physical current-current response function cancel in the uniform static limit [85, 86], as discussed more fully in App. D.3, i.e. it expresses gauge invariance. Using Eq. (8.8) we can finally rewrite Eq. (8.7) as

$$\boxed{4\Delta>\hbar\omega_{\rm c}+4\Delta\ ,} \tag{8.9}$$

which cannot be satisfied. We conclude that photon condensation cannot occur and that, upon minimization with respect to $|\psi\rangle$, the ground state is $|\psi_0\rangle$ and $\bar{\beta}=0$. From this analysis it is clear that first-order transitions to states with finite photon density are also excluded, because interactions with a coherent equilibrium photon field do not lower the matter energy [1]. Gauge invariance excludes photon condensation for any Hamiltonian of the form (8.2). This is the first important result of this Chapter.

8.3 Cavity QED of an extended Falikov-Kimball model

We now illustrate how this general conclusion applies to a specific properly gauge invariant model of strongly correlated electrons in a cavity. We consider spinless electrons in a one-dimensional (1D) inversion-symmetric crystal with N sites, each with one atom with two atomic orbitals of opposite parity (s and p). When this lattice model is augmented by the addition of on-site repulsive electron-electron interactions, it is often referred to as an extended Falikov-Kimball (EFK) model [199]. The EFK model has been used to discuss exciton condensation [200] and electronic ferroelectricity [201, 202]. The coupling of cavity photons to the matter degrees of freedom of a 1D EFK model can be described [203–206] by employing a Peierls substitution in the site representation with a uniform linearly-polarized vector potential of amplitude A_0, as detailed in App. D.4. We obtain

$$\hat{\mathcal{H}}_{\boldsymbol{A}_0}=\hat{\mathcal{H}}_0+\hat{\mathcal{H}}_{\rm ee}+\hbar\omega_{\rm c}\hat{a}^\dagger\hat{a}+\frac{g_0}{\sqrt{N}}\frac{\hbar}{a}\hat{j}_{\rm p}(\hat{a}+\hat{a}^\dagger)-\frac{g_0^2}{2N}\hat{\mathcal{T}}(\hat{a}+\hat{a}^\dagger)^2\ , \tag{8.10}$$

where $\hat{\mathcal{H}}_0=\sum_{k,\alpha,\beta}\hat{c}^\dagger_{k,\alpha}H_{\alpha\beta}(k)\hat{c}_{k,\beta}$ is the band Hamiltonian,

$$H_{\alpha\beta}(k)=\begin{pmatrix}E_{\rm s}-2t_{\rm s}\cos(ka) & 2i\tilde{t}\sin(ka)\\ -2i\tilde{t}\sin(ka) & E_{\rm p}+2t_{\rm p}\cos(ka)\end{pmatrix}\ , \tag{8.11}$$

[1] In the thermodynamic limit, the ground-state factorization implies a photon coherent state. The matter state for a given β is therefore equivalent to a matter state with a time-independent spatially constant vector potential. In turn, this implies a matter state energy independent of β. According to Eq. (8.3), introducing photons only costs energy, forbidding a first-order transition to a photon condensate.

and the Hubbard interaction term

$$\hat{\mathcal{H}}_{\rm ee} = U \sum_{j=1}^{N} \hat{c}^{\dagger}_{j,{\rm s}} \hat{c}_{j,{\rm s}} \hat{c}^{\dagger}_{j,{\rm p}} \hat{c}_{j,{\rm p}} \ . \tag{8.12}$$

In Eq. (8.10), $\hat{j}_{\rm p} = \sum_{k,\alpha,\beta} \hat{c}^{\dagger}_{k,\alpha} j_{\alpha\beta}(k) \hat{c}_{k,\beta}$ with $j_{\alpha\beta}(k) \equiv \hbar^{-1} \partial H_{\alpha\beta}(k)/\partial k$ is the paramagnetic number current operator, and $\hat{\mathcal{T}} = \sum_{k,\alpha,\beta} \hat{c}^{\dagger}_{k,\alpha} \mathcal{T}_{\alpha\beta}(k) \hat{c}_{k,\beta}$ with $\mathcal{T}_{\alpha\beta}(k) \equiv -a^{-2} \partial^2 H_{\alpha\beta}(k)/\partial k^2$ is the diamagnetic operator. In Eq. (8.11), $E_{\rm s}$ and $E_{\rm p}$ are on-site energies for the s and p orbitals, $t_{\rm s} \in \mathbb{R}$ and $t_{\rm p} \in \mathbb{R}$ are hopping parameters, and $\tilde{t} \in \mathbb{R}$ is the inter-band hopping parameter. At the single-particle level (i.e. for $U = 0$), $\tilde{t}$ is the only term responsible for inter-band transitions due to light. All sums over the wave number k are carried out in the 1D Brillouin zone and become integrals in the thermodynamic limit with the usual rule $N^{-1} \sum_k \to a \int_{-\pi/a}^{+\pi/a} dk/(2\pi)$, where a is the lattice constant. In these equations the Greek labels take values $\alpha, \beta = {\rm s}, {\rm p}$. The momentum-space and site representations for field operators are linked by the usual relationship $\hat{c}^{\dagger}_{j,\alpha} = N^{-1/2} \sum_k \hat{c}^{\dagger}_{k,\alpha} e^{-ikja}$. The dimensionless light-matter coupling constant in Eq. (8.10) is defined by $g \equiv eaA_0/(\hbar c) = g_0/\sqrt{N}$, where $g_0 \equiv \sqrt{2\pi e^2/(\hbar v_0 \omega_{\rm c} \epsilon_{\rm r})}$ and $v_0 = V/N$ is the cavity volume per site.

We emphasize that the operators $\hat{j}_{\rm p}$ and $\hat{\mathcal{T}}$ describing light-matter interactions are completely determined by the matrix elements $H_{\alpha\beta}(k)$ of the band Hamiltonian. This property is crucial to have a properly gauge-invariant model [2] and must be a general feature of *any* strongly correlated lattice model coupled to cavity photons.

In the limit $g_0 \to 0$, the model reduces to a 1D EFK model [199, 201, 202]. In the limit $ka \to 0$ and $U = 0$, Eq. (8.10) reduces to the Dicke model, augmented by the addition of a term proportional to $\sum_{k,\alpha,\beta} \hat{c}^{\dagger}_{k,\alpha} \hat{\sigma}^{z}_{\alpha\beta} \hat{c}_{k,\beta} (\hat{a} + \hat{a}^{\dagger})^2$ [78, 207, 208], where $\hat{\sigma}^{z}_{\alpha\beta}$ are the matrix elements of the corresponding 2×2 Pauli matrix. For non-interacting systems, the diamagnetic term prevents photon condensation from occurring in the thermodynamic limit [39, 40]. We now show that interactions do not help. $\hat{\mathcal{H}}_{\boldsymbol{A}_0}$ does not support photon condensation.

To make progress in analyzing the interacting problem we treat the Hubbard term using an unrestricted Hartree-Fock (HF) approximation [86, 209]. As detailed in App. D.5 we arrive at

$$\begin{aligned} \hat{\mathcal{H}}^{\rm (HF)}_{\rm ee} &= -U \frac{\mathcal{M}}{2} \sum_k (\hat{c}^{\dagger}_{k,{\rm p}} \hat{c}_{k,{\rm p}} - \hat{c}^{\dagger}_{k,{\rm s}} \hat{c}_{k,{\rm s}}) - U \sum_k (\mathcal{I} \hat{c}^{\dagger}_{k,{\rm s}} \hat{c}_{k,{\rm p}} + \mathcal{I}^{*} \hat{c}^{\dagger}_{k,{\rm p}} \hat{c}_{k,{\rm s}}) \\ &+ U \frac{n_0}{2} \sum_{k,\alpha} \hat{n}_{k,\alpha} + UN \left(\frac{\mathcal{M}^2 - n_0^2}{4} + |\mathcal{I}|^2 \right) \ . \end{aligned} \tag{8.13}$$

In Eq. (8.13) we have introduced the following self-consistent fields: i) the electronic polarization

$$\mathcal{M} \equiv \frac{1}{N} \sum_k (\langle \hat{c}^{\dagger}_{k,{\rm p}} \hat{c}_{k,{\rm p}} \rangle - \langle \hat{c}^{\dagger}_{k,{\rm s}} \hat{c}_{k,{\rm s}} \rangle) \ , \tag{8.14}$$

[2] Gauge invariance (of linear-response functions) and the f-sum rule follow from particle (charge) conservation [85, 86]. Consider Eq. (8.10) at $g_0 = 0$ and arbitrary values of U. In this case, the conservation law reads as following, $\partial_t \hat{n}_\ell + (\hat{j}_{{\rm p},\ell+1} - \hat{j}_{{\rm p},\ell})/a = 0$, which is the lattice version of 1D continuity equation. Here, we have defined the local density operator in the site representation, $\hat{n}_\ell \equiv \sum_\alpha \hat{c}^{\dagger}_{\ell,\alpha} \hat{c}_{\ell,\alpha}$ and the local paramagnetic (number) current operator $\hat{j}_{{\rm p},\ell} \equiv it_{\rm s} a(\hat{c}^{\dagger}_{\ell,{\rm s}} \hat{c}_{\ell-1,{\rm s}} - \hat{c}^{\dagger}_{\ell-1,{\rm s}} \hat{c}_{\ell,{\rm s}})/\hbar - it_{\rm p} a(\hat{c}^{\dagger}_{\ell,{\rm p}} \hat{c}_{\ell-1,{\rm p}} - \hat{c}^{\dagger}_{\ell-1,{\rm p}} \hat{c}_{\ell,{\rm p}})/\hbar + i\tilde{t}a(\hat{c}^{\dagger}_{\ell,{\rm s}} \hat{c}_{\ell-1,{\rm p}} - \hat{c}^{\dagger}_{\ell-1,{\rm p}} \hat{c}_{\ell,{\rm s}})/\hbar + i\tilde{t}a(\hat{c}^{\dagger}_{\ell-1,{\rm s}} \hat{c}_{\ell,{\rm p}} - \hat{c}^{\dagger}_{\ell,{\rm p}} \hat{c}_{\ell-1,{\rm s}})/\hbar$. Coupling to the uniform vector potential of the cavity *must* be done via the paramagnetic current operator $\hat{j}_{\rm p} = \sum_{\ell=1}^{N} \hat{j}_{{\rm p},\ell}$ (while, at the same time, including the diamagnetic term). This is manifestly displayed by our Hamiltonian (8.10) at $g_0 \neq 0$. Further details on the f-sum rule can be found in App. D.7.

ii) the complex excitonic order parameter

$$\mathcal{I} \equiv \frac{1}{N}\sum_k \langle \hat{c}^\dagger_{k,\mathrm{p}} \hat{c}_{k,\mathrm{s}} \rangle \ , \tag{8.15}$$

and iii) the number of electrons per site $n_0 \equiv N^{-1}\sum_{k,\alpha}\langle \hat{n}_{k,\alpha}\rangle$, where $\hat{n}_{k,\alpha} \equiv \hat{c}^\dagger_{k,\alpha}\hat{c}_{k,\alpha}$. The term proportional to $n_0/2$ in Eq. (8.13) acts as a renormalization of the chemical potential in the grand-canonical Hamiltonian and can be discarded in this study since we study the phase diagram only at half filling and $n_0 = 1$ in all phases.

In order to reduce the number of free parameters in the problem, from now on we enforce particle-hole symmetry in the bare band Hamiltonian $\hat{\mathcal{H}}_0$ by setting $E_\mathrm{s} \equiv -E_\mathrm{p} = -E_\mathrm{g}/2$ and $t_\mathrm{s} \equiv t_\mathrm{p} = t$ (with $|t| > E_\mathrm{g}/4$, see Fig. (S1)). In order to find the ground state of the Hamiltonian (8.10) with Hubbard interactions treated as in Eq. (8.13), we follow the same steps outlined in the proof of the no-go theorem above. We seek a ground state of the unentangled form $|\Psi\rangle = |\psi\rangle\,|\Phi\rangle$. After removing the term proportional to $(\hat{a}+\hat{a}^\dagger)^2$, one finds that $|\Phi\rangle$ must be a coherent state $|\bar{\beta}\rangle$ with $\bar{\beta} = -g_0\mathcal{J}\sqrt{N}/(\lambda^{3/2}\hbar\omega_\mathrm{c})$. (We remind the reader that the photon condensate order parameter is $\langle\bar{\beta}|\hat{a}|\bar{\beta}\rangle/\sqrt{N} = \langle\bar{\beta}|\cosh(x)\hat{b} - \sinh(x)\hat{b}^\dagger|\bar{\beta}\rangle/\sqrt{N} = \bar{\beta}/\sqrt{N\lambda}$. See App D.6.) Here, $\mathcal{J} \equiv \hbar\,\langle\psi|\,\hat{j}_\mathrm{p}\,|\psi\rangle/(aN)$, λ has the same expression as in the proof of the no-go theorem with $\Delta = -g_0^2\mathcal{T}/2$, and $\mathcal{T} \equiv \langle\psi|\,\hat{\mathcal{T}}\,|\psi\rangle$. Note that both $\mathcal{J}$ and $\mathcal{T}$ have units of energy and are finite in the $N\to\infty$ limit.

The resulting effective Hamiltonian for the matter degrees of freedom, i.e. $\langle\bar{\beta}|\,\hat{\mathcal{H}}_{\boldsymbol{A}_0}\,|\bar{\beta}\rangle$, can be diagonalized exactly since, after the HF decoupling, it is quadratic in the fermionic operators $\hat{c}_{k,\alpha}$, $\hat{c}^\dagger_{k,\alpha}$. To this end, it is sufficient to introduce the Bogoliubov operators $\hat{\gamma}^\dagger_{k,-} = u_k\hat{c}^\dagger_{k,\mathrm{s}} + v_k\hat{c}^\dagger_{k,\mathrm{p}}$ and $\hat{\gamma}^\dagger_{k,+} = v_k^*\hat{c}^\dagger_{k,\mathrm{s}} - u_k^*\hat{c}^\dagger_{k,\mathrm{p}}$, where the quantities u_k and v_k depend on the parameters of the bare Hamiltonian $\hat{\mathcal{H}}_0$, on the Hubbard parameter U, on the light-matter coupling constant g_0, and on the quantities $\mathcal{I}$, $\mathcal{M}$, $\mathcal{J}$, and $\mathcal{T}$. The ground state $|\psi\rangle = \prod_k \hat{\gamma}^\dagger_{k,-}\,|\mathrm{vac}\rangle$ can be written in a BCS-like fashion,

$$|\psi\rangle = \prod_k \left[u_k + v_k\hat{c}^\dagger_{k,\mathrm{p}}\hat{c}_{k,\mathrm{s}}\right]|\emptyset\rangle \ , \tag{8.16}$$

where $|\emptyset\rangle = \prod_k \hat{c}^\dagger_{k,\mathrm{s}}\,|\mathrm{vac}\rangle$ and $|\mathrm{vac}\rangle$ is the state with no electrons. The final ingredients which are needed are the expressions for the quantities $\mathcal{M}$, $\mathcal{I}$, $\mathcal{J}$, and $\mathcal{T}$ in terms of u_k, v_k: $\mathcal{M} = N^{-1}\sum_k(|v_k|^2 - |u_k|^2)$, $\mathcal{I} = N^{-1}\sum_k v_k^*u_k$, $\mathcal{J} = 2N^{-1}\sum_k[-t\sin(ka)(|v_k|^2 - |u_k|^2) - 2\tilde{t}\cos(ka)\mathrm{Im}(u_k^*v_k)]$, and $\mathcal{T} = 2N^{-1}\sum_k[t\cos(ka)\left(|v_k|^2 - |u_k|^2\right) - 2\tilde{t}\sin(ka)\mathrm{Im}(u_k^*v_k)]$. The technical details of this calculation are summarized in App. D.6.

The quantities $\mathcal{I}$, $\mathcal{M}$, $\mathcal{J}$, and $\mathcal{T}$ can be determined by solving this nonlinear system of equations. A typical solution is shown in Fig. 8.1. We have found that all observables are independent of g_0. In other words, in the thermodynamic limit the ground state is given by Eq. (8.16) with u_k and v_k evaluated at $g_0 = 0$, in agreement with the general theorem proven above. The self-consistent solutions always have $\mathcal{J} = 0$ (i.e. $\bar{\beta} = 0$), as clearly seen in Fig. 8.1(c), and therefore display no photon condensation but may have finite excitonic order parameter and finite polarization, as shown in Fig. 8.1(a) and (b), respectively. This is the second important result of this Chapter. We have checked that the self-consistent solutions always have $\mathcal{J} = 0$ on a wide range of parameters (not shown). Also, it is easy to prove that the stability of the solutions is guaranteed by the condition $\mathcal{T} \le 0$. At $\tilde{t} = 0$ the HF ground state has a single transition at $U = U_\mathrm{XC}$. For $0 < U < U_\mathrm{XC}$ the ground state is an exciton condensate with spontaneous coherence between s and p bands [201, 202]

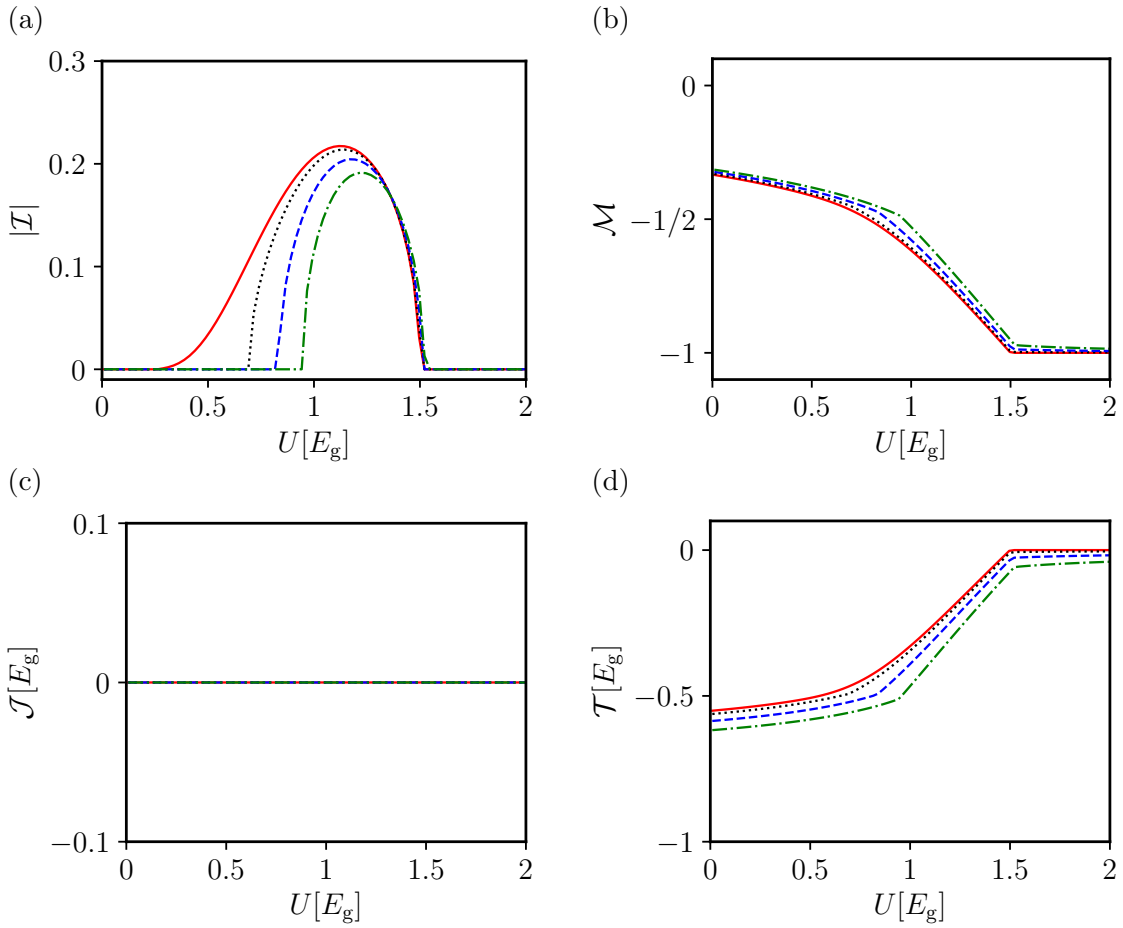

FIGURE 8.1: Panel (a) The excitonic order parameter $|\mathcal{I}|$ is plotted as a function of U (in units of E_g). Numerical results have been obtained by setting $t = 0.5\ E_g$ and $\hbar\omega_c = E_g$. Different curves correspond to different values of $\tilde{t}$. Red solid line: $\tilde{t} = 10^{-4}\ E_g$. Black dotted line: $\tilde{t} = 0.05\ E_g$. Blue dashed line: $\tilde{t} = 0.1\ E_g$. Green dash-dotted line: $\tilde{t} = 0.15\ E_g$. Note that for $\tilde{t} \neq 0$, $|\mathcal{I}| \neq 0$ for $U_{c1} < U < U_{c2}$. Panel (b) Same as in panel (a) but for the electronic polarization $\mathcal{M}$. Panel (c) Same as in other panels but for $\mathcal{J}$. Note that $\mathcal{J} = 0$ for all values of $\tilde{t}$ and U/E_g. This implies $\bar{\beta} = 0$ and therefore no photon condensation. Panel (d) Same as in other panels but for $\mathcal{T}$ (in units of E_g) .

which are not hybridized when $U = 0$. The ordered state appears on the small U side of the transition because interactions favor orbital polarization over coherence. The value of U_{XC} can be determined analytically as detailed in App. D.8. We find, in agreement with earlier work [210, 211], that $U_{XC} = 8t^2/E_g - E_g/2$.

In the limit $\tilde{t} = 0$, $\hat{\mathcal{H}}_{\boldsymbol{A}_0}$ separately conserves the number of electrons with band indices $\alpha = \mathrm{s}, \mathrm{p}$, and has a global $U(1)$ symmetry associated with the arbitrariness of the relative phase between s and p electrons [199]. The HF ground state breaks this symmetry. For $\tilde{t} \neq 0$ the $U(1)$ symmetry is reduced to a discrete Z_2 symmetry reflecting the invariance of the Hamiltonian under spatial inversion. This symmetry is broken for $U_{c1}(\tilde{t}) < U < U_{c2}(\tilde{t})$. Note that $\lim_{\tilde{t}\to 0} U_{c2}(\tilde{t}) = U_{XC}$. Corrections to $U_{c2}(0)$ can be found perturbatively for $\tilde{t}/t \ll 1$ and are of $\mathcal{O}(\tilde{t}^2)$ (see App. D.9). For $0 < U < U_{c1}(\tilde{t})$ inversion symmetry is unbroken and $\mathcal{I} = 0$. For $U > U_{c1}(\tilde{t})$ the ground state is an insulating ferroelectric that breaks the Z_2 symmetry (see App. D.9). The dependence of U_{c1} on $\tilde{t}$ is non-analytical and can be extracted

asymptotically for $\tilde{t}/t \ll 1$. We find that $U_{c1}(\tilde{t}) \to \pi(4t^2 - E_g^2/4)^{1/2}/|\ln(\tilde{t}/t)|$ (see App. D.9).

8.4 Summary and conclusions

In summary, we have presented a no-go theorem for photon condensation that applies to all quantum many-body Hamiltonians of the form (8.1), greatly extending previous no-go theorems for Dicke-type Hamiltonians [40, 73]. Since the proof is non-perturbative in the strength of electron-electron interactions, our arguments against photon condensation apply to all lattice models of strongly correlated electron systems that can be derived from Eq. (8.1). We have then explained how the theorem manifests in practice, presenting a theory of cavity QED of a 1D model that supports insulating ferroeletric and exciton condensate phases. We have shown that these electronic orders are never entwined with photon condensation [3]. In the future, it will be interesting to study the role of spatially-varying multimode cavity fields and their interplay with retarded interactions [212, 213], or strong magnetic fields [214]. Our work emphasizes that theoretical models of interacting light-matter systems must retain precise gauge invariance, which is often lost when the matter system is projected onto a low-energy model.

[3] The influence of strong interactions combined with a uniform single-mode cavity field on the phase diagram of small-gap semiconductors has also been considered in an interesting recent paper by G. Mazza and A. Georges, [72]. Some of the conclusions of this paper are incorrect because the model is not precisely gauge invariant.

9

Theory of Photon Condensation in a Spatially-Varying Electromagnetic Field

In this Chapter we show that the no-go theorem does not apply to spatially-varying quantum cavity fields. Here, we derive a series of criteria for occurrence of photon condensation. The results of this work have been published in Ref. [42] and this Chapter is largely based upon it.

This Chapter is organized as following. Photon condensation in 3D in the presence of purely orbital coupling between the cavity electromagnetic field and matter degrees of freedom is discussed in Sect. 9.2. The role of spin and combined orbital-spin effects (always in 3D) is reported in Sect. 9.3. Finally, the case of 2DESs embedded in quasi-2D cavities is discussed in Sect. 9.4. A brief summary and our main conclusions are finally presented in Sect. 9.5. A number of cumbersome mathematical proofs and useful technical details are reported in Appendix E.

9.1 Synopsis

The Dicke model [25], which describes a system of N qubits coupled to a single-mode spatially-uniform field confined in a cavity of volume V, plays a central role in quantum optics and cavity quantum electrodynamics (QED) [33, 36, 64, 65]. In 1973 Hepp and Lieb [31] and subsequently Wang and Hioe [38] pointed out that for sufficiently strong light-matter coupling the Dicke model in the thermodynamic limit ($N \to \infty$, $V \to \infty$, with $N/V = \text{const}$) has a finite temperature second-order equilibrium phase transition between a normal and "superradiant" state. In the latter, the ground state contains a macroscopically large number of coherent photons, *i.e.* $\langle \hat{a} \rangle \propto \sqrt{N}$, where $\hat{a}$ ($\hat{a}^\dagger$) destroys (creates) a cavity photon. To avoid confusion with the superradiant emission discussed in the original work by Dicke [25], we refer to the equilibrium superradiant phase as a photon condensate. Equilibrium superradiance was shown to be robust against the addition of counter-rotating terms [184, 185] neglected in Refs. 31, 38, but not against restoration of an additional neglected term proportional to

$(\hat{a} + \hat{a}^\dagger)^2$ (Ref. 39). This quadratic term is naturally generated by applying minimal coupling $\hat{\boldsymbol{p}} \to \hat{\boldsymbol{p}} + e\boldsymbol{A}/c$ to the electron kinetic energy $\hat{\boldsymbol{p}}^2/(2m)$. Rzażewski et al. [39] were the first to show that the Thomas-Reiche-Kuhn (TRK) sum rule [84, 186] poses an insurmountable obstacle against equilibrium superradiance in a spatially-uniform quantum cavity field. Physically, this sum rule originates from gauge invariance [85, 86], and in particular from the property that a system cannot respond to a spatially-uniform and time-independent vector potential. The link between gauge invariance and quadratic terms emerges as following. The quadratic term is responsible for the appearance of a *diamagnetic* contribution to the current operator [85, 86]. Only when paramagnetic and diamagnetic contributions are considered on equal footing, does one have a precisely gauge-invariant Hamiltonian satisfying the TRK sum rule. Recent advances in technology have reinvigorated interest in equilibrium superradiance [37, 187], inspiring a literature thread in which the obstacle presented by quadratic terms was periodically resurrected [40, 188]. Complications due to the presence of a superconducting condensate in circuit QED setups were also discussed [40, 73, 189–191].

In the Dicke model direct interactions between two-level systems are neglected. Effective long-range interactions between qubits are solely mediated by the common cavity field. Recent experimental progress has created opportunities to study light-matter interactions in an entirely new regime. For example, two-dimensional (2D) electron systems (ESs) can be embedded in cavities or exposed to the radiation field of metamaterials, making it possible to study strong light-matter interactions in the regime where direct electron-electron interactions may play a pivotal role, as in the quantum Hall regime [192–198].

Similarly, one can imagine cavity QED in which matter exhibits strongly correlated phenomena [212, 213, 215–224] such as exciton condensation, superconductivity, magnetism, or Mott insulating states. For all these exciting new possibilities, the paradigmatic Dicke model needs of course to be transcended. The degrees of freedom of microscopic many-body Hamiltonians—such as the one of the jellium model [86] or the Hubbard model [225] to name two—need to be coupled to the cavity modes. As the Dicke model story has instructed us, theories of the equilibrium properties of these intriguing new systems must be fully gauge invariant. This has not always been the case in the literature. For example, the case of materials with a low-energy linear energy-momentum dispersion relation, such as graphene and Weyl semimetals, is particularly tricky. In this case, the low-energy continuum model Hamiltonian needs to be accompanied by an ultraviolet cut-off, which breaks gauge invariance [226]. Using this model to study superradiant quantum phase transitions, e.g. in graphene [71], incorrectly implies photon condensation because a dynamically generated quadratic term is missed [74, 75]. We therefore conclude that low-energy truncations of the Hilbert space must be carried out carefully in order to preserve gauge invariance [78, 226, 227]. Another example is that of Ref. 72, where the coupling of the matter degrees of freedom of a two-band Hubbard model to the spatially-uniform vector potential of the cavity was carried out via a paramagnetic current operator not satisfying the continuity equation (see Ref. 41 for further details). A no-go theorem for superradiant quantum phase transitions which is applicable to generic interacting many-body systems in a cavity has been recently demonstrated in Ref. 41, under the strong but almost universally made assumption of a spatially-uniform cavity field.

The term “superradiance" is used to describe a plethora of different collective phenomena, ranging from the amplification of radiation due to coherence in the emitting medium [25] to the Zel'dovich-Misner-Unruh [228] amplification of radiation by rotating black holes. To avoid confusion, we will therefore refer to the equilibrium superradiant phase as a photon condensate. Given the impossibility of achieving photon condensation in a spatially-uniform quantum cavity field, in this Chapter we relax this strong assumption. We lay down a theory

of photon condensation in a *spatially-varying* quantum cavity field that does not rely on the smallness of the electron-electron-interaction coupling constant. As such, our theory is applicable to strongly correlated ESs. For pioneering theoretical works on the case of spatially-varying quantum cavity fields see Refs. 229–231.

We separately study three cases:

i) We first consider a three-dimensional (3D) ES embedded in a 3D cavity field. In this case, we reach a condition for the occurrence of photon condensation which is universal, in that it does not depend on the cavity material parameters. Indeed, our criterion depends only on a non-local linear response function of the 3DES, namely the static non-local orbital magnetic susceptibility $\chi_{\rm orb}(q)$. This quantity describes the response of the electron system to a static but spatially-oscillating magnetic field:

$$\chi_{\rm orb}(q) \equiv -\frac{e^2}{c^2}\frac{\chi_{\rm T}(q,0)}{q^2} \ . \tag{9.1}$$

Here, $-e$ is the electron charge, c is the speed of light in vacuum, and $\chi_{\rm T}(q,0)$ is the transverse current response function of the interacting ES [85, 86]. We find that photon condensation occurs if and only if $\chi_{\rm orb}(q) > 1/(4\pi)$.

ii) We then study the role of spin degrees of freedom, by including in the treatment the Zeeman coupling between the electron spin and the spatially-varying cavity field. We also discuss the combined effects of orbital and spin couplings.

iii) Finally, we consider the case of a 2DES embedded in a quasi-2D cavity of extension L_z in the direction perpendicular to the plane hosting the 2DES, i.e. the $\hat{\boldsymbol{x}}$-$\hat{\boldsymbol{y}}$ plane [231]. In this case, the criterion for photon condensation depends on L_z, and not only on the intrinsic orbital magnetic properties of the 2DES.

This Chapter is organized as following. Photon condensation in 3D in the presence of purely orbital coupling between the cavity electromagnetic field and matter degrees of freedom is discussed in Sect. 9.2. The role of spin and combined orbital-spin effects (always in 3D) is reported in Sect. 9.3. Finally, the case of 2DESs embedded in quasi-2D cavities is discussed in Sect. 9.4. A brief summary and our main conclusions are finally presented in Sect. 9.5. A number of cumbersome mathematical proofs and useful technical details are reported in Appendices E.1-E.4.

9.2 3D Photon Condensation

We consider a 3DES interacting with a spatially-varying quantized electromagnetic field. For the sake of concreteness, we assume that the 3DES is described by the jellium model Hamiltonian [85, 86]

$$\hat{\mathcal{H}} = \sum_{i=1}^{N} \frac{\hat{\boldsymbol{p}}_i^2}{2m} + \frac{1}{2}\sum_{i\neq j} v(|\hat{\boldsymbol{r}}_i - \hat{\boldsymbol{r}}_j|) \ . \tag{9.2}$$

This model describes N electrons of mass m interacting via an arbitrary [1] central potential $v(r)$. Charge neutrality (and therefore stability) of the system is guaranteed by a positive background of uniform charge. Electron-background and background-background interactions have not been explicitly written in $\hat{\mathcal{H}}$. For future reference, we denote by $|\psi_m\rangle$ and E_m the

[1] Strictly speaking, in the (unscreened) jellium model [86] $v(r) = e^2/(\epsilon_{\rm r} r)$, where $\epsilon_{\rm r}$ is a suitable background dielectric constant which will be introduced below. Nowhere in our proof we will assume this specific form of $v(r)$.

exact eigenstates and eigenvalues [85, 86] of $\hat{\mathcal{H}}$, with $|\psi_0\rangle$ and E_0 denoting the ground state and ground-state energy, respectively. We also introduce the 3D Fourier transforms of the density and paramagnetic (number) current operators [85, 86]:

$$\hat{n}(\boldsymbol{q}) = \sum_{i=1}^{N} e^{-i\boldsymbol{q}\cdot\hat{\boldsymbol{r}}_i} , \tag{9.3}$$

$$\hat{\boldsymbol{j}}_{\rm p}(\boldsymbol{q}) = \frac{1}{2m}\sum_{i=1}^{N}\left(\hat{\boldsymbol{p}}_i e^{-i\boldsymbol{q}\cdot\hat{\boldsymbol{r}}_i} + e^{-i\boldsymbol{q}\cdot\hat{\boldsymbol{r}}_i}\hat{\boldsymbol{p}}_i\right) , \tag{9.4}$$

with $\hat{n}(-\boldsymbol{q}) = \hat{n}^\dagger(\boldsymbol{q})$ and $\hat{\boldsymbol{j}}_{\rm p}(-\boldsymbol{q}) = \hat{\boldsymbol{j}}_{\rm p}^\dagger(\boldsymbol{q})$.

We treat the spatially-varying cavity electromagnetic field $\hat{\boldsymbol{A}}(\boldsymbol{r})$ in a quantum fashion [76, 232]. We consider a cavity of volume $V = L_x L_y L_z$, impose periodic boundary conditions on the cavity field, and represent it in terms of plane waves:

$$\hat{\boldsymbol{A}}(\boldsymbol{r}) = \sum_{\boldsymbol{q},\sigma} A_{\boldsymbol{q}}\boldsymbol{u}_{\boldsymbol{q},\sigma}(\hat{a}_{\boldsymbol{q},\sigma}e^{i\boldsymbol{q}\cdot\boldsymbol{r}} + \hat{a}^\dagger_{\boldsymbol{q},\sigma}e^{-i\boldsymbol{q}\cdot\boldsymbol{r}}) . \tag{9.5}$$

Here, $\boldsymbol{q} = (2\pi n_x/L_x, 2\pi n_y/L_y, 2\pi n_z/L_z)$ with (n_x, n_y, n_z) relative integers, $\sigma = 1, 2$ is the polarization index, $\boldsymbol{u}_{\boldsymbol{q},\sigma}$ is the linear polarization vector, $A_{\boldsymbol{q}} = \sqrt{2\pi\hbar c^2/(V\omega_{\boldsymbol{q}}\epsilon_{\rm r})}$, $\omega_{\boldsymbol{q}} = cq/\sqrt{\epsilon_{\rm r}}$, and $\epsilon_{\rm r}$ is a relative dielectric constant. The following properties hold [232]: $\omega_{-\boldsymbol{q}} = \omega_{\boldsymbol{q}}$, $\boldsymbol{u}_{-\boldsymbol{q},\sigma} = \boldsymbol{u}_{\boldsymbol{q},\sigma}$, $A_{-\boldsymbol{q}} = A_{\boldsymbol{q}}$, and $\boldsymbol{u}_{\boldsymbol{q},\sigma}\cdot\boldsymbol{u}_{\boldsymbol{q},\sigma'} = \delta_{\sigma,\sigma'}$. In the Coulomb gauge, we have the transversality condition

$$\boldsymbol{u}_{\boldsymbol{q},\sigma}\cdot\boldsymbol{q} = 0 , \tag{9.6}$$

for every $\boldsymbol{q}$ and σ. The photonic annihilation and creation operators in Eq. (9.5) satisfy bosonic commutation relations, $[\hat{a}_{\boldsymbol{q},\sigma}, \hat{a}^\dagger_{\boldsymbol{q}',\sigma'}] = \delta_{\boldsymbol{q},\boldsymbol{q}'}\delta_{\sigma,\sigma'}$.

Being a quantum object, the field $\hat{\boldsymbol{A}}(\boldsymbol{r})$ has its own dynamics, which is determined by the photon Hamiltonian

$$\hat{\mathcal{H}}_{\rm ph} = \sum_{\boldsymbol{q},\sigma}\hbar\omega_{\boldsymbol{q}}\left(\hat{a}^\dagger_{\boldsymbol{q},\sigma}\hat{a}_{\boldsymbol{q},\sigma} + \frac{1}{2}\right) . \tag{9.7}$$

The full Hamiltonian, including light-matter interactions, is therefore given by

$$\hat{\mathcal{H}}_{\boldsymbol{A}} = \hat{\mathcal{H}} + \hat{\mathcal{H}}_{\rm ph} + \sum_{i=1}^{N}\frac{e}{mc}\hat{\boldsymbol{A}}(\boldsymbol{r}_i)\cdot\hat{\boldsymbol{p}}_i + \sum_{i=1}^{N}\frac{e^2}{2mc^2}\hat{\boldsymbol{A}}^2(\boldsymbol{r}_i) . \tag{9.8}$$

The third and fourth terms in Eq. (9.8) are often referred to respectively as the paramagnetic and diamagnetic contributions to the light-matter coupling Hamiltonian.

With the aim of studying the potential existence of a quantum phase transition to a photon condensate and make therefore general statements about the ground state $|\Psi\rangle$ of $\hat{\mathcal{H}}_{\boldsymbol{A}}$, the model (9.8) must be extrapolated to the thermodynamic limit [31] $N \to \infty$, $V \to \infty$, with constant N/V. As shown in Appendix. E.1, in this limit, $|\Psi\rangle$ does not contain light-matter entanglement, i.e. we can take $|\Psi\rangle = |\psi\rangle\,|\Phi\rangle$, where $|\psi\rangle$ and $|\Phi\rangle$ are matter and light states. We can therefore introduce the effective Hamiltonian for the photonic degrees of freedom, $\hat{\mathcal{H}}^{\rm eff}_{\rm ph}[\psi] \equiv \langle\psi|\hat{\mathcal{H}}_{\boldsymbol{A}}|\psi\rangle$. Explicitly,

$$\hat{\mathcal{H}}_{\rm ph}^{\rm eff}\ [\psi] = \hat{\mathcal{H}}_{\rm ph} + \langle\psi|\hat{\mathcal{H}}|\psi\rangle + \sum_{\boldsymbol{q},\sigma}\frac{e}{c}A_{\boldsymbol{q}}\left[\hat{a}_{\boldsymbol{q},\sigma}\boldsymbol{j}_{\rm p}(-\boldsymbol{q})\cdot\boldsymbol{u}_{\boldsymbol{q},\sigma} + {\rm h.c.}\right] +$$
$$+ \quad \frac{e^2}{2mc^2}\sum_{\boldsymbol{q},\boldsymbol{q}',\sigma}A_{\boldsymbol{q}}A_{\boldsymbol{q}'}\boldsymbol{u}_{\boldsymbol{q},\sigma}\cdot\boldsymbol{u}_{\boldsymbol{q}',\sigma}\big[\hat{a}^\dagger_{\boldsymbol{q}',\sigma}\hat{a}_{\boldsymbol{q},\sigma}n(\boldsymbol{q}'-\boldsymbol{q}) + \hat{a}_{\boldsymbol{q},\sigma}\hat{a}^\dagger_{\boldsymbol{q}',\sigma}n(\boldsymbol{q}-\boldsymbol{q}') +$$
$$+ \quad \hat{a}_{\boldsymbol{q},\sigma}\hat{a}_{\boldsymbol{q}',\sigma}n(-\boldsymbol{q}-\boldsymbol{q}') + \hat{a}^\dagger_{\boldsymbol{q}',\sigma}\hat{a}^\dagger_{\boldsymbol{q},\sigma}n(\boldsymbol{q}+\boldsymbol{q}')\big]\ . \tag{9.9}$$

where we have used the transversality condition in Eq. (9.6), and introduced

$$n(\boldsymbol{q}) \equiv \langle\psi|\hat{n}(\boldsymbol{q})|\psi\rangle \tag{9.10}$$

and

$$\boldsymbol{j}_{\rm p}(\boldsymbol{q}) \equiv \langle\psi|\hat{\boldsymbol{j}}_{\rm p}(\boldsymbol{q})|\psi\rangle\ . \tag{9.11}$$

In the Coulomb gauge, 3D photon condensation is manifested by a non-zero value of the order parameter $\bar{\alpha}_{\boldsymbol{q},\sigma} \equiv \langle\Phi|\hat{a}_{\boldsymbol{q},\sigma}|\Phi\rangle$ emerging at a critical value of a suitable light-matter coupling constant [31, 38]. At the quantum critical point (QCP), $\bar{\alpha}_{\boldsymbol{q},\sigma}$ is small. Note also that, near the QCP, the matter state can be written as $|\bar{\psi}\rangle = |\psi_0\rangle + \sum_{\boldsymbol{q},\sigma}\bar{\alpha}_{\boldsymbol{q},\sigma}\,|\delta\psi_{\boldsymbol{q},\sigma}\rangle + \mathcal{O}(\bar{\alpha}^2_{\boldsymbol{q},\sigma})$. Since the diamagnetic term in Eq. (9.9) is quadratic in $\bar{\alpha}_{\boldsymbol{q},\sigma}$, we can approximate the quantity $n(\boldsymbol{q})$ in the last two lines of this equation with its value in the absence of light-matter interactions, i.e. we can safely take $n(\boldsymbol{q}) \simeq \langle\psi_0|\hat{n}(\boldsymbol{q})|\psi_0\rangle$. We now assume that the ground state $|\Psi_0\rangle$ of the 3DES in the absence of light-matter interactions is homogenous and isotropic, i.e. $\langle\psi_0|\hat{n}(\boldsymbol{q})|\psi_0\rangle = N\delta_{\boldsymbol{q},\boldsymbol{0}}$. The reason why this assumption was made is obvious from the form of the diamagnetic term in Eq. (9.9): inhomogeneous ground states with $\langle\psi_0|\hat{n}(\boldsymbol{q})|\psi_0\rangle \neq N\delta_{\boldsymbol{q},\boldsymbol{0}}$ would couple modes with $\boldsymbol{q} \neq \boldsymbol{q}'$, rapidly leading to a problem that is intractable with purely analytical methods. Under this assumption, the effective Hamiltonian reduces to:

$$\hat{\mathcal{H}}_{\rm ph}^{\rm eff}\ [\psi] = \langle\psi|\hat{\mathcal{H}}|\psi\rangle + \sum_{\boldsymbol{q},\sigma}\frac{eA_{\boldsymbol{q}}}{c}\left[\hat{a}_{\boldsymbol{q},\sigma}\boldsymbol{j}_{\rm p}(-\boldsymbol{q})\cdot\boldsymbol{u}_{\boldsymbol{q},\sigma} + \hat{a}^\dagger_{\boldsymbol{q},\sigma}\boldsymbol{j}_{\rm p}(\boldsymbol{q})\cdot\boldsymbol{u}_{\boldsymbol{q},\sigma}\right]$$
$$+ \quad \frac{1}{2}\sum_{\boldsymbol{q},\sigma}\left[\hbar\widetilde{\omega}_{\boldsymbol{q}} + \hbar\widetilde{\omega}_{\boldsymbol{q}}\left(\hat{a}^\dagger_{\boldsymbol{q},\sigma}\hat{a}_{\boldsymbol{q},\sigma} + \hat{a}^\dagger_{-\boldsymbol{q},\sigma}\hat{a}_{-\boldsymbol{q},\sigma}\right) + 2\Delta_{\boldsymbol{q}}\left(\hat{a}_{-\boldsymbol{q},\sigma}\hat{a}_{\boldsymbol{q},\sigma} + \hat{a}^\dagger_{\boldsymbol{q},\sigma}\hat{a}^\dagger_{-\boldsymbol{q},\sigma}\right)\right]\ , \tag{9.12}$$

where $\Delta_{\boldsymbol{q}} \equiv Ne^2A^2_{\boldsymbol{q}}/(2mc^2)$ with $\Delta_{\boldsymbol{q}} = \Delta_{-\boldsymbol{q}}$, and $\hbar\widetilde{\omega}_{\boldsymbol{q}} = \hbar\omega_{\boldsymbol{q}} + 2\Delta_{\boldsymbol{q}}$. The term $\sum_{\boldsymbol{q},\sigma}\hbar\widetilde{\omega}_{\boldsymbol{q}}/2$ is a vacuum contribution. Eq. (9.12) is a quadratic function of the photonic operators and can be diagonalized via the following Bogoliubov transformation:

$$\hat{a}^\dagger_{\boldsymbol{q},\sigma} \quad = \quad \cosh(x_{\boldsymbol{q}})\hat{b}^\dagger_{\boldsymbol{q},\sigma} - \sinh(x_{\boldsymbol{q}})\hat{b}_{-\boldsymbol{q},\sigma}\ , \tag{9.13}$$

where $\cosh(x_{\boldsymbol{q}}) = (\lambda_{\boldsymbol{q}}+1)/(2\sqrt{\lambda_{\boldsymbol{q}}})$, $\sinh(x_{\boldsymbol{q}}) = (\lambda_{\boldsymbol{q}}-1)/(2\sqrt{\lambda_{\boldsymbol{q}}})$, and $\lambda_{\boldsymbol{q}} = \sqrt{1+4\Delta_{\boldsymbol{q}}/\hbar\omega_{\boldsymbol{q}}}$. In terms of the new bosonic operators $\hat{b}^\dagger_{\boldsymbol{q},\sigma}, \hat{b}_{\boldsymbol{q},\sigma}$ the effective Hamiltonian reads as follows:

$$\hat{\mathcal{H}}^{\rm eff}_{\rm ph}[\psi] = \langle\psi|\hat{\mathcal{H}}|\psi\rangle + \sum_{\boldsymbol{q},\sigma}\hbar\Omega_{\boldsymbol{q}}\left(\hat{b}^\dagger_{\boldsymbol{q},\sigma}\hat{b}_{\boldsymbol{q},\sigma} + \frac{1}{2}\right) + \sum_{\boldsymbol{q},\sigma}\frac{eA_{\boldsymbol{q}}}{c\sqrt{\lambda_{\boldsymbol{q}}}}\left[\boldsymbol{j}_{\rm p}(-\boldsymbol{q})\cdot\boldsymbol{u}_{\boldsymbol{q},\sigma}\hat{b}_{\boldsymbol{q},\sigma} + {\rm H.c.}\right]\ , \tag{9.14}$$

where $\hbar\Omega_{\boldsymbol{q}} = \hbar\omega_{\boldsymbol{q}}\lambda_{\boldsymbol{q}}$.

Being a sum of displaced harmonic oscillators, the ground state $|\Phi\rangle$ of $\hat{\mathcal{H}}^{\rm eff}_{\rm ph}[\psi]$, for every matter state $|\psi\rangle$, is a tensor product $|\mathscr{B}\rangle \equiv \otimes_{\boldsymbol{q},\sigma} |\beta_{\boldsymbol{q},\sigma}\rangle$ of coherent states of the $\hat{b}_{\boldsymbol{q},\sigma}$ operators[47, 76], i.e. $\hat{b}_{\boldsymbol{q}',\sigma'} |\mathscr{B}\rangle = \beta_{\boldsymbol{q}',\sigma'} |\mathscr{B}\rangle$. Note that the order parameter $\alpha_{\boldsymbol{q},\sigma}$ introduced above is linearly-dependent on $\beta_{\boldsymbol{q},\sigma}$, i.e. $\alpha_{\boldsymbol{q},\sigma} = \cosh(x_{\boldsymbol{q}})\beta^*_{\boldsymbol{q},\sigma} - \sinh(x_{\boldsymbol{q}})\beta_{-\boldsymbol{q},\sigma}$. Hence, a non-zero $\beta_{\boldsymbol{q},\sigma}$ implies a non-zero $\alpha_{\boldsymbol{q},\sigma}$. From now on, we will therefore consider $\beta_{\boldsymbol{q},\sigma}$ as the order parameter, which can again be considered small at the QCP.

We now introduce the following energy functional, obtained by taking the expectation value of $\hat{\mathcal{H}}^{\rm eff}_{\rm ph}[\psi]$ over $|\mathscr{B}\rangle$: $E[\{\beta_{\boldsymbol{q},\sigma}\},\psi] \equiv \langle\Psi|\hat{\mathcal{H}}_{\boldsymbol{A}}|\Psi\rangle = \langle\mathscr{B}|\hat{\mathcal{H}}^{\rm eff}_{\rm ph}[\psi]|\mathscr{B}\rangle$:

$$E[\{\beta_{\boldsymbol{q},\sigma}\},\psi] = \langle\psi|\hat{\mathcal{H}}|\psi\rangle + \sum_{\boldsymbol{q},\sigma} \hbar\Omega_{\boldsymbol{q}} \left(|\beta_{\boldsymbol{q},\sigma}|^2 + \frac{1}{2}\right) + \sum_{\boldsymbol{q},\sigma} \frac{eA_{\boldsymbol{q}}}{c\sqrt{\lambda_{\boldsymbol{q}}}} \left[\boldsymbol{j}_{\rm p}(-\boldsymbol{q})\cdot\boldsymbol{u}_{\boldsymbol{q},\sigma}\beta_{\boldsymbol{q},\sigma} + \text{c.c.}\right] \ .$$

This needs to be minimized with respect to $\{\beta_{\boldsymbol{q},\sigma}\}$ and $|\psi\rangle$. The minimization with respect to $\{\beta_{\boldsymbol{q},\sigma}\}$ can be done analytically by imposing the condition $\partial_{\beta^*_{\boldsymbol{q},\sigma}} E[\{\beta_{\boldsymbol{q},\sigma}\},\psi] = 0$. We find that the optimal value of $\{\beta_{\boldsymbol{q},\sigma}\}$ is given by:

$$\bar{\beta}_{\boldsymbol{q},\sigma} = -\frac{A_{\boldsymbol{q}}}{\hbar\omega_{\boldsymbol{q}}\lambda_{\boldsymbol{q}}^{3/2}} \frac{e}{c} \boldsymbol{j}_{\rm p}(\boldsymbol{q})\cdot\boldsymbol{u}_{\boldsymbol{q},\sigma} \ , \tag{9.15}$$

which depends on $|\psi\rangle$ through Eq. (9.11). Note that this equation can be written in terms of the operator

$$\hat{B}_{\boldsymbol{q},\sigma} \equiv -\frac{A_{\boldsymbol{q}}}{\hbar\omega_{\boldsymbol{q}}\lambda_{\boldsymbol{q}}^{3/2}} \frac{e}{c} \hat{\boldsymbol{j}}_{\rm p}(\boldsymbol{q})\cdot\boldsymbol{u}_{\boldsymbol{q},\sigma} \ , \tag{9.16}$$

i.e. $\bar{\beta}_{\boldsymbol{q},\sigma} = \langle\psi|\hat{B}_{\boldsymbol{q},\sigma}|\psi\rangle$.

Using Eq. (9.15) into Eq. (9.15), we finally find the energy functional that needs to be minimized with respect to $|\psi\rangle$:

$$E[\{\bar{\beta}_{\boldsymbol{q},\sigma}\},\psi] = \langle\psi|\hat{\mathcal{H}}|\psi\rangle - \sum_{\boldsymbol{q},\sigma} \hbar\Omega_{\boldsymbol{q}} \left(|\bar{\beta}_{\boldsymbol{q},\sigma}|^2 - \frac{1}{2}\right) \ . \tag{9.17}$$

As in the case of a spatially-uniform cavity field [41], we are therefore left with a *constrained* minimum problem for the matter degrees of freedom: we need to seek the minimum of (9.17) among the normalized anti-symmetric states $|\psi\rangle$ which yield (9.15). Such constrained minimum problems can be effectively handled with the stiffness theorem [86].

For photon condensation to occur we need the photon condensate phase to be energetically favored with respect to the normal phase, i.e. we need $E[\{\bar{\beta}_{\boldsymbol{q},\sigma}\},\psi] < E[0,\psi_0]$ or, equivalently,

$$\langle\psi|\hat{\mathcal{H}}|\psi\rangle - \langle\psi_0|\hat{\mathcal{H}}|\psi_0\rangle < \sum_{\boldsymbol{q},\sigma} \hbar\Omega_{\boldsymbol{q}}|\bar{\beta}_{\boldsymbol{q},\sigma}|^2 \ . \tag{9.18}$$

Note that the left-hand side of the previous inequality is the energy difference $E[\{\bar{\beta}_{\boldsymbol{q},\sigma}\},\psi] - E[0,\psi_0]$, so that the vacuum contribution $\sum_{\boldsymbol{q},\sigma}\hbar\Omega_{\boldsymbol{q}}/2$ drops out of the right-hand side.

The dependence of $\langle\psi|\hat{\mathcal{H}}|\psi\rangle - \langle\psi_0|\hat{\mathcal{H}}|\psi_0\rangle$ on $\bar{\beta}_{\boldsymbol{q},\sigma}$ can be calculated *exactly* up to order $\bar{\beta}^2_{\boldsymbol{q},\sigma}$ by using the stiffness theorem [86]. The expansion of the left hand side of the inequality (9.18) up to order $\bar{\beta}^2_{\boldsymbol{q},\sigma}$ is justified by the smallness of $\bar{\beta}_{\boldsymbol{q},\sigma}$ at the QCP. From now on, we exclude the trivial case $\langle\psi_0|\hat{\boldsymbol{j}}_{\rm p}(\boldsymbol{q})|\psi_0\rangle \neq 0$, requiring that $\langle\psi_0|\hat{\boldsymbol{j}}_{\rm p}(\boldsymbol{q})|\psi_0\rangle = 0$ for all values of

$\boldsymbol{q}$: for non-trivial photon condensate phases to occur, the ground state of the 3DES described by (9.2) is required to display no ground-state currents at all length scales.

Using the stiffness theorem [86], we find, up to second order in $\bar{\beta}_{\boldsymbol{q},\sigma}$,

$$\langle\psi|\hat{\mathcal{H}}|\psi\rangle - \langle\psi_0|\hat{\mathcal{H}}|\psi_0\rangle = -\frac{1}{2}\sum_{\boldsymbol{q},\sigma}\sum_{\boldsymbol{q}',\sigma'}\chi^{-1}_{\hat{B}_{\boldsymbol{q},\sigma},\hat{B}_{-\boldsymbol{q}',\sigma'}}(0)\bar{\beta}^{*}_{\boldsymbol{q},\sigma}\bar{\beta}_{\boldsymbol{q}',\sigma'} \ , \tag{9.19}$$

where $\chi^{-1}_{\hat{B}_{\boldsymbol{q},\sigma},\hat{B}_{-\boldsymbol{q}',\sigma'}}(0)$ is the inverse of the static response function $\chi_{\hat{B}_{\boldsymbol{q},\sigma},\hat{B}_{-\boldsymbol{q}',\sigma'}}(0)$, the operator $\hat{B}_{\boldsymbol{q},\sigma}$ has been introduced in Eq. (9.16), and we have used the notation of Ref. 86. Since the ground state of the 3DES has been taken to be homogenous and isotropic [86],

$$\chi_{\hat{B}_{\boldsymbol{q},\sigma},\hat{B}_{-\boldsymbol{q}',\sigma'}}(0) = \chi_{\hat{B}_{\boldsymbol{q},\sigma},\hat{B}_{-\boldsymbol{q},\sigma}}(0)\delta_{\boldsymbol{q},\boldsymbol{q}'}\delta_{\sigma,\sigma'} \ . \tag{9.20}$$

As any other response function, $\chi_{\hat{B}_{\boldsymbol{q},\sigma},\hat{B}_{-\boldsymbol{q},\sigma}}(0)$ has a Lehmann representation [85, 86] in terms of the exact eigenstates of the Hamiltonian (9.2),

$$\chi_{\hat{B}_{\boldsymbol{q},\sigma},\hat{B}_{-\boldsymbol{q},\sigma}}(0) = -\frac{2A^2_{\boldsymbol{q}}}{\hbar^2\omega^2_{\boldsymbol{q}}\lambda^3_{\boldsymbol{q}}}\frac{e^2}{c^2}\sum_{n\neq 0}\frac{|\langle\psi_n|\hat{\boldsymbol{j}}_{\rm p}(\boldsymbol{q})\cdot\boldsymbol{u}_{\boldsymbol{q},\sigma}|\psi_0\rangle|^2}{E_n - E_0} < 0 \ . \tag{9.21}$$

We readily recognize $\chi_{\hat{B}_{\boldsymbol{q},\sigma},\hat{B}_{-\boldsymbol{q},\sigma}}(0)$ to be intimately linked to the static, paramagnetic current-current response tensor [86]

$$\begin{aligned}\chi_{\hat{j}_{\boldsymbol{p},i}(\boldsymbol{q}),\hat{j}_{\boldsymbol{p},k}(-\boldsymbol{q})}(0) &= -\frac{1}{V}\sum_{n\neq 0}\frac{\langle\psi_n|\hat{j}_{{\rm p},i}(\boldsymbol{q})|\psi_0\rangle\,\langle\psi_0|\hat{j}_{{\rm p},k}(-\boldsymbol{q})|\psi_n\rangle}{E_n - E_0} \\ &- \frac{1}{V}\sum_{n\neq 0}\frac{\langle\psi_0|\hat{j}_{{\rm p},i}(\boldsymbol{q})|\psi_n\rangle\,\langle\psi_n|\hat{j}_{{\rm p},k}(-\boldsymbol{q})|\psi_0\rangle}{E_n - E_0} \ ,\end{aligned} \tag{9.22}$$

where $\hat{j}_{{\rm p},i}(\boldsymbol{q})$, with $i = x, y, z$, denotes the i-th Cartesian component of $\hat{\boldsymbol{j}}_{\rm p}(\boldsymbol{q})$. Indeed, it is easy to show that

$$\chi_{\hat{B}_{\boldsymbol{q},\sigma},\hat{B}_{-\boldsymbol{q},\sigma}}(0) = \frac{A^2_{\boldsymbol{q}}N}{\hbar^2\omega^2_{\boldsymbol{q}}\lambda^3_{\boldsymbol{q}}n}\frac{e^2}{c^2}\sum_{i,k}u^{(i)}_{\boldsymbol{q},\sigma}u^{(k)}_{\boldsymbol{q},\sigma}\chi_{\hat{j}_{\boldsymbol{p},i}(\boldsymbol{q}),\hat{j}_{\boldsymbol{p},k}(-\boldsymbol{q})}(0) \ , \tag{9.23}$$

where $u^{(i)}_{\boldsymbol{q},\sigma}$ denotes the i-th Cartesian component of the vector $\boldsymbol{u}_{\boldsymbol{q},\sigma}$ and we have introduced the electron density $n = N/V$. The previous result can be written in a more transparent manner by introducing the *physical* current-current response tensor [86], which contains a diamagnetic as well as a paramagnetic contribution:

$$\chi^{\rm J}_{i,k}(\boldsymbol{q},0) = \frac{n}{m}\delta_{i,k} + \chi_{\hat{j}_{{\rm p},i}(\boldsymbol{q}),\hat{j}_{{\rm p},k}(-\boldsymbol{q})}(0) \ . \tag{9.24}$$

In a homogeneous and isotropic system, the rank-2 tensor $\chi^{\rm J}_{i,k}(\boldsymbol{q},0)$ can be decomposed in terms of the longitudinal and transverse current-current response functions [86], $\chi^{\rm J}_{\rm L}(q,0)$ and $\chi^{\rm J}_{\rm T}(q,0)$, respectively:

$$\chi^{\rm J}_{i,k}(\boldsymbol{q},0) = \chi^{\rm J}_{\rm L}(q,0)\frac{q_i q_k}{q^2} + \chi^{\rm J}_{\rm T}(q,0)\left(\delta_{i,k} - \frac{q_i q_k}{q^2}\right) \ . \tag{9.25}$$

Note that, as a consequence of gauge invariance, $\chi^{\rm J}_{\rm L}(q,0) = 0$ for every q [86]. Using Eqs. (9.24)-(9.25) in Eq. (9.23), we finally find

$$\chi_{\hat{B}_{\boldsymbol{q},\sigma},\hat{B}_{-\boldsymbol{q},\sigma}}(0) = \frac{A^2_{\boldsymbol{q}} N}{\hbar^2 \omega^2_{\boldsymbol{q}} \lambda^3_{\boldsymbol{q}} n} \frac{e^2}{c^2} \left[\chi^{\rm J}_{\rm T}(q,0) - \frac{n}{m} \right] . \tag{9.26}$$

As a natural consequence of the transversality of the electromagnetic field, imposed by the Coulomb gauge, only the transverse current-current response function $\chi^{\rm J}_{\rm T}(q,0)$ enters Eq. (9.26).

We now return to the result of the stiffness theorem. Inserting Eq. (9.19) inside Eq. (9.18), we finally find the condition for photon condensation in a 3DES embedded in a spatially-varying electromagnetic field:

$$-\sum_{\boldsymbol{q},\sigma} \left[\frac{1}{2\chi_{\hat{B}_{\boldsymbol{q},\sigma},\hat{B}_{-\boldsymbol{q},\sigma}}(0)} + \hbar\Omega_{\boldsymbol{q}} \right] |\bar{\beta}_{\boldsymbol{q},\sigma}|^2 < 0 . \tag{9.27}$$

Since we want to minimize the energy difference $E[\{\bar{\beta}_{\boldsymbol{q},\sigma}\},\psi] - E[0,\psi_0]$, the optimal choice of $\bar{\beta}_{\boldsymbol{q}\sigma}$ is constructed as follows: i) modes with momentum $\boldsymbol{q}$ and polarization σ such that Eq. (9.27) is satisfied acquire a finite displacement $\bar{\beta}_{\boldsymbol{q}\sigma} \neq 0$, since this choice lowers the energy difference; ii) on the other hand, modes for which Eq. (9.27) is not satisfied, are forced to be unpopulated, i.e. to have $\bar{\beta}_{\boldsymbol{q},\sigma} = 0$. A finite occupation of these modes would indeed increase the energy difference. Hence, we can analyze the inequality (9.27) for a fixed $\boldsymbol{q}$:

$$-\chi_{\hat{B}_{\boldsymbol{q},\sigma},\hat{B}_{-\boldsymbol{q},\sigma}}(0) > \frac{1}{2\hbar\Omega_{\boldsymbol{q}}} . \tag{9.28}$$

Using Eq. (9.26) and the microscopic expression of $A_{\boldsymbol{q}}$, we can rewrite Eq. (9.28) as follows:

$$-4\pi \frac{c^2}{\omega^2_{\boldsymbol{q}} \epsilon_{\rm r}} \frac{e^2}{c^2} \left[\chi^{\rm J}_{\rm T}(q,0) - \frac{n}{m} \right] > 1 + 4\frac{\Delta_{\boldsymbol{q}}}{\hbar\omega_{\boldsymbol{q}}} . \tag{9.29}$$

Before further simplifying Eq. (9.29), we wish to make a few observations on the special case of a single-mode spatially-uniform field:

i) *No-go theorem in the presence of the diamagnetic term.* Let us consider the standard situation in the literature, in which matter degrees of freedom are minimally coupled to a quantum field, which is assumed to be single mode and spatially uniform, with angular frequency ω_0 and amplitude $A_{\boldsymbol{q}} = A_0 = \sqrt{2\pi\hbar c^2/(V\omega_0\epsilon_{\rm r})}$. Consistently, if the assumption of spatial uniformity is done from the very beginning, by setting $\boldsymbol{q} = \boldsymbol{0}$ in Eq. (9.5), one has to replace $\chi^{\rm J}_{\rm T}(q,0)$ with $\lim_{q\to 0} \chi^{\rm J}_{\rm T}(q,0)$ inside the square bracket in Eq. (9.29). In systems with no long-range order (i.e. in systems that do not become superconducting), it is well known [86] that the "diamagnetic sum rule" holds true: $\lim_{q\to 0} \chi^{\rm J}_{\rm T}(q,0) = 0$. In this case, Eq. (9.29) reduces to:

$$4\pi \frac{c^2}{\omega^2_0 \epsilon_{\rm r}} \frac{e^2}{c^2} \frac{n}{m} > 1 + 4\frac{\Delta_0}{\hbar\omega_0} , \tag{9.30}$$

with $\Delta_0 = e^2 N A_0^2/(2mc^2)$. The left-hand-side of Eq. (9.30) can be easily seen to be equal to $4\Delta_0/(\hbar\omega_0)$ and this inequality therefore reduces to $0 > 1$, which is clearly absurd. This is the no-go theorem [41] for photon condensation in a single-mode spatially-uniform quantum field.

ii) *Spurious "go theorem" in the absence of the diamagnetic term.* Neglecting artificially the diamagnetic contribution to Eq. (9.8) is equivalent to setting $\Delta_0 = 0$ in the right-hand-side of Eq. (9.30). In this case a photon condensate occurs provided that the Drude weight $\mathcal{D} = \pi e^2 n/m$ of the 3DES satisfies the following inequality:

$$\mathcal{D} > \frac{\omega_0^2 \epsilon_{\rm r}}{4} \ . \tag{9.31}$$

Returning to Eq. (9.29) and using in it the microscopic expressions for $\omega_{\boldsymbol{q}}$ and $\Delta_{\boldsymbol{q}}$ given above (below Eq.(9.5) and Eq.(9.12), respectively), we finally conclude that a photon condensate phase occurs if and only if the following inequality is satisfied:

$$-\frac{e^2}{c^2}\frac{\chi_{\rm T}^{\rm J}(q,0)}{q^2} > \frac{1}{4\pi} \ . \tag{9.32}$$

The left-hand-side of Eq. (9.32) has a very clear physical interpretation. It is the non-local orbital magnetic susceptibility [86]

$$\chi_{\rm orb}(q) \equiv -\frac{e^2}{c^2}\frac{\chi_{\rm T}^{\rm J}(q,0)}{q^2} \ , \tag{9.33}$$

which, in the long-wavelength $q \to 0$ limit, reduces to the thermodynamic (i.e. macroscopic) orbital magnetic susceptibility (OMS)

$$\chi_{\rm OMS} \equiv \lim_{q\to 0} \chi_{\rm orb}(q) = \left.\frac{\partial M_{\rm O}}{\partial B}\right|_{B=0} \ . \tag{9.34}$$

Here, $M_{\rm O}$ is the orbital contribution to the magnetization. This limit exists in systems with no long-range order: indeed, $\chi_{\rm T}^{\rm J}(q,0)$ vanishes like q^2 in the long-wavelength $q \to 0$ limit, in agreement with the diamagnetic sum rule [86].

In summary, introducing $\chi_{\rm orb}(q)$, we can write Eq. (9.32) as

$$\boxed{\chi_{\rm orb}(q) > \frac{1}{4\pi}} \ . \tag{9.35}$$

Eq. (9.35) is the most important result of this Section, representing a rigorous criterion for the occurrence of photon condensation in a 3DES.

9.2.1 Discussion

A few comments are now in order.

i) In 3D, as clear from Eq. (9.35), $\chi_{\rm orb}(q)$ is dimensionless. It therefore naturally plays the role of a coupling constant determining the strength of light-matter interactions. Only when it exceeds the value $1/(4\pi) \sim 0.08$ can photon condensation take place.

ii) The criterion (9.35) does not depend *explicitly* on $\epsilon_{\rm r}$ but only implicitly, through the $\epsilon_{\rm r}$-dependence of the e-e interaction potential $v(r)$. The latter, in turn, has an impact on $\chi_{\rm orb}(q)$.

iii) Note that, while $\chi_{\hat{B}_{\boldsymbol{q},\sigma},\hat{B}_{-\boldsymbol{q},\sigma}}(0)$ in Eq. (9.21) and (9.26) is negative definite, the transverse contribution $\chi_{\rm T}(q,0)$ to the current-current response function satisfies the inequality $\chi_{\rm T}(q,0) < n/m$ and can therefore be both positive or negative. In turn, this implies that, for a given 3DES, $\chi_{\rm OMS}$ can be positive or negative (and perhaps change sign with microscopic

parameters such as the electron density n). Broadly speaking, materials can be divided intro two groups, from the point of view of their orbital response: a) orbital *diamagnets*, those which have $\chi_{\rm OMS} < 0$, are most common. They will not display photon condensation, according to our criterion (9.35); b) orbital *paramagnets*, those for which $\chi_{\rm OMS} > 0$, are much more rare in nature but, as discussed below, do exist. Only orbital paramagnets with $\chi_{\rm OMS} > 1/(4\pi)$ can display photon condensation.

Just as an example, we remind the reader that for free (i.e. non-interacting) parabolic-band fermions in 3D [86],

$$\chi^{(0)}_{\rm OMS} = -\frac{\alpha^2}{r_{\rm s}} \left(\frac{1}{768\pi^5} \right)^{1/3} < 0 \ , \tag{9.36}$$

where $r_{\rm s} = [3/(4\pi n a_{\rm B}^3)]^{1/3}$ is the so-called Wigner-Seitz or gas parameter, $a_{\rm B} = \hbar^2/(me^2)$ is the Bohr radius, and $\alpha = e^2/(\hbar c)$ is the fine structure constant.

iv) The result in Eq. (9.35) can be understood as the condition for the occurrence of a static magnetic instability [231]. Indeed, let us consider the energy functional of a material subject to a magnetic field $\boldsymbol{H}(\boldsymbol{r})$:

$$E[\boldsymbol{B}(\boldsymbol{r})] = \frac{1}{2} \int d^3\boldsymbol{r} \ \boldsymbol{H}(\boldsymbol{r}) \cdot \boldsymbol{B}(\boldsymbol{r}) \ , \tag{9.37}$$

where $\boldsymbol{B}(\boldsymbol{r})$ is the magnetic induction. The latter is related to the magnetic field via the orbital magnetization $\boldsymbol{M}(\boldsymbol{r})$, i.e. $\boldsymbol{B}(\boldsymbol{r}) = \boldsymbol{H}(\boldsymbol{r}) + 4\pi \boldsymbol{M}(\boldsymbol{r})$. The difference between $\boldsymbol{H}$ and $\boldsymbol{B}$ stems from the flow of charges in response to $\boldsymbol{H}$, which creates an orbital magnetization $\boldsymbol{M}$. In the realm of linear response theory, we can relate the orbital magnetization to the magnetic induction, $\boldsymbol{M}(\boldsymbol{r}) = \int d^3\boldsymbol{r}' \chi_{\rm orb}(|\boldsymbol{r} - \boldsymbol{r}'|) \boldsymbol{B}(\boldsymbol{r}')$. We can therefore write the energy as a quadratic function of $\boldsymbol{B}(\boldsymbol{r})$:

$$\begin{aligned} E[\boldsymbol{B}(\boldsymbol{r})] &= \frac{1}{2} \int d^3\boldsymbol{r} \int d^3\boldsymbol{r}' \Big[\delta(\boldsymbol{r} - \boldsymbol{r}') \\ &- 4\pi \chi_{\rm orb}(|\boldsymbol{r} - \boldsymbol{r}'|) \Big] \boldsymbol{B}(\boldsymbol{r}') \cdot \boldsymbol{B}(\boldsymbol{r}) \ . \end{aligned} \tag{9.38}$$

An instability occurs if $E[\boldsymbol{B}(\boldsymbol{r})] < 0$, i.e. if and only if $\boldsymbol{B}(\boldsymbol{r}) < 4\pi \int d\boldsymbol{r}' \chi_{\rm orb}(|\boldsymbol{r} - \boldsymbol{r}'|) \boldsymbol{B}(\boldsymbol{r}')$. Fourier transforming with respect to $\boldsymbol{r}$ yields Eq. (9.35).

Magnetostatic instabilities and the criterion (9.35) have been discussed long ago [233–238]. In a 3D metal, the de Haas-van Alphen effect (oscillations of the magnetization in response to an applied magnetic field) can lead to a thermodynamic instability of the electron gas. The magnetization is a function of the magnetic induction and when the orbital magnetic susceptibility $\chi_{\rm OMS}$ obeys the inequality (9.35), the magnetic induction is a multi-valued function of the field. Condon first pointed out that Maxwell's construction yields phase coexistence and the formation of (paramagnetic and diamagnetic) domains. These "Condon domains", although first predicted for Be [233], were first unambiguously observed in Ag [239]. Since then, Condon domains have been observed also in Be [240], Sn [241], and also Al, Pb, and In (for a recent review see, for example, Ref. 237). They have also been observed in Br_2-intercalated graphite [242], which is a layered compound with quasi-2D character.

The derivation in Sect. 9.2 shows that 3D photon condensation and Condon domain formation are the *same* phenomenon [231]. In essence, the proof reported in Sect. 9.2 is a fully quantum mechanical derivation of the condition for the occurrence of Condon domains, which transcends the usual semiclassical approximations [235] used to derive (9.35).

v) For the remainder of this Chapter (particularly for Sect. 9.4), it is useful to derive Eq. (9.12) in an alternative way.

Instead of determining the exact photonic state, as we did above, we now follow a much more humble approach. We evaluate the expectation value of the Hamiltonian (9.12) on a trial photonic wavefunction of the form $|\mathscr{A}\rangle \equiv \otimes_{\boldsymbol{q},\sigma} |\alpha_{\boldsymbol{q},\sigma}\rangle$, namely a tensor product of coherent states of the $\hat{a}_{\boldsymbol{q},\sigma}$ operators, i.e. $\hat{a}_{\boldsymbol{q}',\sigma'} |\mathscr{A}\rangle = \alpha_{\boldsymbol{q}',\sigma'} |\mathscr{A}\rangle$. (We know that the exact eigenstate is not of this form, i.e. it is a tensor product $|\mathscr{B}\rangle \equiv \otimes_{\boldsymbol{q},\sigma} |\beta_{\boldsymbol{q},\sigma}\rangle$ of coherent states of the $\hat{b}_{\boldsymbol{q},\sigma}$ operators. Momentarily, we will understand what error is made in using $|\mathscr{A}\rangle$ rather than $|\mathscr{B}\rangle$.) Such expectation value is easily obtained by replacing the photonic operators in Eq. (9.12) with c-numbers, i.e. by replacing $\hat{a}_{\boldsymbol{q},\sigma} \to \alpha_{\boldsymbol{q},\sigma}$. Up to a constant factor, we find

$$\begin{aligned}
\tilde{E} \quad & [\{\alpha_{\boldsymbol{q},\sigma}\}, \psi] \equiv \langle \mathscr{A} | \hat{\mathcal{H}}^{\rm eff}_{\rm ph}[\psi] | \mathscr{A} \rangle = \langle \psi | \hat{\mathcal{H}} | \psi \rangle + \\
+ \quad & \sum_{\boldsymbol{q},\sigma} \frac{eA_{\boldsymbol{q}}}{c} \left[\alpha_{\boldsymbol{q},\sigma} \boldsymbol{j}_{\rm p}(-\boldsymbol{q}) \cdot \boldsymbol{u}_{\boldsymbol{q},\sigma} + \alpha^*_{\boldsymbol{q},\sigma} \boldsymbol{j}_{\rm p}(\boldsymbol{q}) \cdot \boldsymbol{u}_{\boldsymbol{q},\sigma} \right] \\
+ \quad & \frac{1}{2} \sum_{\boldsymbol{q},\sigma} \left[\hbar\widetilde{\omega}_{\boldsymbol{q}} \left(\alpha^*_{\boldsymbol{q},\sigma} \alpha_{\boldsymbol{q},\sigma} + \alpha^*_{-\boldsymbol{q},\sigma} \alpha_{-\boldsymbol{q},\sigma} + 1 \right) + 2\Delta_{\boldsymbol{q}} \left(\alpha_{-\boldsymbol{q},\sigma} \alpha_{\boldsymbol{q},\sigma} + \alpha^*_{\boldsymbol{q},\sigma} \alpha^*_{-\boldsymbol{q},\sigma} \right) \right] \ . \quad (9.39)
\end{aligned}$$

Performing in Eq. (9.39) the linear transformation $\alpha^*_{\boldsymbol{q},\sigma} = \cosh(x_{\boldsymbol{q}}) \beta^*_{\boldsymbol{q},\sigma} - \sinh(x_{\boldsymbol{q}}) \beta_{-\boldsymbol{q},\sigma}$, analogous to Eq. (9.13), we get:

$$\tilde{E}[\{\beta_{\boldsymbol{q},\sigma}\}, \psi] = \langle \psi | \hat{\mathcal{H}} | \psi \rangle + \sum_{\boldsymbol{q},\sigma} \left(\frac{\hbar\widetilde{\omega}_{\boldsymbol{q}}}{2} + \hbar\Omega_{\boldsymbol{q}} |\beta_{\boldsymbol{q},\sigma}|^2 \right) + \sum_{\boldsymbol{q},\sigma} \frac{eA_{\boldsymbol{q}}}{c\sqrt{\lambda_{\boldsymbol{q}}}} \left[\boldsymbol{j}_{\rm p}(-\boldsymbol{q}) \cdot \boldsymbol{u}_{\boldsymbol{q},\sigma} \beta_{\boldsymbol{q},\sigma} + \text{c.c.} \right] \ .$$

The quantity $\tilde{E}[\{\beta_{\boldsymbol{q},\sigma}\}, \psi]$ differs from the exact result in Eq. (9.15) only for the vacuum contribution, which is $\sum_{\boldsymbol{q},\sigma} \hbar\widetilde{\omega}_{\boldsymbol{q}}/2$ instead of the correct one $\sum_{\boldsymbol{q},\sigma} \hbar\Omega_{\boldsymbol{q}}/2$. However, since we are interested only in energy differences, the vacuum contribution drops out of the problem and the two procedures yield the same energy difference: $E[\{\bar{\beta}_{\boldsymbol{q},\sigma}\}, \psi] - E[0, \psi_0] = \tilde{E}[\{\bar{\beta}_{\boldsymbol{q},\sigma}\}, \psi] - E[0, \psi_0]$.

In conclusion, if one is solely interested in energy differences, it is not necessary to determine the eigenstates exactly but it is sufficient to assume the photonic wave-function to be a tensor product of coherent states of the $\hat{a}_{\boldsymbol{q},\sigma}$ operators.

9.3 The role of Zeeman coupling and combined orbital-spin effects

In this Section we investigate the role of the Zeeman coupling. To begin with, we consider (Sect. 9.3.1) the case in which the 3DES couples to the radiation field only via the Zeeman term. In the second part of this Section (Sect. 9.3.2), we consider the combined role of orbital and Zeeman couplings. The derivation of the corresponding criteria for photon condensation closely follows the case of pure orbital coupling discussed in Sect. 9.2.

9.3.1 Light-matter interactions via the Zeeman term

If the 3DES couples to the spatially-varying cavity electromagnetic field only via the Zeeman term, the full Hamiltonian is:

$$\hat{\mathcal{H}}_{\boldsymbol{B}} = \hat{\mathcal{H}} + \hat{\mathcal{H}}_{\rm ph} + \frac{g\mu_{\rm B}}{2} \sum_{i=1}^{N} \hat{\boldsymbol{\sigma}}_i \cdot \hat{\boldsymbol{B}}(\boldsymbol{r}_i) \ , \quad (9.40)$$

where g is the Landé g-factor, $\mu_{\rm B}$ is the Bohr magneton, $\hat{\boldsymbol{\sigma}}_i$ is the spin operator of the i-th electron, and $\hat{\boldsymbol{B}}(\boldsymbol{r}) = \boldsymbol{\nabla} \times \hat{\boldsymbol{A}}(\boldsymbol{r})$ is the magnetic component of the cavity electromagnetic field, $\hat{\boldsymbol{A}}(\boldsymbol{r})$ being given in Eq. (9.5). Explicitly, the magnetic field reads as follows:

$$\hat{\boldsymbol{B}}(\boldsymbol{r}) = \sum_{\boldsymbol{q},\sigma} iqA_{\boldsymbol{q}} \boldsymbol{u}_{\mathrm{T},\boldsymbol{q},\sigma} \left(\hat{a}_{\boldsymbol{q}} e^{i\boldsymbol{q}\cdot\boldsymbol{r}} - \hat{a}^{\dagger}_{\boldsymbol{q}} e^{-i\boldsymbol{q}\cdot\boldsymbol{r}} \right) , \tag{9.41}$$

where $\boldsymbol{u}_{\mathrm{T},\boldsymbol{q},\sigma} \equiv (\boldsymbol{q}/q) \times \boldsymbol{u}_{\boldsymbol{q},\sigma}$. (Note that $\{\boldsymbol{q}, \boldsymbol{u}_{\boldsymbol{q},\sigma}, \boldsymbol{u}_{\mathrm{T},\boldsymbol{q},\sigma}\}$ is a set of orthogonal vectors.)

As shown in Appendix E.2, the ground state $|\Psi\rangle$ of $\hat{\mathcal{H}}_{\boldsymbol{B}}$ does not contain light-matter entanglement in the thermodynamic limit, i.e. we can take $|\Psi\rangle = |\psi\rangle\,|\Phi\rangle$, where $|\psi\rangle$ and $|\Phi\rangle$ are matter and light states. As in Sect. 9.2, we are therefore led to introduce an effective Hamiltonian for the photonic degrees of freedom, $\hat{\mathcal{H}}^{\rm eff}_{\rm ph}[\psi] \equiv \langle\psi|\hat{\mathcal{H}}_{\boldsymbol{B}}|\psi\rangle$:

$$\hat{\mathcal{H}}^{\rm eff}_{\rm ph}[\psi] = \langle\psi|\hat{\mathcal{H}}|\psi\rangle + \hat{\mathcal{H}}_{\rm ph} + \sum_{\boldsymbol{q},\sigma} \frac{g\mu_{\rm B}A_{\boldsymbol{q}}}{2} \left[\boldsymbol{S}(-\boldsymbol{q}) \hat{a}_{\boldsymbol{q},\sigma} - \boldsymbol{S}(\boldsymbol{q}) \hat{a}^{\dagger}_{\boldsymbol{q},\sigma} \right] \cdot iq\boldsymbol{u}_{\mathrm{T},\boldsymbol{q},\sigma} ,$$

where [86]

$$\hat{\boldsymbol{S}}(\boldsymbol{q}) = \sum_{i=1}^{N} e^{-i\boldsymbol{q}\cdot\boldsymbol{r}_i} \hat{\boldsymbol{\sigma}}_i \tag{9.42}$$

is the 3D Fourier transform of the spin density $\hat{\boldsymbol{S}}(\boldsymbol{q}) = \sum_{i=1}^{N} \hat{\boldsymbol{\sigma}}_i \delta(\boldsymbol{r} - \boldsymbol{r}_i)$ and $\boldsymbol{S}(\boldsymbol{q}) = \langle\psi|\hat{\boldsymbol{S}}(\boldsymbol{q})|\psi\rangle$.

Since Eq. (9.42) is a sum of displaced harmonic oscillators, we can assume without loss of generality that the ground state $|\Phi\rangle$ of $\hat{\mathcal{H}}^{\rm eff}_{\rm ph}[\psi]$ is a tensor product $|\mathscr{A}\rangle \equiv \otimes_{\boldsymbol{q},\sigma} |\alpha_{\boldsymbol{q},\sigma}\rangle$ of coherent states of the $\hat{a}_{\boldsymbol{q},\sigma}$ operators[47, 76], i.e. $\hat{a}_{\boldsymbol{q}',\sigma'}\,|\mathscr{A}\rangle = \alpha_{\boldsymbol{q}',\sigma'}\,|\mathscr{A}\rangle$.

The total energy, defined as $E[\{\alpha_{\boldsymbol{q},\sigma}\}, \psi] \equiv \langle\Psi|\hat{\mathcal{H}}_{\boldsymbol{B}}|\Psi\rangle = \langle\mathscr{A}|\hat{\mathcal{H}}^{\rm eff}_{\rm ph}[\psi]|\mathscr{A}\rangle$, is given by:

$$\begin{aligned} E \quad [\{\alpha_{\boldsymbol{q},\sigma}\}, \psi] &= \langle\psi|\hat{\mathcal{H}}|\psi\rangle + \sum_{\boldsymbol{q},\sigma} \hbar\omega_{\boldsymbol{q}} \left(|\alpha_{\boldsymbol{q},\sigma}|^2 + \frac{1}{2} \right) + \\ + \quad & \sum_{\boldsymbol{q},\sigma} \frac{g\mu_{\rm B}A_{\boldsymbol{q}}}{2} \left[\boldsymbol{S}(-\boldsymbol{q}) \alpha_{\boldsymbol{q},\sigma} - \boldsymbol{S}(\boldsymbol{q}) \alpha^{*}_{\boldsymbol{q},\sigma} \right] \cdot iq\boldsymbol{u}_{\mathrm{T},\boldsymbol{q},\sigma} . \end{aligned} \tag{9.43}$$

Minimization can be performed with respect to $\{\alpha_{\boldsymbol{q},\sigma}\}$ analytically by imposing the condition $\partial_{\alpha^{*}_{\boldsymbol{q},\sigma}} E[\{\alpha_{\boldsymbol{q},\sigma}\}, \psi] = 0$. We find that the optimal value of $\{\alpha_{\boldsymbol{q},\sigma}\}$ is given by:

$$\bar{\alpha}_{\boldsymbol{q},\sigma} = \frac{g\mu_{\rm B}A_{\boldsymbol{q}}}{2\hbar\omega_{\rm c}} \langle\psi|\hat{\boldsymbol{S}}(\boldsymbol{q})|\psi\rangle \cdot iq\boldsymbol{u}_{\mathrm{T},\boldsymbol{q},\sigma} . \tag{9.44}$$

Note that this equation can be written in terms of the operator

$$\hat{C}_{\boldsymbol{q},\sigma} \quad \equiv \quad \frac{g\mu_{\rm B}A_{\boldsymbol{q}}}{2\hbar\omega_{\boldsymbol{q}}} \hat{\boldsymbol{S}}(\boldsymbol{q}) \cdot iq\boldsymbol{u}_{\mathrm{T},\boldsymbol{q},\sigma} , \tag{9.45}$$

i.e. $\langle\psi|\hat{C}_{\boldsymbol{q},\sigma}|\psi\rangle = \bar{\alpha}_{\boldsymbol{q},\sigma}$. Using Eq. (9.44) into Eq. (9.43) we finally find the energy functional that needs to be minimized with respect to $|\psi\rangle$:

$$E \quad [\{\bar{\alpha}_{\boldsymbol{q},\sigma}\}, \psi] = \langle\psi|\hat{\mathcal{H}}|\psi\rangle - \sum_{\boldsymbol{q},\sigma} \hbar\omega_{\boldsymbol{q}} \left(|\bar{\alpha}_{\boldsymbol{q},\sigma}|^2 - \frac{1}{2} \right) . \tag{9.46}$$

Once again, for photon condensation to occur we need $E[\{\bar{\alpha}_{\boldsymbol{q},\sigma}\},\psi] < E[0,\psi_0]$ or, equivalently,

$$\langle\psi|\hat{\mathcal{H}}|\psi\rangle - \langle\psi_0|\hat{\mathcal{H}}|\psi_0\rangle < \sum_{\boldsymbol{q},\sigma} \hbar\omega_{\boldsymbol{q}} |\bar{\alpha}_{\boldsymbol{q},\sigma}|^2 \ . \tag{9.47}$$

As in Sect. 9.2, the dependence of $\langle\psi|\hat{\mathcal{H}}|\psi\rangle - \langle\psi_0|\hat{\mathcal{H}}|\psi_0\rangle$ on $\bar{\alpha}_{\boldsymbol{q},\sigma}$ can be calculated exactly up to order $\bar{\alpha}^2_{\boldsymbol{q},\sigma}$ by using the stiffness theorem [86]:

$$\langle\psi|\hat{\mathcal{H}}|\psi\rangle - \langle\psi_0|\hat{\mathcal{H}}|\psi_0\rangle = -\frac{1}{2}\sum_{\boldsymbol{q},\sigma}\sum_{\boldsymbol{q}',\sigma'} \chi^{-1}_{\hat{C}_{\boldsymbol{q},\sigma},\hat{C}_{-\boldsymbol{q}',\sigma'}}(0)\bar{\alpha}^*_{\boldsymbol{q},\sigma}\bar{\alpha}_{\boldsymbol{q}',\sigma'} \ , \tag{9.48}$$

where $\chi^{-1}_{\hat{C}_{\boldsymbol{q},\sigma},\hat{C}_{-\boldsymbol{q}',\sigma'}}(0)$ is the inverse of the static response function $\chi_{\hat{C}_{\boldsymbol{q},\sigma},\hat{C}_{-\boldsymbol{q}',\sigma'}}(0)$ and the operator $\hat{C}_{\boldsymbol{q},\sigma}$ has been introduced in Eq. (9.45). Inserting Eq. (9.48) inside Eq. (9.47) we find:

$$-\sum_{\boldsymbol{q},\sigma}\left[\frac{1}{2\chi_{\hat{C}_{\boldsymbol{q},\sigma},\hat{C}_{-\boldsymbol{q},\sigma}}(0)} + \hbar\omega_{\boldsymbol{q}}\right]|\bar{\alpha}_{\boldsymbol{q},\sigma}|^2 < 0 \ . \tag{9.49}$$

Following the same logical steps discussed in Sect. 9.2, we can consider the previous inequality for a fixed $\boldsymbol{q}$:

$$-\chi_{\hat{C}_{\boldsymbol{q},\sigma},\hat{C}_{-\boldsymbol{q},\sigma}}(0) > \frac{1}{2\hbar\omega_{\boldsymbol{q}}} \ . \tag{9.50}$$

We now observe that the homogenous and isotropic nature of the ground state of the 3DES implies [86] $\chi_{\hat{C}_{\boldsymbol{q},\sigma},\hat{C}_{-\boldsymbol{q}',\sigma'}}(0) = \chi_{\hat{C}_{\boldsymbol{q},\sigma},\hat{C}_{-\boldsymbol{q},\sigma}}(0)\delta_{\boldsymbol{q},\boldsymbol{q}'}\delta_{\sigma,\sigma'}$. We readily recognize $\chi_{\hat{C}_{\boldsymbol{q},\sigma},\hat{C}_{-\boldsymbol{q},\sigma}}(0)$ to be intimately linked to the static, spin-spin response tensor $\chi^{\rm S}_{i,k}(\boldsymbol{q},0)$. Indeed, it is easy to show that

$$\chi_{\hat{C}_{\boldsymbol{q},\sigma},\hat{C}_{-\boldsymbol{q},\sigma}}(0) = \frac{q^2 g^2 \mu_{\rm B}^2 A^2_{\boldsymbol{q}} V}{4\hbar^2\omega^2_{\boldsymbol{q}}} \sum_{i,k} u^{(i)}_{{\rm T},\boldsymbol{q},\sigma} u^{(k)}_{{\rm T},\boldsymbol{q},\sigma} \chi^{\rm S}_{i,k}(\boldsymbol{q},0) \ , \tag{9.51}$$

where

$$\begin{aligned}\chi^{\rm S}_{i,k}(\boldsymbol{q},0) &= -\frac{1}{V}\sum_{n\neq 0}\frac{\langle\psi_0|\hat{S}_i(-\boldsymbol{q})|\psi_n\rangle\,\langle\psi_n|\hat{S}_k(\boldsymbol{q})|\psi_0\rangle}{E_n - E_0} \\ &- \frac{1}{V}\sum_{n\neq 0}\frac{\langle\psi_0|\hat{S}_i(\boldsymbol{q})|\psi_n\rangle\,\langle\psi_n|\hat{S}_k(-\boldsymbol{q})|\psi_0\rangle}{E_n - E_0} \ ,\end{aligned} \tag{9.52}$$

and $\hat{S}_i(\boldsymbol{q})$, with $i = x, y, z$, denotes the i-th Cartesian component of $\hat{\boldsymbol{S}}(\boldsymbol{q})$.

Isotropy, translational- and spin-rotational invariance imply that the rank-2 tensor $\chi^{\rm S}_{i,k}(\boldsymbol{q},0)$ can be decomposed in terms of the longitudinal, $\chi^{\rm S}_{\rm L}(q,0)$, and transverse, $\chi^{\rm S}_{\rm T}(q,0)$, spin-spin response functions:

$$\chi^{\rm S}_{i,k}(\boldsymbol{q},0) = \chi^{\rm S}_{\rm L}(q,0)\frac{q_i q_k}{q^2} + \chi^{\rm S}_{\rm T}(q,0)\left(\delta_{i,k} - \frac{q_i q_k}{q^2}\right) \ . \tag{9.53}$$

Replacing Eq. (9.53) into Eq. (9.51), we finally find

$$\chi_{\hat{C}_{\boldsymbol{q},\sigma},\hat{C}_{-\boldsymbol{q},\sigma}}(0) = \frac{q^2 g^2 \mu_{\rm B} A^2_{\boldsymbol{q}} V}{4\hbar^2\omega^2_{\boldsymbol{q}}}\chi^{\rm S}_{\rm T}(q,0) \ . \tag{9.54}$$

Using Eqs. (9.51) and (9.53) and the microscopic expressions of $\omega_{\boldsymbol{q}} = cq/\sqrt{\epsilon_{\rm r}}$ and $A_{\boldsymbol{q}} = \sqrt{2\pi\hbar c^2/(V\omega_{\boldsymbol{q}}\epsilon_{\rm r})}$ given above, Eq. (9.50) can be written as follows:

$$-\frac{g^2\mu_{\rm B}^2}{4}\,\chi_{\rm T}^{\rm S}(q,0) > \frac{1}{4\pi}\ , \tag{9.55}$$

Again, the left-hand-side of Eq. (9.55) has a very clear physical interpretation. It is the non-local transverse spin susceptibility [86]

$$\chi_{\rm spin}(q) \equiv -\frac{g^2\mu_{\rm B}^2}{4}\,\chi_{\rm T}^{\rm S}(q,0)\ , \tag{9.56}$$

which, in the long-wavelength $q \to 0$ limit, reduces to the thermodynamic (i.e. macroscopic) spin magnetic susceptibility (SMS)

$$\chi_{\rm SMS} \equiv \lim_{q\to 0}\chi_{\rm spin}(q) = \left.\frac{\partial M_{\rm S}}{\partial B}\right|_{B=0}\ . \tag{9.57}$$

Here, $M_{\rm S}$ is the spin contribution to the magnetization. For free (i.e. non-interacting) parabolic-band fermions in 3D, $\chi_{\rm SMS}$ reduces to the well-known Pauli spin susceptibility [86], i.e.

$$\chi_{\rm SMS}^{(0)} = \frac{\alpha^2}{r_s}\left(\frac{9}{256\pi^5}\right)^{1/3} > 0\ , \tag{9.58}$$

where we have used a Landé g-factor $g = 2$. Comparing Eq. (9.58) with Eq. (9.36), we find the very well-known result,

$$\chi_{\rm SMS}^{(0)} = -3\chi_{\rm OMS}^{(0)}\ . \tag{9.59}$$

In summary, the condition for the occurrence of photon condensation in a 3DES, when the cavity electromagnetic field couples to matter degrees of freedom via the Zeeman coupling only, is:

$$\boxed{\chi_{\rm spin}(q) > \frac{1}{4\pi}}\ . \tag{9.60}$$

9.3.2 Combined orbital and Zeeman couplings

In general, when both orbital and spin light-matter interactions are taken into account the total Hamiltonian is:

$$\hat{\mathcal{H}}_{\boldsymbol{A}+\boldsymbol{B}} = \hat{\mathcal{H}} + \hat{\mathcal{H}}_{\rm ph} + \frac{g\mu_{\rm B}}{2}\sum_{i=1}^{N}\hat{\boldsymbol{\sigma}}_i\cdot\hat{\boldsymbol{B}}(\boldsymbol{r}_i) + \sum_{i=1}^{N}\frac{e}{mc}\hat{\boldsymbol{A}}(\boldsymbol{r}_i)\cdot\hat{\boldsymbol{p}}_i + \sum_{i=1}^{N}\frac{e^2}{2mc^2}\hat{\boldsymbol{A}}^2(\boldsymbol{r}_i)\ . \tag{9.61}$$

Following the same steps discussed in Sects. 9.2 and 9.3.1, one reaches the following condition for the occurrence of photon condensation in a 3DES:

$$-\chi_{\hat{B}_{\boldsymbol{q},\sigma}+\hat{C}_{\boldsymbol{q},\sigma},\hat{B}_{-\boldsymbol{q},\sigma}+\hat{C}_{-\boldsymbol{q},\sigma}}(0) > \frac{1}{2\hbar\Omega_{\boldsymbol{q}}}\ . \tag{9.62}$$

Now, the key point is that, in the absence of spin-orbit coupling, cross response functions vanish:

$$\chi_{\hat{C}_{\boldsymbol{q},\sigma},\hat{B}_{-\boldsymbol{q},\sigma}}(0) = \chi_{\hat{B}_{\boldsymbol{q},\sigma},\hat{C}_{-\boldsymbol{q},\sigma}}(0) = 0\ . \tag{9.63}$$

This is due to the following facts. Consider for example $\chi_{\hat{C}_{\boldsymbol{q},\sigma},\hat{B}_{-\boldsymbol{q},\sigma}}(0)$. We have [86]

$$\chi_{\hat{C}_{\boldsymbol{q},\sigma},\hat{B}_{-\boldsymbol{q},\sigma}}(\omega) = -\frac{i}{\hbar V}\lim_{\eta\to 0}\int_0^\infty d\tau [\hat{C}_{\boldsymbol{q},\sigma}(\tau),\hat{B}_{-\boldsymbol{q},\sigma}]e^{i(\omega+i\eta)\tau} \; . \tag{9.64}$$

Since the operators $\hat{C}_{\boldsymbol{q},\sigma}(t)$ and $\hat{B}_{-\boldsymbol{q},\sigma}$ have disjoint supports, the former acting on the spin degrees of freedom while the latter on the charge degrees of freedom, we have $[\hat{C}_{\boldsymbol{q},\sigma}(t),\hat{B}_{-\boldsymbol{q},\sigma}] = 0$. We therefore conclude that

$$\chi_{\hat{B}_{\boldsymbol{q},\sigma}+\hat{C}_{\boldsymbol{q},\sigma},\hat{B}_{-\boldsymbol{q},\sigma}+\hat{C}_{-\boldsymbol{q},\sigma}}(0) = \chi_{\hat{B}_{\boldsymbol{q},\sigma},\hat{B}_{-\boldsymbol{q},\sigma}}(0) + \chi_{\hat{C}_{\boldsymbol{q},\sigma},\hat{C}_{-\boldsymbol{q},\sigma}}(0) \; . \tag{9.65}$$

Using Eqs. (9.65), (9.26), and (9.54) inside Eq. (9.62), we find that the condition for occurrence of photon condensation is:

$$2A_{\boldsymbol{q}}^2 V\big[\chi_{\rm orb}(q)+\chi_{\rm spin}(q)\big]q^2 > \hbar\omega_{\boldsymbol{q}} \; , \tag{9.66}$$

which, upon substitution of $\omega_{\boldsymbol{q}} = cq/\sqrt{\epsilon_{\rm r}}$ and $A_{\boldsymbol{q}} = \sqrt{2\pi\hbar c^2/(V\omega_{\boldsymbol{q}}\epsilon_{\rm r})}$, becomes

$$\boxed{\chi_{\rm orb}(q)+\chi_{\rm spin}(q) > \frac{1}{4\pi}} \; . \tag{9.67}$$

This is the most important result for 3DESs: in the absence of spin-orbit coupling in the matter degrees of freedom—or other microscopic mechanisms that are responsible for non-zero cross response function such as $\chi_{\hat{B}_{\boldsymbol{q},\sigma},\hat{C}_{-\boldsymbol{q},\sigma},}(0)$ and $\chi_{\hat{C}_{\boldsymbol{q},\sigma},\hat{B}_{-\boldsymbol{q},\sigma}}(0)$—the condition for the occurrence of photon condensation involves the sum of the orbital and spin transverse static response functions.

When electron-electron interactions are negligible (i.e. $r_{\rm s} \ll 1$), the condition (9.67) for the occurrence of 3D photon condensation (i.e. formation of Condon domains) can be made more explicit. Indeed, consider for example the case of a non-interacting parabolic-band 3D Fermi gas. Using the long-wavelength expression (9.36) and (9.58) inside Eq. (9.67), we immediately see that photon condensation can occur in the absence of electron-electron interactions provided that

$$r_{\rm s} < \left(\frac{2}{3\pi^2}\right)^{1/3}\alpha^2 \; , \tag{9.68}$$

or, equivalently, provided that the electron density is sufficiently high,

$$n > n_{\rm c} = \frac{9\pi}{8\alpha^6}\frac{1}{a_{\rm B}^3} \; . \tag{9.69}$$

Unscreened current-current interactions at low temperatures under strong magnetic fields, which may result in non-Fermi-liquid behavior [243], lead to the occurrence of long-range magnetic orbital order even at low densities [236].

9.4 2D Photon Condensation

In this Section, we consider the problem of a 2DES located in the middle of a quasi-2D cavity.

Similarly to the 3D case discussed above in Sect. 9.2, we describe the 2DES with the jellium model Hamiltonian

$$\hat{\mathcal{H}}_{\rm 2D} = \sum_{i=1}^N \frac{\hat{\boldsymbol{p}}_{\parallel,i}^2}{2m} + \frac{1}{2}\sum_{i\neq j} v(|\hat{\boldsymbol{r}}_{\parallel,i}-\hat{\boldsymbol{r}}_{\parallel,j}|) \; , \tag{9.70}$$

where $\hat{\boldsymbol{r}}_{\parallel,i}$ and $\hat{\boldsymbol{p}}_{\parallel,i}$ denote respectively the position and momentum operators of the i-th electron moving in the $\hat{\boldsymbol{x}}$-$\hat{\boldsymbol{y}}$ plane. For future use, we introduce the 2D Fourier transforms of the density and paramagnetic (number) current operators:

$$\hat{n}(\boldsymbol{q}_\parallel) = \sum_{i=1}^{N} e^{-i\boldsymbol{q}_\parallel \cdot \hat{\boldsymbol{r}}_{\parallel,i}} , \tag{9.71}$$

$$\hat{\boldsymbol{j}}_{\rm p}(\boldsymbol{q}_\parallel) = \frac{1}{2m}\sum_{i=1}^{N}\left(\hat{\boldsymbol{p}}_{\parallel,i} e^{-i\boldsymbol{q}_\parallel \cdot \hat{\boldsymbol{r}}_{\parallel,i}} + e^{-i\boldsymbol{q}_\parallel \cdot \hat{\boldsymbol{r}}_{\parallel,i}}\hat{\boldsymbol{p}}_{\parallel,i}\right) , \tag{9.72}$$

with the usual properties $\hat{n}(-\boldsymbol{q}_\parallel) = \hat{n}^\dagger(\boldsymbol{q}_\parallel)$ and $\hat{\boldsymbol{j}}_{\rm p}(-\boldsymbol{q}_\parallel) = \hat{\boldsymbol{j}}_{\rm p}^\dagger(\boldsymbol{q}_\parallel)$.

We consider a cavity with length L_z in the $\hat{\boldsymbol{z}}$ direction, satisfying the quasi-2D condition $L_z \ll L_x, L_y$. The walls of the cavity in the $\hat{\boldsymbol{z}}$ direction are assumed to perfectly conducting. Accordingly, the tangential component of the electric field and the normal component of the magnetic field must vanish at the cavity boundaries [244] $z = \pm L_z/2$. In addition, we impose periodic boundary conditions along the $\hat{\boldsymbol{x}}$ and $\hat{\boldsymbol{y}}$ directions. In the Coulomb gauge, the vector potential fulfilling the cavity boundary conditions can be expressed as follows [244]:

$$\hat{\boldsymbol{A}}(\boldsymbol{r}) = \sum_{\boldsymbol{q}_\parallel,\sigma,n_z} A^{(\rm 2D)}_{\boldsymbol{q}_\parallel,n_z}\boldsymbol{e}_{\boldsymbol{q}_\parallel,\sigma,n_z}(z)(\hat{a}_{\boldsymbol{q}_\parallel,\sigma,n_z} e^{i\boldsymbol{q}_\parallel \cdot \boldsymbol{r}_\parallel} + \hat{a}^\dagger_{\boldsymbol{q}_\parallel,\sigma,n_z} e^{-i\boldsymbol{q}_\parallel \cdot \boldsymbol{r}_\parallel}) , \tag{9.73}$$

where

$$\boldsymbol{e}_{\boldsymbol{q}_\parallel,1,n_z}(z) = \boldsymbol{u}_{\boldsymbol{q}_\parallel,1}\sin\left[\frac{\pi n_z}{L_z}\left(z+\frac{L_z}{2}\right)\right] , \tag{9.74}$$

$$\begin{aligned}\boldsymbol{e}_{\boldsymbol{q}_\parallel,2,n_z}(z) &= \frac{\boldsymbol{q}_\parallel}{q_\parallel}\sin\left[\frac{\pi n_z}{L_z}\left(z+\frac{L_z}{2}\right)\right]\frac{\pi n_z}{L_z\sqrt{q_\parallel^2+(\frac{\pi n_z}{L_z})^2}} \\ &+ \hat{\boldsymbol{z}}\cos\left[\frac{\pi n_z}{L_z}\left(z+\frac{L_z}{2}\right)\right]\frac{iq_\parallel}{\sqrt{q_\parallel^2+(\frac{\pi n_z}{L_z})^2}} .\end{aligned} \tag{9.75}$$

Here, n_z is an integer index, $\boldsymbol{q}_\parallel = (2\pi n_x/L_x, 2\pi n_y/L_y)$ with (n_x, n_y) relative integers, $\sigma = 1, 2$ is the polarization index, $\boldsymbol{u}_{\boldsymbol{q}_\parallel,1}$ is the linear polarization vector lying in the $\hat{\boldsymbol{x}}$-$\hat{\boldsymbol{y}}$ plane and transverse to $\boldsymbol{q}_\parallel$, i.e. $\boldsymbol{u}_{\boldsymbol{q}_\parallel,1}\cdot\boldsymbol{q}_\parallel = 0$, $A^{(\rm 2D)}_{\boldsymbol{q}_\parallel,n} = \sqrt{4\pi\hbar c^2/(L_z S\omega_{\boldsymbol{q}_\parallel,n_z}\epsilon_{\rm r})}$, $S = L_x L_y$, $\epsilon_{\rm r}$ is the cavity relative dielectric constant, and $\omega_{\boldsymbol{q}_\parallel,n_z} = (c/\epsilon_{\rm r})\sqrt{q_\parallel^2 + (\pi n_z/L_z)^2}$. In the $\hat{\boldsymbol{x}}$-$\hat{\boldsymbol{y}}$ plane ($z = 0$), where the 2DES lays, modes labeled by the polarization index $\sigma = 1$ are transverse waves, i.e. $\boldsymbol{e}_{\boldsymbol{q}_\parallel,1,n_z}(0)\cdot\boldsymbol{q}_\parallel = 0$. The second mode labelled by $\sigma = 2$ can be dropped for arbitrarily large wave vector if the 2DES is located exactly in the middle of the cavity since:

- For odd values of n_z, the vector $\boldsymbol{e}_{\boldsymbol{q}_\parallel,2,\text{ odd }n_z}(z=0)$ is longitudinal, i.e. it is parallel to $\boldsymbol{q}_\parallel$. Since, as a consequence of gauge invariance, the static longitudinal current-current response function is zero [86] for arbitrary $\boldsymbol{q}_\parallel$, light-matter interactions with longitudinal photonic modes cannot induce photon condensation.

- For even values of n_z, the vector $\boldsymbol{e}_{\boldsymbol{q}_\parallel,2,\text{ even }n_z}(z=0)$ is along the $\hat{\boldsymbol{z}}$ direction. Therefore, electronic degrees of freedom cannot couple to modes with $\sigma = 2$ and even n_z.

From now on, we will take into account only modes with $\sigma = 1$. In particular, since the 2DES is placed in the middle of the photonic cavity, at $z = 0$, only photonic modes with odd n_z couple to the matter degrees of freedom [245]. Similarly to the 3D case, the following properties hold true: $\omega_{-\boldsymbol{q}_\parallel,n_z} = \omega_{\boldsymbol{q}_\parallel,n_z}$, $\boldsymbol{u}_{-\boldsymbol{q}_\parallel,1} = \boldsymbol{u}_{\boldsymbol{q}_\parallel,1}$, $A^{(2D)}_{-\boldsymbol{q}_\parallel,n_z} = A^{(2D)}_{\boldsymbol{q}_\parallel,n_z}$.

The Hamiltonian of the 2DES coupled to the cavity field is expressed as

$$\hat{\mathcal{H}}_{\boldsymbol{A}} = \hat{\mathcal{H}}_{\rm 2D} + \hat{\mathcal{H}}_{\rm ph} + \sum_{i=1}^{N} \frac{e}{mc} \hat{\boldsymbol{A}}(\boldsymbol{r}_{\parallel,i}, z=0) \cdot \hat{\boldsymbol{p}}_{\parallel,i} + \sum_{i=1}^{N} \frac{e^2}{2mc^2} \hat{\boldsymbol{A}}^2(\boldsymbol{r}_{\parallel,i}, z=0) \ , \tag{9.76}$$

where the cavity Hamiltonian $\hat{\mathcal{H}}_{\rm ph}$ reads as following

$$\hat{\mathcal{H}}_{\rm ph} = \sum_{\boldsymbol{q}_\parallel,\sigma,n_z} \hbar\omega_{\boldsymbol{q}_\parallel,n_z} \hat{a}^\dagger_{\boldsymbol{q}_\parallel,\sigma,n_z} \hat{a}_{\boldsymbol{q}_\parallel,\sigma,n_z} \ . \tag{9.77}$$

This needs to be compared with the 3D one in Eq. (9.8). Once again, the third and the fourth term in Eq. (9.76) are the paramagnetic and diamagnetic contributions, respectively. A constant term in Eq. (9.77) has been dropped, since below we will be only interested in energy differences. From now on, we will follows steps similar to those described in Sect. 9.2. We will therefore mainly highlight differences between the 3D case discussed there and the 2D case discussed in this Section and cut short on the algebraic steps that are identical in the two cases. On purpose, and with notational abuse, we will denote by the same symbols quantities that in both cases have an identical physical meaning.

As in the 3D case, we are interested in the possible occurrence of a quantum phase transition to a photon condensate, and we therefore wish to make general statements about the ground state $|\Psi\rangle$ of $\hat{\mathcal{H}}_{\boldsymbol{A}}$, in the 2D thermodynamic limit $N \to \infty$, $S \to \infty$, with constant $n_{\rm 2D} = N/S$. In this limit, we can safely assume that $|\Psi\rangle$ does not contain light-matter entanglement, i.e. we can take $|\Psi\rangle = |\psi\rangle\,|\Phi\rangle$, where $|\psi\rangle$ and $|\Phi\rangle$ are matter and light states. The effective Hamiltonian for the photonic degrees of freedom is $\hat{\mathcal{H}}^{\rm eff}_{\rm ph}[\psi] \equiv \langle\psi|\hat{\mathcal{H}}_{\boldsymbol{A}}|\psi\rangle$. The order parameter for 2D photon condensation is $\bar{\alpha}_{\boldsymbol{q}_\parallel,1,n_z} \equiv \langle\Phi|\hat{a}_{\boldsymbol{q}_\parallel,1,n_z}|\Phi\rangle$, which, at the putative QCP, is small. Since the diamagnetic term in Eq. (9.76) is quadratic in $\bar{\alpha}_{\boldsymbol{q}_\parallel,1,n_z}$, close to the QCP we can approximate the matter content in the diamagnetic term with its value in the absence of light-matter interactions. By further assuming, as in the 3D case, that the ground state of the 2DES in the absence of light-matter interactions is homogenous and isotropic, i.e. that $\langle\psi_0|\hat{n}(\boldsymbol{q}_\parallel)|\psi_0\rangle = N\delta_{\boldsymbol{q}_\parallel,\boldsymbol{0}}$, the effective photon Hamiltonian can be written as

$$\hat{\mathcal{H}}^{\rm eff}_{\rm ph} \quad [\psi] = \langle\psi|\hat{\mathcal{H}}_{\rm 2D}|\psi\rangle + \hat{\mathcal{H}}_{\rm ph} + \hat{\mathcal{H}}_{\rm p} + \hat{\mathcal{H}}_{\rm d} \ , \tag{9.78}$$

where the paramagnetic contribution is given by

$$\hat{\mathcal{H}}_{\rm p} = \sum_{\text{odd } n_z} \sum_{\boldsymbol{q}_\parallel} (-1)^{\frac{n_z-1}{2}} \frac{e}{c} A^{(2D)}_{\boldsymbol{q}_\parallel,n_z} \left[\hat{a}_{\boldsymbol{q}_\parallel,1,n_z} \boldsymbol{u}_{\boldsymbol{q}_\parallel,1} \cdot \boldsymbol{j}_{\rm p}(-\boldsymbol{q}_\parallel) + \hat{a}^\dagger_{\boldsymbol{q}_\parallel,1,n_z} \boldsymbol{u}_{\boldsymbol{q}_\parallel,1} \cdot \boldsymbol{j}_{\rm p}(\boldsymbol{q}_\parallel) \right] \tag{9.79}$$

and the diamagnetic one by

$$\hat{\mathcal{H}}_{\rm d} = \sum_{\text{odd } n_z,n_z'} \sum_{\boldsymbol{q}_\parallel} (-1)^{\frac{n_z+n_z'-2}{2}} \frac{e^2}{2mc^2} A^{(2D)}_{\boldsymbol{q}_\parallel,n_z} A^{(2D)}_{\boldsymbol{q}_\parallel,n_z'} (\hat{a}_{\boldsymbol{q}_\parallel,1,n_z} + \hat{a}^\dagger_{-\boldsymbol{q}_\parallel,1,n_z})(\hat{a}^\dagger_{\boldsymbol{q}_\parallel,1,n_z'} + \hat{a}_{-\boldsymbol{q}_\parallel,1,n_z'}) \ . \tag{9.80}$$

In Eq. (9.79) we have introduced

$$\boldsymbol{j}_{\rm p}(\boldsymbol{q}_\parallel) \equiv \langle\psi|\hat{\boldsymbol{j}}_{\rm p}(\boldsymbol{q}_\parallel)|\psi\rangle \ . \tag{9.81}$$

For future use, we also introduce $\mathcal{J}_{\boldsymbol{q}_\parallel,1} = \boldsymbol{u}_{\boldsymbol{q}_\parallel,1} \cdot \boldsymbol{j}_{\rm p}(\boldsymbol{q}_\parallel)$.

As we have seen in Sect. 9.2.1, point v), in order to calculate the energy functional, it is sufficient to evaluate the expectation value of the effective Hamiltonian $\hat{\mathcal{H}}^{\rm eff}_{\rm ph}[\psi]$ on a trial photonic wavefunction of the form $|\mathscr{A}\rangle \equiv \otimes_{\boldsymbol{q},n_z} |\alpha_{\boldsymbol{q},1,n_z}\rangle$, namely on a tensor product of coherent states of the $\hat{a}_{\boldsymbol{q},1,n_z}$ operators, i.e. $\hat{a}_{\boldsymbol{q}',1,n_z} |\mathscr{A}\rangle = \alpha_{\boldsymbol{q}',1,n_z} |\mathscr{A}\rangle$. This procedure corresponds to replacing the photonic operators in Eq. (9.12) with c-numbers, $\hat{a}_{\boldsymbol{q}_\parallel,1,n_z} \to \alpha_{\boldsymbol{q}_\parallel,1,n_z}$. Carrying out this procedure we find:

$$
\begin{aligned}
E\quad [\{\alpha_{\boldsymbol{q}_\parallel,1,n_z}\},\psi] &= \langle\psi|\hat{\mathcal{H}}_{\rm 2D}|\psi\rangle + \sum_{\rm odd\ } \sum_{n_z} \sum_{\boldsymbol{q}_\parallel} \frac{(-1)^{\frac{n_z-1}{2}}\sqrt{2D}}{\sqrt{\omega_{\boldsymbol{q}_\parallel,n_z}}} \Big[\alpha_{\boldsymbol{q}_\parallel,1,n_z}\mathcal{J}_{-\boldsymbol{q}_\parallel,1} + \text{c.c.}\Big] \\
&+ \sum_{\rm odd\ } \sum_{n_z} \sum_{\rm odd\ } \sum_{n_z'} \sum_{\boldsymbol{q}_\parallel} \frac{(-1)^{\frac{n_z+n_z'-2}{2}} DN}{m\sqrt{\omega_{\boldsymbol{q}_\parallel,n_z}\omega_{\boldsymbol{q}_\parallel,n_z'}}} (\alpha_{\boldsymbol{q}_\parallel,1,n_z} + \alpha^*_{-\boldsymbol{q}_\parallel,1,n_z})(\alpha^*_{\boldsymbol{q}_\parallel,1,n_z'} + \alpha_{-\boldsymbol{q}_\parallel,1,n_z'}) \\
&+ \sum_{\boldsymbol{q}_\parallel,1,n_z} \hbar\omega_{\boldsymbol{q}_\parallel,n_z} \alpha^*_{\boldsymbol{q}_\parallel,1,n_z}\alpha_{\boldsymbol{q}_\parallel,1,n_z}\ ,
\end{aligned}
\tag{9.82}
$$

where $D \equiv 2\pi\hbar e^2/(L_z S\epsilon_{\rm r})$. (As discussed in Sect. 9.2, if one is interested in finding the exact photonic eigenstate, a different and much more cumbersome root needs to be followed. This is described at length in Appendix E.3 and related Appendix E.4. The end result, from the point of view of energy differences, is identical to the one that one obtains using Eq. (9.82).) Note that all the modes with even n_z are completely decoupled from matter degrees of freedom. For these modes, the minimum of the energy functional is trivially obtained at $\alpha_{\boldsymbol{q}_\parallel,1,n_z} = 0$. Hence, we can completely disregard even values of n_z: from now on, the index n_z will take only odd values.

It turns out to be useful to express the energy functional $E[\{\alpha_{\boldsymbol{q}_\parallel,1,n_z}\},\psi]$ in terms of $\{\boldsymbol{z}_{\boldsymbol{q}_\parallel,1,n_z}\} = \{(x_{\boldsymbol{q}_\parallel,1,n_z}, y_{\boldsymbol{q}_\parallel,1,n_z})^\top\}$ where $x_{\boldsymbol{q}_\parallel,1,n_z} = (\alpha_{\boldsymbol{q}_\parallel,1,n_z} + \alpha^*_{-\boldsymbol{q}_\parallel,1,n_z})/2$ and $y_{\boldsymbol{q}_\parallel,1,n_z} = (\alpha_{\boldsymbol{q}_\parallel,1,n_z} - \alpha^*_{-\boldsymbol{q}_\parallel,1,n_z})/(2i)$. Introducing $g_j(\boldsymbol{q}_\parallel) = (-1)^j\sqrt{2D/\omega_{\boldsymbol{q}_\parallel,2j+1}}$, we find

$$
\begin{aligned}
E[\{\boldsymbol{z}_{\boldsymbol{q}_\parallel,1,n_z}\},\psi] &= \langle\psi|\hat{\mathcal{H}}_{\rm 2D}|\psi\rangle + \sum_{\boldsymbol{q}_\parallel,1} \sum_{\rm odd\ } \sum_{n_z} \Big[\hbar\omega_{\boldsymbol{q}_\parallel,n_z}(x_{\boldsymbol{q}_\parallel,1,n_z}x_{-\boldsymbol{q}_\parallel,1,n_z} + y_{\boldsymbol{q}_\parallel,1,n_z}y_{-\boldsymbol{q}_\parallel,1,n_z}) \\
&+ \frac{2N}{m} \sum_{\rm odd\ } \sum_{n_z'} g_{(n_z-1)/2}(\boldsymbol{q}_\parallel) g_{(n_z'-1)/2}(\boldsymbol{q}_\parallel) x_{\boldsymbol{q}_\parallel,1,n_z} x_{-\boldsymbol{q}_\parallel,1,n_z'} 2\mathcal{J}_{-\boldsymbol{q}_\parallel,1} g_{(n_z-1)/2}(\boldsymbol{q}_\parallel) x_{\boldsymbol{q}_\parallel,1,n_z}\Big]
\end{aligned}
\tag{9.83}
$$

This needs to be minimized with respect to $\{\boldsymbol{z}_{\boldsymbol{q}_\parallel,1,n_z}\}$ and $|\psi\rangle$. The minimization with respect to $\{\boldsymbol{z}_{\boldsymbol{q}_\parallel,1,n_z}\}$ can be done analytically by imposing the condition $\partial_{\boldsymbol{z}^*_{\boldsymbol{q}_\parallel,1,n_z}} E[\{\boldsymbol{z}_{\boldsymbol{q}_\parallel,1,n_z}\},\psi] = 0$. We find that the optimal value of $\{\boldsymbol{z}_{\boldsymbol{q}_\parallel,1,n_z}\}$ is given by: $\hbar\omega_{\boldsymbol{q}_\parallel,n_z} y_{\boldsymbol{q}_\parallel,1,n_z} = 0$ and

$$
\hbar\omega_{\boldsymbol{q}_\parallel,n_z} x_{\boldsymbol{q}_\parallel,1,n_z} + \frac{2N}{m} \sum_{\rm odd\ } \sum_{n_z'} g_{(n_z-1)/2}(\boldsymbol{q}_\parallel) g_{(n_z'-1)/2}(\boldsymbol{q}_\parallel) x_{\boldsymbol{q}_\parallel,1,n_z'} = -g_{(n_z-1)/2}(\boldsymbol{q}_\parallel)\mathcal{J}_{\boldsymbol{q}_\parallel,1}\ , \tag{9.84}
$$

where n_z is odd.

The first equation is trivially solved by $y_{\boldsymbol{q}_\parallel,1,n_z} = 0$. From Eq. (9.84), we find that the optimal value of $\{x_{\boldsymbol{q}_\parallel,1,n_z}\}$ is the solution of a linear system in terms of $\mathcal{J}_{\boldsymbol{q}_\parallel,1}$, and it is non-trivial (i.e. $x_{\boldsymbol{q}_\parallel,1,n_z} \neq 0$) only if $\mathcal{J}_{\boldsymbol{q}_\parallel,1}$ takes a finite value. Using the stiffness theorem [86], one has, up to second order in $\mathcal{J}_{\boldsymbol{q}_\parallel,1}$,

$$\langle\psi|\hat{\mathcal{H}}_{\rm 2D}|\psi\rangle - \langle\psi_0|\hat{\mathcal{H}}_{\rm 2D}|\psi_0\rangle = -\frac{1}{2S}\sum_{\boldsymbol{q}_\parallel,\boldsymbol{q}'_\parallel} \chi^{-1}_{\boldsymbol{u}_{\boldsymbol{q}_\parallel,1}\cdot\hat{\boldsymbol{j}}_{\rm p}(\boldsymbol{q}_\parallel),\boldsymbol{u}_{\boldsymbol{q}'_\parallel,1}\cdot\hat{\boldsymbol{j}}_{\rm p}(-\boldsymbol{q}'_\parallel)}(0)\mathcal{J}_{\boldsymbol{q}_\parallel,1}\mathcal{J}_{-\boldsymbol{q}'_\parallel,1} \ . \tag{9.85}$$

In writing the previous equation we have assumed, as in the 3D case, that $\langle\psi_0|\hat{\boldsymbol{j}}_{\rm p}(\boldsymbol{q}_\parallel)|\psi_0\rangle = 0$ for all values of $\boldsymbol{q}_\parallel$. Since the ground state of the 2DES has been taken to be homogenous and isotropic, the following property holds true:

$$\chi_{\boldsymbol{u}_{\boldsymbol{q}_\parallel,1}\cdot\hat{\boldsymbol{j}}_{\rm p}(\boldsymbol{q}_\parallel),\boldsymbol{u}_{\boldsymbol{q}'_\parallel,1}\cdot\hat{\boldsymbol{j}}_{\rm p}(-\boldsymbol{q}'_\parallel)}(0) = \chi_{\boldsymbol{u}_{\boldsymbol{q}_\parallel,1}\cdot\hat{\boldsymbol{j}}_{\rm p}(\boldsymbol{q}_\parallel),\boldsymbol{u}_{\boldsymbol{q}_\parallel,1}\cdot\hat{\boldsymbol{j}}_{\rm p}(-\boldsymbol{q})}(0)\delta_{\boldsymbol{q}_\parallel,\boldsymbol{q}'_\parallel} \ . \tag{9.86}$$

Similarly to the 3D case, we now express the response function $\chi_{\boldsymbol{u}_{\boldsymbol{q}_\parallel,1}\cdot\hat{\boldsymbol{j}}_{\rm p}(\boldsymbol{q}_\parallel),\boldsymbol{u}_{\boldsymbol{q}_\parallel,1}\cdot\hat{\boldsymbol{j}}_{\rm p}(-\boldsymbol{q})}(0)$ in terms of the *physical* current-current response tensor [86], which contains a paramagnetic as well as a diamagnetic contribution:

$$\chi^{\rm J}_{i,k}(\boldsymbol{q}_\parallel,0) = \frac{n_{\rm 2D}}{m}\delta_{i,k} + \chi_{\hat{j}_{{\rm p},i}(\boldsymbol{q}),\hat{j}_{{\rm p},k}(-\boldsymbol{q}_\parallel)}(0) \ . \tag{9.87}$$

Since we are considering a homogeneous and isotropic system, the rank-2 tensor $\chi^{\rm J}_{i,k}(\boldsymbol{q}_\parallel,0)$ can be decomposed in terms of the longitudinal, $\chi^{\rm J}_{\rm L}(q_\parallel,0)$, and transverse, $\chi^{\rm J}_{\rm T}(q_\parallel,0)$, current-current response functions [86]:

$$\chi^{\rm J}_{i,k}(\boldsymbol{q}_\parallel,0) = \chi^{\rm J}_{\rm L}(q_\parallel,0)\frac{q_{\parallel,i}q_{\parallel,k}}{q^2_\parallel} + \chi^{\rm J}_{\rm T}(q_\parallel,0)\left(\delta_{i,k} - \frac{q_{\parallel,i}q_{\parallel,k}}{q^2_\parallel}\right) \ . \tag{9.88}$$

Note that, as a consequence of gauge invariance, $\chi^{\rm J}_{\rm L}(q_\parallel,0) = 0$ for every $q_\parallel$ [86]. Using Eqs. (9.87)-(9.88) in Eq. (9.86), we finally find

$$\chi_{\boldsymbol{u}_{\boldsymbol{q}_\parallel,1}\cdot\hat{\boldsymbol{j}}_{\rm p}(\boldsymbol{q}_\parallel),\boldsymbol{u}_{\boldsymbol{q}_\parallel,1}\cdot\hat{\boldsymbol{j}}_{\rm p}(-\boldsymbol{q})}(0) = \left[\chi^{\rm J}_{\rm T}(q_\parallel,0) - \frac{n_{\rm 2D}}{m}\right] \ . \tag{9.89}$$

We now calculate the energy difference between a generic phase with $[\boldsymbol{z}_{\boldsymbol{q}_\parallel,1},\psi]$ and the normal phase with $[\boldsymbol{z}_{\boldsymbol{q}_\parallel,1} = \boldsymbol{0},\psi_0]$ (where $\boldsymbol{z}_{\boldsymbol{q}_\parallel,1} = \{\boldsymbol{z}_{\boldsymbol{q}_\parallel,1,n_z}\}_{\text{odd } n_z}$):

$$\begin{aligned} E[\boldsymbol{z}_{\boldsymbol{q}_\parallel,1},\psi] - E[\boldsymbol{z}_{\boldsymbol{q}_\parallel,1} = \boldsymbol{0},\psi_0] &= \sum_{\boldsymbol{q}_\parallel}\Big\{\frac{1}{2S}\left[\frac{n_{\rm 2D}}{m} - \chi^{\rm J}_{\rm T}(q_\parallel,0)\right]^{-1}\mathcal{J}_{\boldsymbol{q}_\parallel,1}\mathcal{J}_{-\boldsymbol{q}_\parallel,1} \\ &+ \sum_{\text{odd } n_z}\Big[\hbar\omega_{\boldsymbol{q},n_z}(x_{\boldsymbol{q}_\parallel,1,n_z}x_{-\boldsymbol{q}_\parallel,1,n_z} + y_{\boldsymbol{q}_\parallel,1,n_z}y_{-\boldsymbol{q}_\parallel,1,n_z}) \\ &+ \frac{2N}{m}\sum_{\text{odd } n'_z} g_{(n_z-1)/2}(\boldsymbol{q}_\parallel)g_{(n'_z-1)/2}(\boldsymbol{q}_\parallel)x_{\boldsymbol{q}_\parallel,1,n_z}x_{-\boldsymbol{q}_\parallel,1,n'_z} + 2\mathcal{J}_{-\boldsymbol{q}_\parallel,1}g_{(n_z-1)/2}(\boldsymbol{q}_\parallel)x_{\boldsymbol{q}_\parallel,1,n_z}\Big]\Big\} \ . \end{aligned} \tag{9.90}$$

Minimizing this quantity with respect to $\mathcal{J}_{\boldsymbol{q}_\parallel,1}$, we obtain the following result:

$$\mathcal{J}_{\boldsymbol{q}_\parallel,1} = 2S\left[\chi^{\rm J}_{\rm T}(q_\parallel,0) - \frac{n_{\rm 2D}}{m}\right]\sum_{\text{odd } n_z} g_{(n_z-1)/2}(\boldsymbol{q}_\parallel)x_{\boldsymbol{q}_\parallel,1,n_z} \ . \tag{9.91}$$

Replacing Eq. (9.91) in Eq. (9.90), we find that the energy difference, minimized with respect to the matter wave-function and denoted by $\mathcal{E}[\boldsymbol{z}_{\boldsymbol{q}_\parallel,1}] \equiv \min_\psi \left(E[\boldsymbol{z}_{\boldsymbol{q}_\parallel,1},\psi] - E[\boldsymbol{z}_{\boldsymbol{q}_\parallel,1} = \boldsymbol{0},\psi_0]\right)$ takes the following quadratic form:

$$\mathcal{E}[\boldsymbol{z}_{\boldsymbol{q}_\parallel,1}] = \sum_{\boldsymbol{q}_\parallel} \sum_{\text{odd } n_z} \Big[\hbar\omega_{\boldsymbol{q}_\parallel,n_z}(x_{\boldsymbol{q}_\parallel,1,n_z}x_{-\boldsymbol{q}_\parallel,1,n_z} + y_{\boldsymbol{q}_\parallel,1,n_z}y_{-\boldsymbol{q}_\parallel,1,n_z}) + \frac{2S}{m}\chi_{\rm T}^{\rm J}(q_\parallel,0) \sum_{\text{odd } n_z'} g_{(n_z-1)/2}(\boldsymbol{q}_\parallel) g_{(n_z'-1)/2}(\boldsymbol{q}_\parallel) x_{\boldsymbol{q}_\parallel,1,n_z}x_{-\boldsymbol{q}_\parallel,1,n_z'}\Big] , \tag{9.92}$$

which can be written compactly as

$$\mathcal{E}[\boldsymbol{z}_{\boldsymbol{q}_\parallel,1}] = \sum_{\boldsymbol{q}_\parallel} \boldsymbol{z}^\dagger_{\boldsymbol{q}_\parallel,1}\mathcal{M}_{\boldsymbol{q}_\parallel}\boldsymbol{z}_{\boldsymbol{q}_\parallel,1} . \tag{9.93}$$

Here, $\mathcal{M}_{\boldsymbol{q}_\parallel}$ is a symmetric matrix. For photon condensation to occur we need the photon condensate phase to be energetically favored with respect to the normal phase. This occurs, at a given $\boldsymbol{q}_\parallel$, if at least one eigenvalue $\lambda_{\boldsymbol{q}_\parallel,n}$ of $\mathcal{M}_{\boldsymbol{q}_\parallel}$ is negative. For each $\boldsymbol{q}_\parallel$, the determinant $\Delta_{\boldsymbol{q}_\parallel} = \text{Det}(\mathcal{M}_{\boldsymbol{q}_\parallel})$ of the quadratic form in Eq. (9.93) can be written as (see Appendix E.5):

$$\Delta_{\boldsymbol{q}_\parallel} = \left[1 + \chi_{\rm T}^{\rm J}(q_\parallel,0)\frac{2\pi e^2}{c^2 q_\parallel}\tanh\left(\frac{q_\parallel L_z}{2}\right)\right] \prod_{\text{odd } n_z} (\hbar\omega_{\boldsymbol{q}_\parallel,n_z})^2 . \tag{9.94}$$

Using the relation $\Delta_{\boldsymbol{q}_\parallel} = \prod_n \lambda_{\boldsymbol{q}_\parallel,n}$ between eigenvalues and determinant, and noting that the second line in Eq. (9.94) is positive definite, we conclude that, in order to have at least one negative eigenvalue, the following inequality needs to be satisfied:

$$-\chi_{\rm T}^{\rm J}(q_\parallel,0)\frac{2\pi e^2}{c^2 q_\parallel}\tanh\left(\frac{q_\parallel L_z}{2}\right) > 1 . \tag{9.95}$$

This equation generalizes the criterion for photon condensation obtained in Ref. 231 for the case of a 2DES with Rashba spin-orbit coupling, placed in an external uniform magnetic field.

Let us consider first the case of zero photon momentum, $q_\parallel = 0$. In this case, the condition (9.95) for the occurrence of the photon condensation reduces to

$$-\chi_{\rm T}^{\rm J}(0,0)\frac{\pi e^2 L_z}{c^2} > 1 . \tag{9.96}$$

As discussed in Sect. 9.2, in systems with no long-range order [86], $\lim_{q_\parallel\to 0}\chi_{\rm T}^{\rm J}(q_\parallel,0) = 0$. Such diamagnetic sum-rule then yields an absurd $(0 > 1)$, expressing the no-go theorem for the occurrence of photon condensation in a spatially-uniform cavity field.

As in the 3D case, we now introduce the 2D non-local orbital susceptibility

$$\chi_{\rm orb}(q_\parallel) \equiv -\frac{e^2}{c^2}\frac{\chi_{\rm T}^{\rm J}(q_\parallel,0)}{q_\parallel^2} . \tag{9.97}$$

Introducing this definition in Eq. (9.95), we finally obtain the condition for the occurrence of photon condensation in a 2DES:

$$\boxed{\chi_{\rm orb}(q_\parallel) > \frac{1}{2\pi q_\parallel \tanh(q_\parallel L_z/2)}} . \tag{9.98}$$

This is the most important result of this Section.

As in the 3D case discussed in Sect. 9.2, the criterion in Eq. (9.98) emphasizes that the route towards the discovery of photon condensate states relies entirely on the knowledge of the orbital magnetic response function $\chi_{\rm orb}$ of ESs.

9.4.1 Discussion

In order to gain a deeper understanding on the possible occurrence of 2D photon condensation, we multiply both sides of Eq. (9.98) by $2/L_z$ and re-write the criterion as following:

$$\frac{2\chi_{\rm orb}(q_\parallel)}{L_z} > \frac{1}{2\pi(q_\parallel L_z/2)\tanh(q_\parallel L_z/2)} \ . \tag{9.99}$$

Note that, in this form, both sides of the inequality are dimensionless. We now discuss two regimes of $q_\parallel$ (short-wavelength and long-wavelength regimes) where Eq. (9.99) can be satisfied.

The right-hand side of Eq. (9.99) decreases with increasing $q_\parallel$. It therefore seems easy to satisfy Eq. (9.99) at short wavelengths, i.e. at $q_\parallel = 1/\ell_{\rm matter}$, where $\ell_{\rm matter}$ is a characteristic microscopic length scale of the 2DES at hand [2]. Indeed, since $\ell_{\rm matter}$ is expected to be $\ll L_z/2$, the right-hand side of Eq. (9.99) is small at $q_\parallel \sim 1/\ell_{\rm matter}$ and the threshold condition for 2D photon condensation reduces to

$$\frac{2\pi\chi_{\rm orb}(q_\parallel = 1/\ell_{\rm matter})}{\ell_{\rm matter}} \gtrsim 1 \ , \tag{9.100}$$

where we have used that $\tanh(L_z/(2\ell_{\rm matter})) \sim 1$. It may be however very inconvenient to hunt for 2D photon condensation at wave number scales on the order of $1/\ell_{\rm matter}$, as this would require cavities operating at very high energies, on the order of $\hbar\omega \sim \hbar c q_\parallel/\epsilon_{\rm r} = \hbar c/(\epsilon_{\rm r}\ell_{\rm matter})$.

From the argument above, it is advisable to investigate whether the 2D criterion (9.99) can be satisfied in the long-wavelength $q_\parallel \to 0$ limit. In this respect, we invite the reader to compare Eq. (9.99) with the 3D criterion in Eq. (9.35). The two criteria display a dramatic qualitative difference. While in the 3D case photon condensation can occur also in the quasi-homogeneous $q \to 0$ limit (provided that Eq. (9.35) is satisfied in that limit), in the 2D case the right-hand side of Eq. (9.99) diverges as $1/q_\parallel^2$ in the $q_\parallel \to 0$ limit. On the other hand, the left-hand side is usually finite in the same limit. At a first, superficial glance, it therefore seems impossible to satisfy the condition (9.99) in the long-wavelength limit.

However, a useful intermediate small-$q_\parallel$ regime exists. Indeed, the quantity $\chi_{\rm orb}(q_\parallel)$ on the left-hand side of Eq. (9.99) is expected to change on a wave number scale controlled by $1/\ell_{\rm matter}$. Matter is in the quasi-homogenous $q_\parallel \to 0$ limit when $q_\parallel \ll 1/\ell_{\rm matter}$. On the other hand, the right-hand side of Eq. (9.99) changes when $q_\parallel$ changes relatively to $2/L_z$. In order to mitigate the growth of the right-hand side of Eq. (9.99) with decreasing $q_\parallel$, it is therefore wise to work in the regime

$$\frac{2}{L_z} \lesssim q_\parallel \ll \frac{1}{\ell_{\rm matter}} \ , \tag{9.101}$$

assuming, as above, that $L_z/2 \gg \ell_{\rm matter}$.

When $q_\parallel \sim 2/L_z \ll 1/\ell_{\rm matter}$, the right-hand side of Eq. (9.99) is $\approx [2\pi\tanh(1)]^{-1}$, and the criterion for 2D photon condensation reduces to

$$\frac{2\chi_{\rm OMS}}{L_z} \gtrsim 0.21 \ , \tag{9.102}$$

where, in analogy to the 3D case in Eq. (9.34),

$$\chi_{\rm OMS} \equiv \lim_{q_\parallel \to 0} \chi_{\rm orb}(q_\parallel) \ . \tag{9.103}$$

[2] For example, in zero magnetic field, $\ell_{\rm matter}$ is expected to be on the order of $1/k_{\rm F}$, where $k_{\rm F}$ is the Fermi wave number of the 2DES. Similarly, in a perpendicular magnetic field $\boldsymbol{B} = B\hat{\boldsymbol{z}}$, $\ell_{\rm matter} \sim \ell_{\rm B}$, where $\ell_{\rm B} = \sqrt{\hbar c/(eB)}$ is the magnetic length.

In summary, in order to satisfy the inequality (9.99) in the quasi-homogeneous regime (9.101), we need to hunt for 2DESs whose OMS is positive (orbital paramagnets) and larger than $\approx L_z/10$.

We now list 2DESs where the criterion (9.102) is most likely to be satisfied. In 1991, Vignale demonstrated [246] that when the Fermi energy is sufficiently close to a saddle point of the band structure, non-interacting 2DESs in a periodic potential display orbital paramagnetism with $\chi_{\rm OMS}$ diverging logarithmically. The divergence is due to a diverging density of states at the saddle point. The positive sign of $\chi_{\rm OMS}$ is an exquisite quantum effect, which is easy to understand. Near a saddle point the semiclassical approximation breaks down, and tunnelling from one quasi-classical trajectory to the neighboring one occurs. Due to tunneling, electrons rotate around the saddle point in a direction opposite to the classical direction of rotation and the induced magnetic moment is reversed. We emphasize that the positive sign (i.e. paramagnetic character of the response) for non-interacting electrons is surprising, in view of the fact that non-interacting *parabolic-band* ESs are characterized by a negative OMS (Landau diamagnetism). Recently discovered [247] high-order van Hove singularities are expected to give stronger-than-logarithmic orbital paramagnetic behavior.

More recently, the OMS of the 2DES in graphene has received some attention. In the massless Dirac fermion continuum model, the 2DES in graphene is strongly diamagnetic [248], $\chi_{\rm OMS} \propto -\delta(E_{\rm F})$, when the Fermi energy lies at the Dirac point and electron-electron interactions are neglected. On the other hand, the lattice contribution [249] to the OMS beyond the massless Dirac fermion continuum model is positive for a wide range of Fermi energies and diverges at the saddle point, in agreement with Ref. 246. Electron-electron interactions display the same tendency and, in the massless Dirac fermion continuum model, turn the 2DES in graphene into an orbital paramagnet [250] when the Fermi energy is away from the Dirac point.

The OMS of multi-band systems with a pair of Dirac points interpolating between honeycomb and dice lattices has been studied by Raoux et al. [251]. Orbital paramagnetic behavior, stemming from a topological Berry phase changing continuously from π (graphene) to 0 (dice), has been found in this work even at Dirac crossings. A novel geometric contribution to the OMS has been shown to give rise to very strong orbital paramagnetism in models with flat bands [252]. It is therefore very natural to expect the same behavior also in twisted bilayer graphene close to the magic angle [253].

Other instances of orbital paramagnetic behavior have been found recently in a non-interacting 2DES in the presence of Rashba spin-orbit coupling and a perpendicular static magnetic field [231]. In particular, in their model, Nataf et al. [231] showed that Eq. (9.98) is satisfied at $q_{\parallel} \sim 1/\ell_{\rm B}$, every time that two Landau levels with opposite helicity cross.

9.5 Summary and conclusions

In summary, we have derived criterions for the occurrence of “superradiant" (i.e. photon condensate) states in electrons system coupled to a spatially-varying electromagnetic field. In three spatial dimensions, the criterion, reported in Eq. (9.35), is *identical* to the Condon criterion for the occurrence of magnetic domains. The Zeeman coupling of the electronic spin degrees of freedom to the cavity field leads to the criterion in Eq. (9.67) and implies that in a real material one needs to know both orbital and spin non-local response functions to make quantitative predictions on the occurrence of a photon condensate phase.

Finally, the condition for the occurrence of photon condensates in 2D systems embedded

in quasi-2D cavities is reported in Eq. (9.98) and poses severe bounds on the observability of this phenomenon. We have indeed shown that in order to satisfy this criterion in the quasi-homogeneous limit, one needs to hunt for materials with a divergent orbital paramagnetic character. A few possibilities have been discussed in Sect. 9.4.1.

While we have made no assumptions on the electromagnetic field, we have taken the electron system at hand to be homogeneous, i.e . we have worked with the so-called "jellium model [86]. Furthermore, relativistic Hamiltonian terms, such as spin-orbit coupling, have been neglected. In the future we plan to extend our investigations of photon condensate states to more general model Hamiltonians, especially ones that transcend the assumption of homogeneity.

The prediction of the possible coexistence in strongly correlated materials of exotic orders and photon condensate states requires accurate microscopic theories of the non-local orbital and spin response functions that take into account the role of electron-electron interactions.

10 Conclusions

In this Thesis collective effects in many-body quantum physics have been investigated. The properties of many-body systems can be dramatically different from the properties of the individual constituents displaying emergent collective behavior. There is a great deal of interest to exploit such collective many-body effects in the context of quantum technologies to boost the performance of a quantum device or to engineer new exotic phases of matter.

In the first part of the manuscript, we studied many-body quantum batteries, i.e. quantum systems composed by many units which are able to store energy and perform useful work. As we reviewed in Chap. 2, quantum information theorems [22, 23] showed that quantum correlations, established between the battery units, can greatly speed-up the charging process of a quantum battery. The average power of the collective charging protocol proposed in Ref. [22, 23] outperforms the best parallel charging protocol, in which entanglement between units cannot be built, by a factor polynomial in the number of battery units N. However, those studies considered non-local interactions between battery units which however are quite difficult to implement in practice. In this regard, Chap. 3 reviews current experiments on light-matter systems are - up to a certain level of details - well-described by the Dicke model. This model describes atoms in interaction with cavity photons as a collection of two-level systems coupled with a single bosonic mode. Effectively, this cavity mode can be seen as a mediator of long-range forces between atoms. Moreover, it is known that an ensemble of N excited atoms coherently coupled with the same cavity mode emits photons with an intensity N times bigger than the intensity associated with the independent emission of N uncorrelated atoms [25], known as "superradiant emission" in Literature.

Driven by the strong analogy between quantum batteries protocol and the Dicke physics, we proposed a Dicke quantum battery in Chap. 4. By employing exact diagonalization, we demonstrate the emergence of a collective speed-up in the charging power of a Dicke battery scaling like $\sqrt{N}$ for $N \gg 1$.

A battery is generally a complicated machine and its performance it is not only defined by the charging time. In Chap. 5 we study the fraction $\mathcal{E}_{\mathrm{B}}^{(N)}$ of energy stored in a Dicke battery that can be extracted in order to perform thermodynamic work. We first demonstrate that $\mathcal{E}_{\mathrm{B}}^{(N)}$ is highly reduced by the presence of correlations, e.g. the entanglement, between the

charger and the battery or between the two-level systems composing the battery. As this case shows, the presence of quantum effects can be detrimental for work extraction. We conclude by proving that the charger-battery system is asymptotically free of such locking correlations in the $N \to \infty$ limit for the case of the dynamics being dictated by an integrable Hamiltonian.

At this point, the physics behind the charging speed-up in a Dicke quantum battery is still unclear. Is this just due to the collective behavior of the underlying interacting many-body system or does it have its roots in the quantum mechanical nature of the system itself? In Chap. 6 we address these questions by studying three examples of quantum-mechanical many-body batteries with rigorous classical analogs. We find that quantum and classical models perform with the same scaling with the number of battery units N. Within these models it is possible to find only parametric, i.e independent of N, advantages, which are model dependent and, even within the same model, depend on the value of the coupling constant controlling the interaction between the charger and the battery itself. In summary, in these three models under study (and in contrast with the charging protocol exposed in Ref. [22, 23]) the use of quantum mechanical resources does not provide any advantage scaling polynomially in N.

Up to this point, a direct many-body implementation of the quantum speed-up foreseen by Ref. [22, 23] is missing. The exactly solvable Sachdev-Ye-Kitaev (SYK) model has recently received considerable attention in both condensed matter physics and high energy physics because it describes quantum matter without quasiparticles, while being at the same time the holographic dual of a quantum black hole. In Chap. 7, we examined SYK-based charging protocols of quantum batteries with N quantum cells. Extensive calculations based on exact diagonalization for N up to 16 strongly suggest that the optimal charging power of our SYK quantum batteries displays a super-extensive scaling with N that stems from genuine quantum mechanical effects. To the best of our knowledge, this is the first quantum many-body battery model where fast charging occurs due to the maximally-entangling underlying quantum dynamics.

As the Anderson's leitmotif "More is different" [254] teaches us, a quantitative change can lead to a qualitative change. For example, when we deal with a large number N of constituents, transitions between different phases of matter can occur. Quantum phase transitions are phase transition occurring at zero temperature and which are controlled by a Hamiltonian parameter. As we have discussed in Chap. 3, the Dicke model displays a quantum phase transition between a normal phase and a "superradiant"phase characterized by a macroscopic number of photons. This quantum phase transition controlled by the light-matter coupling has been referred to "photon condensation" in this Thesis. A careful derivation of the Dicke model from (a) the microscopical underlying model leads to the inclusion of the diamagnetic term proportional to $(\hat{a} + \hat{a}^\dagger)^2$ [39], which is naturally generated by the minimal coupling procedure $\hat{\boldsymbol{p}} \to \hat{\boldsymbol{p}} + e\boldsymbol{A}/c$. This terms forbids the phase transition if the Thomas-Reiche-Kuhn (TRK) sum-rule [84] is taken into account. Recently there has been a growing interest in quantum materials embedded in photonic cavity. While the Dicke model remains a paradigmatic model of ligh-matter interaction, it fails to describe a plethora of new experimental platform. Whether or not photon condensation can occur in such new experiments remains an open (and debated) question [40, 73].

In Chap. 8, we have shown that an arbitrary non-relativistic electronic system coupled to a single bosonic mode does not display photon condensation, even in presence of strong electron-electron interactions. As an example, we have studied an extended Falikov-Kimball model [199] showing that despite this model exhibits a phase transition to an exciton condensate phase, photon condensation does not occur in this system if light-matter interaction is

correctly implemented through the Peierls substitution.

The proof of the no-go theorem discussed in Chap. 8 relies on the fact that a spatially-uniform electromagnetic mode corresponds to a fictitious gauge field, which cannot have any physical manifestation.

Hence, a natural way to circumvent the theorem is to consider a spatially-varying mode. We have shown in Chap. 9, that it is indeed possible to derive a criterion for the occurrence of photon condensation. This criterion corresponds to a paramagnetic response to an external static magnetic field and is identical to the Condon criterion [233–238] for the occurrence of magnetic domains. Furthermore, we have derived the condition for the occurrence of photon condensates in 2D systems embedded in quasi-2D cavities. We have shown that in order to satisfy this criterion in the quasi-homogeneous limit, one needs materials with a divergent orbital paramagnetic character [246, 250, 251]. Given such findings, in the future, it will be interesting to study such paramagnetic materials inside a photonic cavity. While the ultimate goal of this line of research would be the experimental proof of photon condensation, our works can be seen as a significant step, necessary to identification of materials which, once embedded in a cavity, would display photon condensation.

In conclusions, this Thesis tackled two different topics, both characterized by the crucial role played by collective effects, namely many body quantum batteries and photon condensation. The results reported here show that the collective behavior typical for these systems can be exploited to boost the performance of a quantum device and to realize exotic phase of matter.

A

Appendix: High-power collective charging of a solid-state quantum battery

A.1 Considerations on an alternative charging/discharging protocol

The charging/discharging protocol described in the main text relies on turning on and off the interaction between the array of TLSs and the cavity (see Fig. 4.1 of the main text). Implementing such operation may be experimentally challenging. A more practical way to implement an equivalent charging/discharging protocol can be realized by manipulating the detuning between the TLSs and the cavity mode. When the two subsystems are far detuned, their interaction is effectively quenched. While the cavity frequency $\omega_{\rm c}$ is typically determined by fixed geometric features, it is often possible to temporally tune the TLS level splitting $\omega_{\rm eg}$ e.g. by means of an applied magnetic field.

For a time dependent $\omega_{\rm eg}(t)$ and a fixed interaction strength g, the Hamiltonian of the system reads:

$$\hat{\mathcal{H}}(t) = \omega_{\rm c}\hat{a}^\dagger\hat{a} + \omega_{\rm eg}(t)\hat{J}^z + 2g\hat{J}^x\left(\hat{a}^\dagger + \hat{a}\right) \ . \tag{A.1}$$

This alternative charging/discharging protocol is sketched in Fig. A.1.

Note that the new Hamiltonian (A.1) coincides with the Hamiltonian (6.20) considered in the main text during the charging and discharging steps, i.e. for $t \in [0, \tau_{\rm c}] \cup [\tau_{\rm c}+\tau_{\rm s}, \tau_{\rm c}+\tau_{\rm s}+\tau_{\rm d}]$. Accordingly, during these time intervals, the dynamics does not change with respect to that discussed in the main text.

For all other times, i.e. for $t \notin [0, \tau_{\rm c}] \cup [\tau_{\rm c} + \tau_{\rm s}, \tau_{\rm c} + \tau_{\rm s} + \tau_{\rm d}]$, the TLS and the cavity are far detuned, $|\tilde{\omega}_{\rm eg} - \omega_{\rm c}| \gg \omega_{\rm c} g$. In the case of a Rabi QB, the dynamics of each individual TLS+cavity system is well described in the far-detuned limit by the so-called dispersive Hamiltonian [98, 133]

$$\hat{h}^{\parallel} \approx \hbar\omega_{\rm c}\hat{a}^\dagger\hat{a} + \frac{\hbar\tilde{\omega}_{\rm eg}}{2}\hat{\sigma}^z + \hbar g^2\left[\left(\frac{1}{\delta} + \frac{1}{\Sigma}\right)\hat{a}^\dagger\hat{a}\hat{\sigma}_z + \frac{1}{2}\left(\frac{1}{\delta} - \frac{1}{\Sigma}\right) + \frac{1}{2}\left(\frac{1}{\delta} + \frac{1}{\Sigma}\right)\hat{\sigma}_z\right] , \tag{A.2}$$

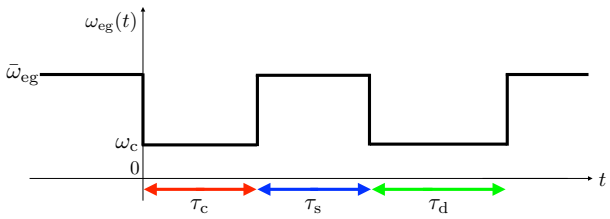

FIGURE A.1: (Color online) Alternative charging/discharging protocol. The TLS-cavity coupling g stays constant while the TLS energy splitting $\omega_{\rm eg}(t)$ is varied in time in a stepwise manner, therefore affecting the detuning.

where $\delta \equiv \tilde{\omega}_{\rm a} - \omega_{\rm c}$ and $\Sigma \equiv \tilde{\omega}_{\rm a} + \omega_{\rm c}$. Similarly, in the case of a Dicke QB and for $t \notin [0, \tau_{\rm c}] \cup [\tau_{\rm c} + \tau_{\rm s}, \tau_{\rm c} + \tau_{\rm s} + \tau_{\rm d}]$, the dynamics is well described by [134]

$$\hat{\mathcal{H}}^{\sharp} \approx \hbar\omega_{\rm c}\hat{a}^{\dagger}\hat{a} + \tilde{\omega}_{\rm eg}\hat{J}^{z} + d\hat{\mathcal{H}} \ , \tag{A.3}$$

where

$$d\hat{\mathcal{H}} = g^{2}\left[\left(\frac{2}{\delta}+\frac{2}{\Sigma}\right)\hat{a}^{\dagger}\hat{a}\hat{J}^{z} + \frac{\hbar}{2}\left(\frac{1}{\delta}-\frac{1}{\Sigma}\right) + \left(\frac{1}{\delta}+\frac{1}{\Sigma}\right)\hat{J}^{z}\right] . \tag{A.4}$$

Notice that the Hamiltonian (A.2) commutes with both $\hat{\sigma}^{z}$ and $\hat{a}^{\dagger}\hat{a}$ and that, similarly, the Hamiltonian (A.3) commutes with both $\hat{J}^{z}$ and $\hat{a}^{\dagger}\hat{a}$. That is, the interaction is effectively quenched in the far detuned case. Accordingly, no exchange of quanta between the TLS and the cavity mode is allowed when the TLSs are far detuned from the cavity. It follows that the overall dynamics of the TLS+cavity system is the same as the one discussed in the main text. However, we emphasize that the energy expectation can be different in the two cases, when considering the non-interacting stages, i.e. at $t \notin [0, \tau_{\rm c}] \cup [\tau_{\rm c} + \tau_{\rm s}, \tau_{\rm c} + \tau_{\rm s} + \tau_{\rm d}]$. Indeed, there can be considerable differences in the values of the energy injection $\delta E^{\rm on/off}$ at each of the turning-on/off point of the two protocols. To see this, consider for simplicity the turning-on point at time $t = 0$ in the limit $g^{2}N/\delta, g^{2}N/\Sigma \ll \min[\tilde{\omega}_{\rm eg}, \omega_{\rm c}]$. In this case, the term proportional to g^{2} in Eq. (A.3) can be neglected and the energy injection amounts to the large value $\delta E^{\rm on} \simeq (\omega_{\rm c} - \tilde{\omega}_{\rm eg})N/2$ (see Fig. A.1). On the other hand, $\delta E^{\rm on}$ vanishes for the protocol discussed in the main text, see Fig. 4.1(c).

A.2 Universality

Fig. A.2(a) and (b) show the maximum stored energy $\tilde{E}_{\sharp}^{(N)}$ and maximum charging power $\bar{P}_{\sharp}^{(N)}$ plotted as functions of the quantity $g_{N} = g\sqrt{N}$, which was already introduced in the main text, for various values of N. It is remarkable to note that the results for different values of N, which were reported in Fig. 4.3(b) and (d) of the main text, collapse onto universal curves in both cases.

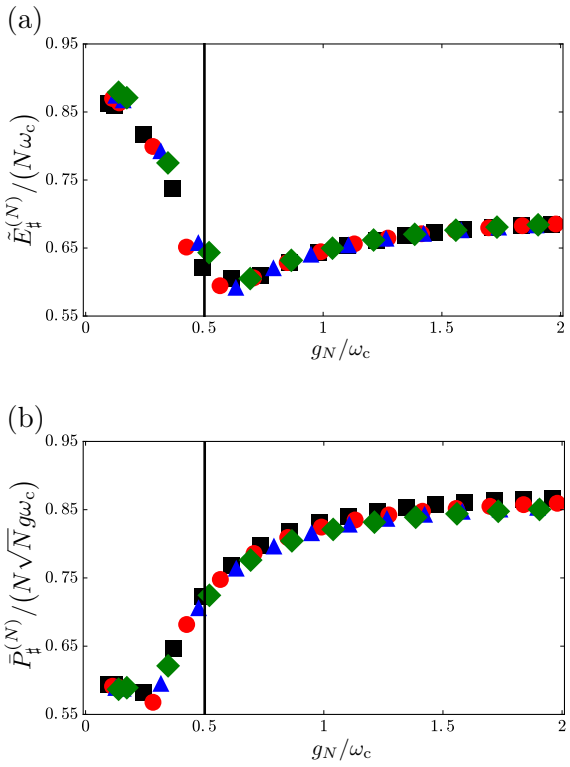

FIGURE A.2: Panel (a) The maximum stored energy $\tilde{E}_\sharp^{(N)}$ (in units of $N\omega_c$) is plotted as a function of g_N/ω_c for $N = 6$ (black squares), $N = 8$ (red circles), $N = 10$ (blue triangles), and $N = 12$ (green diamonds). Panel (b) The maximum charging power $\tilde{P}_\sharp^{(N)}$ (in units of $g\omega_c N\sqrt{N}$) is plotted as a function of g_N/ω_c for $N = 6$ (black squares), $N = 8$ (red circles), $N = 10$ (blue triangles) and $N = 12$ (green diamonds). Vertical black lines indicate the critical coupling $g_N/\omega_c = 0.5$ at which a superradiant quantum phase transition occurs in the ground state of the system, in the thermodynamic limit [37].

A.3 On the role of a quadratic term in the photon field

In certain solid-state experimental implementations of Rabi and Dicke Hamiltonians, it may be necessary to include an extra term proportional to $(\hat{a}^\dagger + \hat{a})^2$ in the Hamiltonian (6.20). As mentioned in the main text, the inclusion of such a term may have important consequences in regard to the achievability of the superradiant quantum phase transition in the thermodynamic limit [40, 69, 70, 73–75]. However, as detailed below for the case of finite N considered in this Appendix, the new Hamiltonian with the extra term $\propto (\hat{a}^\dagger + \hat{a})^2$ takes on exactly the same form of Eq. (6.20) when re-expressed in terms of properly squeezed bosonic operators $\hat{b}$, $\hat{b}^\dagger$. In this case, a renormalized cavity frequency and TLS-cavity coupling constant appear, as we proceed to demonstrate. Consider the new Hamiltonian

$$\hat{\mathcal{H}}^{\sharp\prime} \equiv \hat{\mathcal{H}}^\sharp + \Delta(\hat{a}^\dagger + \hat{a})^2 = \omega_c \hat{a}^\dagger \hat{a} + \omega_a \hat{J}^z + 2gJ_x\left(\hat{a}^\dagger + \hat{a}\right) + \Delta(\hat{a}^\dagger + \hat{a})^2 \,. \tag{A.5}$$

Introducing the squeezed operator

$$\hat{b} = \frac{(\alpha - 1)}{2\sqrt{\alpha}}\hat{a}^\dagger + \frac{(\alpha + 1)}{2\sqrt{\alpha}}\hat{a} \tag{A.6}$$

with $\alpha = \sqrt{4\Delta + 1}$, we obtain

$$\hat{\mathcal{H}}^{\sharp\prime} = \hbar\alpha\omega_{\mathrm{c}}\hat{b}^{\dagger}\hat{b} + \omega_{\mathrm{a}}\hat{J}_z + 2g\alpha^{-1/2}\lambda(t)\hat{J}_x(\hat{b}^{\dagger} + \hat{b}) \ , \tag{A.7}$$

where an irrelevant constant term has been dropped. We therefore immediately see that the new Hamiltonian $\hat{\mathcal{H}}^{\sharp,\prime}$ takes the same form as in Eq. (6.20), but with rescaled parameters. We note, however, that microscopic considerations [40, 73] reveal that there exist a functional relation between Δ, g, ω_{c} and N,

$$\Delta = \xi\frac{Ng^2}{\omega_{\mathrm{c}}} \ , \tag{A.8}$$

where ξ is a free parameter [40, 73]. Consequently, when the $(\hat{a}^{\dagger} + \hat{a})^2$ term is accounted for, a change in the coupling g would be accompanied by a change in Δ, leading to both a change in the dressed cavity mode frequency $\omega_{\mathrm{c}}' = \alpha\omega_{\mathrm{c}}$ and in the cavity eigenstates. This unfortunate situation does not occur when the more realistic protocol described in Appendix A.1 is used. In this case, the coupling stays fixed and only the TLS frequency changes. The new Hamiltonian remains therefore formally the same as in the main text as well as the initial state (involving now the N-photon Fock state associated to the operator $\hat{b}$, instead of $\hat{a}$), leaving unchanged the analysis described in the main text.

B

Appendix: Extractable work, the role of correlations, and asymptotic freedom in quantum batteries

In this appendix we provide additional information on the explicit form of the initial states mentioned in the main text and the scaling of the average charging power with N for these states. Finally, we also elaborate on why the coherent state is optimal for the ergotropy, we present a proof of Eq. (6) of the main text, and we extend our analysis of the ergotropy to the Dicke model.

B.1 Explicit form of the three initial states of the charger

We here provide the explicit form of the three initial states studied in our work, i.e. a Fock state, a coherent state, and a squeezed state:

$$\begin{aligned} |n\rangle_{\rm A} &= \frac{(\hat{a}^\dagger)^n}{\sqrt{n!}}\,|0\rangle \ , \\ |\alpha\rangle_{\rm A} &= \exp\left(\alpha\hat{a}^\dagger - \alpha^*\hat{a}\right)|0\rangle \ , \\ |z\rangle_{\rm A} &= \exp\left(\frac{z\hat{a}^2 - z^*(\hat{a}^\dagger)^2}{2}\right)|0\rangle \ , \end{aligned} \tag{B.1}$$

where $|0\rangle$ is the vacuum of the cavity. The three parameters n, α, and z, are fixed by the requirement to have input energy equal to $E_{\rm A}^{(N)}(0) = N\omega_0$. We therefore have $n = N$, $\alpha = \sqrt{N}$, and $z = \text{arcsinh}(\sqrt{N})$.

B.2 Scaling of the maximum average charging power

Here, we study the maximum average charging power $P_{\rm B}^{(N)}(\bar{\tau})$ as a function of N, for the three initial states introduced in the main text and in the previous section of this file. In

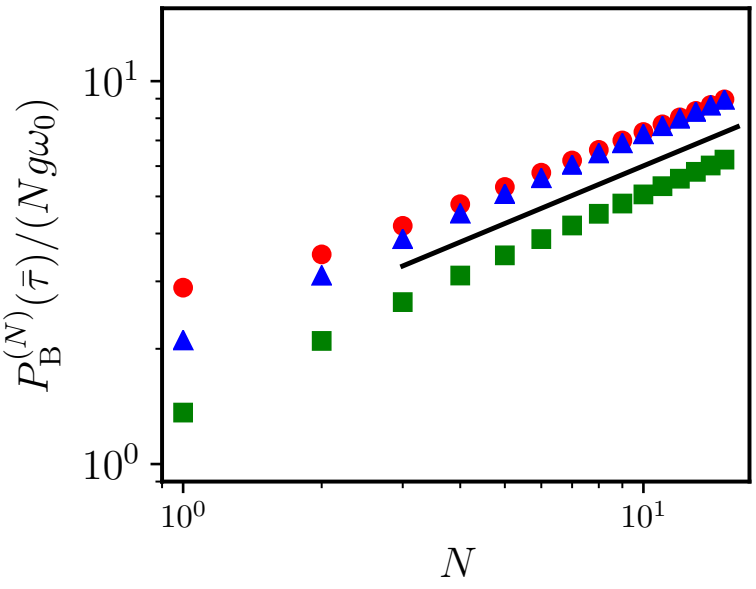

FIGURE B.1: The maximum average charging power $P_{\rm B}^{(N)}(\bar{\tau})$ (in units of $Ng\omega_0$) is plotted as a function of N in a log-log scale. Different symbols refer to three initial states of the charger: a Fock state (red circles), a coherent state (blue triangles), and a squeezed state (green squares).We plot a black solid line with slope 1/2 in the log-log scale, indicating the $\sqrt{N}$ scaling.

Fig. (B.1) we report a log-log scale plot of $P_{\rm B}^{(N)}(\bar{\tau})/N$ as a function of N. A simple inspection of this plot shows that $P_{\rm B}^{(N)}(\bar{\tau})/N \propto \sqrt{N}$, independently of the initial state. Now, by definition, $P_{\rm B}^{(N)}(\bar{\tau}) = E_{\rm B}^{(N)}(\bar{\tau})/\bar{\tau}$. Since $E_{\rm B}^{(N)}(\bar{\tau})$ is an extensive quantity, the collective advantage $P_{\rm B}^{(N)}(\bar{\tau})/N \propto \sqrt{N}$ stems from the scaling $\bar{\tau} \propto 1/\sqrt{N}$ of the optimal time.

B.3 Optimality of coherent states for work extraction

In this Section we offer an argument that explains why coherent states with an high number N of average excitations create weak correlations between A and B for relatively small times $\sqrt{N}g\tau \lesssim \pi/3$, B being initially in the ground state. We start by rewriting the Tavis-Cummings Hamiltonian in terms of collective spins operators:

$$\hat{J}^z \equiv \frac{1}{2}\sum_{i=1}^{N} \hat{\sigma}_i{}^z \tag{B.2}$$

and

$$\hat{J}^+ \equiv \left[\hat{J}^-\right]^\dagger = \sum_{i=1}^{N} \hat{\sigma}_i^+ \ . \tag{B.3}$$

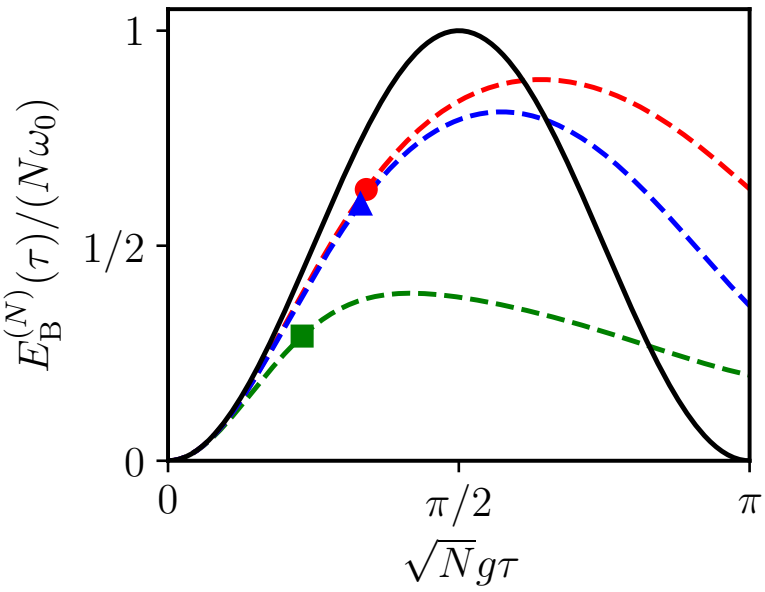

Figure B.2: The stored energy $E_{\rm B}^{(N)}(\tau)$ (in units of $N\omega_0$) as a function of $\sqrt{N}g\tau$. The black solid line denotes the energy calculated from the approximate Hamiltonian (B.5). Dashed lines denote the energy as calculated numerically from the exact dynamics, for three initial states of the charger: a Fock state (red), a coherent state (blue), and a squeezed state (green). Filled symbols denote the value of the energy at the optimal time $\bar{\tau}$.

The Hamiltonian then reads

$$\begin{aligned} \hat{\mathcal{H}}_{\rm A} &= \omega_0 \hat{a}^\dagger \hat{a} \ , \\ \hat{\mathcal{H}}_{\rm B} &= \omega_0 \left[\hat{J}^z + \frac{N}{2} \right] \ , \\ \hat{\mathcal{H}}_1 &= g \left[\hat{a} \hat{J}^+ + \hat{a}^\dagger \hat{J}^- \right] \ . \end{aligned} \tag{B.4}$$

We now use the Holdstein-Primakoff transformation [90] to express the collective spin operators in terms of auxiliary harmonic oscillator operators $\hat{b}$ and $\hat{b}^\dagger$: $\hat{J}^z = (\hat{b}^\dagger \hat{b} - N/2)$ and $\hat{J}^+ = \hat{b}^\dagger \sqrt{N} \sqrt{1 - \hat{b}^\dagger \hat{b}/N}$. If we are interested only in the first few excitations of the spectrum we can neglect terms like $\hat{b}^\dagger \hat{b}/N$ (since $N \gg 1$). In this case, we have $\hat{J}^+ \approx \hat{b}^\dagger \sqrt{N}$, obtaining

$$\begin{aligned} \hat{\mathcal{H}}_{\rm A} &= \omega_0 \hat{a}^\dagger \hat{a} \ , \\ \hat{\mathcal{H}}_{\rm B} &= \omega_0 \hat{b}^\dagger \hat{b} \ , \\ \hat{\mathcal{H}}_1 &\approx g\sqrt{N} (\hat{a} \hat{b}^\dagger + \hat{a}^\dagger \hat{b}) \ . \end{aligned} \tag{B.5}$$

The total Hamiltonian is now approximately the one of two harmonic oscillators coupled via a quadratic term. When this approximation holds, an initial coherent state remains a coherent state under time evolution, i.e.

$$\begin{aligned} |\Psi(t)\rangle &= \exp(-i\hat{\mathcal{H}} t) \, |\sqrt{N}\rangle_{\rm A} \otimes |{\rm G}\rangle_{\rm B} \\ &= |\sqrt{N} \cos(g_N t)\rangle_{\rm A} \otimes |-i\sqrt{N} \sin(g_N t\rangle_{\rm B} \ , \end{aligned} \tag{B.6}$$

where $g_N = \sqrt{N}g$ and $|\alpha(t)\rangle$ is the coherent state defined by the displacement parameter $\alpha(t)$. The energy stored in B, as calculated from Eq. (B.5), is $E_{\rm B}(\tau) \approx N\omega_0 \sin^2(g_N t)$ and is independent of the initial state.

The large-N bosonic approximation is good only for small times, i.e. for $\sqrt{N}g\tau \ll 1$, when the battery is poorly charged and highly excited states are empty. Furthermore, we can verify *a posteriori* the condition $\hat{b}^\dagger\hat{b}/N \ll 1$ by calculating the occupation number in B within the approximation. This yields $\langle \hat{b}^\dagger\hat{b}\rangle /N = \sin^2(g_N t) \ll 1$, which works for $\sqrt{N}g\tau \ll 1$.

In Fig. (B.2) we compare the energy $E_{\rm B}^{(N)}$ calculated within the large-N bosonic approximation (black solid line) with that calculated from the exact dynamics. In addition, we indicate by filled symbols the value $E_{\rm B}^{(N)}(\bar{\tau})$ evaluated at the optimal time $\bar{\tau}$. We clearly see that at the optimal time $\bar{\tau}$ the large-N bosonic approximation is qualitatively correct.

B.4 Proof of Eq. (6)

In this Section we provide a proof for Eq. (6) of the main text, i.e. we show that $\lim_{N\to\infty} \mathcal{E}_{\rm B}^{(N)}/E_{\rm B}^{(N)} \to 1$, or more precisely, that

$$\lim_{N\to\infty} \frac{E_{\rm B}^{(N)} - \mathcal{E}_{\rm B}^{(N)}}{E_{\rm B}^{(N)}} \to 0 \tag{B.7}$$

whenever $\rho_{\rm B}(\tau)$ has a number $\mathcal{N}$ of non-zero eigenvalues λ_i which is at most polynomial in N, i.e. $\mathcal{N} \leq \alpha N^k$ for some $\alpha, k > 0$. This assumption results in a von Neumann entropy $S(\rho_{\rm B}(\tau))$ of the reduced system, which scales at most as $\log N$.

We first notice that the numerator of Eq. (B.7) can be rewritten as $E_{\rm B}^{(N)} - \mathcal{E}_{\rm B}^{(N)} = {\rm tr}_{\rm B}[\hat{\mathcal{H}}_{\rm B}\tilde{\rho}_{\rm B}]$, where $\tilde{\rho}_{\rm B}$ is the passive state corresponding to $\rho_{\rm B}$ and $\hat{\mathcal{H}}_{\rm B}$.

We then define $\bar{\rho}_{\rm B}$ as the density matrix diagonal in the energy basis of $\hat{\mathcal{H}}_{\rm B}$ such that its first αN^k eigenvalues are non-zero and all equal, i.e. $\bar{\lambda}_i = 1/(\alpha N^k)$ for $i = 1 \dots \alpha N^k$. It is now useful to revise the concept of majorization [3]: a state ρ majorizes another state ρ' (and we write $\rho \succ \rho'$) if the eigenvalues of the density matrices satisfy: $\sum_{i=1}^n \lambda_i \geq \sum_{i=1}^n \lambda'_i$, for all n, where $\lambda_i\,(\lambda'_i)$ are the eigenvalues of $\rho\,(\rho')$ in descending order. Notice then that $\bar{\rho}_{\rm B}$ is a passive state and that it is majorized by $\tilde{\rho}_{\rm B}$: i.e. $\tilde{\rho}_{\rm B} \succ \bar{\rho}_{\rm B}$.

It is now useful to write

$${\rm tr}_{\rm B}[\hat{\mathcal{H}}_{\rm B}\tilde{\rho}_{\rm B}] - {\rm tr}_{\rm B}[\hat{\mathcal{H}}_{\rm B}\bar{\rho}_{\rm B}] = \sum_i (\epsilon_{i+1}^{\rm B} - \epsilon_i^{\rm B}) \sum_{j=1}^{i} (\lambda_j - \bar{\lambda}_j) \ , \tag{B.8}$$

which appears to be a negative quantity due to the fact that the energies are ordered, i.e. $(\epsilon_{i+1}^{\rm B} - \epsilon_i^{\rm B}) \geq 0$, and $\tilde{\rho}_{\rm B} \succ \bar{\rho}_{\rm B}$. Accordingly, we arrive at the following inequality

$$E_{\rm B}^{(N)} - \mathcal{E}_{\rm B}^{(N)} = {\rm tr}_{\rm B}[\hat{\mathcal{H}}_{\rm B}\tilde{\rho}_{\rm B}] \leq {\rm tr}_{\rm B}[\hat{\mathcal{H}}_{\rm B}\bar{\rho}_{\rm B}] \ . \tag{B.9}$$

We now observe that the spectrum of B is highly degenerate. Since we have N identical qubits, we have $N+1$ degenerate energy levels, and the j-th level is $\binom{N}{j}$ times degenerate. For large N we can use the Stirling approximation $\binom{N}{j} \sim N^j$. If we select the level $j = k+1$ for large enough N we can construct a state $\rho_{\rm B}^{(k)}$ within this degenerate subspace that populates equally αN^k of these $\binom{N}{k}$ states, where each state has energy $k\omega_0$. As this state has the same spectrum of $\bar{\rho}_{\rm B}$, there is a unitary operation U_k such that $\rho_{\rm B}^{(k)} = U_k \bar{\rho}_{\rm B} U_k^\dagger$.

Now, recalling that $\bar{\rho}_{\rm B}$ is a passive state, the following inequality holds true: $\mathrm{tr}_{\rm B}[\hat{\mathcal{H}}_{\rm B}\bar{\rho}_{\rm B}] \leq \mathrm{tr}_{\rm B}[\hat{\mathcal{H}}_{\rm B}\rho_{\rm B}^{(k)}] = k\,\omega_0$, which inserted into Eq. (B.9) yields

$$E_{\rm B}^{(N)} - \mathcal{E}_{\rm B}^{(N)} \leq k\omega_0 \ . \tag{B.10}$$

Equation (B.7) finally follows from the observation that the energy is extensive, i.e. that $E_{\rm B}^{(N)} \sim N\omega_0$, so that $(E_{\rm B}^{(N)} - \mathcal{E}_{\rm B}^{(N)})/E_{\rm B}^{(N)} \sim k/N$, which goes to zero as $N \to \infty$. We also note that from this proof we can infer a convergence to unity scaling as $1/N$.

B.5 Validity of our main results for the case of the Dicke model

In this Section we study how our analysis can be gerenalized to the Dicke model [24, 25], described by the Hamiltonian

$$\hat{\mathcal{H}}_{\rm A} = \omega_0\ \hat{a}^\dagger\hat{a}\ , \tag{B.11}$$

$$\hat{\mathcal{H}}_{\rm B} = \omega_0 \sum_{i=1}^{N} \hat{\sigma}_i^+\hat{\sigma}_i^-\ , \tag{B.12}$$

$$\hat{\mathcal{H}}_1 = g\sum_{i=1}^{N}\big(\hat{a}\ +\hat{a}^\dagger\big)\hat{\sigma}_i^x\ , \tag{B.13}$$

where all relevant operators and parameters have the save meaning as for the Tavis-Cummings model in the main text. We notice that the Tavis-Cummings Hamiltonian used in the main text can be obtained from the full Dicke Hamiltonian (B.13) in the weak-coupling regime $g/\omega_0 \ll 1$, neglecting the counter-rotating terms $\hat{a}\,\hat{\sigma}_i^-$ and $\hat{a}^\dagger\,\hat{\sigma}_i^+$.

Since $[\hat{\mathcal{H}}_1, \hat{\mathcal{H}}_0] \neq 0$ during the protocol some energy is injected via the modulation of the coupling $\lambda(t)$ and this process does not fall in the class of pure-energy-transfer protocols. (See Ref. [49] for a detailed discussion.) While we are not explicitly studying this issue here, we show that the main results of the main text apply also to the Dicke model. We consider the same three initial optical states considered in the main text. In Fig. B.3 we can clearly see that:

1) Coherent states are still optimal in minimizing the amount of correlations between the charger A and the battery B and hence maximize the ratio $\mathcal{E}_{\rm B}^{(N)}(\tau)/E_{\rm B}^{(N)}(\tau)$. We note that the amount of energy locked in correlations can be bigger than in the Tavis-Cummings case, due to the presence of counter-rotating terms.

2) As explained in the main text, due to the conservation of the total angular momentum J^2, we still have the asymptotic freedoms from correlations, namely $\mathcal{E}_{\rm B}^{(N)}/E_{\rm B}^{(N)} \to 1$ for $N \to \infty$ also for the Dicke model.

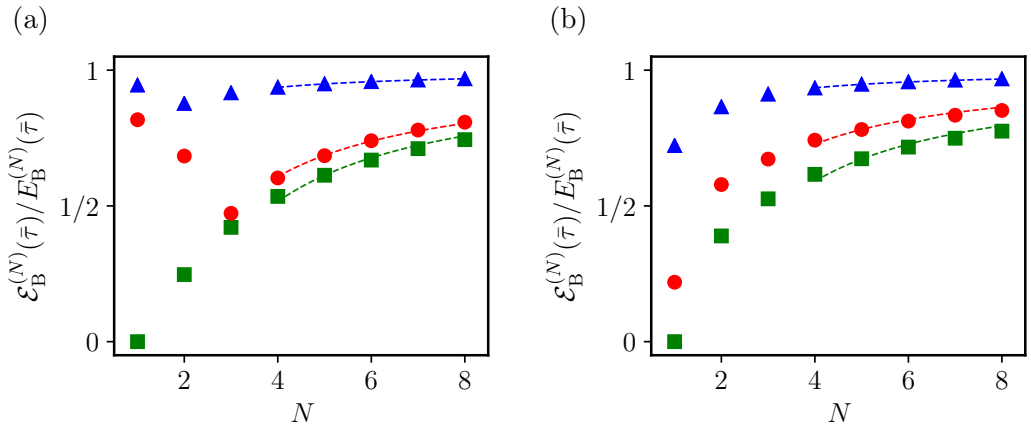

FIGURE B.3: Panel (a) The ratio $\mathcal{E}_{\rm B}^{(N)}(\bar{\tau})/E_{\rm B}^{(N)}(\bar{\tau})$ as a function of N for three initial states of the charger: a Fock state (red circles), a coherent state (blue triangles), and a squeezed state (green squares). Numerical results in this figure have been obtained for the Dicke model and $g/\omega_0 = 0.2$. We fit the last five points of all data sets with a $1/N$ convergence to 1. Panel (b) Same as in panel (a) but for $g/\omega_0 = 2$ (the ultra-strong-coupling regime).

C

Appendix: Quantum advantage in the charging process of Sachdev-Ye-Kitaev batteries

C.1 On the JW transformation and other details on the numerical calculations

The c-SYK model [177] for finite N is best handled numerically after mapping it onto a spin model. This is accomplished through the JW transformation. For the sake of clarity, we here report the c-SYK model Hamiltonian [cf. Eq. (7.4) in Chap. 7]:

$$\hat{\mathcal{H}}_1^{\text{c-SYK}} = \sum_{i,j,k,l=1}^{N} J_{i,j,k,l}\, \hat{c}_i^\dagger\, \hat{c}_j^\dagger\, \hat{c}_k\, \hat{c}_l \ . \tag{C.1}$$

Here, $\hat{c}_j^\dagger$ ($\hat{c}_j$) creates (annihilates) a complex spinless fermion and the usual fermionic anti-commutation relations, $\{c_i^\dagger, c_j\} = \delta_{i,j}$, $\{c_i, c_j\} = 0$, hold true. The JW transformation, which maps spinless fermions into spin-1/2 degrees of freedom, reads as following:

$$\hat{c}_j^\dagger = \hat{\sigma}_j^+ \left[\prod_{m=1}^{j-1} \hat{\sigma}_m^z\right] , \qquad \hat{c}_j = \left[\prod_{m=1}^{j-1} \hat{\sigma}_m^z\right] \hat{\sigma}_j^- \ , \tag{C.2}$$

where $\hat{\sigma}_j^\pm \equiv (\hat{\sigma}_j^x \pm i\hat{\sigma}_j^y)/2$.

Applying such transformation to the model in Eq. (C.1), one has to distinguish three cases [255]:

• All indices are different ($i \neq j \neq k \neq l$). In this case

$$\hat{c}_i^\dagger\, \hat{c}_j^\dagger\, \hat{c}_k\, \hat{c}_l = \beta \left[\prod_{\xi=\zeta_1+1}^{\zeta_2-1} \hat{\sigma}_\xi^z\right] \left[\prod_{\xi'=\zeta_3+1}^{\zeta_4-1} \hat{\sigma}_{\xi'}^z\right] \hat{\sigma}_i^+\, \hat{\sigma}_j^+\, \hat{\sigma}_k^-\, \hat{\sigma}_l^- \ , \tag{C.3}$$

where $\{\zeta_1, \zeta_2, \zeta_3, \zeta_4\} = \{i, j, k, l\}$ are the four reordered indices, such that $\zeta_1 < \zeta_2 < \zeta_3 < \zeta_4$, and $\beta = \text{sign}(i-j)\,\text{sign}(k-l)$;

• Two indices are equal (e.g. $j = l$ and $i \neq j \neq k$). In this case:

$$\hat{c}_i^\dagger \, \hat{c}_j^\dagger \, \hat{c}_j \, \hat{c}_k = \hat{\sigma}_i^+ \left[\prod_{\xi=\zeta_1}^{\zeta_2-1} \hat{\sigma}_\xi^z \right] \hat{\sigma}_j^+ \, \hat{\sigma}_j^- \, \hat{\sigma}_k^- \ , \tag{C.4}$$

where $\{\zeta_1, \zeta_2\} = \{i, k\}$ are reordered such that $\zeta_1 < \zeta_2$;
• Indices are equal in pairs (e.g. $j = k$ and $i = l$). In this case

$$\hat{c}_i^\dagger \, \hat{c}_j^\dagger \, \hat{c}_j \, \hat{c}_i = \hat{\sigma}_i^+ \, \hat{\sigma}_j^+ \, \hat{\sigma}_j^- \, \hat{\sigma}_i^- \ . \tag{C.5}$$

As we mentioned in Chap. 7, in order to enforce PHS, one needs to add extra terms of the form $\hat{c}_i^\dagger \hat{c}_k$ to Eq. (C.1) [cf. (7.5) in Chap. 7]. We can again use the JW transformation in order to write each of these one-body contributions in terms of spin-1/2 operators:

$$\hat{c}_i^\dagger \hat{c}_k = \hat{\sigma}_i^+ \left[\prod_{\xi=\zeta_1}^{\zeta_2-1} \hat{\sigma}_\xi^z \right] \hat{\sigma}_k^- \ , \tag{C.6}$$

where $\{\zeta_1, \zeta_2\} = \{i, k\}$ are reordered such that $\zeta_1 < \zeta_2$.

Once the Hamiltonian is written in the spin-1/2 representation (spin operators do commute on different sites), one can safely write its matrix representation in the usual computational basis where the operator $\hat{\sigma}_j^z$ is diagonal. Notice that, for the b-SYK Hamiltonian [Eq. (7.6)], the JW string is not required.

In order to evaluate the properties of the time-evolved state during our charging protocol ($\hbar = 1$),

$$|\psi(\tau)\rangle = e^{-i\hat{\mathcal{H}}_1 \tau} \left(\bigotimes_{j=1}^{N} |{\downarrow}^{(y)}\rangle_j \right) \ , \tag{C.7}$$

we numerically integrated the equation of motion for $|\psi(\tau)\rangle$ using a fixed-stepsize fourth-order Runge-Kutta method. To ensure convergence, typical integration time steps of order $\delta t \approx 10^{-3}$ (in units of $1/J$) were used. We checked that our choice of δt is always conservative (i.e., it guarantees convergence in time of all our results, within an error bar that is negligible on the scale of the figures).

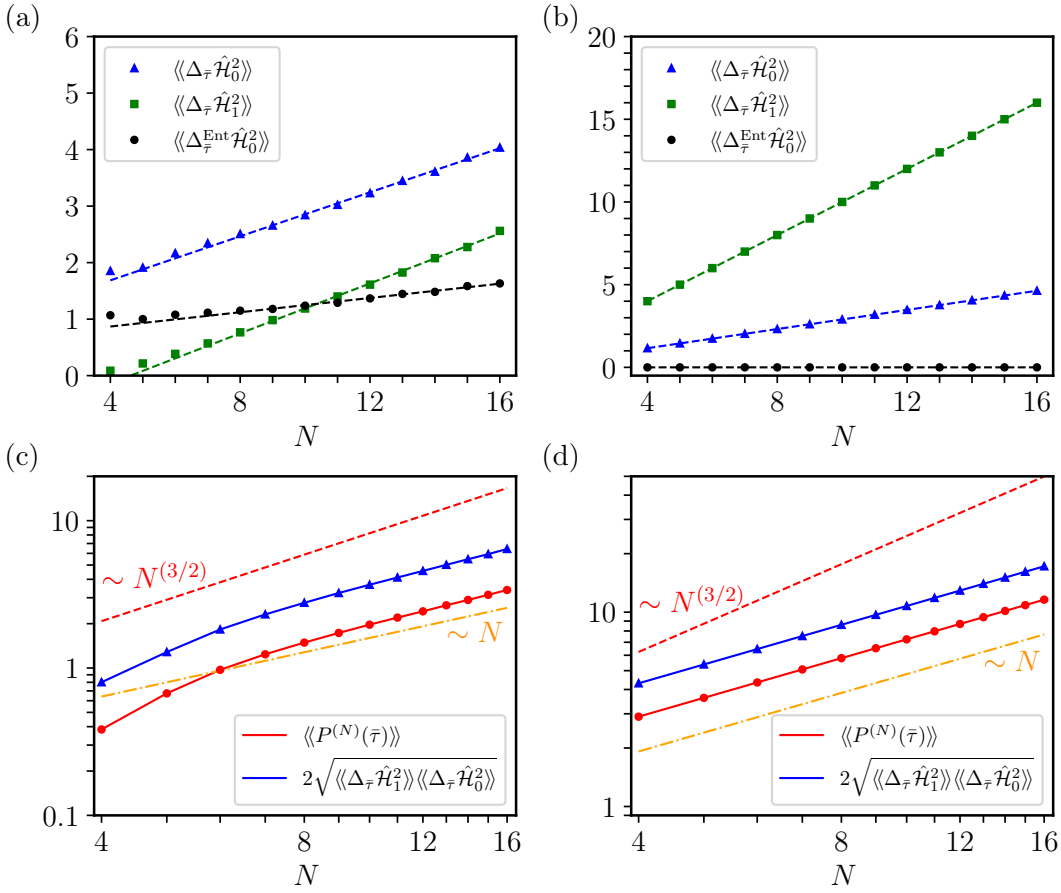

FIGURE C.1: (Color online) Panels (a,b) The relevant quantities for the bound (7.12) in Chap. 7, evaluated at the optimal time $\bar\tau$ and averaged over disorder: time-averaged variances $\langle\langle\Delta_{\bar\tau}\hat{\mathcal{H}}_0^2\rangle\rangle$ (blue triangles), $\langle\langle\Delta_{\bar\tau}\hat{\mathcal{H}}_1^2\rangle\rangle$ (green squares), $\langle\langle\Delta_{\bar\tau}^{\rm Ent}\hat{\mathcal{H}}_0^2\rangle\rangle$ (black circles), as functions of N. Dashed lines denote linear fits to the numerical results. The four data points corresponding to the smallest N have been always eliminated from the fits. Panels (c,d) The optimal power (red) $\langle\langle P^{(N)}(\bar\tau)\rangle\rangle$ and the quantity in the right-hand-side of the bound (12) (blue) are plotted as functions of N, in a log-log scale. Dashed lines correspond to power laws $\sim N^{1+k}$ ($k = 0.5$: red; $k = 0$: orange) and are plotted as guides to the eye. Data in panels (a,c) refer to the b-SYK QB model. Data in panels (b,d), instead, refer to the parallel QB model.In panels (a,b), $\langle\langle\Delta_{\bar\tau}\hat{\mathcal{H}}_0^2\rangle\rangle$ and $\langle\langle\Delta_{\bar\tau}^{\rm Ent}\hat{\mathcal{H}}_0^2\rangle\rangle$ are measured in units of ω_0^2, while $\langle\langle\Delta_{\bar\tau}\hat{\mathcal{H}}_1^2\rangle\rangle$ is measured in units of J^2 for both b-SYK and parallel-charging protocols. Data in panels (c,d) are in units of $\omega_0 J$ for both b-SYK and parallel-charging protocols. This implies that choices need to be made for the parameters $\bar J$ and K, in units of J: data in this figure have been obtained by setting $\bar J = J$ and $K = J$. Here and in Fig. C.2, data for both types of SYK models have been obtained after averaging over $N_{\rm dis} = 10^3$ (for $N = 4, \ldots, 10$), 5×10^2 (for $N = 11, 12$), and 10^2 (for $N = 13, \ldots, 16$) instances of disorder in the couplings $\{J_{i,j,k,l}\}$ and $\{\bar J_{i,j,k,l}\}$.

C.2 Derivation of Eq. (7.9) in Chap. 7

From the Heisenberg equation of motion for $0 \leq t \leq \tau$ we get:

$$\left(\frac{dE^{(N)}(t)}{dt}\right)^2 = \left|\,\langle[\hat{\mathcal{H}}_0, \hat{\mathcal{H}}_1]\rangle_t\,\right|^2 . \tag{C.8}$$

The Schrödinger-Robertson (SR) inequality [256] yields: $|\langle[\hat{\mathcal{H}}_0,\hat{\mathcal{H}}_1]\rangle_t|^2 \leq 4\,(\delta_t\hat{\mathcal{H}}_0^2)\,(\delta_t\hat{\mathcal{H}}_1^2)$, where $\delta_t\hat{\mathcal{H}}^2 \equiv \langle\hat{\mathcal{H}}^2\rangle_t - \langle\hat{\mathcal{H}}\rangle_t^2$. Taking the square root of Eq. (C.8), using the SR inequality, applying the integral $\int_0^\tau dt/\tau$ to both members of Eq. (C.8), and using $E^{(N)}(0)=0$, we finally get the inequality:

$$P^{(N)}(\tau) \equiv \frac{E^{(N)}(\tau)}{\tau} \leq 2\int_0^\tau \frac{dt}{\tau}\sqrt{(\delta_t\hat{\mathcal{H}}_0^2)\,(\delta_t\hat{\mathcal{H}}_1^2)}\,. \tag{C.9}$$

Using the Cauchy-Schwarz inequality with respect to the scalar product induced by $\int_0^\tau dt/\tau$, we finally get Eq. (7.9) in Chap. 7, i.e.

$$P^{(N)}(\tau) \leq 2\sqrt{\Delta_\tau\hat{\mathcal{H}}_0^2\,\Delta_\tau\hat{\mathcal{H}}_1^2}\,. \tag{C.10}$$

Since the evolution is generated by the charging Hamiltonian $\hat{\mathcal{H}}_1$ itself, the time-average $\int_0^\tau dt/\tau$ involved in the second term in the r.h.s of Eq. (C.10) can be computed trivially as

$$\Delta_\tau\hat{\mathcal{H}}_1^2 = \langle\hat{\mathcal{H}}_1^2\rangle - \langle\hat{\mathcal{H}}_1\rangle^2. \tag{C.11}$$

C.3 Comparison between quantum and classical many-body batteries

Consider the bound in Eq. (C.10) [Eq. (7.9) in Chap. 7]. In order to ensure thermodynamic consistency, the average value of the charging Hamiltonian is required to be extensive, $\langle\hat{\mathcal{H}}_1\rangle \sim N$, while its standard deviation, $\left[\langle\hat{\mathcal{H}}_1^2\rangle - \langle\hat{\mathcal{H}}_1\rangle^2\right]^{1/2}$ should scale as $\sqrt{N}$. This ensures that relative fluctuations, $\langle\hat{\mathcal{H}}_1\rangle\,/\left[\langle\hat{\mathcal{H}}_1^2\rangle - \langle\hat{\mathcal{H}}_1\rangle^2\right]^{1/2}$, drop to zero as N goes to infinity, implying the equivalence of all the thermodynamic ensembles (microcanonical, canonical, and grand canonical). This constraint forces $\Delta_\tau\hat{\mathcal{H}}_1^2$ to scale at most linearly with N. In Chap. 7, we have ensured thermodynamic consistency of the SYK QB by choosing the appropriate scaling [177] with N of the variance $\langle\!\langle J_{i,j,k,l}^2\rangle\!\rangle = J^2/N^3$ of the coupling parameters.

Exploiting the locality of $\hat{\mathcal{H}}_0 = \sum_j \hat{h}_j$, with $\hat{h}_j = \omega_0\hat{\sigma}_j^y/2$, the first term in the r.h.s. of Eq. (C.10) can be written as the sum of two contributions: $\Delta_\tau\hat{\mathcal{H}}_0^2 = \Delta_\tau^{\rm Loc}\hat{\mathcal{H}}_0^2 + \Delta_\tau^{\rm Ent}\hat{\mathcal{H}}_0^2$, see Eqs. (7.10,7.11) in Chap. 7,

$$\Delta_\tau^{\rm Loc}\hat{\mathcal{H}}_0^2 \equiv \frac{1}{\tau}\int_0^\tau dt\sum_i\left[\,\langle\hat{h}_i^2\rangle_t - \langle\hat{h}_i\rangle_t^2\,\right], \tag{C.12}$$

$$\Delta_\tau^{\rm Ent}\hat{\mathcal{H}}_0^2 \equiv \frac{1}{\tau}\int_0^\tau dt\sum_{i\neq j}\Big[\,\langle\hat{h}_i\hat{h}_j\rangle_t - \langle\hat{h}_i\rangle_t\,\langle\hat{h}_j\rangle_t\Big], \tag{C.13}$$

where averages $\langle\,\cdot\,\rangle_t$ are done on the state $|\psi(t)\rangle$ at time t. The first term, being a sum of N factors, is extensive with N by construction. The second term can, in principle, scale quadratically with N if correlations between different sites are established during the dynamics. Here we argue that such correlations have a quantum origin.

Indeed, consider the correlation term

$$C_\phi = \sum_{i\neq j}\Big[\,\langle\hat{h}_i\hat{h}_j\rangle_\phi - \langle\hat{h}_i\rangle_\phi\,\langle\hat{h}_j\rangle_\phi\,\Big] \tag{C.14}$$

inside the integral in Eq. (C.13), where averages $\langle \cdot \rangle_\phi$ are done over a given state $|\phi\rangle$. Evaluating it on the highly nonclassical Greenberger-Horne-Zeilinger (GHZ) state [3],

$$|\mathrm{GHZ}\rangle = \frac{1}{\sqrt{2}}\left(\bigotimes_{j=1}^{N} |{\downarrow^{(y)}}\rangle_j + \bigotimes_{j=1}^{N} |{\uparrow^{(y)}}\rangle_j \right), \tag{C.15}$$

would result in a quadratic scaling with N, i.e., $C_{\mathrm{GHZ}} = N(N-1)\,\omega_0^2$. Conversely such correlation term evaluated over a separable state, $|\phi\rangle = \bigotimes_{j=1}^{N} |\varphi\rangle_j$ ($|\varphi\rangle_j$ being an arbitrary local state), would trivially vanish. This means that, in order to have a super-linear scaling in the contribution $\Delta_{\bar\tau}^{\mathrm{Ent}}\hat{\mathcal{H}}_0^2$, the system has to evolve through highly nonlocal states, as the GHZ state, during the dynamics. By definition, classical systems do not build up any entanglement during the charging dynamics, therefore different battery units are uncorrelated $\langle \hat{h}_i \hat{h}_j \rangle_t = \langle \hat{h}_i \rangle_t \langle \hat{h}_j \rangle_t$ and $\Delta_{\bar\tau}^{\mathrm{Ent}}\hat{\mathcal{H}}_0^2 = 0$, meaning that the power scales linearly with N.

In conclusion, in classical many-body batteries the term $\Delta_{\bar\tau}\hat{\mathcal{H}}_0^2$ scales at most linearly with N, while the term $\Delta_{\bar\tau}\hat{\mathcal{H}}_1^2$ is constrained to scale linearly by thermodynamic consistency. On the other hand, in quantum many-body batteries the entanglement production enables $\Delta_{\bar\tau}\hat{\mathcal{H}}_0^2$ to scale quadratically with N, which in turn implies that the power may scale at most as $N^{3/2}$.

A more detailed analysis of the relation between power and entanglement is given in Ref. [63], which shows that a finite fraction of quantum cells are required to be entangled in a GHZ-like state in order to imply a superextensive charging power.

C.4 Power and bounds for the b-SYK and the parallel-charging models

In Chap. 7 it has been shown that a QB charged through the c-SYK model is able to outperform any classical battery, since both $\langle\!\langle \Delta_{\bar\tau}\hat{\mathcal{H}}_0^2 \rangle\!\rangle$ and $\langle\!\langle \Delta_{\bar\tau}^{\mathrm{Ent}}\hat{\mathcal{H}}_0^2 \rangle\!\rangle$ grow quadratically with N (see Fig. 7.3 in Chap. 7). Time fluctuations of $\hat{\mathcal{H}}_0$ are thus super-extensive. On the other hand, as expected, $\langle\!\langle \Delta_{\bar\tau}\hat{\mathcal{H}}_1^2 \rangle\!\rangle$ is extensive in N. This suggests that the bound (12), as well as the optimal power, scale as $N^{3/2}$:

$$\langle\!\langle P^{(N)}(\bar\tau) \rangle\!\rangle \sim N^{1+\frac{1}{2}} \quad \text{(for the c-SYK model)}\,, \tag{C.16}$$

a fact that is fully confirmed by our numerical calculations. In Fig. C.1, we show the same quantities for the b-SYK model [panels (a)-(c)] and for the parallel model [panels (b)-(d)]. It is evident that, in both cases, all of the above mentioned time-averaged variances, as well as the optimal charging power, grow linearly in N,

$$\langle\!\langle P^{(N)}(\bar\tau) \rangle\!\rangle \sim N \quad \text{(for the b-SYK \& parallel models)}\,. \tag{C.17}$$

This rules out the possibility to have a genuine quantum speed-up in the charging process, by using the b-SYK and parallel-charging Hamiltonians.

C.5 Comparison between the c-SYK, b-SYK and the parallel-charging models using renormalized Hamiltonians

The charging performances of the various quantum batteries (QBs) can be tested by analyzing the scaling of the optimal power $P^{(N)}(\bar\tau)$ with the number N of cells [see Eq. (7.2) in Chap. 7].

Comparisons between the different models need to be made with great care. We note that the time-evolution operator is $\hat{U}(t) \equiv \exp(-i\hat{\mathcal{H}}_1 t)$. The charging Hamiltonian $\hat{\mathcal{H}}_1$ contains an energy scale, i.e. J ($\bar{J}$) for the c-SYK (b-SYK) model and K for the parallel-charging model. Here it is important to (i) rule out trivial power enhancements determined by an increase in the energy scale, i.e. obtained by multiplying the energy couplings by a factor $\alpha > 1$, and (ii) compare the three models in a fair manner—"fair" in the sense that, trivially, a parallel charging protocol with $K \geq J, \bar{J}$, for example, may outperform c-SYK and b-SYK charging protocols, and we want to avoid that.

To rule out these spurious effects, we consider the rescaled charging Hamiltonians [22, 23],

$$\hat{\mathscr{H}}_1 \equiv \frac{\hat{\mathcal{H}}_1}{\|\hat{\mathcal{H}}_1\|} , \tag{C.18}$$

where $\|\hat{\mathcal{O}}\| = \mu_{\hat{\mathcal{O}}}$ defines the norm of the operator $\hat{\mathcal{O}}$, $\mu_{\hat{\mathcal{O}}}$ being its highest singular value. For the sake of convenience and without loss of generality, we also set to zero the ground-state energy ϵ_0 of all Hamiltonian operators $\hat{\mathcal{H}}$, by adding a suitable constant. The charging Hamiltonian (C.18) allows a fair comparison between different QB models. In Fig. C.2, we report the optimal charging power $\langle\langle P^{(N)}(\bar{\tau})\rangle\rangle$ as a function of N, calculated for the c-SYK, b-SYK, and parallel rescaled charging Hamiltonians. For the case of the c-SYK and b-SYK models, data have been obtained after averaging over many disorder realizations. Results in this figure are independent of the microscopic energy scale appearing in $\hat{\mathcal{H}}_1$.

We see that the c-SYK is the only model for which $\langle\langle P^{(N)}(\bar{\tau})\rangle\rangle$ clearly increases with N, thereby presenting a qualitative advantage over the b-SYK and parallel-charging QBs. Concerning the b-SYK QB, its poor performance with respect to its fermionic cousin, the c-SYK QB, indicates that random pair hopping, which both models share, is not enough to guarantee a quantum advantage. The non-local JW strings for fermions are crucial, as they maximize entanglement production during the time evolution and therefore correlations between the N quantum cells. Note that there is no contradiction between the scaling of the optimal charging power shown in Fig. C.2 for the c-SYK charging protocol and the $\sim N^{3/2}$ scaling seen in Fig. 7.3 (b) in Chap. 7. The point is that, in the former, the rescaled Hamiltonian (C.18) was used. We have checked that the ratio between the two optimal charging powers yields the correct bandwidth of the c-SYK model, which scales linearly with N.

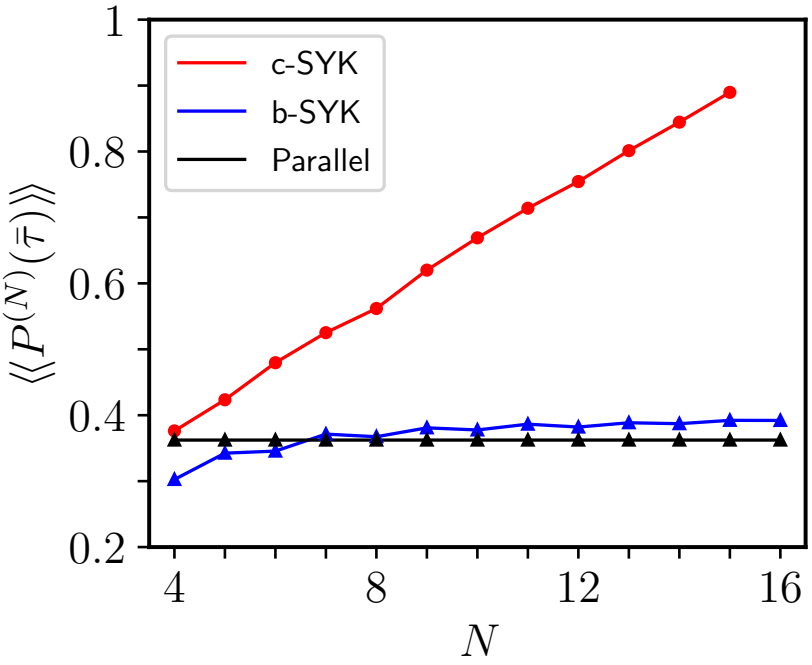

Figure C.2: (Color online) The dependence of the averaged optimal charging power $\langle\langle P^{(N)}(\bar{\tau})\rangle\rangle$ on the number N of quantum cells, using the rescaled Hamiltonian (C.18). The averaged optimal charging power shown in this plot is thus measured in units of ω_0. In red, we show the optimal power calculated for the c-SYK model with PHS. In blue (black) we show the same quantity for the b-SYK (parallel) model.

C.6 Asymptotic dynamics of the SYK model and random states

The SYK model is known to exhibit peculiar properties such as non-integrability, the absence of any local conserved quantity, and quantum chaos [164, 168]. Such properties imply that any time-evolved state at long times can be locally approximated by a suitable thermal state. We therefore expect that in the c-SYK QB charging protocol, after an initial transient time, the population $p_k(\tau)$ of the energy levels of the Hamiltonian $\hat{\mathcal{H}}_0$ becomes independent of τ. More precisely, we expect it to be well approximated by that of a random state in the 2^N-dimensional Hilbert space. In fact, such time independence of p_k for the c-SYK model is clearly visible in Fig. 7.2(a) of Chap. 7 already for $\tau \gtrsim 1$ (in units of $1/J$). Panel (b) of the same figure suggests that a similar situation may also occur for the b-SYK model as well, but at comparatively longer times.

This is quantitatively analyzed in Fig. C.3, where we report the same data of Fig. 2(a), once the time is fixed to $\tau = 4$, in units of $1/J$ (blue triangles). One can immediately recognize that such distribution of energy levels agrees nearly perfectly with the one corresponding to a completely mixed state, $\rho^{(\mathrm{r})} = \mathbb{I}/2^N$ (red squares), The latter is simply given by a binomial distribution

$$p_k^{(\mathrm{r})} = \frac{1}{2^N}\binom{N}{k} . \tag{C.19}$$

A very similar result can be obtained if a random pure state, $|\psi^{(\mathrm{r})}\rangle = \sum_n c_n |n\rangle$, is taken, c_n being complex numbers with randomly distributed amplitude and variance and satisfying

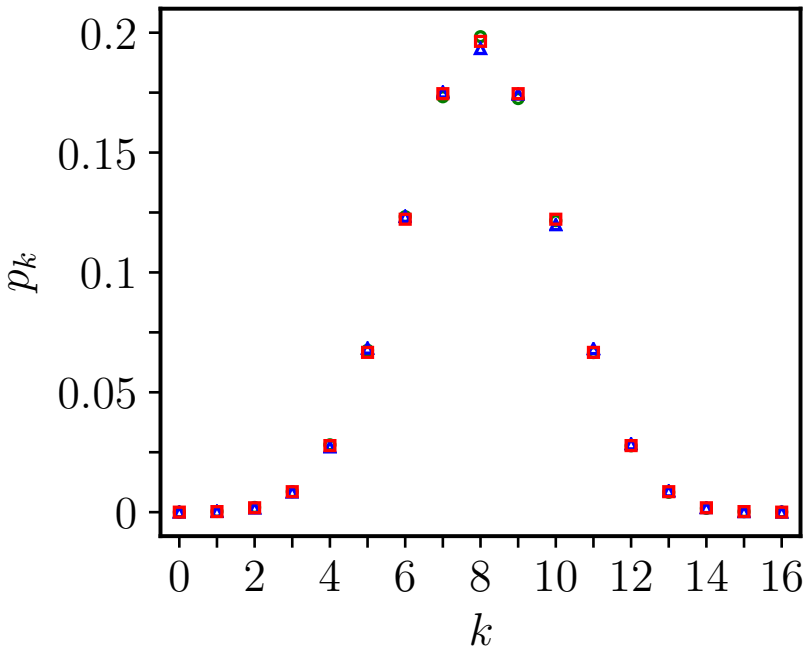

FIGURE C.3: (Color online) The energy-level population (blue triangles) p_k as a function of k, for the c-SYK model, evaluated numerically at $\tau = 4$ (in units of $1/J$). These numerical results are compared against the analytical result in Eq. (C.19) (red squares) and the prediction based on a random state (green circles). The two latter outcomes (red and green symbols) turn out to be indistinguishable from the numerically obtained data (blue symbols).

$\sum_n |c_n|^2 = 1$ (green circles).

This reasoning hints at a fast thermalization of the c-SYK model to an infinite temperature state.

C.7 Charging power of a Dicke battery

Unlike for the c-SYK battery, the power of a Dicke battery [24] does not exhibit a super-linear scaling, provided consistency with the thermodynamic limit is correctly enforced [63]. Dicke batteries are unitarily charged via a protocol that is slightly different from the one described in Eq. (7.2) of Chap. 7. In fact, both the charging system A and the battery B are quantum mechanically described by the time-dependent Hamiltonian

$$\hat{\mathcal{H}}(t) = \hat{\mathcal{H}}_{\rm A} + \hat{\mathcal{H}}_{\rm B} + \lambda(t)\hat{\mathcal{H}}_{\rm int} \ . \tag{C.20}$$

where $\hat{\mathcal{H}}_{\rm A}$ ($\hat{\mathcal{H}}_{\rm B}$) is the free Hamiltonian acting on the system A (B), $\lambda(t)$ is a classical control parameter, which is assumed to be equal to one if $t \in [0, \tau]$ and zero elsewhere, and $\hat{\mathcal{H}}_{\rm int}$ is an interaction Hamiltonian which couples the charging system and the battery, thus enabling the charging process to occur. A Dicke battery is made by N qubits (the battery cells) charged

by a cavity mode. The Hamiltonian terms in Eq. (C.20) are given by

$$\hat{\mathcal{H}}_{\mathrm{A}} = \omega_0 \hat{a}^\dagger \hat{a} \ , \tag{C.21}$$

$$\hat{\mathcal{H}}_{\mathrm{B}} = \frac{\omega_0}{2}\Big(\sum_{i=1}^{N} \hat{\sigma}_i^z + \frac{N}{2}\Big) \ , \tag{C.22}$$

$$\hat{\mathcal{H}}_{\mathrm{int}} = \frac{g}{\sqrt{N}}\big(\hat{a}^\dagger + \hat{a}\big)\sum_{i=1}^{N} \hat{\sigma}_i^x \ , \tag{C.23}$$

where $\hat{a}$ ($\hat{a}^\dagger$) is a bosonic annihilation (creation) operator, ω_0 is the characteristic frequency of both subsystems, and g the coupling strength. The prefactor $1/\sqrt{N}$ ensures the thermodynamic consistency of the model [63]. As a matter of fact, the interaction Hamiltonian $\hat{\mathcal{H}}_{\mathrm{int}}$ can be derived from a dipole light-matter interaction of the form $\sum_{i=1}^{N} \hat{\boldsymbol{d}}_i \cdot \hat{\boldsymbol{E}}_i$, where $\hat{\boldsymbol{d}}_i$ is the dipole operator acting on the i-th cell and $\hat{\boldsymbol{E}}_i$ is the cavity electric field evaluated at the position i. While each dipole operator $\hat{\boldsymbol{d}}_i$ does not carry any scaling with N, the electric field inside a cavity with volume V scales like $1/\sqrt{V}$. In a cavity system, the correct thermodynamic limit consists in considering $N \to \infty$, $V \to \infty$, with $N/V \to$ const. This means that $V \sim N$. Thus $1/\sqrt{N}$ is the correct prefactor to enforce a well-defined thermodynamic limit.

At time $t = 0$, the charger is prepared in a N-photon Fock state, while the qubits are prepared in their ground state, namely

$$|\psi(0)\rangle = |N\rangle_{\mathrm{A}} \otimes |0\rangle_{\mathrm{B}} \ . \tag{C.24}$$

The energy injected in the N cells of the Dicke battery and the corresponding average power are defined as

$$E^{(N)}(\tau) \equiv \mathrm{tr}\big[\hat{\mathcal{H}}_{\mathrm{B}}\, \rho_{\mathrm{B}}(\tau)\big] \ , \tag{C.25}$$

$$P^{(N)}(\tau) \equiv \frac{E^{(N)}(\tau)}{\tau} \ . \tag{C.26}$$

The optimal charging time $\bar{\tau}$ is defined as in Eq. (7.3) in Chap. 7, $P^{(N)}(\bar{\tau}) = \max_{\tau>0} P^{(N)}(\tau)$. In Fig. C.4, we explicitly show the optimal charging power $P^{(N)}(\bar{\tau})$, normalized by N times the optimal charging power of a single cell $P^{(1)}(\bar{\tau})$. This ratio tends to saturate to a constant for N large enough, meaning that the power of a Dicke battery does not display a super-linear scaling.

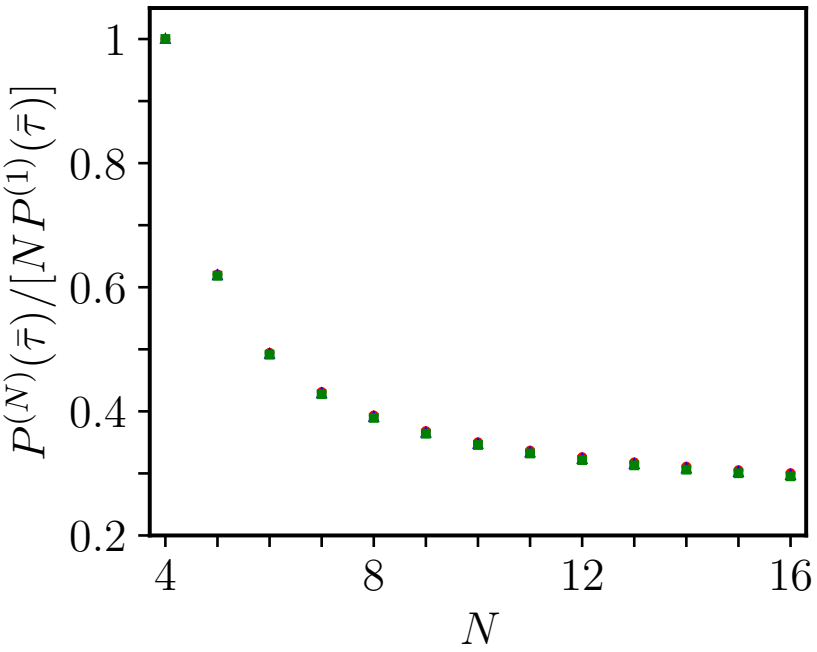

FIGURE C.4: (Color online) The optimal charging power $P^{(N)}(\bar{\tau})$, in units of $NP^{(1)}(\bar{\tau})$, as a function of N. Different symbols and colors refer to various values of the coupling strengh: $g/\omega_0 = 0.05$ (red circles), $g/\omega_0 = 0.5$ (blue triangles), $g/\omega_0 = 2$ (green squares).

D

Appendix: Cavity QED of Strongly Correlated Electron Systems: A No-go Theorem for Photon Condensation

D.1 Disentangling light and matter

In this Section we show that, in the thermodynamic $N \to \infty$ limit, it is permissible to assume a factorized ground state of the form

$$|\Psi\rangle = |\psi\rangle\,|\Phi\rangle \ . \tag{D.1}$$

We begin by defining the electron-photon Hamiltonian

$$\hat{\mathcal{H}}_{\rm el-ph} = \sum_{i=1}^{N} \frac{e}{m_i c}\hat{\boldsymbol{p}}_i \cdot \boldsymbol{A}_0(\hat{a}+\hat{a}^\dagger) + \Delta(\hat{a}+\hat{a}^\dagger)^2 \ , \tag{D.2}$$

where Δ has been defined in the main text. The electron Hamiltonian $\hat{\mathcal{H}}$ and the photon Hamiltonian $\hat{\mathcal{H}}_{\rm ph}$ have been defined in the main text. Each of the Hamiltonians $\hat{\mathcal{H}}$, $\hat{\mathcal{H}}_{\rm ph}$, and $\hat{\mathcal{H}}_{\rm el-ph}$ scales *extensively* in N. While this is obvious for $\hat{\mathcal{H}}$, we note that also $\hat{\mathcal{H}}_{\rm ph}$ and $\hat{\mathcal{H}}_{\rm el-ph}$ scale with N since $\boldsymbol{A}_0 \propto 1/\sqrt{N}$ and $\hat{a}, \hat{a}^\dagger \propto \sqrt{N}$. Below, we therefore work with the operators $\hat{\mathcal{H}}/N$, $\hat{\mathcal{H}}_{\rm ph}/N$, and $\hat{\mathcal{H}}_{\rm el-ph}/N$ which are well defined in the $N \to \infty$ limit. For the sake of simplicity, we now assume that all electrons have the same mass, i.e. $m_i = m$,$\forall i = 1 \ldots N$.

In order to prove Eq. (D.1) we will prove that, in the limit $N \to \infty$

$$[\frac{\hat{\mathcal{H}}}{N}, \frac{\hat{\mathcal{H}}_{\rm el-ph}}{N}] \to 0 \tag{D.3}$$

and

$$[\frac{\hat{\mathcal{H}}_{\rm ph}}{N}, \frac{\hat{\mathcal{H}}_{\rm el-ph}}{N}] \to 0 \ . \tag{D.4}$$

Explicitly, the left-hand side of Eq. (D.3) reads as following:

$$[\frac{\hat{\mathcal{H}}}{N}, \frac{\hat{\mathcal{H}}_{\rm el-ph}}{N}] = [\sum_{i=1}^{N} V(\hat{\boldsymbol{r}}_i) + \frac{1}{2}\sum_{i\neq j} v(\hat{\boldsymbol{r}}_i - \hat{\boldsymbol{r}}_j), \sum_{j=1}^{N} \frac{e}{mc}\hat{\boldsymbol{p}}_j \cdot \boldsymbol{A}_0]\frac{(\hat{a}+\hat{a}^\dagger)}{N^2} \ . \tag{D.5}$$

Using that $[f(\hat{\boldsymbol{r}}_i), \hat{\boldsymbol{p}}_j] = \delta_{i,j} i\hbar \nabla_{\hat{\boldsymbol{r}}_i} f(\hat{\boldsymbol{r}}_i)$ and introducing the external force $\hat{\boldsymbol{F}}_i^{\rm ext} = -\nabla_{\hat{\boldsymbol{r}}_i} V(\hat{\boldsymbol{r}}_i)$ and the Coulomb force $\hat{\boldsymbol{F}}_{i,j}^{\rm C} = -\nabla_{\hat{\boldsymbol{r}}_i} v(\hat{\boldsymbol{r}}_i - \hat{\boldsymbol{r}}_j)/2$ we get:

$$[\frac{\hat{\mathcal{H}}}{N}, \frac{\hat{\mathcal{H}}_{\rm el-ph}}{N}] = -\frac{i\hbar e(\hat{a}+\hat{a}^\dagger)\boldsymbol{A}_0}{mcN^2} \cdot \sum_{i=1}^{N} \hat{\boldsymbol{F}}_i^{\rm ext} \ , \tag{D.6}$$

where $\hat{\boldsymbol{F}}_{i,j}^{\rm C}$ dropped out of the commutator since $\sum_{i,j} \hat{\boldsymbol{F}}_{i,j}^{\rm C} = 0$. Noticing that $(\hat{a}+\hat{a}^\dagger)\boldsymbol{A}_0$ is an *intensive* quantity, which does not scale with N, and that $\sum_{i=1}^{N} \hat{\boldsymbol{F}}_i^{\rm ext} \sim N$, we obtain that the commutator $[\hat{\mathcal{H}}/N, \hat{\mathcal{H}}_{\rm el-ph}/N]$ scales like $1/N$, and therefore vanishes in the thermodynamic limit.

Exploiting the commutator $[\hat{a}, \hat{a}^\dagger] = 1$, we can rewrite the left-hand side of Eq. (D.4) as:

$$[\frac{\hat{\mathcal{H}}_{\rm ph}}{N}, \frac{\hat{\mathcal{H}}_{\rm el-ph}}{N}] = \frac{\hbar\omega_{\rm c}}{N^2}\left\{\sum_{i=1}^{N} \frac{e}{mc}\hat{\boldsymbol{p}}_i \cdot \boldsymbol{A}_0(\hat{a}^\dagger - \hat{a}) + \Delta\big[(\hat{a}^\dagger + \hat{a})(\hat{a}^\dagger - \hat{a}) + (\hat{a}^\dagger - \hat{a})(\hat{a}^\dagger + \hat{a})\big]\right\} \ . \tag{D.7}$$

Again, this quantity scales like $1/N$, since $\sum_{i=1}^{N} \hat{\boldsymbol{p}}_i \sim N$ and $\Delta \sim 1$.

D.2 On the stiffness theorem

In this Section we prove that $\langle\psi_0|\hat{\boldsymbol{j}}_{\rm p}|\psi_0\rangle \cdot \boldsymbol{A}_0 = 0$. We used this property to evaluate the quantity $\langle\psi|\hat{\mathcal{H}}|\psi\rangle - \langle\psi_0|\hat{\mathcal{H}}|\psi_0\rangle$ up to order $\bar{\beta}^2$, via the stiffness theorem.

We introduce the total dipole operator $\hat{\boldsymbol{d}} = -e\sum_i \hat{\boldsymbol{r}}_i$ and note that, because of the fundamental commutator $[\hat{r}_{\ell\alpha}, \hat{p}_{k\beta}] = i\hbar\delta_{\ell,k}\delta_{\alpha,\beta}$, we have

$$-i\hbar e\hat{\boldsymbol{j}}_{\rm p} = [\hat{\boldsymbol{d}}, \hat{\mathcal{H}}] \tag{D.8}$$

and

$$[\hat{j}_{{\rm p}\alpha}, \hat{d}_\beta] = i\hbar\sum_{\ell} \frac{e}{m_\ell}\delta_{\alpha,\beta} \ . \tag{D.9}$$

Using Eq. (D.8) we immediately find for a large but finite system

$$\langle\psi_0|\hat{\boldsymbol{j}}_{\rm p}|\psi_0\rangle \cdot \boldsymbol{A}_0 = \frac{i}{\hbar e}\langle\psi_0|[\hat{\boldsymbol{d}}, \hat{\mathcal{H}}]|\psi_0\rangle \cdot \boldsymbol{A}_0 = \frac{i}{\hbar e}(E_0 - E_0)\langle\psi_0|\hat{\boldsymbol{d}}|\psi_0\rangle \cdot \boldsymbol{A}_0 = 0 \ . \tag{D.10}$$

D.3 On the TRK sum rule

In this Section we prove the TRK sum rule.

Eq. (D.8) implies that

$$\frac{e^2}{c^2}\sum_{n\neq 0} \frac{|\langle\psi_n|\hat{\boldsymbol{j}}_{\rm p} \cdot \boldsymbol{A}_0|\psi_0\rangle|^2}{E_n - E_0} = \frac{1}{\hbar^2 c^2}\sum_{n\neq 0}(E_n - E_0)|\langle\psi_n|\hat{\boldsymbol{d}} \cdot \boldsymbol{A}_0|\psi_0\rangle|^2 \ . \tag{D.11}$$

Eq. (D.9) implies that we can rewrite Δ as:

$$\Delta = \sum_{\ell=1}^{N} \frac{e^2 A_0^2}{2m_\ell c^2} = \frac{ie}{2\hbar c^2} \langle \psi_0 | [\hat{\boldsymbol{d}} \cdot \boldsymbol{A}_0, \hat{\boldsymbol{j}}_{\rm p} \cdot \boldsymbol{A}_0] | \psi_0 \rangle \ . \tag{D.12}$$

We then manipulate the right-hand side of Eq. (D.12) by inserting exact identities [85, 86] $\mathbb{I} = \sum_n |\psi_n\rangle\langle\psi_n|$ in the appropriate positions,

$$\begin{aligned} & \langle \psi_0 | [\hat{\boldsymbol{d}} \cdot \boldsymbol{A}_0, \hat{\boldsymbol{j}}_{\rm p} \cdot \boldsymbol{A}_0] | \psi_0 \rangle = \sum_n \langle \psi_0 | \hat{\boldsymbol{d}} \cdot \boldsymbol{A}_0 | \psi_n \rangle \langle \psi_n | \hat{\boldsymbol{j}}_{\rm p} \cdot \boldsymbol{A}_0 | \psi_0 \rangle - \sum_n \langle \psi_0 | \hat{\boldsymbol{j}}_{\rm p} \cdot \boldsymbol{A}_0 | \psi_n \rangle \langle \psi_n | \hat{\boldsymbol{d}} \cdot \boldsymbol{A}_0 | \psi_0 \rangle \\ = \ & \frac{i}{\hbar e} \sum_n \langle \psi_0 | \hat{\boldsymbol{d}} \cdot \boldsymbol{A}_0 | \psi_n \rangle \langle \psi_n | [\hat{\boldsymbol{d}} \cdot \boldsymbol{A}_0, \hat{\mathcal{H}}] | \psi_0 \rangle - \frac{i}{\hbar e} \sum_n \langle \psi_0 | [\hat{\boldsymbol{d}} \cdot \boldsymbol{A}_0, \hat{\mathcal{H}}] | \psi_n \rangle \langle \psi_n | \hat{\boldsymbol{d}} \cdot \boldsymbol{A}_0 | \psi_0 \rangle \\ = \ & -\frac{2i}{\hbar e} \sum_n (E_n - E_0) |\langle \psi_n | \hat{\boldsymbol{d}} \cdot \boldsymbol{A}_0 | \psi_0 \rangle|^2 = -\frac{2i}{\hbar e} \sum_{n \neq 0} (E_n - E_0) |\langle \psi_n | \hat{\boldsymbol{d}} \cdot \boldsymbol{A}_0 | \psi_0 \rangle|^2 \ . \end{aligned} \tag{D.13}$$

Using the previous result inside Eq. (D.12), we find

$$\Delta = \frac{1}{\hbar^2 c^2} \sum_{n \neq 0} (E_n - E_0) |\langle \psi_n | \hat{\boldsymbol{d}} \cdot \boldsymbol{A}_0 | \psi_0 \rangle|^2 \ . \tag{D.14}$$

Comparing Eq. (D.14) with Eq. (D.11) we reach the desired result.

We now present a more physical, alternative proof. We first remind the reader that the physical current operator corresponding to the Hamiltonian $\hat{\mathcal{H}}_{\boldsymbol{A}_0}$ is

$$\hat{\boldsymbol{J}}_{\rm phys} = \frac{c}{e} \frac{\delta \hat{\mathcal{H}}_{\boldsymbol{A}_0}}{\delta \boldsymbol{A}_0} = \hat{\boldsymbol{j}}_{\rm p} + \sum_{i=1}^{N} \frac{e}{m_i c} \boldsymbol{A}_0 \ . \tag{D.15}$$

We now observe that the electron system cannot respond to $\boldsymbol{A}_0$, since the latter is uniform and time-independent. (A current cannot flow along $\boldsymbol{u}$ in response to $\boldsymbol{A}_0$.) This property, i.e. gauge invariance, implies that the physical current-current response function in response to $\boldsymbol{A}_0$ must vanish [85, 86], i.e.

$$0 = -\frac{2}{L^d} \sum_{n \neq 0} \frac{|\langle \psi_n | \hat{\boldsymbol{j}}_{\rm p} \cdot \boldsymbol{u} | \psi_0 \rangle|^2}{E_n - E_0} + \frac{1}{L^d} \sum_{i=1}^{N} \frac{1}{m_i} \ , \tag{D.16}$$

where the first (second) term on the right-hand side is the paramagnetic (diamagnetic) contribution and L^d is the electron system volume. Eq. (D.16) can be written as

$$2 \sum_{n \neq 0} \frac{|\langle \psi_n | \hat{\boldsymbol{j}}_{\rm p} \cdot \boldsymbol{u} | \psi_0 \rangle|^2}{E_n - E_0} = \sum_{i=1}^{N} \frac{1}{m_i} \ , \tag{D.17}$$

which is easily seen to be equivalent to Eq. (8). In other words, Eq. (8) simply expresses the fact that paramagnetic and diamagnetic contributions to the physical current-current response function cancel out in the uniform and static limit [85, 86].

D.4 Coupling the EFK model to cavity photons

Consider spinless electrons hopping in a one-dimensional inversion-symmetric crystal with N sites, one atom per site, and two atomic orbitals of opposite parity (s and p), in a tight-binding scheme. The second-quantized single-particle Hamiltonian in the site representation reads as following:

$$\begin{aligned}\hat{\mathcal{H}}_0 &= \sum_{j=1}^{N}\sum_{\alpha=\mathrm{s,p}} E_\alpha \hat{c}^\dagger_{j,\alpha}\hat{c}_{j,\alpha} - t_\mathrm{s}\sum_{j=1}^{N}(\hat{c}^\dagger_{j+1,\mathrm{s}}\hat{c}_{j,\mathrm{s}} + \hat{c}^\dagger_{j,\mathrm{s}}\hat{c}_{j+1,\mathrm{s}}) + t_\mathrm{p}\sum_{j=1}^{N}(\hat{c}^\dagger_{j+1,\mathrm{p}}\hat{c}_{j,\mathrm{p}} + \hat{c}^\dagger_{j,\mathrm{p}}\hat{c}_{j+1,\mathrm{p}}) \\ &- \tilde{t}\sum_{j=1}^{N}(\hat{c}^\dagger_{j+1,\mathrm{s}}\hat{c}_{j,\mathrm{p}} + \hat{c}^\dagger_{j,\mathrm{p}}\hat{c}_{j+1,\mathrm{s}}) + \tilde{t}\sum_{j=1}^{N}(\hat{c}^\dagger_{j,\mathrm{s}}\hat{c}_{j+1,\mathrm{p}} + \hat{c}^\dagger_{j+1,\mathrm{p}}\hat{c}_{j,\mathrm{s}}) \equiv \sum_{j=1}^{N}\sum_{\alpha=\mathrm{s,p}} E_\alpha \hat{c}^\dagger_{j,\alpha}\hat{c}_{j,\alpha} + \hat{\mathcal{T}}\ ,\end{aligned} \tag{D.18}$$

where t_s, t_p, $\tilde{t} \in \mathbb{R}$ are for the moment completely arbitrary, we assumed periodic boundary conditions ($\hat{c}_{N+1,\alpha} = \hat{c}_{1,\alpha}$), and defined the kinetic operator $\hat{\mathcal{T}} = -t_\mathrm{s}\sum_{j=1}^{N}(\hat{c}^\dagger_{j+1,\mathrm{s}}\hat{c}_{j,\mathrm{s}} + \hat{c}^\dagger_{j,\mathrm{s}}\hat{c}_{j+1,\mathrm{s}}) + t_\mathrm{p}\sum_{j=1}^{N}(\hat{c}^\dagger_{j+1,\mathrm{p}}\hat{c}_{j,\mathrm{p}} + \hat{c}^\dagger_{j,\mathrm{p}}\hat{c}_{j+1,\mathrm{p}}) - \tilde{t}\sum_{j=1}^{N}(\hat{c}^\dagger_{j+1,\mathrm{s}}\hat{c}_{j,\mathrm{p}} + \hat{c}^\dagger_{j,\mathrm{p}}\hat{c}_{j+1,\mathrm{s}}) + \tilde{t}\sum_{j=1}^{N}(\hat{c}^\dagger_{j,\mathrm{s}}\hat{c}_{j+1,\mathrm{p}} + \hat{c}^\dagger_{j+1,\mathrm{p}}\hat{c}_{j,\mathrm{s}})$. We now add repulsive on-site electron-electron interactions in the site representation:

$$\hat{\mathcal{H}}_\mathrm{ee} = U\sum_{j=1}^{N}\hat{n}_{j,s}\hat{n}_{j,p}\ , \tag{D.19}$$

where $U > 0$ and $\hat{n}_{j,\alpha} \equiv \hat{c}^\dagger_{j,\alpha}\hat{c}_{j,\alpha}$ is the orbitally-resolved local density operator.

The full Hamiltonian of our 1D EFK model in the absence of cavity photons is

$$\hat{\mathcal{H}} = \hat{\mathcal{H}}_0 + \hat{\mathcal{H}}_\mathrm{ee}\ . \tag{D.20}$$

We now couple the matter Hamiltonian $\hat{\mathcal{H}}$ in Eq. (D.20) to light by employing a uniform linearly-polarized vector potential $\boldsymbol{A}(t) = A(t)\hat{\boldsymbol{u}}$ where $\boldsymbol{u} = \pm\hat{\boldsymbol{x}}$ in the ring geometry above with periodic boundary conditions. This is accomplished, as usual [203–206], by means of the Peierls factor:

$$\begin{aligned}\hat{\mathcal{H}}_{A(t)} &= \sum_{j=1}^{N}\sum_{\alpha=\mathrm{s,p}} E_\alpha \hat{c}^\dagger_{j,\alpha}\hat{c}_{j,\alpha} - t_\mathrm{s}\sum_{j=1}^{N}\left(e^{-ieaA(t)/(\hbar c)}\hat{c}^\dagger_{j+1,\mathrm{s}}\hat{c}_{j,\mathrm{s}} + e^{+ieaA(t)/(\hbar c)}\hat{c}^\dagger_{j,\mathrm{s}}\hat{c}_{j+1,\mathrm{s}}\right) \\ &+ t_\mathrm{p}\sum_{j=1}^{N}\left(e^{-ieaA(t)/(\hbar c)}\hat{c}^\dagger_{j+1,\mathrm{p}}\hat{c}_{j,\mathrm{p}} + e^{+ieaA(t)/(\hbar c)}\hat{c}^\dagger_{j,\mathrm{p}}\hat{c}_{j+1,\mathrm{p}}\right) \\ &- \tilde{t}\sum_{j=1}^{N}\left(e^{-ieaA(t)/(\hbar c)}\hat{c}^\dagger_{j+1,\mathrm{s}}\hat{c}_{j,\mathrm{p}} + e^{+ieaA(t)/(\hbar c)}\hat{c}^\dagger_{j,\mathrm{p}}\hat{c}_{j+1,\mathrm{s}}\right) \\ &+ \tilde{t}\sum_{j=1}^{N}\left(e^{+ieaA(t)/(\hbar c)}\hat{c}^\dagger_{j,\mathrm{s}}\hat{c}_{j+1,\mathrm{p}} + e^{-ieaA(t)/(\hbar c)}\hat{c}^\dagger_{j+1,\mathrm{p}}\hat{c}_{j,\mathrm{s}}\right) \\ &+ \hat{\mathcal{H}}_\mathrm{ee}\ ,\end{aligned} \tag{D.21}$$

where a is the lattice constant.

We expand $\hat{\mathcal{H}}_{A(t)}$ in powers of $A(t)$ for small $A(t)$, retaining terms of $\mathcal{O}(A^2(t))$. We find:

$$\hat{\mathcal{H}}_{A(t)} = \hat{\mathcal{H}}_0 + \hat{\mathcal{H}}_\mathrm{ee} + \frac{e}{c}A(t)\hat{j}_\mathrm{p} - \frac{1}{2}\frac{e^2a^2A^2(t)}{\hbar^2c^2}\hat{\mathcal{T}}\ , \tag{D.22}$$

where

$$\hat{j}_{\rm p} \equiv \frac{c}{e}\left.\frac{\delta\hat{\mathcal{H}}_{A(t)}}{\delta A(t)}\right|_{A(t)=0} = \frac{it_{\rm s}a}{\hbar}\sum_{j=1}^{N}(\hat{c}^{\dagger}_{j+1,{\rm s}}\hat{c}_{j,{\rm s}} - \hat{c}^{\dagger}_{j,{\rm s}}\hat{c}_{j+1,{\rm s}}) - \frac{it_{\rm p}a}{\hbar}\sum_{j=1}^{N}(\hat{c}^{\dagger}_{j+1,{\rm p}}\hat{c}_{j,{\rm p}} - \hat{c}^{\dagger}_{j,{\rm p}}\hat{c}_{j+1,{\rm p}}) + \frac{i\tilde{t}a}{\hbar}\sum_{j=1}^{N}(\hat{c}^{\dagger}_{j+1,{\rm s}}\hat{c}_{j,{\rm p}} - \hat{c}^{\dagger}_{j,{\rm p}}\hat{c}_{j+1,{\rm s}}) + \frac{i\tilde{t}a}{\hbar}\sum_{j=1}^{N}(\hat{c}^{\dagger}_{j,{\rm s}}\hat{c}_{j+1,{\rm p}} - \hat{c}^{\dagger}_{j+1,{\rm p}}\hat{c}_{j,{\rm s}}) \ , \tag{D.23}$$

is the paramagnetic (number) current operator and $\hat{\mathcal{T}}$ is the kinetic operator in Eq. (D.18). The physical (number) current operator is therefore

$$\hat{J}_{\rm phys} \equiv \frac{c}{e}\frac{\delta\hat{\mathcal{H}}_{A(t)}}{\delta A(t)} = \hat{j}_{\rm p} - \frac{e}{c}A(t)\frac{a^2}{\hbar^2}\hat{\mathcal{T}} \ , \tag{D.24}$$

with contains paramagnetic and diamagnetic terms.

We finally quantize the e.m. field by writing $A(t) \to A_0(\hat{a}+\hat{a}^{\dagger})$, where A_0 has been defined in the main text, and we give dynamics to the field by means of the photon Hamiltonian $\hat{\mathcal{H}}_{\rm ph} = \hbar\omega_{\rm c}\hat{a}^{\dagger}\hat{a}$. The full Hamiltonian, which includes light-matter interactions, is therefore given by:

$$\hat{\mathcal{H}}_{\boldsymbol{A}_0} = \hat{\mathcal{H}}_0 + \hat{\mathcal{H}}_{\rm ee} + \hat{\mathcal{H}}_{\rm ph} + \frac{e}{c}A_0\hat{j}_{\rm p}(\hat{a}+\hat{a}^{\dagger}) - \frac{1}{2}\frac{e^2a^2}{\hbar^2c^2}A_0^2\hat{\mathcal{T}}(\hat{a}+\hat{a}^{\dagger})^2 \ . \tag{D.25}$$

The fourth and fifth terms in the right-hand side of Eq. (D.25) are called paramagnetic and diamagnet contributions.

Eq. (D.25) is written in the site representation. In the main text, however, the quantities $\hat{\mathcal{H}}_0$, $\hat{j}_{\rm p}$, and $\hat{\mathcal{T}}$ have been given in momentum space. The link between momentum-space and site representations is offered by

$$\hat{c}^{\dagger}_{j,\alpha} = \frac{1}{\sqrt{N}}\sum_{k\in{\rm BZ}}\hat{c}^{\dagger}_{k,\alpha}e^{-ikja} \ , \tag{D.26}$$

where the sum is carried over the 1D Brillouin zone (BZ). In the thermodynamic $N\to\infty$ limit we can replace

$$\frac{1}{N}\sum_{k\in{\rm BZ}} \to a\int_{-\pi/a}^{+\pi/a}\frac{dk}{2\pi} \ . \tag{D.27}$$

We find

$$\hat{\mathcal{H}}_0 = \sum_{k\in{\rm BZ}}\begin{pmatrix}\hat{c}^{\dagger}_{k,{\rm s}} & \hat{c}^{\dagger}_{k,{\rm p}}\end{pmatrix}\begin{pmatrix}E_{\rm s}-2t_{\rm s}\cos(ka) & 2i\tilde{t}\sin(ka)\\ -2i\tilde{t}\sin(ka) & E_{\rm p}+2t_{\rm p}\cos(ka)\end{pmatrix}\begin{pmatrix}\hat{c}_{k,{\rm s}}\\ \hat{c}_{k,{\rm p}}\end{pmatrix} \equiv \sum_{k\in{\rm BZ}}\sum_{\alpha,\beta={\rm s,p}}\hat{c}^{\dagger}_{k,\alpha}H_{\alpha\beta}(k)\hat{c}_{k,\beta} \ , \tag{D.28}$$

$$\hat{j}_{\rm p} = \frac{2a}{\hbar}\sum_{k\in{\rm BZ}}\begin{pmatrix}\hat{c}^{\dagger}_{k,{\rm s}} & \hat{c}^{\dagger}_{k,{\rm p}}\end{pmatrix}\begin{pmatrix}t_{\rm s}\sin(ka) & i\tilde{t}\cos(ka)\\ -i\tilde{t}\cos(ka) & -t_{\rm p}\sin(ka)\end{pmatrix}\begin{pmatrix}\hat{c}_{k,{\rm s}}\\ \hat{c}_{k,{\rm p}}\end{pmatrix} \equiv \sum_{k\in{\rm BZ}}\sum_{\alpha,\beta={\rm s,p}}\hat{c}^{\dagger}_{k,\alpha}j_{\alpha\beta}(k)\hat{c}_{k,\beta} \ , \tag{D.29}$$

and

$$\begin{aligned}\hat{\mathcal{T}} &= 2\sum_{k\in\mathrm{BZ}}\begin{pmatrix}\hat{c}^\dagger_{k,\mathrm{s}} & \hat{c}^\dagger_{k,\mathrm{p}}\end{pmatrix}\begin{pmatrix}-t_\mathrm{s}\cos(ka) & i\tilde{t}\sin(ka)\\ -i\tilde{t}\sin(ka) & +t_\mathrm{p}\cos(ka)\end{pmatrix}\begin{pmatrix}\hat{c}_{k,\mathrm{s}}\\ \hat{c}_{k,\mathrm{p}}\end{pmatrix}\\ &\equiv \sum_{k\in\mathrm{BZ}}\sum_{\alpha,\beta=\mathrm{s,p}}\hat{c}^\dagger_{k,\alpha}\mathcal{T}_{\alpha\beta}(k)\hat{c}_{k,\beta}\ . \end{aligned} \tag{D.30}$$

It is easy to check that

$$j_{\alpha\beta}(k) = \frac{1}{\hbar}\frac{\partial H_{\alpha\beta}(k)}{\partial k} \tag{D.31}$$

and

$$\mathcal{T}_{\alpha\beta}(k) = -\frac{1}{a^2}\frac{\partial^2 H_{\alpha\beta}(k)}{\partial k^2}\ . \tag{D.32}$$

Equations (D.31)-(D.32) heavily constrain the paramagnetic and diamagnetic terms of the full Hamiltonian $\hat{\mathcal{H}}_{\boldsymbol{A}_0}$, which rule light-matter interactions. In other words, one cannot simply couple light to matter with arbitrary operators $\hat{j}_\mathrm{p}$ and $\hat{\mathcal{T}}$. Instead the form of these operators is specified by $\hat{\mathcal{H}}_0$ and must be constructed with perfect consistency.

D.5 Hartree-Fock treatment of electron-electron interactions

We treat the electron-electron interaction term in Eq. (11) of the main text—or, equivalently, Eq. (D.19)—within Hartree-Fock (HF) mean-field theory (see, e.g., Chapter 2 of Ref. [86]). We replace $\hat{\mathcal{H}}_\mathrm{ee}$ with

$$\begin{aligned}\hat{\mathcal{H}}^{(\mathrm{HF})}_\mathrm{ee} \equiv U\sum_{j=1}^{N}&[\hat{c}^\dagger_{j,\mathrm{s}}\hat{c}_{j,\mathrm{s}}\langle\hat{c}^\dagger_{j,\mathrm{p}}\hat{c}_{j,\mathrm{p}}\rangle + \hat{c}^\dagger_{j,\mathrm{p}}\hat{c}_{j,\mathrm{p}}\langle\hat{c}^\dagger_{j,\mathrm{s}}\hat{c}_{j,\mathrm{s}}\rangle - \hat{c}^\dagger_{j,\mathrm{s}}\hat{c}_{j,\mathrm{p}}\langle\hat{c}^\dagger_{j,\mathrm{p}}\hat{c}_{j,\mathrm{s}}\rangle - \hat{c}^\dagger_{j,\mathrm{p}}\hat{c}_{j,\mathrm{s}}\langle\hat{c}^\dagger_{j,\mathrm{s}}\hat{c}_{j,\mathrm{p}}\rangle]\\ - U\sum_{i}&[\langle\hat{c}^\dagger_{j,\mathrm{s}}\hat{c}_{j,\mathrm{s}}\rangle\langle\hat{c}^\dagger_{j,\mathrm{p}}\hat{c}_{j,\mathrm{p}}\rangle - \langle\hat{c}^\dagger_{j,\mathrm{s}}\hat{c}_{j,\mathrm{p}}\rangle\langle\hat{c}^\dagger_{j,\mathrm{p}}\hat{c}_{j,\mathrm{s}}\rangle]\ . \end{aligned} \tag{D.33}$$

Each of the mean fields above can be written as

$$\langle\hat{c}^\dagger_{j,\alpha}\hat{c}_{j,\beta}\rangle = \frac{1}{N}\sum_{k,k'\in\mathrm{BZ}} e^{-i(k-k')ja}\langle\hat{c}^\dagger_{k,\alpha}\hat{c}_{k',\beta}\rangle\ . \tag{D.34}$$

We assume that $\langle\hat{c}^\dagger_{j,\alpha}\hat{c}_{j,\beta}\rangle$ is independent of the site index j (translational invariance), i.e. we take $\langle\hat{c}^\dagger_{k,\alpha}\hat{c}_{k',\beta}\rangle = \delta_{k,k'}\langle\hat{c}^\dagger_{k,\alpha}\hat{c}_{k,\beta}\rangle$.

We are therefore naturally led to introduce the following quantities:

$$\mathcal{M} \equiv \langle\hat{c}^\dagger_{j,\mathrm{p}}\hat{c}_{j,\mathrm{p}}\rangle - \langle\hat{c}^\dagger_{j,\mathrm{s}}\hat{c}_{j,\mathrm{s}}\rangle = \frac{1}{N}\sum_{k\in\mathrm{BZ}}(\langle\hat{c}^\dagger_{k,\mathrm{p}}\hat{c}_{k,\mathrm{p}}\rangle - \langle\hat{c}^\dagger_{k,\mathrm{s}}\hat{c}_{k,\mathrm{s}}\rangle)\ , \tag{D.35}$$

$$\mathcal{I} \equiv \langle\hat{c}^\dagger_{j,\mathrm{p}}\hat{c}_{j,\mathrm{s}}\rangle = \frac{1}{N}\sum_{k\in\mathrm{BZ}}\langle\hat{c}^\dagger_{k,\mathrm{p}}\hat{c}_{k,\mathrm{s}}\rangle\ , \tag{D.36}$$

and

$$n_0 \equiv \langle\hat{c}^\dagger_{j,\mathrm{p}}\hat{c}_{j,\mathrm{p}}\rangle + \langle\hat{c}^\dagger_{j,\mathrm{s}}\hat{c}_{j,\mathrm{s}}\rangle = \frac{1}{N}\sum_{k\in\mathrm{BZ}}(\langle\hat{c}^\dagger_{k,\mathrm{p}}\hat{c}_{k,\mathrm{p}}\rangle + \langle\hat{c}^\dagger_{k,\mathrm{s}}\hat{c}_{k,\mathrm{s}}\rangle)\ . \tag{D.37}$$

Under the assumption of homogeneity, we can rewrite the HF interaction term (D.33) as

$$\hat{\mathcal{H}}_{\rm ee}^{(\rm HF)} = -U\sum_{k\in \rm BZ}\left[\frac{\mathcal{M}}{2}(\hat{c}^\dagger_{k,\rm p}\hat{c}_{k,\rm p} - \hat{c}^\dagger_{k,\rm s}\hat{c}_{k,\rm s}) + \mathcal{I}\hat{c}^\dagger_{k,\rm s}\hat{c}_{k,\rm p} + \mathcal{I}^*\hat{c}^\dagger_{k,\rm p}\hat{c}_{k,\rm s}\right] + U\sum_{k\in \rm BZ}\frac{n_0}{2}(\hat{c}^\dagger_{k,\rm p}\hat{c}_{k,\rm p} + \hat{c}^\dagger_{k,\rm s}\hat{c}_{k,\rm s}) + UN\left(\frac{\mathcal{M}^2 - n_0^2}{4} + |\mathcal{I}|^2\right) . \tag{D.38}$$

The term proportional to $n_0/2$ acts as a renormalization of the chemical potential μ in the grand-canonical Hamiltonian $\hat{\mathcal{K}} = \hat{\mathcal{H}}_{\boldsymbol{A}_0} - \mu\hat{\mathcal{N}}$, where $\hat{\mathcal{N}} = \sum_{k\in \rm BZ}\sum_{\alpha=\rm s,p}\hat{c}^\dagger_{k,\alpha}\hat{c}_{k,\alpha}$ is the total electron number operator. In this work we study only the phase diagram at half filling. We therefore have $n_0 = 1\ \forall j = 1\dots N$ in all phases and can discard such term. The last term in Eq. (D.38) instead must be retained (after discarding n_0) since it takes different values in different phases. (It is a trivial constant: it therefore only matters when one compares total energies of different phases.)

The HF mean-field Hamiltonian (D.38) can be written in a 2×2 fashion:

$$\hat{\mathcal{H}}_{\rm ee}^{(\rm HF)} = U\sum_{k\in \rm BZ}\begin{pmatrix}\hat{c}^\dagger_{k,\rm s} & \hat{c}^\dagger_{k,\rm p}\end{pmatrix}\begin{pmatrix}\mathcal{M}/2 & -\mathcal{I}\\ -\mathcal{I}^* & -\mathcal{M}/2\end{pmatrix}\begin{pmatrix}\hat{c}_{k,\rm s}\\ \hat{c}_{k,\rm p}\end{pmatrix} + UN\left(\frac{\mathcal{M}^2}{4} + |\mathcal{I}|^2\right) . \tag{D.39}$$

D.6 Details on the Bogoliubov transformation

In this Section we give all technical details relevant to the diagonalization of the problem posed by Eq. (9) in the main text, with $\hat{\mathcal{H}}_{\rm ee}$ replaced by its HF mean-field expression (D.39):

$$\hat{\mathcal{H}}_{\boldsymbol{A}_0}^{(\rm HF)} \equiv \hat{\mathcal{H}}_0 + \hat{\mathcal{H}}_{\rm ee}^{(\rm HF)} + \hat{\mathcal{H}}_{\rm ph} + \frac{g_0}{\sqrt{N}}\frac{\hbar}{a}\hat{j}_{\rm p}(\hat{a}+\hat{a}^\dagger) - \frac{g_0^2}{2N}\hat{\mathcal{T}}(\hat{a}+\hat{a}^\dagger)^2 . \tag{D.40}$$

We seek ground-state wave functions of the unentangled form $|\Psi\rangle = |\psi\rangle\,|\Phi\rangle$, where $|\psi\rangle$ is the wave function for the matter degrees of freedom and $|\Phi\rangle$ is the analog for the e.m. field.

In order to reduce the number of free parameters in the problem, we enforce particle-hole symmetry by setting $E_{\rm s} = -E_{\rm g}/2 = -E_{\rm p}$ and $t_{\rm s} = t_{\rm p} = t$.

An effective mean-field Hamiltonian for matter degrees of freedom can be obtained by taking the expectation value of $\hat{\mathcal{H}}_{\boldsymbol{A}_0}^{(\rm HF)}$ over the light state $|\Phi\rangle$, i.e.

$$\begin{aligned}\hat{\mathcal{H}}_{\rm eff-matter} \equiv \langle\Phi|\hat{\mathcal{H}}_{\boldsymbol{A}_0}^{(\rm HF)}|\Phi\rangle &= \sum_{k\in \rm BZ}\begin{pmatrix}\hat{c}^\dagger_{k,\rm s} & \hat{c}^\dagger_{k,\rm p}\end{pmatrix}\mathcal{H}(k)\begin{pmatrix}\hat{c}_{k,\rm s}\\ \hat{c}_{k,\rm p}\end{pmatrix} +\\ &+ \hbar\omega_{\rm c}\langle\Phi|a^\dagger a|\Phi\rangle + UN\left(\frac{\mathcal{M}^2}{4} + |\mathcal{I}|^2\right) .\end{aligned} \tag{D.41}$$

$\mathcal{H}(k)$ can be conveniently written in terms of ordinary 2×2 Pauli matrices $\{\sigma_i, i = 1,2,3\}$, i.e. $\mathcal{H}(k) = \sum_i h_i(k)\sigma_i$ with

$$h_1(k) = -U\mathrm{Re}(\mathcal{I}) , \tag{D.42}$$

$$h_2(k) = -2\tilde{t}\sin(ka)\left(1 - \frac{g_0^2}{2}\mathcal{A}_2\right) - 2\tilde{t}g_0\cos(ka)\mathcal{A}_1 + U\mathrm{Im}(\mathcal{I}) , \tag{D.43}$$

and

$$h_3(k) = -\frac{E_{\rm g}}{2} - 2t\cos(ka)\left(1 - \frac{g_0^2}{2}\mathcal{A}_2\right) + 2tg_0\sin(ka)\mathcal{A}_1 + U\frac{\mathcal{M}}{2} . \tag{D.44}$$

In Eqs. (D.42)-(D.44) we have introduced

$$\mathcal{A}_1 \equiv \frac{1}{\sqrt{N}} \langle \Phi | \hat{a} + \hat{a}^\dagger | \Phi \rangle \tag{D.45}$$

and

$$\mathcal{A}_2 \equiv \frac{1}{N} \langle \Phi | \left(\hat{a} + \hat{a}^\dagger \right)^2 | \Phi \rangle \ . \tag{D.46}$$

The Hamiltonian (D.41) can be diagonalized by introducing the following Bogoliubov transformation:

$$\hat{\gamma}^\dagger_{k,-} = u_k \hat{c}^\dagger_{k,\mathrm{s}} + v_k \hat{c}^\dagger_{k,\mathrm{p}} \ , \tag{D.47}$$

$$\hat{\gamma}^\dagger_{k,+} = v^*_k \hat{c}^\dagger_{k,\mathrm{s}} - u^*_k \hat{c}^\dagger_{k,\mathrm{p}} \ , \tag{D.48}$$

where $u_k = \cos(\theta_k/2)$ and $v_k = \sin(\theta_k/2) e^{i\phi_k}$ with

$$\cos(\theta_k) = -\frac{h_3(k)}{\epsilon(k)} \ , \tag{D.49}$$

$$\sin(\theta_k) = -\frac{\sqrt{h_1^2(k) + h_2^2(k)}}{\epsilon(k)} \ , \tag{D.50}$$

$$e^{i\phi_k} = \frac{h_1(k) + i h_2(k)}{\sqrt{h_1^2(k) + h_2^2(k)}} \ , \tag{D.51}$$

$$\epsilon(k) = \sqrt{h_1^2(k) + h_2^2(k) + h_3^2(k)} \ . \tag{D.52}$$

Note that u_k and v_k are functions of $\mathcal{I}$, $\mathcal{M}$, $\mathcal{A}_1$, and $\mathcal{A}_2$, i.e. $u_k = u_k(\mathcal{I}, \mathcal{M}, \mathcal{A}_1, \mathcal{A}_2)$ and $v_k = v_k(\mathcal{I}, \mathcal{M}, \mathcal{A}_1, \mathcal{A}_2)$. We find

$$\hat{\mathcal{H}}_{\mathrm{eff-matter}} = \sum_{k \in \mathrm{BZ}} \sum_{\xi = \pm} \xi \epsilon(k) \hat{\gamma}^\dagger_{k,\xi} \hat{\gamma}_{k,\xi} + \mathcal{C} \ , \tag{D.53}$$

where

$$\mathcal{C} \equiv UN \left(\frac{\mathcal{M}^2}{4} + |\mathcal{I}|^2 \right) + \hbar \omega_{\mathrm{c}} \langle \Phi | a^\dagger a | \Phi \rangle \ . \tag{D.54}$$

The ground state of (D.53) is $|\psi\rangle = \prod_{k \in \mathrm{BZ}} \hat{\gamma}^\dagger_{k,-} |\mathrm{vac}\rangle$, where $|\mathrm{vac}\rangle$ is the state with no electrons. Mimicking the BCS theory, we find that

$$|\psi\rangle = \prod_{k \in \mathrm{BZ}} \left[u_k + v_k \hat{c}^\dagger_{k,\mathrm{p}} \hat{c}_{k,\mathrm{s}} \right] |\emptyset\rangle \ , \tag{D.55}$$

where $|\emptyset\rangle = \prod_{k \in \mathrm{BZ}} \hat{c}^\dagger_{k,\mathrm{s}} |\mathrm{vac}\rangle$. The following quantities $\langle \psi | \hat{c}^\dagger_{k,\mathrm{s}} \hat{c}_{k,\mathrm{s}} | \psi \rangle = |u_k|^2$, $\langle \psi | \hat{c}^\dagger_{k,\mathrm{p}} \hat{c}_{k,\mathrm{p}} | \psi \rangle = |v_k|^2$, and $\langle \psi | \hat{c}^\dagger_{k,\mathrm{p}} \hat{c}_{k,\mathrm{s}} | \psi \rangle = v^*_k u_k$ are useful to write the order parameters in terms of u_k and v_k. We find

$$\mathcal{I} = \frac{1}{N} \sum_{k \in \mathrm{BZ}} \langle \psi | \hat{c}^\dagger_{k,\mathrm{p}} \hat{c}_{k,\mathrm{s}} | \psi \rangle = \frac{1}{N} \sum_{k \in \mathrm{BZ}} v^*_k u_k \tag{D.56}$$

and

$$\mathcal{M} = \frac{1}{N} \sum_{k \in \mathrm{BZ}} \left(\langle \psi | \hat{c}^\dagger_{k,\mathrm{p}} \hat{c}_{k,\mathrm{p}} | \psi \rangle - \langle \psi | \hat{c}^\dagger_{k,\mathrm{s}} \hat{c}_{k,\mathrm{s}} | \psi \rangle \right) = \frac{1}{N} \sum_{k \in \mathrm{BZ}} \left(|v_k|^2 - |u_k|^2 \right) \ . \tag{D.57}$$

We also write the expectation values of $\hat{j}_{\rm p}$ and $\hat{\mathcal{T}}$ over the HF state $|\psi\rangle$ in terms of u_k and v_k:

$$\mathcal{J} \equiv \frac{\hbar}{aN}\langle\psi|\hat{j}_{\rm p}|\psi\rangle = \frac{2}{N}\sum_{k\in \rm BZ}\left[-t\sin(ka)(|v_k|^2-|u_k|^2) - 2\tilde{t}\cos(ka)\mathrm{Im}(u_k^* v_k)\right] \tag{D.58}$$

and

$$\mathcal{T} \equiv \langle\psi|\hat{\mathcal{T}}|\psi\rangle = \frac{2}{N}\sum_{k\in \rm BZ}\left[t\cos(ka)\big(|v_k|^2-|u_k|^2\big) - 2\tilde{t}\sin(ka)\mathrm{Im}(u_k^* v_k)\right] \ . \tag{D.59}$$

Note that both $\mathcal{J}$ and $\mathcal{T}$ have units of energy and are finite in the thermodynamic $N\to\infty$ limit.

Following exactly the same steps described in the proof of the no-go theorem in the main text and defining

$$\Delta = -\frac{g_0^2}{2}\mathcal{T} \tag{D.60}$$

and

$$\lambda = \sqrt{1+\frac{4\Delta}{\hbar\omega_{\rm c}}} \ , \tag{D.61}$$

we find that $|\Phi\rangle$ must be a coherent state $|\bar{\beta}\rangle$, i.e. $\hat{b}\,|\bar{\beta}\rangle = \bar{\beta}\,|\bar{\beta}\rangle$, with

$$\bar{\beta} = -\frac{g_0}{\lambda^{3/2}}\frac{\mathcal{J}}{\hbar\omega_{\rm c}}\sqrt{N} \ , \tag{D.62}$$

to be compared with Eq. (4) in the main text. As in the case of the proof of the no-go theorem, $\hat{b} = \cosh(x)\hat{a} + \sinh(x)\hat{a}^\dagger$, with $\cosh(x) = (\lambda+1)/(2\sqrt{\lambda})$ and $\sinh(x) = (\lambda-1)/(2\sqrt{\lambda})$. The inverse transformation reads as following: $\hat{a} = \cosh(x)\hat{b} - \sinh(x)\hat{b}^\dagger$. Note that $\mathcal{J}$ depends on $\bar{\beta}$ and therefore the previous equation defines $\bar{\beta}$ only implicitly.

Since we have found the ground state $|\Phi\rangle$ (i.e. a coherent state $|\bar{\beta}\rangle$ of the $\hat{b}$ operator), we can evaluate Eqs. (D.45)-(D.46):

$$\mathcal{A}_1 = \frac{1}{\sqrt{N\lambda}}\langle\bar{\beta}|\hat{b}+\hat{b}^\dagger|\bar{\beta}\rangle = \frac{2\bar{\beta}}{\sqrt{N\lambda}} = -\frac{2g_0}{\lambda^2}\frac{\mathcal{J}}{\hbar\omega_{\rm c}} \tag{D.63}$$

and

$$\mathcal{A}_2 = \frac{1}{N\lambda}\,\langle\bar{\beta}|\big(\hat{b}+\hat{b}^\dagger\big)^2|\bar{\beta}\rangle = \frac{4\bar{\beta}^2+1}{N\lambda} = \mathcal{A}_1^2 + \frac{1}{\lambda N} \ . \tag{D.64}$$

To derive Eq. (D.64) we have used that $\big(\hat{b}+\hat{b}^\dagger\big)^2 = \hat{b}^2+\hat{b}^{\dagger 2}+2\hat{b}^\dagger\hat{b}+1$. Using Eqs. (D.53)-(D.54) and using that $\hat{a}^\dagger\hat{a} = (\lambda^2+1)\hat{b}^\dagger\hat{b}/(2\lambda) - (\lambda^2-1)(\hat{b}^2+\hat{b}^{\dagger 2})/(4\lambda) + (\lambda-1)^2/(4\lambda)$, we can also write the ground-state energy per particle as

$$\epsilon_{\rm GS} = \frac{E_{\rm GS}}{N} = -\frac{1}{N}\sum_{k\in\rm BZ}\epsilon(k) + \frac{\hbar\omega_{\rm c}[4\bar{\beta}^2+(\lambda-1)^2]}{4\lambda N} + U\left(\frac{\mathcal{M}^2}{4}+|\mathcal{I}|^2\right) \ . \tag{D.65}$$

In the thermodynamic $N\to\infty$ limit we find $\mathcal{A}_2 = \mathcal{A}_1^2$ (i.e. the vacuum contribution can be neglected) and

$$\lim_{N\to\infty}\epsilon_{\rm GS} = -a\int_{-\pi/a}^{+\pi/a}\frac{dk}{2\pi}\epsilon(k) + \frac{\hbar\omega_{\rm c}}{4}\mathcal{A}_1^2 + U\left(\frac{\mathcal{M}^2}{4}+|\mathcal{I}|^2\right) \ . \tag{D.66}$$

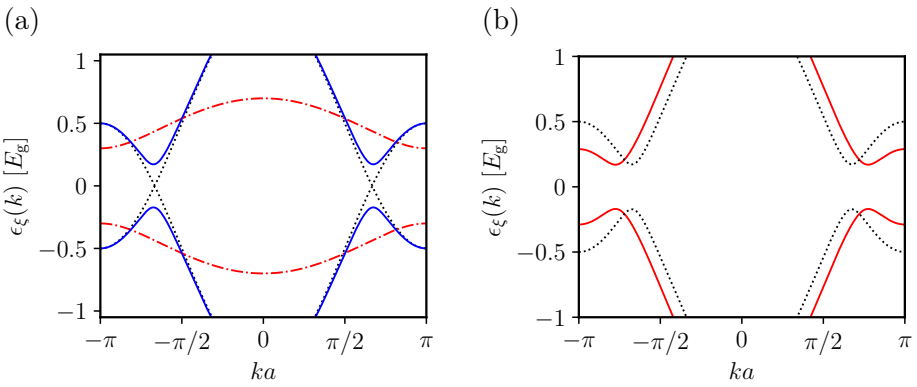

FIGURE D.1: (Color online) Panel (a) The non-interacting $U = 0$ spectrum $\epsilon_\xi(k) = \xi\epsilon(k) = \pm\epsilon(k)$ (in units of E_g) as a function of ka in the first BZ, $ka \in (-\pi/\pi)$. The red dashed line is the spectrum in an insulating non-interacting case $|t| < E_g/4$, $t = 0.1\ E_g$, and $\tilde{t} = 0$. The black dotted line shows the metallic phase $|t| > E_g/4$, $t = 0.5\ E_g$, and $\tilde{t} = 0$. The blue solid line—obtained by setting $t = 0.5\ E_g$ and $\tilde{t} = 0.1\ E_g$—shows that a finite value of $\tilde{t}$ opens a single-particle hybridization gap. Panel (b) A comparison between the non-interacting and the interacting spectrum. The black dotted line is the non-interacting spectrum (i.e. obtained by setting $U = 0$), for $t = 0.5\ E_g$ and $\tilde{t} = 0.1\ E_g$. The red solid line is the HF mean-field spectrum obtained for the same values of t and $\tilde{t}$, at $U = E_g$ (i.e. $U/t = 2$).

Since $\epsilon(k)$ depends only on ka, it is useful to change integration variable in Eq. (D.66) from k to $k' = ka \in (\pi, +\pi)$.

Eqs. (D.56), (D.57), (D.58), (D.59), (D.63), and (D.64) fully determine all the relevant quantities in the problem, i.e. $\mathcal{I}$, $\mathcal{M}$, $\mathcal{J}$, and $\mathcal{T}$.

In Fig. D.1 we present a summary of our main results for the bands $\pm\epsilon(k)$ both in the simple non-interacting $U = 0$ case—panel a)—and in the interacting $U \neq 0$ case—panel b).

D.7 Optical conductivity, Drude weight, and the f-sum rule

In this Section we discuss the optical conductivity $\sigma(\omega)$ and the f-sum rule for the EFK model. The longitudinal conductivity $\sigma(\omega)$ is defined as the response of the physical *charge* current operator to the electric field $E(t) = -c^{-1}\partial A(t)/\partial t$. Assuming $A(t) = A_\omega e^{-i\omega t}e^{\eta t} + \text{c.c.}$ with $\eta = 0^+$ (as usual, for the applicability of linear response theory the applied field must vanish in the far past [85, 86]), we have $E(t) = ic^{-1}(\omega + i\eta)A_\omega e^{-i\omega t}e^{\eta t} + \text{c.c.} = E_\omega e^{-i\omega t}e^{\eta t} + \text{c.c.}$.

We therefore find that the response of the physical current is given by

$$-e\delta J_{\text{phys}}(\omega) \equiv \sigma(\omega)E_\omega = \frac{i}{c}\sigma(\omega)(\omega + i\eta)A_\omega \ . \tag{D.67}$$

We conclude that the pre-factor in front of A_ω in the right-hand side Eq. (D.67) can be calculated from the current-current response function [85, 86], with its paramagnetic and diamagnetic contributions.

Here, we focus on the EFK model, i.e. Eq. (9) for $g_0 = 0$. Using Eq. (D.67) and linear response theory [85, 86], we immediately find that the optical conductivity of the EFK model

is given by

$$\sigma(\omega) = \frac{i}{\omega + i\eta}\frac{e^2a^2}{\hbar^2 L}\langle -\hat{\mathcal{T}}\rangle + \frac{e^2}{\hbar L}\frac{i}{\omega+i\eta}\sum_{n,m}(P_m - P_n)\frac{|\langle\psi_n|\hat{j}_{\rm p}|\psi_m\rangle|^2}{\omega - \omega_{nm} + i\eta}\ , \tag{D.68}$$

where $|\psi_n\rangle$ are the exact eigenstates of the Hamiltonian $\hat{\mathcal{H}}_0+\hat{\mathcal{H}}_{\rm ee}$ with eigenvalues E_n, $\langle\dots\rangle \equiv \sum_n P_n\langle\psi_n|\dots|\psi_n\rangle$ denotes a thermal average, and $P_n = \exp(-\beta E_n)/\mathcal{Z}$, with $\beta = (k_{\rm B}T)^{-1}$ and $\mathcal{Z} = \sum_n \exp(-\beta E_n)$ is the canonical partition function. In deriving the exact eigenstate representation (D.68) we have used that $\hat{j}_{\rm p}^\dagger = \hat{j}_{\rm p}$ and therefore $\langle\psi_n|\hat{j}_{\rm p}|\psi_m\rangle = \langle\psi_m|\hat{j}_{\rm p}|\psi_n\rangle^*$.

Separating the real and imaginary parts of $\sigma(\omega)$ and taking the zero-temperature limit ($P_n = 0$ for $n \neq 0$ and $P_0 = 1$), we finally find:

$${\rm Re}[\sigma(\omega)] = D\delta(\omega) + \frac{\pi e^2}{L}\sum_{n\neq 0}\frac{|\langle\psi_n|\hat{j}_{\rm p}|\psi_0\rangle|^2}{E_n - E_0}[\delta(\omega-\omega_{n0}) + \delta(\omega+\omega_{n0})] \tag{D.69}$$

where D is the so-called Drude weight [203–206]

$$D = \frac{\pi e^2 a^2}{\hbar^2 L}\langle\psi_0| - \hat{\mathcal{T}}|\psi_0\rangle - \frac{2\pi e^2}{L}\sum_{n\neq 0}\frac{|\langle\psi_n|\hat{j}_{\rm p}|\psi_0\rangle|^2}{E_n - E_0} \equiv D_{\rm d} + {\rm D_p}\ . \tag{D.70}$$

Here, $D_{\rm d}$ (${\rm D_p}$) defines the diamagnetic (paramagnetic) contribution to D.

We immediately notice the f-sum rule [85, 86, 204–206]

$$\int_{-\infty}^{+\infty} d\omega {\rm Re}[\sigma(\omega)] = 2\int_0^{+\infty} d\omega {\rm Re}[\sigma(\omega)] = D + \frac{2\pi e^2}{L}\sum_{n\neq 0}\frac{|\langle\psi_n|\hat{j}_{\rm p}|\psi_0\rangle|^2}{E_n - E_0} = D_{\rm d}\ . \tag{D.71}$$

We now show that the f-sum rule is satisfied in our HF treatment of the EFK model. In the absence of light, the complete HF Hamiltonian including electron-electron interactions and neglecting an irrelevant constant is (see Eq. (D.53)):

$$\hat{\mathcal{H}}^{\rm HF} = \sum_{k\in{\rm BZ}}\sum_{\xi=\pm}\xi\epsilon(k)\hat{\gamma}^\dagger_{k,\xi}\hat{\gamma}_{k,\xi}\ . \tag{D.72}$$

The eigenstates and eigenvalues are $|\xi,k\rangle = \hat{\gamma}^\dagger_{\xi,k}|{\rm vac}\rangle$ and $\epsilon_\xi(k) = \xi\epsilon(k)$. We remind the reader that $\epsilon(k)$ has been defined in Eq. (D.52) and, in this Section, needs to be evaluated at $g_0 = 0$. The ground state, as noticed above, is $|\psi_0\rangle = \prod_{k\in{\rm BZ}}\hat{\gamma}^\dagger_{-,k}|{\rm vac}\rangle$. We have

$${\rm D_p} = -\frac{2\pi e^2}{Na}\sum_{k\in{\rm BZ}}\frac{|\langle +,k|\hat{j}_{\rm p}|-,k\rangle|^2}{2\epsilon(k)} \tag{D.73}$$

and

$$D_{\rm d} = \frac{\pi e^2 a}{\hbar^2 N}\sum_{k\in{\rm BZ}}\langle -,k| - \hat{\mathcal{T}}|-,k\rangle\ . \tag{D.74}$$

The quantity $2\epsilon(k)$ is the energy necessary to promote an electron with wave number k vertically from the lower band $\xi = -$ to the upper band $\xi = +$. Fig. D.2(a) shows the quantity $2\epsilon(k)$ (in units of $E_{\rm g}$) as a function of ka. The extrema of $2\epsilon(k)$ give rise to logarithmic divergences in the optical conductivity.

In order to calculate both contributions to the Drude weight, we need the following matrix elements:

$$\langle +,k|\hat{j}_{\rm p}|-,k\rangle = \frac{2a}{\hbar}e^{i\phi_k}[t\sin(ka)\sin(\theta_k)+\tilde{t}\cos(ka)\cos(\theta_k)\sin(\phi_k)+i\tilde{t}\cos(ka)\cos(\phi_k)] \quad \text{(D.75)}$$

and

$$\langle -,k|-\hat{\mathcal{T}}|-,k\rangle = [t\cos(ka)\cos(\theta_k)+\tilde{t}\sin(ka)\sin(\theta_k)\sin(\phi_k)]\ , \quad \text{(D.76)}$$

where θ_k and ϕ_k are the Bogoliubov angles defined in Sec. VI. From Eq. (D.75), we notice that, for $\tilde{t}=0$ and $U=0$, one has $\langle +,k|\hat{j}_{\rm p}|-,k\rangle = 0$. This is expected since, in the absence of many-body effects and for $\tilde{t}=0$, the eigenstates have no orbital mixing (i.e. $\sin(\theta_k)=0$). Switching on $\tilde{t}$ or U, however, yields $\langle +,k|\hat{j}_{\rm p}|-,k\rangle \neq 0$. In particular, for $\tilde{t}=0$, repulsive interactions allow $\langle +,k|\hat{j}_{\rm p}|-,k\rangle \neq 0$ when $\sin(\theta_k)\neq 0$, i.e. for $0<U<U_{\rm XC}=U_{\rm c2}(0)$, since, from Eqs. (D.42)-(D.44), one has $\sin^2(\theta_k)=[U|\mathcal{I}|/\epsilon(k)]^2$.

Using Eqs. (D.75) and (D.76), it is possible to calculate $D_{\rm p}$ and $D_{\rm d}$, and therefore D. Fig. D.2(b) shows these quantities as functions of $U/E_{\rm g}$.

We now calculate the smooth part $\sigma'(\omega)$ of $\mathrm{Re}[\sigma(\omega)]$,

$$\sigma'(\omega) \equiv \frac{\pi e^2}{Na}\sum_{k\in{\rm BZ}}\frac{|\langle +,k|\hat{j}_{\rm p}|-,k\rangle|^2}{2\epsilon(k)}[\delta(\omega-2\epsilon(k)/\hbar)+\delta(\omega+2\epsilon(k)/\hbar)]\ . \quad \text{(D.77)}$$

Note that $\sigma'(\omega)=\mathrm{Re}[\sigma(\omega\neq 0)]$. Because of $\delta(\omega\mp 2\epsilon(k)/\hbar)$ in the integrand of Eq. (D.77), the integral over k (in the thermodynamic limit) can be carried out analytically. We find

$$\sigma'(\omega) = \frac{e^2\hbar}{8}\sum_i \left.\frac{|\langle +,k|\hat{j}_{\rm p}|-,k\rangle|^2}{|\sum_{j=1}^3 h_j(k)\partial_k h_j(k)|}\right|_{k=k_i(\omega)}\ , \quad \text{(D.78)}$$

where $k_i(\omega)$ are the solutions of $\epsilon(k_i(\omega))=\hbar|\omega|/2$ and the quantities $h_1(k)$, $h_2(k)$, and $h_3(k)$ have been defined in Eqs. (D.42)-(D.44). Fig. D.2(c) shows $\sigma'(\omega)$ as a function $\hbar\omega/E_{\rm g}$. Each vertical dashed line marks the energy $E_{\rm VHS}=\min_{k\in{\rm BZ}}[2\epsilon(k)]$ at which the quantity $2\epsilon(k)$ is minimal. At this energy a logarithmic enhancement of $\sigma'(\omega)$ occurs. (Similarly, another singularity occurs at $E'_{\rm VHS}=\max_{k\in{\rm BZ}}[2\epsilon(k)]$, but that is weaker in our numerical calculations.)

Using Eq. (D.78) we can finally calculate numerically the quantity

$$S'_{\rm p} = -2\int_0^{+\infty} d\omega\ \sigma'(\omega)\ . \quad \text{(D.79)}$$

We have verified numerically that

$$S'_{\rm p} = D_{\rm p}\ . \quad \text{(D.80)}$$

This is seen in Fig. D.2(d). It follows that

$$2\int_0^{+\infty} d\omega \mathrm{Re}[\sigma(\omega)] = D_{\rm d}\ , \quad \text{(D.81)}$$

which is exactly the f-sum rule (D.71).

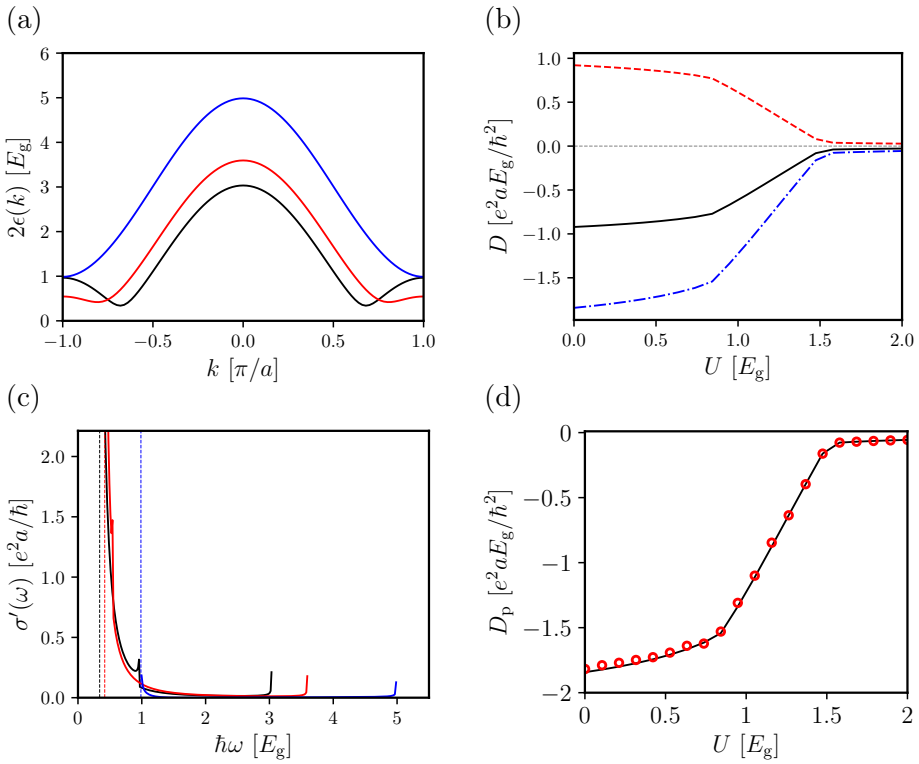

FIGURE D.2: (Color online) (a) The quantity $2\epsilon(k)$ (in units of E_g) as a function ka in the first BZ. Different curves refer to different values of the Hubbard U parameter: $U = E_g/10$ (black), $U = E_g$ (red), and $U = 2E_g$ (blue). (b) The Drude weight D (black solid line) and the contributions D_p (blue dash-dotted line) and D_d (red dashed line) are plotted as functions of U/E_g. The three quantities D, D_p, and D_d are in units of $e^2aE_g/\hbar^2$. (c) The smooth contribution $\sigma'(\omega)$—see Eq. (D.78)—to the real part of the optical conductivity (in units of $e^2aE_g/\hbar$) is plotted as a function $\hbar\omega/E_g$. Different curves refer to different values of the Hubbard U parameter: $U = E_g/10$ (black solid line), $U = E_g$ (red solid line), and $U = 2E_g$ (blue solid line). Black, red, and blue vertical dashed lines mark the energy $E_{VHS} = \min_{k\in BZ}[2\epsilon(k)]$ at which a logarithmic divergence of $\sigma'(\omega)$ occurs. Clearly, E_{VHS} shifts with U. (d) The paramagnetic contribution to the Drude weight D_p (black solid line, in units of $e^2aE_g/\hbar^2$) is compared with the quantity S'_p (red circles) defined in Eq. (D.79). All numerical results in this figure have been obtained by setting $t = E_g/2$ and $\tilde{t} = E_g/10$.

D.8 On the phase diagram of the EFK model

In this Section we demonstrate the existence of two critical values of U, U_{c1} and U_{c2}, at which $\mathcal{I} = 0$, where $\mathcal{I}$ has been introduced in the self-consistent field equation (Eq. (14)) of the main text and Eq. (D.56). The latter yields the following equations:

$$\left[1 - \frac{1}{N}\sum_{k\in \mathrm{BZ}} \frac{U}{2\epsilon(k)}\right] \mathrm{Re}(\mathcal{I}) = 0 \tag{D.82}$$

and

$$\left[1 - \frac{1}{N}\sum_{k\in \mathrm{BZ}} \frac{U}{2\epsilon(k)}\right] \mathrm{Im}(\mathcal{I}) = -\tilde{t}\frac{1}{N}\sum_{k\in \mathrm{BZ}} \frac{\sin(ka)}{\epsilon(k)} \ . \tag{D.83}$$

In the absence of hybridization, i.e. for $\tilde{t} = 0$, the previous expressions become identical. This implies a degeneracy with to respect the phase of $\mathcal{I}$. For $\tilde{t} \neq 0$, these equations can be satisfied by solutions of the HF equations which yield $\mathrm{Im}(\mathcal{I}) = 0$ and $\epsilon(-k) = \epsilon(k)$. The latter condition implies that the left-hand side of Eq. (D.83) vanishes. All the solutions we find are of this type.

The condition $\mathrm{Re}(\mathcal{I}) \neq 0$ implies that the following equation must be satisfied:

$$1 - \frac{1}{N}\sum_{k\in \mathrm{BZ}} \frac{U}{2\epsilon(k)} = 0 \ . \tag{D.84}$$

Before proceeding to prove the existence of U_{c1} and U_{c2} we write Eq. (D.84) in a more appealing form. We define $\psi_k = \mathrm{Re}(\mathcal{I})/[2\epsilon(k)]$, and we rewrite Eq. (D.84) as

$$2\epsilon(k)\psi_k = \frac{1}{N}\sum_{k'\in \mathrm{BZ}} U\psi_{k'} \ . \tag{D.85}$$

This establishes an immediate link between Eq. (D.84) and the equation for the exciton binding energy.

We first demonstrate the existence of upper critical value of U, i.e. $U_{c2}(\tilde{t})$. Let us first set $\tilde{t} = 0$. For $U/t \gg 1$, the system is in a trivial insulating phase in which all electrons occupy the s band and $\mathcal{M} = \mathcal{M}_0 \equiv -1$. Upon decreasing U down to $U_{\mathrm{XC}} = U_{c2}(0)$, the system develops an infinitesimal excitonic order parameter. The value U_{XC} at which this occurs can be found by solving Eq. (D.84) for an infinitesimal $\mathcal{I}$, i.e.

$$\frac{1}{N}\sum_{k\in \mathrm{BZ}} \frac{U_{\mathrm{XC}}}{4t\cos(ka) + E_{\mathrm{g}} + U_{\mathrm{XC}}} = 1 \ , \tag{D.86}$$

or, in the thermodynamic limit,

$$\int_{-\pi}^{\pi} \frac{dx}{2\pi} \frac{1}{\cos(x) + [E_{\mathrm{g}} + U_{\mathrm{XC}}]/(4t)} = \frac{4t}{U_{\mathrm{XC}}} \ . \tag{D.87}$$

Carrying out the integral analytically we find

$$U_{\mathrm{XC}} = \frac{8t^2}{E_{\mathrm{g}}} - \frac{E_{\mathrm{g}}}{2} \ . \tag{D.88}$$

Corrections to U_{XC} and $\mathcal{M}_0$ due to $\tilde{t} \neq 0$ can be found perturbatively in the limit $\tilde{t}/t \ll 1$. They start at second order in the small parameter $\tilde{t}/t$: $\delta U_{c2}(\tilde{t}) = (\tilde{t}/t)^2 u$ and $\delta\mathcal{M}_0(\tilde{t}) =$

$(\tilde{t}/t)^2 m_0$. The latter is the change in the electronic polarization from the value $\mathcal{M}_0 = -1$ in the limit $\tilde{t} = 0$. We find $m_0 = E_{\rm g}/(2U_{\rm XC})$ and $u = E_{\rm g}^3/[t(3E_{\rm g}^2 + 16t^2)]$. For example, for $t = E_{\rm g}/2$ we find $m_0 = 1/3$ and $u = 2/7$. In conclusion, we have

$$U_{\rm c2}(\tilde{t}) = U_{\rm XC} + \frac{E_{\rm g}^3(\tilde{t}/t)^2}{t(3E_{\rm g}^2 + 16t^2)} + \mathcal{O}(\tilde{t}^3) \ . \tag{D.89}$$

We now demonstrate the existence of a lower critical value of U, i.e. $U_{\rm c1}(\tilde{t})$. Following similar steps to the ones above, one can demonstrate that there is also a lower-threshold for the existence of the exciton insulating phase. Up to leading order in an asymptotic expansion for small $\tilde{t}/t$ (and under the single-particle condition $|t| > E_{\rm g}/4$ discussed in Fig. D.1) we find

$$U_{\rm c1}(\tilde{t}) \to \frac{\pi\sqrt{4t^2 - E_{\rm g}^2/4}}{|\ln(\tilde{t}/t)|} \ . \tag{D.90}$$

We clearly see that $\lim_{\tilde{t}\to 0} U_{\rm c1}(\tilde{t}) = 0$. But, for finite $\tilde{t}/t$, $U_{\rm c1}(\tilde{t}) \neq 0$. We will come back to Eq. (D.90) below.

We have checked that the analytical results (D.89) and (D.90) match very well our numerical results, in their regime of validity.

D.9 Pseudospin analysis

In this Section we present a few more remarks on the ground state of the EFK model in the HF approximation.

We view the mean-field problem as a variational problem and use a trial ground-state wave function of the form

$$|\psi\rangle = \prod_{k\in{\rm BZ}} \hat{\gamma}^\dagger_{k,-}|{\rm vac}\rangle \ . \tag{D.91}$$

We then express the full Hamiltonian of the 1D EFK model defined by Eq. (D.20) in terms of the Bogoliubov operators $\hat{\gamma}^\dagger_{k,\pm}$ and $\hat{\gamma}_{k,\pm}$:

$$\hat{c}^\dagger_{k,{\rm s}} = u_k\hat{\gamma}^\dagger_{k,-} - v_k\hat{\gamma}^\dagger_{k,+} \ , \tag{D.92}$$

$$\hat{c}^\dagger_{k,{\rm p}} = v^*_k\hat{\gamma}^\dagger_{k,-} + u^*_k\hat{\gamma}^\dagger_{k,+} \ , \tag{D.93}$$

where $u_k = \cos(\theta_k/2)$ and $v_k = \sin(\theta_k/2)e^{i\phi_k}$.

By writing the Hamiltonian in its normal ordered form, exploiting the following property of the variational wave function

$$\langle\psi|\hat{\gamma}^\dagger_{k_1,\lambda_1}\cdots\hat{\gamma}^\dagger_{k_n,\lambda_n}\hat{\gamma}_{k_{n+1},\lambda_{n+1}}\cdots\hat{\gamma}_{k_{2n},\lambda_{2n}}|\psi\rangle = \prod_{j=1}^{2n}\delta_{\lambda_j,-}\langle\psi|\hat{\gamma}^\dagger_{k_1,-}\cdots\hat{\gamma}^\dagger_{k_n,-}\hat{\gamma}_{k_{n+1},-}\cdots\hat{\gamma}_{k_{2n},-}|\psi\rangle \ , \tag{D.94}$$

and enforcing particle-hole symmetry, we find the following ground-state energy:

$$\begin{aligned}\langle\psi|\hat{\mathcal{H}}|\psi\rangle &= \sum_{k\in{\rm BZ}}\left\{[E_{\rm g}/2 + 2t\cos(ka)]\cos(\theta_k) + 2\tilde{t}\sin(ka)\sin(\theta_k)\cos(\phi_k)\right\}\langle\psi|\hat{\gamma}^\dagger_{k,-}\hat{\gamma}_{k,-}|\psi\rangle \\ &+ \frac{U}{N}\sum_{k,k',q\in{\rm BZ}}\sin(\theta_{k'-q}/2)\cos(\theta_{k+q}/2)\cos(\theta_k/2)\sin(\theta_{k'}/2)\times \\ &\times\ e^{i(\phi_{k'}-\phi_{k'-q})}\langle\psi|\hat{\gamma}^\dagger_{k'-q,-}\hat{\gamma}^\dagger_{k+q,-}\hat{\gamma}_{k,-}\hat{\gamma}_{k',-}|\psi\rangle \ .\end{aligned} \tag{D.95}$$

Using the ansatz (D.91) in the previous equation and the properties

$$\langle\psi|\hat{\gamma}^{\dagger}_{k,-}\hat{\gamma}^{\dagger}_{k,-}|\psi\rangle = 1 \ , \tag{D.96}$$

$$\langle\psi|\hat{\gamma}^{\dagger}_{k'-q,-}\hat{\gamma}^{\dagger}_{k+q,-}\hat{\gamma}_{k,-}\hat{\gamma}_{k',-}|\psi\rangle = \delta_{q,0} - \delta_{q,k'-k} \ , \tag{D.97}$$

we finally find

$$\begin{aligned}\langle\psi|\hat{\mathcal{H}}|\psi\rangle &= \sum_{k\in\mathrm{BZ}} [E_{\mathrm{g}}/2 + 2t\cos(ka)]\cos(\theta_k) + 2\tilde{t}\sin(ka)\sin(\theta_k)\cos(\phi_k) \\ &- \frac{U}{N}\sum_{k,k'\in\mathrm{BZ}} \sin(\theta_k/2)\cos(\theta_k/2)\sin(\theta_{k'}/2)\cos(\theta_{k'}/2)\cos(\phi_{k'}-\phi_k) \\ &+ \frac{U}{N}\sum_{k,k'\in\mathrm{BZ}} \cos^2(\theta_k/2)\sin^2(\theta_{k'}/2) \ . \end{aligned} \tag{D.98}$$

We therefore note that the ground-state energy can be written in a form that resembles the energy of a chain of classical interacting spins in an external magnetic field, i.e.

$$\mathcal{E}[\boldsymbol{\tau}_k] \equiv \langle\psi|\hat{\mathcal{H}}|\psi\rangle - \frac{UN}{4} = -\sum_{k\in\mathrm{BZ}} \left[B_y(k)\tau^y_k + B_z(k)\tau^z_k\right] - \frac{U}{4N}\sum_{k,k'\in\mathrm{BZ}} \boldsymbol{\tau}_k\cdot\boldsymbol{\tau}_{k'} \ , \tag{D.99}$$

where $\boldsymbol{B}(k) = [0, 2\tilde{t}\sin(ka), E_{\mathrm{g}}/2 + 2t\cos(ka)]^{\mathrm{T}}$ and $\boldsymbol{\tau}_k$ is a unit vector with Cartesian components:

$$\tau^x_k \equiv \langle\psi|\hat{c}^{\dagger}_{\mathrm{p},k}\hat{c}_{\mathrm{s},k} + \hat{c}^{\dagger}_{\mathrm{s},k}\hat{c}_{\mathrm{p},k}|\psi\rangle = \sin(\theta_k)\cos(\phi_k) \ , \tag{D.100}$$

$$\tau^y_k \equiv i\,\langle\psi|\hat{c}^{\dagger}_{\mathrm{p},k}\hat{c}_{\mathrm{s},k} - \hat{c}^{\dagger}_{\mathrm{s},k}\hat{c}_{\mathrm{p},k}|\psi\rangle = \sin(\theta_k)\sin(\phi_k) \ , \tag{D.101}$$

$$\tau^z_k \equiv \langle\psi|\hat{c}^{\dagger}_{\mathrm{s},k}\hat{c}_{\mathrm{s},k} - \hat{c}^{\dagger}_{\mathrm{p},k}\hat{c}_{\mathrm{p},k}|\psi\rangle = \cos(\theta_k) \ . \tag{D.102}$$

Notice that the "lattice" of spins is in momentum rather than real space. In this pseudospin description, the repulsive Hubbard-U interaction becomes a ferromagnetic rotationally-invariant spin-spin interaction term. The spin configuration which minimizes the energy satisfies the self-consistent field equations

$$\tau^x_k = -\frac{U}{2\mu_k N}\sum_{k\in\mathrm{BZ}} \tau^x_k \ , \tag{D.103}$$

$$\tau^y_k = -\frac{B_y(k)}{\mu_k} - \frac{U}{2\mu_k N}\sum_{k\in\mathrm{BZ}} \tau^y_k \ , \tag{D.104}$$

$$\tau^z_k = -\frac{B_z(k)}{\mu_k} - \frac{U}{2\mu_k N}\sum_{k\in\mathrm{BZ}} \tau^z_k \ , \tag{D.105}$$

where

$$\mu_k = -\sqrt{\left[\frac{U}{2N}\sum_{k\in\mathrm{BZ}}\tau^x_k\right]^2 + \left[B_y(k) - \frac{U}{2N}\sum_{k\in\mathrm{BZ}}\tau^y_k\right]^2 + \left[B_z(k) - \frac{U}{2N}\sum_{k\in\mathrm{BZ}}\tau^z_k\right]^2} \ . \tag{D.106}$$

The quantities $\mathcal{I}$ and $\mathcal{M}$ can also be expressed in terms of pseudospins:

$$\mathcal{I} = \frac{1}{2N}\sum_{k\in\mathrm{BZ}} (\tau^x_k - i\tau^y_k) \tag{D.107}$$

and

$$\mathcal{M} = -\frac{1}{N}\sum_{k\in \mathrm{BZ}} \tau_k^z \ . \tag{D.108}$$

Within this description, we consider two limiting cases. Firstly, we consider the limit $U \gg E_{\mathrm{g}}, t, \tilde{t}$. Neglecting $E_{\mathrm{g}}, t, \tilde{t}$ with respect to U, it follows that the following configurations

$$\boldsymbol{\tau}_k^{(\mathrm{n})} = -\hat{\boldsymbol{z}} \ , \tag{D.109}$$

$$\boldsymbol{\tau}_k^{(\mathrm{fx})} = \hat{\boldsymbol{x}} \ , \tag{D.110}$$

and

$$\boldsymbol{\tau}_k^{(\mathrm{fy})} = \hat{\boldsymbol{y}} \ , \tag{D.111}$$

are degenerate (i.e. $\mathcal{E}[\boldsymbol{\tau}_k^{(\mathrm{n})}] = \mathcal{E}[\boldsymbol{\tau}_k^{(\mathrm{fx})}] = \mathcal{E}[\boldsymbol{\tau}_k^{(\mathrm{fy})}] = -UN/2$). For $U \gg E_{\mathrm{g}}, t, \tilde{t}$ the system is invariant under rotations. The configuration corresponding to $\boldsymbol{\tau}_k^{(\mathrm{n})}$ describes the normal phase ($\mathcal{I} = 0$), while the ones corresponding to $\boldsymbol{\tau}_k^{(\mathrm{fx})}$ and $\boldsymbol{\tau}_k^{(\mathrm{fy})}$ correspond to HF states with $\mathrm{Re}(\mathcal{I}) \neq 0$ and $\mathrm{Im}(\mathcal{I}) \neq 0$, respectively. This implies that all configurations of the form

$$\boldsymbol{\tau}_k^{(\theta,\phi)} = \cos(\theta)\boldsymbol{\tau}_k^{(\mathrm{n})} + \sin(\theta)\cos(\phi)\boldsymbol{\tau}_k^{(\mathrm{fx})} + \sin(\theta)\sin(\phi)\boldsymbol{\tau}_k^{(\mathrm{fy})} \tag{D.112}$$

are degenerate. By turning on E_{g}, t and $\tilde{t}$, and treating them as weak perturbations, we find that the energy associated to the configurations (D.112) is given by $\mathcal{E}[\boldsymbol{\tau}_k^{(\theta,\phi)}] = -[U + E_{\mathrm{g}}\cos(\theta)]N/2$. This means that the gap energy E_{g} makes the *normal* phase expressed in (D.109) energetically preferred. This simple example shows why at large values of the Hubbard-U parameter, the HF phases with $\mathcal{I} \neq 0$ do not occur.

Before concluding, we discuss a second limiting case. We set $E_{\mathrm{g}} = 0$ (which is compatible with the condition $|t| > E_{\mathrm{g}}/4$ described in Fig. D.1) and we assume $0 < \tilde{t} < t$. Under these conditions, the external magnetic field $\boldsymbol{B}(k)$ lays on the $\hat{\boldsymbol{y}}$-$\hat{\boldsymbol{z}}$ plane and and its average value is zero, i.e. $N^{-1}\sum_{k\in \mathrm{BZ}} \boldsymbol{B}(k) = \boldsymbol{0}$, but $B(k) \neq 0 \ \forall k$ if $t, \tilde{t} \neq 0$. The spin configuration which minimizes the energy is

$$\tau_k^x = -\frac{U\mathrm{Re}(\mathcal{I})}{\mu_k} \ , \tag{D.113}$$

$$\tau_k^y = -\frac{2\tilde{t}\sin(ka)}{\mu_k} \ , \tag{D.114}$$

$$\tau_k^z = -\frac{2t\cos(ka)}{\mu_k} \ , \tag{D.115}$$

$$\mu_k = -\sqrt{[U\mathrm{Re}(\mathcal{I})]^2 + \left[2\tilde{t}\sin(ka)\right]^2 + [2t\cos(ka)]^2} \ , \tag{D.116}$$

with $\mathrm{Re}(\mathcal{I}) \neq 0$ only if the following implicit equation is satisfied:

$$\frac{U}{2N}\sum_{k\in \mathrm{BZ}} \frac{1}{\sqrt{[U\mathrm{Re}(\mathcal{I})]^2 + \left[2\tilde{t}\sin(ka)\right]^2 + [2t\cos(ka)]^2}} = 1 \ . \tag{D.117}$$

In the thermodynamic limit the latter can be rewritten as

$$\frac{t}{U} = \frac{1}{2\pi\sqrt{1 + [U\mathrm{Re}(\mathcal{I})]^2/(4t^2)}}\mathrm{K}\left(\sqrt{\frac{1-(\tilde{t}/t)^2}{1 + [U\mathrm{Re}(\mathcal{I})]^2/(4t^2)}}\right) \ , \tag{D.118}$$

where $\mathrm{K}(x)$ is the complete elliptic integral of the first kind. Inspecting the right-hand side of the previous equation, one finds that, for fixed values of t, $\tilde{t}$, and U,

$$0 \leq \frac{t}{U} \leq \frac{t}{U_{\mathrm{c1}}(\tilde{t})} \equiv \frac{1}{2\pi}\mathrm{K}\left(\sqrt{1-(\tilde{t}/t)^2}\right) \ , \tag{D.119}$$

where U_{c1} is the minimum value of the Hubbard U parameter which gives $\mathrm{Re}(\mathcal{I}) \neq 0$. For small values of $\tilde{t}$ we find

$$U_{\mathrm{c1}}(\tilde{t}) \to \frac{2\pi t}{|\ln(\tilde{t}/t)|} \ . \tag{D.120}$$

Note the logarithmic divergence, as we has seen previously in Eq. (D.90). The only role of $E_{\mathrm{g}} \neq 0$ is to replace $2t \to \sqrt{4t^2 - E_{\mathrm{g}}^2/4}$ in Eq. (D.120).

If $0 < U < U_{\mathrm{c1}}$, the configuration which minimizes the energy is

$$\tau_k^x = 0 \ , \tag{D.121}$$

$$\tau_k^y = -\frac{2\tilde{t}\sin(ka)}{\mu_k} \ , \tag{D.122}$$

$$\tau_k^z = -\frac{2t\cos(ka)}{\mu_k} \ , \tag{D.123}$$

$$\mu_k = -\sqrt{\left[2\tilde{t}\sin(ka)\right]^2 + \left[2t\cos(ka)\right]^2} \ , \tag{D.124}$$

which means that $\mathrm{Re}(\mathcal{I}) = 0$. This second liming case well describes what occurs in the EFK model in the HF approximation for $U \sim U_{\mathrm{c1}}$.

E

Appendix: Theory of Photon Condensation in a Spatially-Varying Electromagnetic Field

E.1 Disentangling light and matter

In this Appendix, we show that, in the thermodynamic $N \to \infty$, $V \to \infty$ limit (with $N/V =$ constant), it is permissible to assume a factorized ground state of the form

$$|\Psi\rangle = |\psi\rangle\,|\Phi\rangle \ . \tag{E.1}$$

We begin by defining the electron-photon Hamiltonian $\hat{\mathcal{H}}_{\rm el-ph} \equiv \hat{\mathcal{H}}^{(1)}_{\rm el-ph} + \hat{\mathcal{H}}^{(2)}_{\rm el-ph}$, where

$$\hat{\mathcal{H}}^{(1)}_{\rm el-ph} \equiv \sum_{i=1}^{N} \frac{e}{mc} \hat{\boldsymbol{A}}(\hat{\boldsymbol{r}}_i) \cdot \hat{\boldsymbol{p}}_i \tag{E.2}$$

and

$$\hat{\mathcal{H}}^{(2)}_{\rm el-ph} \equiv \sum_{i=1}^{N} \frac{e^2}{2mc^2} \hat{\boldsymbol{A}}^2(\hat{\boldsymbol{r}}_i) \ . \tag{E.3}$$

The photon Hamiltonian $\hat{\mathcal{H}}_{\rm ph}$ has been defined in the main text. Let us split the matter Hamiltonian into the sum of kinetic and potential terms, i.e. we write $\hat{\mathcal{H}} \equiv \hat{\mathcal{H}}_{\rm K} + \hat{\mathcal{H}}_{\rm V}$, where:

$$\hat{\mathcal{H}}_{\rm K} \equiv \sum_{i=1}^{N} \frac{\hat{\boldsymbol{p}}_i^2}{2m} \tag{E.4}$$

and

$$\hat{\mathcal{H}}_{\rm V} \equiv \frac{1}{2} \sum_{i \neq j} v(\hat{\boldsymbol{r}}_i - \hat{\boldsymbol{r}}_j) \ . \tag{E.5}$$

In order to guarantee the correct thermodynamic limit, $\hat{\mathcal{H}}_{\rm el-ph}$, $\hat{\mathcal{H}}_{\rm ph}$, and $\hat{\mathcal{H}}$ must scale *extensively* with N. This implies that photonic and electronic operators must scale properly with N in the $N \to \infty$ limit. Let us discuss this fact explicitly.

We begin by considering the photon Hamiltonian $\hat{\mathcal{H}}_{\rm ph}$. We denote by the symbol $N_{\rm modes}$ the number of "non-negligible" modes, i.e. modes that cannot be neglected in the thermodynamic limit. The photon Hamiltonian $\hat{\mathcal{H}}_{\rm ph}$ can have an extensive scaling with N in two different cases:

- $N_{\rm modes}$ is an *intensive* quantity (i.e. $N_{\rm modes}$ does not scale with N). In this case, the operator $\hat{a}_{\boldsymbol{q}_0,\sigma}$ characterized by a given $\boldsymbol{q}_0$ acquires a macroscopic occupation $\hat{a}_{\boldsymbol{q}_0,\sigma} \sim \sqrt{N}$;
- $N_{\rm modes}$ is an *extensive* quantity, while the occupation number $\hat{a}^\dagger_{\boldsymbol{q}_0,\sigma}\hat{a}_{\boldsymbol{q}_0,\sigma}$ of each mode is not macroscopic, i.e. $\hat{a}_{\boldsymbol{q},\sigma} \sim \sqrt{N/N_{\rm modes}} \sim 1$. We now show that this case is not relevant for the occurrence of photon condensation. The paramagnetic electron-photon interaction $\hat{\mathcal{H}}^{(1)}_{\rm el-ph}$ scales like:

$$\hat{\mathcal{H}}^{(1)}_{\rm el-ph} \;\sim\; \sum_{\boldsymbol{q}} A_{\boldsymbol{q}}\hat{a}^\dagger_{\boldsymbol{q},\sigma}\hat{\boldsymbol{j}}_{\rm p}(\boldsymbol{q}) \; . \tag{E.6}$$

  In the case of interest, $A_{\boldsymbol{q}}\hat{a}^\dagger_{\boldsymbol{q},\sigma} \sim 1/\sqrt{N_{\rm modes}} \sim 1/\sqrt{N}$, while $\sum_{\boldsymbol{q}}\hat{\boldsymbol{j}}_{\rm p}(\boldsymbol{q})$ is *extensive* in N. We therefore get the following scaling with N of the paramagnetic contribution: $\hat{\mathcal{H}}^{(1)}_{\rm el-ph} \sim N/\sqrt{N_{\rm modes}} \sim \sqrt{N}$. In summary, if $N_{\rm modes}$ is extensive, we have $\hat{\mathcal{H}}^{(1)}_{\rm el-ph}/N \sim 1/\sqrt{N} \to 0$ in the limit $N \to \infty$. Since $\hat{\mathcal{H}}^{(1)}_{\rm el-ph}$ is responsible for lowering the energy of the photon condensate phase, the fact that it scales to zero in the thermodynamic limit excludes the possibility of a phase transition.

Since we are interested in photon condensation, from now on we will consider only the case in which a finite number of modes acquires a macroscopic occupation number, i.e. we assume that $N_{\rm modes}$ is an *intensive* quantity. In this case, Hamiltonians (E.2) and (E.3) are *extensive*. Let us now focus on electronic operators. Being a sum of N independent terms, $\hat{\mathcal{H}}_{\rm K}$ in Eq. (E.4) is explicitly *extensive*. Conversely, $\hat{\mathcal{H}}_{\rm V}$ in Eq. (E.5) contains a double sum, and is therefore expected to scale like N^2. Nevertheless, it is possible to show that, due to the ground-state equilibrium condition (i.e. charge neutrality [86]), the expectation value of $\hat{\mathcal{H}}_{\rm V}$ over the equilibrium ground-state $|\psi\rangle$ scales with N. Below, we will therefore work with the rescaled operators $\hat{\mathcal{H}}/N$, $\hat{\mathcal{H}}_{\rm ph}/N$, and $\hat{\mathcal{H}}_{\rm el-ph}/N$, which are well defined in the thermodynamic $N \to \infty$ limit.

In order to prove Eq. (E.1) we will show that in the limit $N \to \infty$

$$[\frac{\hat{\mathcal{H}}}{N}, \frac{\hat{\mathcal{H}}_{\rm el-ph}}{N}] \to 0 \; , \tag{E.7}$$

and

$$[\frac{\hat{\mathcal{H}}_{\rm ph}}{N}, \frac{\hat{\mathcal{H}}_{\rm el-ph}}{N}] \to 0 \; . \tag{E.8}$$

The left-hand side of Eq. (E.7) contains three contributions, which we now carefully examine:

a) The first contribution is

$$\begin{aligned}[\frac{\hat{\mathcal{H}}_{\rm K}}{N}, \frac{\hat{\mathcal{H}}^{(1)}_{\rm el-ph}}{N}] \;=\; & \sum_{i=1}^{N} \frac{e\hbar}{2cm^2N^2}\Big[\hat{\boldsymbol{p}}_i\cdot\boldsymbol{q} - \sum_{\boldsymbol{q},\sigma} A_{\boldsymbol{q}}\big(\hat{a}_{\boldsymbol{q},\sigma}e^{i\boldsymbol{q}\cdot\hat{\boldsymbol{r}}_i} - \hat{a}^\dagger_{\boldsymbol{q},\sigma}e^{-i\boldsymbol{q}\cdot\hat{\boldsymbol{r}}_i}\big)\boldsymbol{u}_{\boldsymbol{q},\sigma}\cdot\hat{\boldsymbol{p}}_i + \\ & + \sum_{\boldsymbol{q},\sigma} A_{\boldsymbol{q}}\big(\hat{a}_{\boldsymbol{q},\sigma}e^{i\boldsymbol{q}\cdot\hat{\boldsymbol{r}}_i} - \hat{a}^\dagger_{\boldsymbol{q},\sigma}e^{-i\boldsymbol{q}\cdot\hat{\boldsymbol{r}}_i}\big)\hat{\boldsymbol{p}}_i\cdot\boldsymbol{q}\;\boldsymbol{u}_{\boldsymbol{q},\sigma}\cdot\hat{\boldsymbol{p}}_i\Big] \; .\end{aligned} \tag{E.9}$$

This commutator vanishes like $1/N$, since $\sum_{i=1}^{N}$ scales like N, while terms like $\sum_{\boldsymbol{q}} A_{\boldsymbol{q}}\hat{a}_{\boldsymbol{q},\sigma} \sim \sqrt{N/V}$ are of order unity in the limit $N, V \to \infty$ with $N/V =$ constant.

b) The second contribution is

$$[\frac{\hat{\mathcal{H}}_{\rm V}}{N}, \frac{\hat{\mathcal{H}}^{(1)}_{\rm el-ph}}{N}] = \frac{1}{N^2}[\frac{1}{2}\sum_{i\neq j} v(\hat{\boldsymbol{r}}_i - \hat{\boldsymbol{r}}_j), \sum_{j=1}^{N} \frac{e}{mc}\hat{\boldsymbol{A}}(\hat{\boldsymbol{r}}_j)\cdot\hat{\boldsymbol{p}}_j] \ . \tag{E.10}$$

Using that $[f(\hat{\boldsymbol{r}}_i), \hat{\boldsymbol{p}}_j] = \delta_{i,j} i\hbar\nabla_{\hat{\boldsymbol{r}}_i} f(\hat{\boldsymbol{r}}_i)$ and introducing the Coulomb force $\hat{\boldsymbol{F}}^{\rm C}_{i,j} = -\nabla_{\hat{\boldsymbol{r}}_i} v(\hat{\boldsymbol{r}}_i - \hat{\boldsymbol{r}}_j)/2$ we get:

$$[\frac{\hat{\mathcal{H}}_{\rm V}}{N}, \frac{\hat{\mathcal{H}}^{(1)}_{\rm el-ph}}{N}] = -\sum_{i=1}^{N} \frac{i\hbar e\hat{\boldsymbol{A}}(\hat{\boldsymbol{r}}_i)}{mcN^2}\cdot\sum_{j\neq i}\hat{\boldsymbol{F}}^{\rm C}_{i,j} \ . \tag{E.11}$$

The quantity $\hat{\boldsymbol{F}}^{\rm T}_i \equiv \sum_{j\neq i}\hat{\boldsymbol{F}}^{\rm C}_{i,j}$ is the total force acting on the i-th particle. Even though the double sum in Eq. (E.11) brings in a factor scaling like N^2 in the large-N limit, the expectation value of the commutator in Eq. (E.11) vanishes like $1/N$ in the $N \to \infty$ limit. This is due to the aforementioned charge-neutrality condition, which imposes that the expectation value of $\sum_{i=1}^{N}\hat{\boldsymbol{F}}^{\rm T}_i$ over the matter ground state $|\psi\rangle$ scales like N in the $N \to \infty$ limit.

c) The third contribution is

$$\begin{aligned}
[\frac{\hat{\mathcal{H}}}{N}, \frac{\hat{\mathcal{H}}^{(2)}_{\rm el-ph}}{N}] = [\frac{\hat{\mathcal{H}}_{\rm K}}{N}, \frac{\hat{\mathcal{H}}^{(2)}_{\rm el-ph}}{N}] \ &= \ \sum_{i=1}^{N}\frac{e^2\hbar}{2m^2c^2N^2}\sum_{\boldsymbol{q},\sigma}\Big\{\hat{\boldsymbol{p}}_i\cdot\boldsymbol{q}\hat{\boldsymbol{A}}(\hat{\boldsymbol{r}}_i)\cdot\boldsymbol{u}_{\boldsymbol{q},\sigma}\times \\
&\times \ A_{\boldsymbol{q}}\big(\hat{a}_{\boldsymbol{q},\sigma}e^{i\boldsymbol{q}\cdot\hat{\boldsymbol{r}}_i} - \hat{a}^{\dagger}_{\boldsymbol{q},\sigma}e^{-i\boldsymbol{q}\cdot\hat{\boldsymbol{r}}_i}\big) + \\
&+ \ \sum_{\boldsymbol{q},\sigma}\hat{\boldsymbol{A}}(\hat{\boldsymbol{r}}_i)\cdot\boldsymbol{u}_{\boldsymbol{q},\sigma}A_{\boldsymbol{q}}\big(\hat{a}_{\boldsymbol{q},\sigma}e^{i\boldsymbol{q}\cdot\hat{\boldsymbol{r}}_i} - \hat{a}^{\dagger}_{\boldsymbol{q},\sigma}e^{-i\boldsymbol{q}\cdot\hat{\boldsymbol{r}}_i}\big)\hat{\boldsymbol{p}}_i\cdot\boldsymbol{q}\Big\} \ .
\end{aligned} \tag{E.12}$$

Again, this quantity scales to zero like $1/N$, since the sum $\sum_{i=1}^{N}$ brings in a factor N, while terms like $\sum_{\boldsymbol{q},\sigma} A_{\boldsymbol{q}}\hat{a}_{\boldsymbol{q},\sigma}$ and $\hat{\boldsymbol{A}}(\hat{\boldsymbol{r}}_i)$ are of order unity with respect to N.

In order to prove Eq. (E.8), it is convenient to rewrite the light-matter interaction Hamiltonian in terms of the real-space paramagnetic current $\hat{\boldsymbol{j}}_{\rm p}(\boldsymbol{r})$ and density $\hat{n}(\boldsymbol{r})$ operators:

$$\hat{n}(\boldsymbol{r}) \ = \ \sum_{i=1}^{N}\delta(\hat{\boldsymbol{r}}_i - \boldsymbol{r}) \ , \tag{E.13}$$

$$\hat{\boldsymbol{j}}_{\rm p}(\boldsymbol{r}) \ = \ \frac{1}{2m}\sum_{i=1}^{N}\big[\hat{\boldsymbol{p}}_i\delta(\hat{\boldsymbol{r}}_i - \boldsymbol{r}) + \delta(\hat{\boldsymbol{r}}_i - \boldsymbol{r})\hat{\boldsymbol{p}}_i\big] \ . \tag{E.14}$$

Exploiting these definitions, we can write Eqs. (E.2)-(E.3) as:

$$\hat{\mathcal{H}}^{(1)}_{\rm el-ph} \ = \ \frac{e}{c}\int d^3\boldsymbol{r} \ \hat{\boldsymbol{j}}_{\rm p}(\boldsymbol{r})\cdot\hat{\boldsymbol{A}}(\boldsymbol{r}) \ , \tag{E.15}$$

$$\hat{\mathcal{H}}^{(2)}_{\rm el-ph} \ = \ \frac{e^2}{2mc^2}\int d^3\boldsymbol{r} \ \hat{n}(\boldsymbol{r})\hat{\boldsymbol{A}}^2(\boldsymbol{r}) \ . \tag{E.16}$$

Using the commutator $[\hat{a}_{\boldsymbol{q},\sigma}, \hat{a}^{\dagger}_{\boldsymbol{q}',\sigma'}] = \delta_{\boldsymbol{q},\boldsymbol{q}'}\delta_{\sigma,\sigma'}$, we can rewrite the left-hand side of Eq. (E.8) as the sum of the following two terms:

$$[\frac{\hat{\mathcal{H}}_{\rm ph}}{N}, \frac{\hat{\mathcal{H}}^{(1)}_{\rm el-ph}}{N}] = \sum_{\boldsymbol{q},\sigma} \frac{\hbar\omega_{\boldsymbol{q}}}{N^2}\Big\{\frac{e}{c}\int d^3\boldsymbol{r}\ \hat{\boldsymbol{j}}_{\rm p}(\boldsymbol{r})\cdot\boldsymbol{u}_{\boldsymbol{q},\sigma}A_{\boldsymbol{q}}\big(\hat{a}_{\boldsymbol{q},\sigma}e^{i\boldsymbol{q}\cdot\boldsymbol{r}} - \hat{a}^{\dagger}_{\boldsymbol{q},\sigma}e^{-i\boldsymbol{q}\cdot\boldsymbol{r}}\big)\Big\} \tag{E.17}$$

and

$$\begin{aligned}[\frac{\hat{\mathcal{H}}_{\rm ph}}{N}, \frac{\hat{\mathcal{H}}^{(2)}_{\rm el-ph}}{N}] \ &= \ \sum_{\boldsymbol{q},\sigma} \frac{\hbar\omega_{\boldsymbol{q}}}{N^2}\Big\{\frac{e}{2mc}\int d^3\boldsymbol{r}\ \hat{n}(\boldsymbol{r})\hat{\boldsymbol{A}}(\boldsymbol{r})\cdot\boldsymbol{u}_{\boldsymbol{q},\sigma}A_{\boldsymbol{q},\sigma}\big(\hat{a}_{\boldsymbol{q},\sigma}e^{i\boldsymbol{q}\cdot\boldsymbol{r}} - \hat{a}^{\dagger}_{\boldsymbol{q},\sigma}e^{-i\boldsymbol{q}\cdot\boldsymbol{r}}\big) \\ &+ \ \frac{e}{2mc}\int d^3\boldsymbol{r}\ \hat{n}(\boldsymbol{r})A_{\boldsymbol{q},\sigma}\big(\hat{a}_{\boldsymbol{q},\sigma}e^{i\boldsymbol{q}\cdot\boldsymbol{r}} - \hat{a}^{\dagger}_{\boldsymbol{q},\sigma}e^{-i\boldsymbol{q}\cdot\boldsymbol{r}}\big)\hat{\boldsymbol{A}}(\boldsymbol{r})\cdot\boldsymbol{u}_{\boldsymbol{q},\sigma}\Big\}\ .\end{aligned} \tag{E.18}$$

Again, both quantities scale like $1/N$, since $\int d^3\boldsymbol{r}\ \hat{n}(\boldsymbol{r}) \sim N$ and $\int d^3\boldsymbol{r}\ \hat{\boldsymbol{j}}_{\rm p}(\boldsymbol{r}) \sim N$, while $\hat{\boldsymbol{A}}(\boldsymbol{r})$ and $\sum_{\boldsymbol{q},\sigma}$ do not scale with N (since, as stated at the beginning of this Appendix, we are considering the situation in which $N_{\rm modes}$ does not scale with N).

E.2 Disentangling light and matter in the Zeeman coupling case

In this Appendix, we show that, in the thermodynamic $N \to \infty$, $V \to \infty$ limit (with $N/V =$ constant), it is allowed to assume a factorized ground state of the form

$$|\Psi\rangle = |\psi\rangle\,|\Phi\rangle\ , \tag{E.19}$$

also when a Zeeman-type electron-photon interaction is taken into account. In this case, the electron-photon Hamiltonian is given by

$$\hat{\mathcal{H}}_{\rm el-ph} \ \equiv \ \frac{g\mu_{\rm B}}{2}\sum_{i=1}^{N}\hat{\boldsymbol{\sigma}}_i\cdot\hat{\boldsymbol{B}}(\boldsymbol{r}_i)\ . \tag{E.20}$$

The electron Hamiltonian $\hat{\mathcal{H}}$ and the photon Hamiltonian $\hat{\mathcal{H}}_{\rm ph}$ have been defined in the main text. We here report again the explicit form of the cavity magnetic field: $\hat{\boldsymbol{B}}(\boldsymbol{r}) = \sum_{\boldsymbol{q},\sigma} A_{\boldsymbol{q}} iq \boldsymbol{u}_{\rm T,q,\sigma}\big(\hat{a}_{\boldsymbol{q}}e^{i\boldsymbol{q}\cdot\boldsymbol{r}} - \hat{a}^{\dagger}_{\boldsymbol{q}}e^{-i\boldsymbol{q}\cdot\boldsymbol{r}}\big)$. Again, in order to assure thermodynamic consistency, we assume that a finite number of relevant modes (i.e. a number that does not scale with N), parametrized by $\boldsymbol{q}_0$, acquires macroscopic occupation, i.e. $\hat{a}_{\boldsymbol{q}_0,\sigma} \sim \sqrt{N}$. Since the electron Hamiltonian does not depend on the spin operators $\hat{\boldsymbol{\sigma}}_i$, we have $[\hat{\mathcal{H}}/N, \hat{\mathcal{H}}_{\rm el-ph}/N] = 0$.

In order to prove Eq. (E.19) we only need to show that

$$[\frac{\hat{\mathcal{H}}_{\rm ph}}{N}, \frac{\hat{\mathcal{H}}_{\rm el-ph}}{N}] \to 0 \tag{E.21}$$

in the $N \to \infty$ limit.

To this end, it is convenient to rewrite the electron-photon Hamiltonian $\hat{\mathcal{H}}_{\rm el-ph}$ as a function of the real-space spin density $\hat{\boldsymbol{S}}(\boldsymbol{r})$, which is defined as following:

$$\hat{\boldsymbol{S}}(\boldsymbol{r}) \ = \ \sum_{i=1}^{N}\hat{\boldsymbol{\sigma}}_i\delta(\hat{\boldsymbol{r}}_i - \boldsymbol{r})\ . \tag{E.22}$$

Using this definition, we can rewrite Eq. (E.20) as

$$\hat{\mathcal{H}}_{\rm el-ph} \;=\; \frac{g\mu_{\rm B}}{2}\int d^3\boldsymbol{r}\;\hat{\boldsymbol{S}}(\boldsymbol{r})\cdot\hat{\boldsymbol{B}}(\boldsymbol{r})\;. \tag{E.23}$$

Exploiting the bosonic commutator $[\hat{a}_{\boldsymbol{q},\sigma},\hat{a}^{\dagger}_{\boldsymbol{q}',\sigma'}]=\delta_{\boldsymbol{q},\boldsymbol{q}'}\delta_{\sigma,\sigma'}$, we can rewrite the left-hand side of Eq. (E.21) as

$$[\frac{\hat{\mathcal{H}}_{\rm ph}}{N},\frac{\hat{\mathcal{H}}_{\rm el-ph}}{N}]=-\sum_{\boldsymbol{q},\sigma}\frac{i\hbar q\omega_{\boldsymbol{q}}g\mu_{\rm B}}{2N^2}\Big\{\int d^3\boldsymbol{r}\;\hat{\boldsymbol{S}}(\boldsymbol{r})\cdot\boldsymbol{u}_{\mathrm{T,q},\sigma}A_{\boldsymbol{q}}\big(\hat{a}_{\boldsymbol{q},\sigma}e^{i\boldsymbol{q}\cdot\boldsymbol{r}}+\hat{a}^{\dagger}_{\boldsymbol{q},\sigma}e^{-i\boldsymbol{q}\cdot\boldsymbol{r}}\big)\Big\}\;. \tag{E.24}$$

This quantity scales like $1/N$, since $\int d^3\boldsymbol{r}\;\hat{\boldsymbol{S}}(\boldsymbol{r})\sim N$, while $\sum_{\boldsymbol{q},\sigma}$ and $A_{\boldsymbol{q}}\hat{a}_{\boldsymbol{q},\sigma}$ are of order unity with respect to N.

E.3 Proof of Eq. (9.82)

The Hamiltonian in Eq. (9.78) is a quadratic form of the photonic fields. We now carry out a suitable Bogoliubov transformation, switching from the bosonic operators $\hat{a}_{\boldsymbol{q}_\parallel,1,n_z}$ and $\hat{a}^{\dagger}_{-\boldsymbol{q}_\parallel,1,n_z}$ with odd n_z to new bosonic operators $\hat{b}_{\boldsymbol{q}_\parallel,1,j}$ and $\hat{b}^{\dagger}_{-\boldsymbol{q}_\parallel,1,j}$ with integer j. Bosonic operators $\hat{a}_{\boldsymbol{q}_\parallel,1,n_z}$ and $\hat{a}^{\dagger}_{-\boldsymbol{q}_\parallel,1,n_z}$ with even mode index n_z are decoupled from matter degrees of freedom. The Bogoliubov transformation reads as following:

$$\hat{b}_{\boldsymbol{q}_\parallel,1,j}=\sum_{\ell}[X_{j,\ell}(\boldsymbol{q}_\parallel)\hat{a}_{\boldsymbol{q}_\parallel,1,2\ell+1}+Y_{j,\ell}(\boldsymbol{q}_\parallel)\hat{a}^{\dagger}_{-\boldsymbol{q}_\parallel,1,2\ell+1}]\;, \tag{E.25}$$

with ℓ,j integers. Applying the Hermitian conjugation to the expression above and replacing $\boldsymbol{q}_\parallel\to-\boldsymbol{q}_\parallel$, one has

$$\hat{b}^{\dagger}_{-\boldsymbol{q}_\parallel,1,j}=\sum_{\ell}[Y^{*}_{j,\ell}(-\boldsymbol{q}_\parallel)\hat{a}_{\boldsymbol{q}_\parallel,1,2\ell+1}X^{*}_{j,\ell}(-\boldsymbol{q}_\parallel)\hat{a}^{\dagger}_{-\boldsymbol{q}_\parallel,1,2\ell+1}]\;. \tag{E.26}$$

For every $\boldsymbol{q}_\parallel$, we can therefore write the Bogoliubov transformation in the following compact form

$$\begin{bmatrix}\{\hat{b}_{\boldsymbol{q}_\parallel,1,j}\}\\ \{\hat{b}^{\dagger}_{-\boldsymbol{q}_\parallel,1,j}\}\end{bmatrix}=\begin{bmatrix}X(\boldsymbol{q}_\parallel) & Y(\boldsymbol{q}_\parallel)\\ Y^{*}(-\boldsymbol{q}_\parallel) & X^{*}(-\boldsymbol{q}_\parallel)\end{bmatrix}\begin{bmatrix}\{\hat{a}_{\boldsymbol{q}_\parallel,1,2\ell+1}\}\\ \{\hat{a}^{\dagger}_{-\boldsymbol{q}_\parallel,1,2\ell+1}\}\end{bmatrix}\;. \tag{E.27}$$

It acts only on the photon modes with odd mode index and it is independent of the direction of the polarization vector $\boldsymbol{u}_{\boldsymbol{q}_\parallel,1}$. For this reason, we have omitted the polarization label $\sigma=1$ from the Bogoliubov transformation matrices $X(\boldsymbol{q}_\parallel)$ and $Y(\boldsymbol{q}_\parallel)$.

We would like to find $X(\boldsymbol{q}_\parallel)$ and $Y(\boldsymbol{q}_\parallel)$ such that:

$$\hat{\mathcal{H}}_{\rm ph}+\hat{\mathcal{H}}_{\rm d}=\sum_{\boldsymbol{q}_\parallel}\left[\sum_{\text{even }n_z}\hbar\omega_{\boldsymbol{q}_\parallel,n_z}\left(\hat{a}^{\dagger}_{\boldsymbol{q}_\parallel,1,n_z}\hat{a}_{\boldsymbol{q},1,n_z}+\frac{1}{2}\right)+\sum_{j}\hbar\Omega_{\boldsymbol{q}_\parallel,j}\left(\hat{b}^{\dagger}_{\boldsymbol{q}_\parallel,1,j}\hat{b}_{\boldsymbol{q},1,j}+\frac{1}{2}\right)\right]\;, \tag{E.28}$$

with a suitable choice of $\Omega_{\boldsymbol{q}_\parallel,j}$. Notice that, differently from the main text, we have restored the vacuum contribution. If (E.28) holds true, one has

$$[\hat{\mathcal{H}}_{\rm ph}+\hat{\mathcal{H}}_{\rm d},\hat{b}_{\boldsymbol{q}_\parallel,1,j}]=-\hbar\Omega_{\boldsymbol{q}_\parallel,j}\hat{b}_{\boldsymbol{q}_\parallel,1,j}\;. \tag{E.29}$$

Using Eq. (E.25) we can write Eq. (E.29) as

$$\begin{aligned}&\sum_{\ell}[\hat{\mathcal{H}}_{\rm ph}+\hat{\mathcal{H}}_{\rm d}, X_{j,\ell}(\boldsymbol{q}_\parallel)\hat{a}_{\boldsymbol{q}_\parallel,1,2\ell+1}+Y_{j,\ell}(\boldsymbol{q}_\parallel)\hat{a}^\dagger_{-\boldsymbol{q}_\parallel,1,2\ell+1}]\\ =\;& -\hbar\Omega_{\boldsymbol{q}_\parallel,j}\sum_{\ell}X_{j,\ell}(\boldsymbol{q}_\parallel)\hat{a}_{\boldsymbol{q}_\parallel,1,2\ell+1}+Y_{j,\ell}(\boldsymbol{q}_\parallel)\hat{a}^\dagger_{-\boldsymbol{q}_\parallel,1,2\ell+1}\ ,\end{aligned} \tag{E.30}$$

which is equivalent to

$$\begin{aligned}&\hbar\Omega_{\boldsymbol{q}_\parallel,j}\sum_{\ell}X_{j,\ell}(\boldsymbol{q}_\parallel)\hat{a}_{\boldsymbol{q}_\parallel,1,2\ell+1}+Y_{j,\ell}(\boldsymbol{q}_\parallel)\hat{a}^\dagger_{-\boldsymbol{q}_\parallel,1,2\ell+1}\\ =\;&\sum_{k}X_{jk}(\boldsymbol{q}_\parallel)[\hbar\omega_{\boldsymbol{q}_\parallel,2k+1}\hat{a}_{\boldsymbol{q}_\parallel,1,2k+1}+\frac{N}{m}\sum_{\ell}g_k(\boldsymbol{q}_\parallel)g_\ell(\boldsymbol{q}_\parallel)(\hat{a}_{\boldsymbol{q}_\parallel,1,2\ell+1}+\hat{a}^\dagger_{-\boldsymbol{q}_\parallel,1,2\ell+1})]\\ -\;&Y_{jk}(\boldsymbol{q}_\parallel)[\hbar\omega_{\boldsymbol{q}_\parallel,2\ell+1}\hat{a}^\dagger_{\boldsymbol{q}_\parallel,1,2k+1}+\frac{N}{m}\sum_{\ell}g_k(\boldsymbol{q}_\parallel)g_\ell(\boldsymbol{q}_\parallel)(\hat{a}_{\boldsymbol{q}_\parallel,1,2\ell+1}+\hat{a}^\dagger_{-\boldsymbol{q}_\parallel,1,2\ell+1})]\ ,\end{aligned} \tag{E.31}$$

where $g_j(\boldsymbol{q}_\parallel)=(-1)^j\sqrt{2D/\omega_{\boldsymbol{q}_\parallel,2j+1}}$. The expression above can be written compactly as

$$\left(\mathcal{K}_{\boldsymbol{q}_\parallel}-\hbar\Omega_{\boldsymbol{q}_\parallel,j}\mathbb{I}_{2N_{\rm max}}\right)\boldsymbol{v}_j(\boldsymbol{q}_\parallel)=0\ , \tag{E.32}$$

where we introduced a cutoff $N_{\rm max}$ on the number of modes in order to deal with finite-size matrices. The vector $\boldsymbol{v}_j(\boldsymbol{q}_\parallel)$ reads as following:

$$\begin{aligned}\boldsymbol{v}_j(\boldsymbol{q}_\parallel)\;=\;&[X_{j,0}(\boldsymbol{q}_\parallel)\hat{a}_{\boldsymbol{q}_\parallel,1,1},\cdots,X_{j,N_{\rm max}-1}(\boldsymbol{q}_\parallel)\hat{a}_{\boldsymbol{q}_\parallel,1,2N_{\rm max}-1},\\ &Y_{j,0}(\boldsymbol{q}_\parallel)\hat{a}^\dagger_{-\boldsymbol{q}_\parallel,1,1},\cdots,Y_{j,N_{\rm max}-1}(\boldsymbol{q}_\parallel)\hat{a}^\dagger_{-\boldsymbol{q}_\parallel,1,2N_{\rm max}-1}]^\top\ .\end{aligned} \tag{E.33}$$

The solutions of the linear-algebra problem posed by Eq. (E.32) can be found by setting to zero the determinant of the matrix $\mathcal{K}_{\boldsymbol{q}_\parallel}-\hbar\Omega_{\boldsymbol{q}_\parallel,j}\mathbb{I}_{2N_{\rm max}}$:

$$\mathrm{Det}[\mathcal{K}_{\boldsymbol{q}_\parallel}-\hbar\Omega_{\boldsymbol{q}_\parallel,j}\mathbb{I}_{2N_{\rm max}}]=0\ . \tag{E.34}$$

The calculation of this determinant is a purely mathematical issue and is postponed to Appendix E.4. The final result is reported in Eq. (E.63). Using this result and taking the $N_{\rm max}\to\infty$ limit, we find that the eigenvalues of the matrix $\mathcal{K}_{\boldsymbol{q}_\parallel}$ are the roots of the following transcendental equation:

$$1+\frac{n_{\rm 2D}}{m}\frac{2\pi e^2}{c^2}\frac{\tan\left(L_z\sqrt{\epsilon_{\rm r}\Omega_{\boldsymbol{q}_\parallel,j}{}^2/c^2-q_\parallel^2}/2\right)}{\sqrt{\epsilon_{\rm r}\Omega_{\boldsymbol{q}_\parallel,j}{}^2/c^2-q_\parallel^2}}=0\ , \tag{E.35}$$

where $n_{\rm 2D}=N/S$. Since $\mathcal{K}_{\boldsymbol{q}_\parallel}=\mathcal{K}_{-\boldsymbol{q}_\parallel}$, one has $\Omega_{\boldsymbol{q}_\parallel,j}=\Omega_{-\boldsymbol{q}_\parallel,j}$ and $\boldsymbol{v}_j(\boldsymbol{q}_\parallel)=\boldsymbol{v}_j(-\boldsymbol{q}_\parallel)$, i.e. $X(\boldsymbol{q}_\parallel)=X(-\boldsymbol{q}_\parallel)$ and $Y(\boldsymbol{q}_\parallel)=Y(-\boldsymbol{q}_\parallel)$.

Similarly to what done above, we now calculate the following commutator:

$$[\hat{\mathcal{H}}_{\rm ph}+\hat{\mathcal{H}}_{\rm d},\hat{b}^\dagger_{-\boldsymbol{q}_\parallel,1,j}]=\hbar\Omega_{-\boldsymbol{q}_\parallel,j}\hat{b}^\dagger_{-\boldsymbol{q}_\parallel,1,j}\ . \tag{E.36}$$

Using Eq. (E.26), we find

$$\begin{aligned}
&\hbar\Omega_{-\boldsymbol{q}_\parallel,j}\sum_\ell Y^*_{j,\ell}(-\boldsymbol{q}_\parallel)\hat{a}_{\boldsymbol{q}_\parallel,1,2\ell+1}+X^*_{j,\ell}(-\boldsymbol{q}_\parallel)\hat{a}^\dagger_{-\boldsymbol{q}_\parallel,1,2\ell+1}\\
=\;&\sum_k X^*_{jk}(-\boldsymbol{q}_\parallel)[\hbar\omega_{\boldsymbol{q}_\parallel,2k+1}\hat{a}^\dagger_{-\boldsymbol{q}_\parallel,1,2k+1}+\frac{N}{m}\sum_\ell g_k(\boldsymbol{q}_\parallel)g_\ell(\boldsymbol{q}_\parallel)(\hat{a}_{\boldsymbol{q}_\parallel,1,2\ell+1}+\hat{a}^\dagger_{-\boldsymbol{q}_\parallel,1,2\ell+1})]\\
-\;&Y^*_{jk}(-\boldsymbol{q}_\parallel)[\hbar\omega_{\boldsymbol{q}_\parallel,2\ell+1}\hat{a}_{\boldsymbol{q}_\parallel,1,2k+1}+\frac{N}{m}\sum_\ell g_k(\boldsymbol{q}_\parallel)g_\ell(\boldsymbol{q}_\parallel)(\hat{a}_{\boldsymbol{q}_\parallel,1,2\ell+1}+\hat{a}^\dagger_{-\boldsymbol{q}_\parallel,1,2\ell+1})]\;. \qquad \text{(E.37)}
\end{aligned}$$

The expression above can be written as

$$[\mathcal{K}_{\boldsymbol{q}_\parallel}-\hbar\Omega_{-\boldsymbol{q}_\parallel,j}\mathbb{I}_{2N_{\max}}]\boldsymbol{v}^*_j(-\boldsymbol{q}_\parallel)=0\;, \qquad \text{(E.38)}$$

where $\Omega_{-\boldsymbol{q}_\parallel,j}=\Omega_{\boldsymbol{q}_\parallel,j}$. Since this eigenvalue problem is identical to Eq. (E.32), one has $\boldsymbol{v}^*_j(-\boldsymbol{q}_\parallel)=\boldsymbol{v}_j(\boldsymbol{q}_\parallel)$, i.e. $X(\boldsymbol{q}_\parallel)=X^*(-\boldsymbol{q}_\parallel)$ and $Y(\boldsymbol{q}_\parallel)=Y^*(-\boldsymbol{q}_\parallel)$.

Because of the properties of the matrices $X(\boldsymbol{q}_\parallel)$ and $Y(\boldsymbol{q}_\parallel)$, i.e. $X(\boldsymbol{q}_\parallel)=X^*(-\boldsymbol{q}_\parallel)=X(-\boldsymbol{q}_\parallel)$ and $Y(\boldsymbol{q}_\parallel)=Y^*(-\boldsymbol{q}_\parallel)=Y(-\boldsymbol{q}_\parallel)$, we can write

$$\begin{bmatrix}\{\hat{b}_{\boldsymbol{q}_\parallel,1,j}\}\\ \{\hat{b}^\dagger_{-\boldsymbol{q}_\parallel,1,j}\}\end{bmatrix}=\begin{bmatrix}X(\boldsymbol{q}_\parallel) & Y(\boldsymbol{q}_\parallel)\\ Y(\boldsymbol{q}_\parallel) & X(\boldsymbol{q}_\parallel)\end{bmatrix}\begin{bmatrix}\{\hat{a}_{\boldsymbol{q}_\parallel,1,2\ell+1}\}\\ \{\hat{a}^\dagger_{-\boldsymbol{q}_\parallel,1,2\ell+1}\}\end{bmatrix}\;. \qquad \text{(E.39)}$$

Imposing the bosonic commutation rules, $[\hat{b}_{\boldsymbol{q}_\parallel,1,j},\hat{b}^\dagger_{\boldsymbol{q}'_\parallel,1,j'}]=\delta_{\boldsymbol{q}_\parallel,\boldsymbol{q}'_\parallel}\delta_{j,j'}$ and $[\hat{b}_{\boldsymbol{q}_\parallel,1,j},\hat{b}_{\boldsymbol{q}'_\parallel,1,j'}]=0$, we obtain the following properties

$$X(\boldsymbol{q}_\parallel)X^\top(\boldsymbol{q}_\parallel)-Y(\boldsymbol{q}_\parallel)Y^\top(\boldsymbol{q}_\parallel)=\mathbb{I}\;, \qquad \text{(E.40)}$$

and

$$X(\boldsymbol{q}_\parallel)Y^\top(\boldsymbol{q}_\parallel)-Y(\boldsymbol{q}_\parallel)X^\top(\boldsymbol{q}_\parallel)=0\;. \qquad \text{(E.41)}$$

By using the properties above, it is easy to obtain the inverse Bogoliubov transformation

$$\begin{bmatrix}\{\hat{a}_{\boldsymbol{q}_\parallel,1,2\ell+1}\}\\ \{\hat{a}^\dagger_{-\boldsymbol{q}_\parallel,1,2\ell+1}\}\end{bmatrix}=\begin{bmatrix}X^\top(\boldsymbol{q}_\parallel) & -Y^\top(\boldsymbol{q}_\parallel)\\ -Y^\top(\boldsymbol{q}_\parallel) & X^\top(\boldsymbol{q}_\parallel)\end{bmatrix}\begin{bmatrix}\{\hat{b}_{\boldsymbol{q}_\parallel,1,j}\}\\ \{\hat{b}^\dagger_{-\boldsymbol{q}_\parallel,1,j}\}\end{bmatrix}\;. \qquad \text{(E.42)}$$

In terms of the new bosonic operators $\hat{b}^\dagger_{\boldsymbol{q}_\parallel,1,j},\hat{b}_{\boldsymbol{q}_\parallel,1,j}$, the effective Hamiltonian reads as following:

$$\begin{aligned}
\hat{\mathcal{H}}^{\text{eff}}_{\text{ph}}\;[\psi]=\langle\psi|\hat{\mathcal{H}}_{\text{2D}}|\psi\rangle+\sum_{\boldsymbol{q}_\parallel}\Bigg\{&\sum_{\text{even }n_z}\hbar\omega_{\boldsymbol{q}_\parallel,n_z}\left(\hat{a}^\dagger_{\boldsymbol{q}_\parallel,1,n_z}\hat{a}_{\boldsymbol{q},1,n_z}+\frac{1}{2}\right)\\
+\;&\sum_j\hbar\Omega_{\boldsymbol{q}_\parallel,j}\left(\hat{b}^\dagger_{\boldsymbol{q}_\parallel,1,j}\hat{b}_{\boldsymbol{q},1,j}+\frac{1}{2}\right)+\mathcal{J}_{\boldsymbol{q}_\parallel,1}\sum_{j,\ell}g_\ell(\boldsymbol{q}_\parallel)\left(\hat{b}^\dagger_{\boldsymbol{q}_\parallel,1,j}+\hat{b}_{-\boldsymbol{q}_\parallel,1,j}\right)\left[X_{j\ell}(\boldsymbol{q}_\parallel)-Y_{j\ell}(\boldsymbol{q}_\parallel)\right]\Bigg\}\;.
\end{aligned} \qquad \text{(E.43)}$$

The previous Hamiltonian can be written in a form that is manifestly Hermitian:

$$\begin{aligned}
\hat{\mathcal{H}}^{\text{eff}}_{\text{ph}}\;[\psi]=\langle\psi|\hat{\mathcal{H}}_{\text{2D}}|\psi\rangle+\sum_{\boldsymbol{q}_\parallel,1}\Bigg\{&\sum_{\text{even }n_z}\hbar\omega_{\boldsymbol{q}_\parallel,n_z}\left(\hat{a}^\dagger_{\boldsymbol{q}_\parallel,1,n_z}\hat{a}_{\boldsymbol{q},1,n_z}+\frac{1}{2}\right)\\
+\;&\sum_j\hbar\Omega_{\boldsymbol{q}_\parallel,j}\left(\hat{b}^\dagger_{\boldsymbol{q}_\parallel,1,j}\hat{b}_{\boldsymbol{q},1,j}+\frac{1}{2}\right)+\left[\mathcal{J}_{\boldsymbol{q}_\parallel,1}\sum_{j,\ell}g_\ell(\boldsymbol{q}_\parallel)\hat{b}^\dagger_{\boldsymbol{q}_\parallel,1,j}\left[X_{j\ell}(\boldsymbol{q}_\parallel)-Y_{j\ell}(\boldsymbol{q}_\parallel)\right]+\text{H.c.}\right]\Bigg\}\;.
\end{aligned} \qquad \text{(E.44)}$$

In the effective Hamiltonian above, the even photon modes are independent of the light-matter interaction, while the odd photon modes are renormalized by the diamagnetic term and expressed as a sum of displaced harmonic oscillators. For every matter state $|\psi\rangle$, the ground state $|\Phi\rangle$ of $\hat{\mathcal{H}}^{\rm eff}_{\rm ph}[\psi]$ is therefore a tensor product $|\mathscr{B}\rangle \equiv \otimes_{\boldsymbol{q}_\parallel,j} |\beta_{\boldsymbol{q}_\parallel,1,j}\rangle$ of coherent states of the $\hat{b}_{\boldsymbol{q}_\parallel,1,j}$ operators, i.e. $\hat{b}_{\boldsymbol{q}'_\parallel,1,\ell}\,|\mathscr{B}\rangle = \beta_{\boldsymbol{q}'_\parallel,1,\ell}\,|\mathscr{B}\rangle$.

We now introduce the following energy functional, obtained by taking the expectation value of $\hat{\mathcal{H}}^{\rm eff}_{\rm ph}[\psi]$ over $|\mathscr{B}\rangle$: $E[\{\beta_{\boldsymbol{q}_\parallel,1,j}\},\psi] \equiv \langle\Psi|\hat{\mathcal{H}}_{\boldsymbol{A}}|\Psi\rangle = \langle\mathscr{B}|\hat{\mathcal{H}}^{\rm eff}_{\rm ph}[\psi]|\mathscr{B}\rangle$:

$$\begin{aligned} E[\{\beta_{\boldsymbol{q}_\parallel,1,j}\},\psi] &= \langle\psi|\mathcal{H}_{\rm 2D}|\psi\rangle + \sum_{\boldsymbol{q}_\parallel,j}\Big[\hbar\Omega_{\boldsymbol{q}_\parallel,j}\big(\beta^*_{\boldsymbol{q}_\parallel,1,j}\beta_{\boldsymbol{q}_\parallel,1,j}+\frac{1}{2}\big) \\ &+ \mathcal{J}(\boldsymbol{q}_\parallel,1)(\beta^*_{\boldsymbol{q}_\parallel,1,j}+\beta_{-\boldsymbol{q}_\parallel,1,j})\sum_\ell g_\ell(\boldsymbol{q}_\parallel)(X_{j\ell}(\boldsymbol{q}_\parallel)-Y_{j\ell}(\boldsymbol{q}_\parallel))\Big]\ . \end{aligned} \tag{E.45}$$

We now observe that the order parameter $\alpha_{\boldsymbol{q}_\parallel,1,2\ell+1}$ introduced in the main text is linearly-dependent on $\beta_{\boldsymbol{q}_\parallel,1,j}$, i.e.

$$\begin{bmatrix}\{\alpha_{\boldsymbol{q}_\parallel,1,2\ell+1}\}\\ \{\alpha^*_{-\boldsymbol{q}_\parallel,1,2\ell+1}\}\end{bmatrix} = \begin{bmatrix}X^\top(\boldsymbol{q}_\parallel) & -Y^\top(\boldsymbol{q}_\parallel)\\ -Y^\top(\boldsymbol{q}_\parallel) & X^\top(\boldsymbol{q}_\parallel)\end{bmatrix}\begin{bmatrix}\{\beta_{\boldsymbol{q}_\parallel,1,j}\}\\ \{\beta^*_{-\boldsymbol{q}_\parallel,1,j}\}\end{bmatrix}\ . \tag{E.46}$$

By using the linear relation above, we can express the energy functional $E[\{\beta_{\boldsymbol{q}_\parallel,1,j}\},\psi]$ in terms of $\{\alpha_{\boldsymbol{q}_\parallel,1,j}\}$. Carrying out such procedure and neglecting the vacuum energy, we finally obtain Eq. (9.82) of the main text.

E.4 Calculation of the determinant in Eq. (E.34)

In this Appendix we calculate the determinant in the left-hand side of Eq. (E.34). To this end, it is useful to write the matrix $\mathcal{K}_{\boldsymbol{q}_\parallel} - \hbar\Omega_{\boldsymbol{q}_\parallel,j}\mathbb{I}_{2N_{\rm max}}$ defined in Eq. (E.32) in the following block form:

$$\mathcal{K}_{\boldsymbol{q}_\parallel} - \hbar\Omega_{\boldsymbol{q}_\parallel,j}\mathbb{I}_{2N_{\rm max}} = \begin{bmatrix}Q(\boldsymbol{q}_\parallel)+V(\boldsymbol{q}_\parallel)-\hbar\Omega_{\boldsymbol{q}_\parallel,j}\mathbb{I}_{N_{\rm max}} & -V(\boldsymbol{q}_\parallel)\\ V(\boldsymbol{q}_\parallel) & -Q(\boldsymbol{q}_\parallel)-V(\boldsymbol{q}_\parallel)-\hbar\Omega_{\boldsymbol{q}_\parallel,j}\mathbb{I}_{N_{\rm max}}\end{bmatrix}\ , \tag{E.47}$$

where

$$Q_{k,\ell}(\boldsymbol{q}_\parallel) = \hbar\omega_{\boldsymbol{q}_\parallel,2\ell+1}\delta_{k,\ell} \tag{E.48}$$

and

$$V_{k,\ell}(\boldsymbol{q}_\parallel) = \frac{N}{m}g_k(\boldsymbol{q}_\parallel)g_\ell(\boldsymbol{q}_\parallel)\ . \tag{E.49}$$

Carrying out simple algebraic manipulations, we find

$$\mathcal{K}_{\boldsymbol{q}_\parallel} - \hbar\Omega_{\boldsymbol{q}_\parallel,j}\mathbb{I}_{2N_{\rm max}} = [\mathbb{I}_{2N_{\rm max}}+\mathcal{W}(\boldsymbol{q}_\parallel)]\begin{bmatrix}Q(\boldsymbol{q}_\parallel)-\hbar\Omega_{\boldsymbol{q}_\parallel,j}\mathbb{I}_{N_{\rm max}} & 0\\ 0 & -Q(\boldsymbol{q}_\parallel)-\hbar\Omega_{\boldsymbol{q}_\parallel,j}\mathbb{I}_{N_{\rm max}}\end{bmatrix}\ , \tag{E.50}$$

where

$$\mathcal{W}(\boldsymbol{q}_\parallel) = \begin{bmatrix}\mathcal{W}_-(\boldsymbol{q}_\parallel) & \mathcal{W}_+(\boldsymbol{q}_\parallel)\\ \mathcal{W}_-(\boldsymbol{q}_\parallel) & \mathcal{W}_+(\boldsymbol{q}_\parallel)\end{bmatrix} \tag{E.51}$$

and

$$\mathcal{W}_\pm(\boldsymbol{q}_\parallel) = V(\boldsymbol{q}_\parallel)\Big(\pm\hbar\Omega_{\boldsymbol{q}_\parallel,j}\mathbb{I}_{N_{\rm max}}+Q(\boldsymbol{q}_\parallel)\Big)^{-1}\ . \tag{E.52}$$

Using the expressions above, we can write the determinant at hand as

$$\mathrm{Det}[\mathcal{K}_{\boldsymbol{q}_\parallel} - \hbar\Omega_{\boldsymbol{q}_\parallel,j}\mathbb{I}_{2N_{\max}}] = \prod_\ell [(\hbar\Omega_{\boldsymbol{q}_\parallel,j})^2 - (\hbar\omega_{\boldsymbol{q}_\parallel,2\ell+1})^2]\mathrm{Det}[\mathbb{I}_{2N_{\max}} + \mathcal{W}(\boldsymbol{q}_\parallel)] \ . \tag{E.53}$$

We now focus on $\mathrm{Det}[\mathbb{I}_{2N_{\max}} + \mathcal{W}(\boldsymbol{q}_\parallel)]$ and use the following well-known algebraic property,

$$\mathrm{Det}[\mathbb{I}_{2N_{\max}} + \mathcal{W}(\boldsymbol{q}_\parallel)] = \exp\{\mathrm{Tr}[\ln(\mathbb{I}_{2N_{\max}} + \mathcal{W}(\boldsymbol{q}_\parallel)]\} \ . \tag{E.54}$$

The trace in the right-hand side of the previous equation can be written as

$$\mathrm{Tr}[\ln(\mathbb{I}_{2N_{\max}} + \mathcal{W}(\boldsymbol{q}_\parallel)] = \sum_{j=1}^{\infty} \frac{(-1)^{j-1}}{j}\mathrm{Tr}[\mathcal{W}^j(\boldsymbol{q}_\parallel)] \ . \tag{E.55}$$

For block matrices, the following property holds true:

$$\mathrm{Tr}\left\{\begin{bmatrix} A & B \\ A & B \end{bmatrix}\begin{bmatrix} C & D \\ C & D \end{bmatrix}\right\} = \mathrm{Tr}\{(A+B)(C+D)\} \ . \tag{E.56}$$

We therefore have

$$\mathrm{Tr}[\mathcal{W}^j(\boldsymbol{q}_\parallel)] = \mathrm{Tr}\{[\mathcal{W}_+(\boldsymbol{q}_\parallel) + \mathcal{W}_-(\boldsymbol{q}_\parallel)]^j\} \ . \tag{E.57}$$

Furthermore, it is possible to show that

$$\mathrm{rank}[\mathcal{W}_+(\boldsymbol{q}_\parallel) + \mathcal{W}_-(\boldsymbol{q}_\parallel)] = 1 \ . \tag{E.58}$$

The previous property of the matrix $\mathcal{W}_+(\boldsymbol{q}_\parallel) + \mathcal{W}_-(\boldsymbol{q}_\parallel)$ can be proved by direct inspection, showing that all the columns of $\mathcal{W}_+(\boldsymbol{q}_\parallel)+\mathcal{W}_-(\boldsymbol{q}_\parallel)$ can be obtained, for example, by multiplying the first column for a suitable constant.

We therefore conclude that $\mathcal{W}_+(\boldsymbol{q}_\parallel) + \mathcal{W}_-(\boldsymbol{q}_\parallel)$ has only one non-zero eigenvalue. As a consequence, we find that

$$\mathrm{Tr}[\mathcal{W}^j(\boldsymbol{q}_\parallel)] = \mathrm{Tr}\{\mathcal{W}_+(\boldsymbol{q}_\parallel) + \mathcal{W}_-(\boldsymbol{q}_\parallel)]^j\} = \mathrm{Tr}[(\mathcal{W}_+(\boldsymbol{q}_\parallel) + \mathcal{W}_-(\boldsymbol{q}_\parallel)]^j = \mathrm{Tr}[\mathcal{W}(\boldsymbol{q}_\parallel)]^j \ . \tag{E.59}$$

Replacing this result in Eq. (E.55), we therefore find that

$$\mathrm{Tr}\{\ln[\mathbb{I}_{2N_{\max}} + \mathcal{W}(\boldsymbol{q}_\parallel)]\} = \sum_{j=1}^{\infty} \frac{(-1)^{j-1}}{j}\mathrm{Tr}[\mathcal{W}(\boldsymbol{q}_\parallel)]^j = \ln(1 + \mathrm{Tr}[\mathcal{W}(\boldsymbol{q}_\parallel)]) \ , \tag{E.60}$$

where

$$\begin{aligned} \mathrm{Tr}[\mathcal{W}(\boldsymbol{q}_\parallel)] = \mathrm{Tr}[\mathcal{W}_+(\boldsymbol{q}_\parallel) + \mathcal{W}_+(\boldsymbol{q}_\parallel)] &= \sum_{\ell=0}^{N_{\max}-1} \frac{2\omega_{\boldsymbol{q}_\parallel,2\ell+1} N g_\ell^2(\boldsymbol{q}_\parallel)}{m\hbar(\omega^2_{\boldsymbol{q}_\parallel,2\ell+1} - \Omega^2)} \\ &= \sum_{\ell=0}^{N_{\max}-1} \frac{4DN}{m\hbar(\omega^2_{\boldsymbol{q}_\parallel,2\ell+1} - \Omega^2_{\boldsymbol{q}_\parallel,j})} \ . \end{aligned} \tag{E.61}$$

Replacing Eq. (E.61) in Eq. (E.54), we find

$$\begin{aligned} \mathrm{Det}[\mathbb{I}_{2N_{\max}} + \mathcal{W}_{\boldsymbol{q}_\parallel}] &= 1 + \sum_{\ell=0}^{N_{\max}-1} \frac{4DN}{m\hbar(\omega^2_{\boldsymbol{q}_\parallel,2\ell+1} - \Omega^2_{\boldsymbol{q}_\parallel,j})} \\ &= 1 + \frac{n_{2\mathrm{D}}}{m}\frac{2\pi e^2}{c^2}\frac{\tan\left(L_z\sqrt{\epsilon_{\mathrm{r}}\Omega^2/c^2 - q_\parallel^2}/2\right)}{\sqrt{\epsilon_{\mathrm{r}}\Omega_{\boldsymbol{q}_\parallel,j}{}^2/c^2 - q_\parallel^2}} \ . \end{aligned} \tag{E.62}$$

In the last equality we have used that $\sum_\ell[(2\ell+1)^2-x^2]^{-1}=\pi\tan(\pi x/2)/(4x)$ and the limit $N_{\rm max}\to\infty$ has been taken. In summary, the final desired result is:

$$\begin{aligned}\mathrm{Det}[\mathcal{K}_{\boldsymbol{q}_\parallel}-\hbar\Omega_{\boldsymbol{q}_\parallel,j}\mathbb{I}_{2N_{\rm max}}] &= \prod_\ell[(\hbar\Omega_{\boldsymbol{q}_\parallel,j})^2-(\hbar\omega_{\boldsymbol{q}_\parallel,2\ell+1})^2]\times \\ &\times \left[1+\frac{n_{2D}}{m}\frac{2\pi e^2}{c^2}\frac{\tan\left(L_z\sqrt{\epsilon_{\rm r}{\Omega_{\boldsymbol{q}_\parallel,j}}^2/c^2-q_\parallel^2}/2\right)}{\sqrt{\epsilon_{\rm r}{\Omega_{\boldsymbol{q}_\parallel,j}}^2/c^2-q_\parallel^2}}\right] . \quad \text{(E.63)}\end{aligned}$$

E.5 Calculation of the determinant in Eq. (9.94)

In this Appendix we calculate the determinant of the matrix $\mathcal{M}_{\boldsymbol{q}_\parallel}$ defined in Eq. (9.93). To this end, it is useful to write $\mathcal{M}_{\boldsymbol{q}_\parallel}$ in the following block form:

$$\mathcal{M}_{\boldsymbol{q}_\parallel}=\begin{bmatrix}\mathcal{M}^{(x)}_{\boldsymbol{q}_\parallel} & 0\\ 0 & \mathcal{M}^{(y)}_{\boldsymbol{q}_\parallel}\end{bmatrix} , \quad \text{(E.64)}$$

where

$$\mathcal{M}^{(x)}_{\boldsymbol{q}_\parallel}=Q(\boldsymbol{q}_\parallel)+U(\boldsymbol{q}_\parallel) , \quad \text{(E.65)}$$

$$\mathcal{M}^{(y)}_{\boldsymbol{q}_\parallel}=Q(\boldsymbol{q}_\parallel) , \quad \text{(E.66)}$$

$Q(\boldsymbol{q}_\parallel)$ has been defined in Eq. (E.48), and

$$U_{k,\ell}(\boldsymbol{q}_\parallel)=\frac{2S\chi^{\rm J}_{\rm T}(q_\parallel,0)}{m}g_k(\boldsymbol{q}_\parallel)g_\ell(\boldsymbol{q}_\parallel) . \quad \text{(E.67)}$$

By exploiting the block decomposition, the determinant of $\mathcal{M}_{\boldsymbol{q}_\parallel}$ can be expressed as

$$\Delta_{\boldsymbol{q}_\parallel}=\mathrm{Det}(\mathcal{M}_{\boldsymbol{q}_\parallel})=\mathrm{Det}(\mathcal{M}^{(x)}_{\boldsymbol{q}_\parallel})\mathrm{Det}(\mathcal{M}^{(y)}_{\boldsymbol{q}_\parallel}) , \quad \text{(E.68)}$$

where

$$\mathrm{Det}(\mathcal{M}^{(y)}_{\boldsymbol{q}_\parallel})=\prod_{\ell=0}^{N_{\rm max}-1}\hbar\omega_{\boldsymbol{q}_\parallel,2\ell+1} . \quad \text{(E.69)}$$

Carrying out simple algebraic manipulations, we find

$$\mathcal{M}^{(x)}_{\boldsymbol{q}_\parallel}=[\mathbb{I}_{N_{\rm max}}+U(\boldsymbol{q}_\parallel)Q^{-1}(\boldsymbol{q}_\parallel)]Q(\boldsymbol{q}_\parallel) . \quad \text{(E.70)}$$

The expression of $\mathrm{Det}[\mathcal{M}_{\boldsymbol{q}_\parallel}]$ can be further simplified as

$$\Delta_{\boldsymbol{q}_\parallel}=\mathrm{Det}[\mathbb{I}_{N_{\rm max}}+U(\boldsymbol{q}_\parallel)Q^{-1}(\boldsymbol{q}_\parallel)]\prod_{\ell=0}^{N_{\rm max}-1}[\hbar\omega_{\boldsymbol{q}_\parallel,2\ell+1}]^2 . \quad \text{(E.71)}$$

It is easy to verify that each column of matrix $U(\boldsymbol{q}_\parallel)Q^{-1}(\boldsymbol{q}_\parallel)$ can be obtained by multiplying the first column for a suitable constant: this implies that $\mathrm{rank}[U(\boldsymbol{q}_\parallel)Q^{-1}(\boldsymbol{q}_\parallel)]=1$. Using this property, and following the same procedure discussed in the Appendix E.4, we have

$$\begin{aligned}\mathrm{Det}[\mathbb{I}_{N_{\rm max}}+W_{\boldsymbol{q}_\parallel}] &= 1+\mathrm{Tr}[U(\boldsymbol{q}_\parallel)Q^{-1}(\boldsymbol{q}_\parallel)]=1+\frac{2S\chi^{\rm J}_{\rm T}(q_\parallel,0)}{m}\sum_{\ell=0}^{N_{\rm max}-1}\frac{g^2_\ell(\boldsymbol{q}_\parallel)}{\hbar\omega_{\boldsymbol{q}_\parallel,2\ell+1}} \\ &= 1+\frac{4S\chi^{\rm J}_{\rm T}(q_\parallel,0)D}{m\hbar}\sum_{\ell=0}^{N_{\rm max}-1}\frac{1}{\omega^2_{\boldsymbol{q}_\parallel,2\ell+1}} . \quad \text{(E.72)}\end{aligned}$$

Taking the limit $N_{\max} \to \infty$, we find

$$\mathrm{Det}[\mathbb{I}_{N_{\max}} + W_{\boldsymbol{q}_\parallel}] = 1 + \chi_{\mathrm{T}}^{\mathrm{J}}(q_\parallel, 0)\frac{2\pi e^2}{c^2 q_\parallel}\tanh\left(\frac{q_\parallel L_z}{2}\right) . \tag{E.73}$$

In summary, the determinant of the matrix $\mathcal{M}_{\boldsymbol{q}_\parallel}$ is given by

$$\Delta_{\boldsymbol{q}_\parallel} = \left[1 + \chi_{\mathrm{T}}^{\mathrm{J}}(q_\parallel, 0)\frac{2\pi e^2}{c^2 q_\parallel}\tanh\left(\frac{q_\parallel L_z}{2}\right)\right]\prod_\ell [\hbar\omega_{\boldsymbol{q}_\parallel, 2\ell+1}]^2 , \tag{E.74}$$

as in Eq. (9.94) of the main text.

References

[1] J.P. Dowling and G.J. Milburn, Phil. Trans. R. Soc. A **361**, 3655 (2003).

[2] M. Planck, Verhandl. Dtsch. phys. Ges. **2**, 237 (1900).

[3] M.A. Nielsen and I.L. Chuang, *Quantum Computation and Quantum Information* (Cambridge University Press, Cambridge, England, 2000).

[4] P.W. Shor, Proceedings of the 35th Annual Symposium on the Foundations of Computer Science (IEEE Computer Society Press, Los Alamitos, CA), p. 124, (1994).

[5] F. Arute et al., Nature **574**, 505 (2019).

[6] J. Cirac and P. Zoller, Nat. Phys. **8**, 264-266 (2012).

[7] I.M. Georgescu, S. Ashhab, and F. Nori, Rev. Mod. Phys. **86**, 153 (2014).

[8] V. Giovannetti, S. Lloyd, and L. Maccone, Nature Photonics **5**, 222 (2011).

[9] L. Pezzè, A. Smerzi, M.K. Oberthaler, R. Schmied, and P. Treutlein, Rev. Mod. Phys. **90**, 035005 (2018).

[10] E. Fermi, *Thermodynamics*, (Dover, 1956).

[11] R. Uzdin, A. Levy, and R. Kosloff, Phys. Rev. X **5**, 031044 (2015).

[12] M. Campisi and R. Fazio, J. Phys. A: Math. Theor. **49**, 345002 (2016).

[13] B. Karimi and J.P. Pekola, Phys. Rev. B **94**, 184503 (2016).

[14] G. Marchegiani, P. Virtanen, F. Giazotto, and M. Campisi, Phys. Rev. Applied **6**, 054014 (2016).

[15] A.Ü.C. Hardal and Ö.E. Müstecaplioğlu, Sci. Rep. **5**, 12953 (2015).

[16] M.N. Bera, A. Riera, M. Lewenstein and A. Winter, Nat. Comm. **8**, 2180 (2017).

[17] M.N. Bera, A. Riera, M. Lewenstein, and A. Winter, Quantum **3**, 121 (2019).

[18] M. Perarnau-Llobet, H. Wilming, A. Riera, R. Gallego, and J. Eisert, Phys. Rev. Lett. **120**, 120602 (2018).

[19] B. Karimi and J. P. Pekola and M. Campisi and R. Fazio, Quantum Sci. Technol. **2**, 044007 (2017).

[20] R. Alicki and M. Fannes, Phys. Rev. E **87**, 042123 (2013).

[21] K.V. Hovhannisyan, M. Perarnau-Llobet, M. Huber, and A. Acín, Phys. Rev. Lett. **111**, 240201 (2013).

[22] F.C. Binder, S. Vinjanampathy, K. Modi, and J. Goold, New J. Phys. **17**, 075015 (2015).

[23] F. Campaioli, F.A. Pollock, F.C. Binder, L. Céleri, J. Goold, S. Vinjanampathy, and K. Modi, Phys. Rev. Lett. **118**, 150601 (2017).

[24] D. Ferraro, M. Campisi, G.M. Andolina, V. Pellegrini, and M. Polini, Phys. Rev. Lett. **120**, 117702 (2018).

[25] R.H. Dicke, Phys. Rev. **93**, 99 (1954).

[26] G.M. Andolina, M. Keck, A. Mari, M. Campisi, V. Giovannetti, and M. Polini, Phys. Rev. Lett. **122**, 047702 (2019).

[27] G.M. Andolina, M. Keck, A. Mari, V. Giovannetti, and M. Polini, Phys. Rev. B **99**, 205437 (2019).

[28] D. Rossini, G.M. Andolina, D. Rosa, M. Carrega, and M. Polini, Phys. Rev. Lett. **125**, 236402 (2020).

[29] S. Sachdev and J. Ye, Phys. Rev. Lett. **70**, 3339 (1993).

[30] A.Y. Kitaev, Talks at KITP, University of California, Santa Barbara (USA), Entanglement in Strongly Correlated Quantum Matter (2015).

[31] K. Hepp and E.H. Lieb, Ann. Phys. **76**, 360 (1973) and Phys. Rev. A **8**, 2517 (1973).

[32] Y. Kaluzny, P. Goy, M. Gross, J. M. Raimond, and S. Haroche, Phys. Rev. Lett. **51**, 1175 (1983).

[33] M. Gross and S. Haroche, Phys. Rep. **93**, 301 (1982).

[34] S. Haroche, Rev. Mod. Phys. **85**, 1083 (2013).

[35] S. Haroche and J.M. Raimond, *Exploring the Quantum: Atoms, Cavities, and Photons* (Oxford University Press, 2006).

[36] A.F. Kockum, A. Miranowicz, S. De Liberato, S. Savasta, and F. Nori, Nat. Rev. Phys. **1**, 19 (2019).

[37] C. Emary and T. Brandes, Phys. Rev. Lett. **90**, 044101 (2003) and Phys. Rev. E **67**, 066203 (2003).

[38] Y.K. Wang and F.T. Hioe, Phys. Rev. A **7**, 831 (1973).

[39] K. Rzażewski, K. Wódkiewicz, and W. Żakowicz, Phys. Rev. Lett. **35**, 432 (1975); I. Bialynicki-Birula and K. Rzążewski, Phys. Rev. A **19**, 301 (1979); K. Gawędzki and K. Rzążewski, Phys. Rev. A **23**, 2134 (1981).

[40] P. Nataf and C. Ciuti, Nat. Comm. **1**, 72 (2010).

[41] G.M. Andolina, F.M.D. Pellegrino, V. Giovannetti, A.H. MacDonald, and M. Polini, Phys. Rev. B **100**, 121109(R) (2019).

[42] G.M. Andolina, F.M.D. Pellegrino, V. Giovannetti, A.H. MacDonald, and M. Polini, Phys. Rev. B **102**, 125137 (2020).

[43] A.E. Allahverdyan, R. Balian, and T.M. Nieuwenhuizen, Europhys. Lett. **67**, 565 (2004).

[44] A. Lenard, J. Stat. Phys. **19**, 575 (1978).

[45] W. Pusz and S.L. Woronowicz, Comm. Math. Phys. **58**, 273 (1978).

[46] D. Farina, G.M. Andolina, A. Mari, M. Polini, and V. Giovannetti, Phys. Rev. B **99**, 035421 (2019).

[47] A. Serafini, *Quantum Continuous Variables: A Primer of Theoretical Methods* (CRC Press, Boca Raton, FL, 2017).

[48] T.P. Le, J. Levinsen, K. Modi, M.M. Parish, and F.A. Pollock, Phys. Rev. A **97**, 022106 (2018).

[49] G.M. Andolina, D. Farina, A. Mari, V. Pellegrini, V. Giovannetti, and M. Polini, Phys. Rev. B **98**, 205423 (2018).

[50] Y.-Y. Zhang, T.-R. Yang, L. Fu, and X. Wang, Phys. Rev. E **99**, 052106 (2019).

[51] X. Zhang and M. Blaauboer, arXiv:1812.10139.

[52] F. Barra, Phys. Rev. Lett. **122**, 210601 (2019).

[53] D. Rossini, G.M. Andolina, and M. Polini, Phys. Rev. B **100**, 115142 (2019).

[54] S. Ghosh, T. Chanda, and A. Sen De, Phys. Rev. A **101**, 032115 (2020).

[55] A.C. Santos, B. Çakmak, S. Campbell, and N.T. Zinner, Phys. Rev. E **100**, 032107 (2019).

[56] F. Pirmoradian and K. Mølmer, Phys. Rev. A **100**, 043833 (2019).

[57] J. Chen, L. Zhan, L. Shao, X. Zhang, Y. Zhang, and X. Wang, Ann. Phys. (Berlin) **532**, 1900487 (2020).

[58] J. Monsel, M. Fellous-Asiani, B. Huard, and A. Auffèves, Phys. Rev. Lett. **124**, 130601 (2020).

[59] F. Caravelli, G. Coulter-De Wit, L.P. Garcia-Pintos, and A. Hamma, Phys. Rev. Research **2**, 023095 (2020).

[60] L.P. García-Pintos, A. Hamma, and A. del Campo, Phys. Rev. Lett. **125**, 040601 (2020).

[61] S. Gherardini, F. Campaioli, F. Caruso, and F. C. Binder, Phys. Rev. Research **2**, 013095 (2020).

[62] F.H. Kamin, F.T. Tabesh, S. Salimi, and F. Kheirandish, New J. Phys. **22**, 083007 (2020).

[63] S. Juliá-Farrè, T. Salamon, A. Riera, M.N. Bera, and M. Lewenstein, Phys. Rev. Research **2**, 023113 (2020).

[64] K. Cong, Q. Zhang, Y. Wang, G.T. Noe II, A. Belyanin, and J. Kono, J. Opt. Soc. Am. B **33**, C80 (2016).

[65] P. Kirton, M.M. Roses, J. Keeling, and E.G. Dalla Torre, Adv. Quantum Technol. **2**, 1970013 (2019).

[66] A.A. Anappara, S. De Liberato, A. Tredicucci, C. Ciuti, G. Biasiol, L. Sorba, and F. Beltram, Phys. Rev. B **79**, 201303 (2009).

[67] T. Niemczyk, F. Deppe, H. Huebl, E. P. Menzel, F. Hocke, M. J. Schwarz, J. J. Garcia-Ripoll, D. Zueco, T. Hümmer, E. Solano, A. Marx, and R. Gross, Nat. Phys. **6**, 772 (2010).

[68] A. Bayer, M. Pozimski, S. Schambeck, D. Schuh, R. Huber, D. Bougeard, and C. Lange, Nano Lett. **17**, 6340 (2017).

[69] G. Chen, Z. Chen, and J. Liang, Phys. Rev. A **76**, 055803 (2007).

[70] P. Nataf and C. Ciuti, Phys. Rev. Lett. **104**, 023601 (2010).

[71] D. Hagenmüller and C. Ciuti, Phys. Rev. Lett. **109**, 267403 (2012).

[72] G. Mazza and A. Georges, Phys. Rev. Lett. **122**, 017401 (2019).

[73] O. Viehmann, J. von Delft, and F. Marquardt, Phys. Rev. Lett. **107**, 113602 (2011).

[74] L. Chirolli, M. Polini, V. Giovannetti, and A.H. MacDonald, Phys. Rev. Lett. **109**, 267404 (2012).

[75] F.M.D. Pellegrino, L. Chirolli, R. Fazio, V. Giovannetti, and M. Polini, Phys. Rev. B **89**, 165406 (2014).

[76] D.F. Walls and G.J. Milburn, *Quantum Optics* (Springer Science & Business Media, 2007).

[77] B. M. Garraway, Phil. Trans. R. Soc. A **369**, 1137-1155 (2011).

[78] O. Di Stefano, A. Settineri, V. Macrì, L. Garziano, R. Stassi, S. Savasta, and F. Nori, Nat. Phys. **15**, 803 (2019).

[79] J. Keeling, J. Phys.: Condens. Matter **19**, 295213 (2007).

[80] A. Vukics and P. Domokos, Phys. Rev. A **86**, 053807 (2012).

[81] A. Vukics, T. Griesser, and P. Domokos, Phys. Rev. A **92**, 043835 (2015).

[82] A. Stokes and A. Nazir, Phys. Rev. Lett. **125**, 143603 (2020).

[83] J.J. Hopfield, Phys. Rev. **112**, 1555 (1958).

[84] J.J. Sakurai, *Modern Quantum Mechanics* (Addison-Wesley, Reading-MA, 1994).

[85] D. Pines and P. Noziéres, *The Theory of Quantum Liquids* (W.A. Benjamin, Inc., New York, 1966).

[86] G.F. Giuliani and G. Vignale, *Quantum Theory of the Electron Liquid* (Cambridge University Press, Cambridge, 2005).

[87] H.P. Breuer and F. Petruccione, *The Theory of Open Quantum Systems* (Oxford University Press on Demand, 2007).

[88] D. Braun, *Dissipative Quantum Chaos and Decoherence* (Springer Tracts in Modern Physics, 2001).

[89] S. Sachdev, *Quantum Phase Transitions* (Cambridge University Press, 2011).

[90] T. Holstein and H. Primakoff, Phys. Rev. **58**, 1098 (1940).

[91] C.A. Vincent and B. Scrosati, *Modern Batteries* (Butterworth-Heinemann, Oxford, 1997).

[92] R.M. Dell and D.A.J. Rand, *Understanding Batteries* (The Royal Society of Chemistry, Cambridge, 2001).

[93] *Advances in Battery Technologies for Electric Vehicles*, edited by B. Scrosati, J. Garche, and W. Tillmetz (Woodhead Publishing, Cambridge, 2015).

[94] X. Luo, J. Wang, M. Dooner, and J. Clarke, Applied Energy **137**, 511 (2015).

[95] G. Wang, L. Zhang, and J. Zhang, Chem. Soc. Rev. **41**, 797 (2012).

[96] S.P.S. Badwal, S.S. Giddey, C. Munnings, A.I. Bhatt, and A.F. Hollenkamp, Front. Chem. **2**, 79 (2014).

[97] F. Bonaccorso, L. Colombo, G. Yu, M. Stoller, V. Tozzini, A.C. Ferrari, R.S. Ruoff, and V. Pellegrini, Science **347**, 1246501 (2015).

[98] A. Blais, R.-S. Huang, A. Wallraff, S.M. Girvin, and R.J. Schoelkopf, Phys. Rev. A **69**, 062320 (2004).

[99] M.H. Devoret and R.J. Schoelkopf, Science **339**, 1169 (2013).

[100] D.P. Di Vincenzo, Science **270**, 255 (1995).

[101] S. Vinjanampathy and J. Anders, Contemporary Physics **57**, 545 (2016).

[102] J. Clarke and F.K. Wilhelm, Nature **453**, 1031 (2008).

[103] A. Wallraff, D.I. Schuster, A. Blais, L. Frunzio, R.-S. Huang, J. Majer, S. Kumar, S.M. Girvin, and R.J. Schoelkopf, Nature **431**, 162 (2004).

[104] J.M. Fink, R. Bianchetti, M. Baur, M. Göppl, L. Steffen, S. Filipp, P.J. Leek, A. Blais, and A. Wallraff, Phys. Rev. Lett. **103**, 083601 (2009).

[105] Z.-L. Xiang, S. Ashhab, J.Q. You, and F. Nori, Rev. Mod. Phys. **85**, 623 (2013).

[106] Y. Ben, Z. Hao, C. Sun, F. Ren, N. Tan, and Y. Luo, Opt. Express **12**, 5146 (2004).

[107] A. Singha, M. Gibertini, B. Karmakar, S. Yuan, M. Polini, G. Vignale, M.I. Katsnelson, A. Pinczuk, L.N. Pfeiffer, K.W. West, and V. Pellegrini, Science **332**, 1176 (2011).

[108] T. Hensgens, T. Fujita, L. Janssen, X. Li, C.J. Van Diepen, C. Reichl, W. Wegscheider, S. Das Sarma, and L.M.K. Vandersypen, Nature **548**, 70 (2017).

[109] B. Küng, C. Rössler, M. Beck, M. Marthaler, D. S. Golubev, Y. Utsumi, T. Ihn, and K. Ensslin, Phys. Rev. X **7**, 011001 (2012).

[110] J. Basset, D.-D. Jarausch, A. Stockklauser, T. Frey, C. Reichl, W. Wegscheider, T.M. Ihn, K. Ensslin, and A. Wallraff, Phys. Rev. B **88**, 125312 (2013).

[111] C. Rössler, D. Oehri, O. Zilberberg, G. Blatter, M. Karalic, J. Pijnenburg, A. Hofmann, T. Ihn, K. Ensslin, C. Reichl, and W. Wegscheider, Phys. Rev. Lett. **115**, 166603 (2015).

[112] A. Hofmann, V.F. Maisi, C. Rössler, J. Basset, T. Krähenmann, P. Märki, T. Ihn, K. Ensslin, C. Reichl, and W. Wegscheider, Phys. Rev. B **93**, 035425 (2016).

[113] A. Stockklauser, P. Scarlino, J.V. Koski, S. Gasparinetti, C.K. Andersen, C. Reichl, W. Wegscheider, T. Ihn, K. Ensslin, and A. Wallraff, Phys. Rev. X **7**, 011030 (2017).

[114] A. Comin and L. Manna, Chem. Soc. Rev. **43**, 3957 (2014).

[115] L. De Trizio and L. Manna, Chem. Rev. **116**, 10852 (2016).

[116] M. Hofheinz, E.M. Weig, M. Ansmann, R.C. Bialczak, E. Lucero, M. Neeley, A.D. O'Connell, H. Wang, J.M. Martinis, and A.N. Cleland, Nature **454**, 310 (2008).

[117] M. Hofheinz, H. Wang, M. Ansmann, R.C. Bialczak, Erik Lucero, M. Neeley, A.D. O'Connell, D. Sank, J. Wenner, J.M. Martinis, and A.N. Cleland, Nature **459**, 546 (2009).

[118] R.W. Heeres, B. Vlastakis, E. Holland, S. Krastanov, V.V. Albert, L. Frunzio, L. Jiang, and R.J. Schoelkopf, Phys. Rev. Lett. **115**, 137002 (2015).

[119] S. Gasparinetti, S. Berger, A.A. Abdumalikov, M. Pechal, S. Filipp, and A.J. Wallraff, Sci. Adv. **2**, e1501732 (2016).

[120] S.P. Premaratne, F.C. Wellstood, and B.S. Palmer, Nature Commun. **8**, 14148 (2017).

[121] I.I. Rabi, Phys. Rev. **49**, 324 (1936).

[122] I.I. Rabi, Phys. Rev. **51**, 652 (1937).

[123] D. Braak, Phys. Rev. Lett. **107**, 100401 (2011).

[124] E.T. Jaynes and F.W. Cummings, Proc. IEEE **51**, 89 (1963).

[125] M. Tavis and F.W. Cummings, Phys. Rev. **170**, 379 (1968).

[126] M. Tavis and F.W. Cummings, Phys. Rev. **188**, 692 (1969).

[127] M.A. Bastarrachea-Magnani and J.G. Hirsch, Rev. Mex. de Fis. S **57**, 69 (2011).

[128] Q. Zhang, M. Lou, X. Li, J.L. Reno, W. Pan, J.D. Watson, M.J. Manfra, and J. Kono, Nature Phys. **12**, 1005 (2016).

[129] R.J. Schoelkopf and S.M. Girvin, Nature **451**, 664 (2008).

[130] F. Yoshihara, T. Fuse, S. Ashhab, K. Kakuyanagi, S. Saito, and K. Semba, Nature Phys. **13**, 44 (2017).

[131] N.K. Langford, R. Sagastizabal, M. Kounalakis, C. Dickel, A. Bruno, F. Luthi, D.J. Thoen, A. Endo, and L. DiCarlo, Nature Communications **8**, 1715 (2017).

[132] J. Braumüller, M. Marthaler, A. Schneider, A. Stehli, H. Rotzinger, M. Weides, and A.V. Ustinov, Nature Communications **8**, 779 (2017).

[133] W.P. Schleich, *Quantum Optics in Phase Space* (Wiley, Berlin, 2001).

[134] A.B. Klimov and S.M. Chumakov, *A Group-Theoretical Approach to Quantum Optics* (Wiley, Weinheim, 2009).

[135] For a recent review on QBs see e.g. F. Campaioli, F.A. Pollock, and S. Vinjanampathy, in *Thermodynamics in the Quantum Regime*, F. Binder, L.A. Correa, C. Gogolin, J. Anders, and G. Adesso (eds.), (Springer, 2018). Also available as arXiv:1805.05507.

[136] I. Henao and R.M. Serra, Phys. Rev. E **97**, 062105, (2018).

[137] S. Deffner and S. Campbell, J. Phys. A: Math. Theor. **50**, 453001 (2017).

[138] V. Giovannetti, S. Lloyd, and L. Maccone, Europhys. Lett. **62**, 615 (2003).

[139] J. Oppenheim, M. Horodecki, P. Horodecki, and R. Horodecki, Phys. Rev. Lett. **89**, 180402 (2002).

[140] G. Vitagliano, C. Klöckl, M. Huber, and N. Friis, in *Thermodynamics in the Quantum Regime*, F. Binder, L.A. Correa, C. Gogolin, J. Anders, and G. Adesso (eds.), (Springer, 2018). Also available as arXiv:1803.06884.

[141] J. Goold, M. Huber, A. Riera, L. del Rio, and P. Skrzypczyk, J. Phys. A: Math. Theor. **49**, 143001 (2016).

[142] G. Manzano, F. Plastina, and R. Zambrini, Phys. Rev. Lett. **121**, 120602 (2018).

[143] P. Yang, J.D. Brehm, J. Leppäkangas, L. Guo, M. Marthaler, I. Boventer, A. Stehli, T. Wolz, A.V. Ustinov, and M. Weides, Phys. Rev. Applied **14**, 024025 (2020).

[144] P.J. Leek, S. Filipp, P. Maurer, M. Baur, R. Bianchetti, J.M. Fink, M. Göppl, L. Steffen, and A. Wallraff, Phys. Rev. B **79**, 180511(R) (2009).

[145] J. Lolli, A. Baksic, D. Nagy, Vladimir E. Manucharyan, and C. Ciuti, Phys. Rev. Lett. **114**, 183601 (2015).

[146] P. Strasberg, G. Schaller, T. Brandes, and M. Esposito, Phys. Rev. X **7**, 021003 (2017).

[147] N. Lörch, C. Bruder, N. Brunner, and P.P. Hofer, Quantum Sci. Technol. **3** 035014 (2018).

[148] G. Francica, J. Goold, F. Plastina, and M. Paternostro, npj Quantum Information **3**, 12 (2017).

[149] S. Seah, S. Nimmrichter, and V. Scarani, New J. Phys. **20**, 043045 (2018).

[150] W. Niedenzu, V. Mukherjee, A. Ghosh, A.G. Kofman, and G. Kurizki, Nat. Comm. **9**, 165 (2018).

[151] N. Samkharadze, G. Zheng, N. Kalhor, D. Brousse, A. Sammak, U.C. Mendes, A. Blais, G. Scappucci, and L.M.K. Vandersypen, Science **25**, eaar4054 (2018).

[152] J. Goold, C. Gogolin, S.R. Clark, J. Eisert, A. Scardicchio, and A. Silva, Phys. Rev. B **92**, 180202(R) (2015).

[153] R. Nandkishore and D.A. Huse, Annu. Rev. Condens. Matter Phys. **6**, 15 (2015).

[154] J. Eisert, M. Cramer, and M.B. Plenio, Rev. Mod. Phys. **82**, 277 (2010).

[155] N.M. Bogoliubov, R.K. Bullough, and J. Timonen, J. Phys. A: Math. Gen. **29**, 6305 (1996).

[156] M.A. Bastarrachea-Magnani and J.G. Hirsch, Rev. Mex. Fis. S **57**, 69 (2011).

[157] P.A.M. Dirac, *Principles of Quantum Mechanics* (Oxford University Press, 1982).

[158] J. Chávez-Carlos, B. López-del-Carpio, M.A. Bastarrachea-Magnani, P. Stránsky, S. Lerma-Hernández, L.F. Santos, and J.G. Hirsch, Phys. Rev. Lett. **122**, 024101 (2019).

[159] C. Ciuti, G. Bastard, and I. Carusotto, Phys. Rev. B **72** 115303 (2005).

[160] M.A.M. de Aguiar, K. Furuya, C.H. Lewenkopf, and M.C. Nemes, Ann. Phys. **216**, 291 (1992).

[161] J.P.J. Rodriguez, S.A. Chilingaryan, and B.M. Rodríguez-Lara, Phys. Rev. A **98**, 043805 (2018).

[162] Y. Gu, A. Kitaev, S. Sachdev, and G. Tarnopolsky, J. High Energ. Phys. **2020**, 157 (2020).

[163] For a recent review see e.g. V. Rosenhaus, J. Phys. A: Math. Theor. **52**, 323001 (2019).

[164] J. Maldacena and D. Stanford, Phys. Rev. D **94**, 106002 (2016).

[165] D.A. Roberts, D. Stanford, and A. Streicher, J. High Energ. Phys. **2018**, 122 (2018).

[166] A. Georges, O. Parcollet, and S. Sachdev, Phys. Rev. B **63**, 134406 (2001).

[167] S. Sachdev, Phys. Rev. X **5**, 041025 (2015).

[168] C. Liu, X. Chen, and L. Balents, Phys. Rev. B **97**, 245126 (2018).

[169] Y. Huang and Y. Gu, Phys. Rev. D 100, 041901(R) (2019).

[170] S. Sachdev, Phys. Rev. Lett. **105**, 151602 (2010).

[171] S. Sachdev, J. Stat. Mech. (2010) P11022.

[172] I. Danshita, M. Hanada, and M. Tezuka, Prog. Theor. Exp. Phys. **2017**, 083I01 (2017).

[173] A. Chen, R. Ilan, F. de Juan, D.I. Pikulin, and M. Franz, Phys. Rev. Lett. **121**, 036403 (2018).

[174] A. Chew, A. Essin, and J. Alicea, Phys. Rev. B **96**, 121119(R) (2017).

[175] D.I. Pikulin and M. Franz, Phys. Rev. X **7**, 031006 (2017).

[176] A. Polkovnikov, K. Sengupta, A. Silva, and M. Vengalattore, Rev. Mod. Phys. **83**, 863 (2011).

[177] W. Fu and S. Sachdev, Phys. Rev. B **94**, 035135 (2016).

[178] R.A. Davison, W. Fu, A. Georges, Y. Gu, K. Jensen, and S. Sachdev, Phys. Rev. B **95**, 155131 (2017).

[179] A.M. García-García and J.J.M. Verbaarschot, Phys. Rev. D **94**, 126010 (2016).

[180] A. Eberlein, V. Kasper, S. Sachdev, and J. Steinberg, Phys. Rev. B **96**, 205123 (2017).

[181] V. Holubec and A. Ryabov, Phys. Rev. Lett. **121**, 120601 (2018).

[182] G.T. Noe II, J.-H. Kim, J. Lee, Y. Wang, A.K. Wójcik, S.A. McGill, D.H. Reitze, A.A. Belyanin, and J. Kono, Nat. Phys. **8**, 219 (2012).

[183] See, however, experimental work on Dicke superradiance in open systems formed by Bose-Einstein condensates coupled to optical cavities: K. Baumann, C. Guerlin, F. Brennecke, and T. Esslinger, Nature **464**, 1301 (2010); K. Baumann, R. Mottl, F. Brennecke, and T. Esslinger, Phys. Rev. Lett. **107**, 140402 (2011); H. Ritsch, P. Domokos, F. Brennecke, and T. Esslinger, Rev. Mod. Phys. **85**, 553 (2013).

[184] K. Hepp and E. H. Lieb, Phys. Rev. A **8**, 2517 (1973).

[185] H.J. Carmichael, C.W. Gardiner, and D.F. Walls, Phys. Lett. **46A**, 47 (1973).

[186] T. Tufarelli, K.R. McEnery, S.A. Maier, and M.S. Kim, Phys. Rev. A **91**, 063840 (2015).

[187] V. Bužek, M. Orszag, and M. Roško, Phys. Rev. Lett. **94**, 163601 (2005).

[188] K. Rzążewski and K. Wódkiewicz, Phys. Rev. Lett. **96**, 089301 (2006).

[189] C. Ciuti and P. Nataf, Phys. Rev. Lett. **109**, 179301 (2012).

[190] T. Jaako, Z.-L. Xiang, J.J. Garcia-Ripoll, and P. Rabl, Phys. Rev. A **94**, 033850 (2016).

[191] M. Bamba, K. Inomata, and Y. Nakamura, Phys. Rev. Lett. **117**, 173601 (2016).

[192] F.M.D. Pellegrino, V. Giovannetti, A.H. MacDonald, and M. Polini, Nat. Comm. **7**, 13355 (2016).

[193] G. Scalari, C. Maissen, D. Turčinková, D. Hagenmüller, S. De Liberato, C. Ciuti, C. Reichl, D. Schuh, W. Wegscheider, M. Beck, and J. Faist, Science **335**, 1323 (2012).

[194] V.M. Muravev, P.A. Gusikhin, I.V. Andreev, and I.V. Kukushkin, Phys. Rev. B **87**, 045307 (2013).

[195] S. Smolka, W. Wuester, F. Haupt, S. Faelt, W. Wegscheider, and A. Imamoglu, Science **346**, 332 (2014).

[196] S. Ravets, P. Knüppel, S. Faelt, M. Kroner, W. Wegscheider, and A. Imamoglu, Phys. Rev. Lett. **120**, 057401 (2018).

[197] G.L. Paravicini-Bagliani, F. Appugliese, E. Richter, F. Valmorra, J. Keller, M. Beck, N. Bartolo, C. Rössler, T. Ihn, K. Ensslin, C. Ciuti, G. Scalari, and J. Faist, Nat. Phys. **15**, 186 (2019).

[198] P. Knüppel, S. Ravets, M. Kroner, S. Fält, W. Wegscheider, and A. Imamoglu, Nature **572**, 91 (2019).

[199] For a recent review see e.g. J. Kuneš, J. Phys.: Condens. Matter **27**, 333201 (2015).

[200] See, for example, D. Jérome, T.M. Rice, and W. Kohn, Phys. Rev. **158**, 462 (1967); B.I. Halperin and T.M. Rice, Solid State Phys. **21**, 115 (1968); B.I. Halperin and T.M. Rice, Rev. Mod. Phys. **40**, 755 (1968).

[201] T. Portengen, Th. Östreich, and L.J. Sham, Phys. Rev. Lett. **76**, 3384 (1996) and Phys. Rev. B **54**, 17452 (1996).

[202] C.D. Batista, Phys. Rev. Lett. **89**, 166403 (2002).

[203] W. Kohn, Phys. Rev. **133**, A171 (1964).

[204] B.S. Shastry and B. Sutherland, Phys. Rev. Lett. **65**, 243 (1990).

[205] A.J. Millis and S.N. Coppersmith, Phys. Rev. B **42**, 10807(R) (1990).

[206] R.M. Fye, M.J. Martins, D.J. Scalapino, J. Wagner, and W. Hanke, Phys. Rev. B **44**, 6909 (1991).

[207] D. De Bernardis, T. Jaako, and P. Rabl, Phys. Rev. A **97**, 043820 (2018).

[208] D. De Bernardis, P. Pilar, T. Jaako, S. De Liberato, and P. Rabl, Phys. Rev. A **98**, 053819 (2018).

[209] J.A. Vergés, E. Louis, P.S. Lomdahl, F. Guinea, and A.R. Bishop, Phys. Rev. B **43**, 6099 (1991); J.A. Vergés, F. Guinea, and E. Louis, Phys. Rev. B **46**, 3562 (1992).

[210] A.N. Kocharian and J.H. Sebold, Phys. Rev. B **53**, 12804 (1996).

[211] S. Ejima, T. Kaneko, Y. Ohta, and H. Fehske, Phys. Rev. Lett. **112**, 026401 (2014).

[212] F. Schlawin, A. Cavalleri, and D. Jaksch, Phys. Rev. Lett. **122**, 133602 (2019).

[213] J.B. Curtis, Z.M. Raines, A.A. Allocca, M. Hafezi, and V.M. Galitski, Phys. Rev. Lett. **122**, 167002 (2019).

[214] S.M. Girvin, A.H. MacDonald, and P.M. Platzman, Phys. Rev. Lett. **54**, 581 (1985) and Phys. Rev. B **33**, 2481 (1986); S.M. Girvin and A.H. MacDonald, Phys. Rev. Lett. **58**, 1252 (1987); F.D.M. Haldane, Phys. Rev. Lett. **107**, 116801 (2011).

[215] A.A. Allocca, Z.M. Raines, J.B. Curtis, and V.M. Galitski, Phys. Rev. B **99**, 020504 (2019).

[216] M. Kiffner, J. Coulthard, F. Schlawin, A. Ardavan, and D. Jaksch, Phys. Rev. B **99**, 085116 (2019) and Phys. Rev. B **99**, 099907(E) (2019).

[217] Z.M. Raines, A.A. Allocca, M. Hafezi, and V.M. Galitski, Phys. Rev. Research **2**, 013143 (2020).

[218] J. Li, D. Golez, G. Mazza, A. J. Millis, A. Georges, and M. Eckstein, Phys. Rev. B **101**, 205140 (2020).

[219] Y. Ashida, A. Imamoglu, J. Faist, D. Jaksch, A. Cavalleri, and E. Demler, arXiv:2003.13695.

[220] J. Li and M. Eckstein, arXiv:2005.07643.

[221] V. Rokaj, D. Welakuh, M. Ruggenthaler, and A. Rubio, J. Phys. B: At. Mol. Opt. Phys. **51**, 034005 (2018).

[222] C. Schäfer, M. Ruggenthaler, and A. Rubio, Phys. Rev. A **98**, 043801 (2018).

[223] C. Schäfer, M. Ruggenthaler, H. Appel, and A. Rubio, Proc. Natl. Acad. Sci. (USA) **12**, 4883 (2019).

[224] C. Schäfer, M. Ruggenthaler, V. Rokaj, and A. Rubio, ACS Photon. **7**, 975 (2020).

[225] F.H.L. Essler, H. Frahm, F. Göhmann, A. Klümper, and V.E. Korepin, *The One-Dimensional Hubbard Model* (Cambridge University Press, Cambridge, 2005).

[226] S.H. Abedinpour, G. Vignale, A. Principi, M. Polini, W.-K. Tse, and A.H. MacDonald, Phys. Rev. B **84**, 045429 (2011).

[227] A. Stokes and A. Nazir, arXiv:2005.06499.

[228] Ya.B. Zel'dovich, JETP Lett. **14**, 180 (1971) and Sov. Phys. JETP **35**, 1085 (1971); C.W. Misner, Phys. Rev. Lett. **28**, 994 (1972); W. Unruh, Phys. Rev. D **10**, 3194 (1974).

[229] K. Gawędzki and K. Rzążewski, Phys. Rev. A **23**, 2134 (1981).

[230] M. Bamba and T. Ogawa, Phys. Rev. A **90**, 063825 (2014).

[231] P. Nataf, T. Champel, G. Blatter, and D.M. Basko, Phys. Rev. Lett. **123**, 207402 (2019).

[232] G. Grynberg, A. Aspect, and C. Fabre, *Introduction to Quantum Optics* (Cambridge University Press, Cambridge, 2010).

[233] J.H. Condon, Phys. Rev. **145**, 526 (1966).

[234] S.C. Ying, B. J. McIntyre, and J.J. Quinn, Phys. Rev. B **2**, 1801 (1970).

[235] D. Shoenberg, *Magnetic Oscillations in Metals* (Cambridge University Press, Cambridge, 1984).

[236] A. Gordon, M.A. Itskovsky, I.D. Vagner, and P. Wyder, Phys. Rev. Lett. **81**, 2787 (1998).

[237] G. Solta and V.S. Egorov, Physica B **318** 231 (2002).

[238] N. Logoboy and W. Joss, Physica B **403**, 3464 (2008).

[239] J.H. Condon and R.E. Walstedt, Phys. Rev. Lett. **21**, 612 (1968).

[240] G. Solt, C. Baines, V.S. Egorov, D. Herlach, E. Krasnoperov, and U. Zimmermann, Phys. Rev. Lett. **76**, 2575 (1996).

[241] G. Solt, V.S. Egorov, C. Baines, D. Herlach, and U. Zimmermann, Phys. Rev. B **62**, R11933(R) (2000).

[242] R.S. Markiewicz, M. Meskoob, and C. Zahopoulos, Phys. Rev. Lett. **54**, 1436 (1985).

[243] T. Holstein, R.E. Norton, and P. Pincus, Phys. Rev. B **8**, 2649 (1973).

[244] K. Kakazu and Y.S. Kim, Phys. Rev. A **50**, 1830 (1994).

[245] D. Hagenmüller, S. De Liberato, and C. Ciuti, Phys. Rev. B **81**, 235303 (2010).

[246] G. Vignale, Phys. Rev. Lett. **67**, 358 (1991).

[247] N.F.Q. Yuan, H. Isobe, and L. Fu, Nat. Commun. **10**, 5769 (2019).

[248] J.W. McClure, Phys. Rev. **104**, 666 (1956).

[249] G. Gómez-Santos and T. Stauber, Phys. Rev. Lett. **106**, 045504 (2011).

[250] A. Principi, M. Polini, G. Vignale, and M.I. Katsnelson, Phys. Rev. Lett. **104**, 225503 (2010).

[251] A. Raoux, M. Morigi, J.-N. Fuchs, F. Piéchon, and G. Montambaux, Phys. Rev. Lett. **112**, 026402 (2014).

[252] F. Piéchon, A. Raoux, J.-N. Fuchs, and G. Montambaux, Phys. Rev. B **94**, 134423 (2016).

[253] R. Bistritzer and A. H. MacDonald, Proc. Natl. Acad. Sci. (USA) **108**, 12233 (2011).

[254] P.W. Anderson, Science **177**, 4047 (1972).

[255] L. García-Álvarez, I.L. Egusquiza, L. Lamata, A. delCampo, J. Sonner, and E. Solano, Phys. Rev. Lett. **119**, 040501 (2017).

[256] H.P. Robertson, Phys. Rev. **34**, 163 (1929).